Woubishet Zewdu Taffese

Data-Driven Method for Enhanced Corrosion Assessment of Reinforced Concrete Structures

Turku Centre *for* Computer Science

TUCS Dissertations
No 253, June 2020

Data-driven method for enhanced corrosion assessment of reinforced concrete structures

Woubishet Zewdu Taffese

To be presented, with the permission of the Faculty of Science and Engineering of the University of Turku, for public criticism remotely using video conferencing application on June 18th, 2020 at 12:00.

University of Turku
Department of Future Technologies
20014 Turun Yliopisto, Finland

2020

Supervisors

Associate Professor Tapio Pahikkala
Department of Future Technologies, University of Turku
Turku, Finland

Professor Jukka Heikkonen
Department of Future Technologies, University of Turku
Turku, Finland

Professor Jouni Isoaho
Department of Future Technologies, University of Turku
Turku, Finland

D.Sc. (Tech.) Esko Sistonen
Department of Civil Engineering, Aalto University
Espoo, Finland

Reviewers

Professor Mahmut Bilgehan
Department of Civil Engineering, Istanbul Arel University
Istanbul, Turkey

Associate Professor Marek Słoński
Department of Civil Engineering, Cracow University of Technology
Kraków, Poland

Opponent

Professor Artūras Kaklauskas
Department of Construction Management and Real Estate
Vilnius Gediminas Technical University
Vilnius, Lithuania

The originality of this thesis has been checked in accordance with the University of Turku quality assurance system using the Turnitin Originality Check service.

ISBN 978-952-12-3952-6
ISSN 1239-1883

Abstract

Corrosion is a major problem affecting the durability of reinforced concrete structures. Corrosion related maintenance and repair of reinforced concrete structures cost multibillion USD per annum globally. It is often triggered by the ingression of carbon dioxide and/or chloride into the pores of concrete. Estimation of these corrosion causing factors using the conventional models results in suboptimal assessment since they are incapable of capturing the complex interaction of parameters. Hygrothermal interaction also plays a role in aggravating the corrosion of reinforcement bar and this is usually counteracted by applying surface-protection systems. These systems have different degree of protection and they may even cause deterioration to the structure unintentionally.

The overall objective of this dissertation is to provide a framework that enhances the assessment reliability of the corrosion controlling factors. The framework is realized through the development of data-driven carbonation depth, chloride profile and hygrothermal performance prediction models.

The carbonation depth prediction model integrates neural network, decision tree, boosted and bagged ensemble decision trees. The ensemble tree based chloride profile prediction models evaluate the significance of chloride ingress controlling variables from various perspectives. The hygrothermal interaction prediction models are developed using neural networks to evaluate the status of corrosion and other unexpected deteriorations in surface-treated concrete elements. Long-term data for all models were obtained from three different field experiments.

The performance comparison of the developed carbonation depth prediction model with the conventional one confirmed the prediction superiority of the data-driven model. The variable importance measure revealed that plasticizers and air contents are among the top six carbonation governing parameters out of 25. The discovered topmost chloride penetration controlling parameters representing the composition of the concrete are aggregate size distribution, amount and type of plasticizers and supplementary cementitious materials. The performance analysis of the developed hygrothermal model revealed its prediction capability with low error. The integrated exploratory data analysis

technique with the hygrothermal model had identified the surface-protection systems that are able to protect from corrosion, chemical and frost attacks.

All the developed corrosion assessment models are valid, reliable, robust and easily reproducible, which assist to define proactive maintenance plan. In addition, the determined influential parameters could help companies to produce optimized concrete mix that is able to resist carbonation and chloride penetration. Hence, the outcomes of this dissertation enable reduction of lifecycle costs.

Tiivistelmä

Korroosio vaikuttaa merkittävästi teräsbetonirakenteiden kestävyyteen, ja sen aiheuttamat maailmanlaajuiset taloudelliset kustannukset rakenteiden huolto- ja korjaustöitten takia ovat vuosittain miljardiluokkaa. Korroosion alkusyynä on usein hiilidioksidin ja/tai kloridin tunkeutuminen huokoiseen betoniin. Perinteiset menetelmät korroosiota aiheuttavien tekijöiden arviointiin eivät ota riittävän hyvin huomioon eri tekijöiden ja parametrien vuorovaikutuksia. Hygroterminen vuorovaikutus vaikuttaa vahvisterakenteiden korroosion etenemiseen, ja sitä pyritään estämään erilaisilla pinnoiteratkaisuilla. Näiden ratkaisujen suojaavat ominaisuudet vaihtelevat, ja osin saattavat jopa aiheuttaa ei-haluttua rakenteiden heikkenemistä.

Tässä tutkielmassa kehitetään viitekehys, jonka avulla voidaan paremmin arvioida korroosiolta suojaavien ratkaisujen luotettavuutta. Kehyksen pohjalta rakennetaan datavetoisia malleja karbonatisoitumisen, kloridirasituksen sekä hygrotermisen suorituskyvyn ennustamiseen.

Karbonatisoitumista ennustetaan integroidulla mallilla, jossa käytetään neuroverkkoja sekä tehostettuja ja bootstrap-aggregoituja kokoonpanopäätöspuita. Kokoonpanopäätöspuuhun pohjautuva kloridirasituksen ennustemalli arvioi kloridien tunkeutumiseen vaikuttavien tekijöiden merkitystä monista eri näkökulmista. Hygrotermisen vuorovaikutuksen mallintamiseen kehitetään neuroverkko, joka pyrkii ennustamaan korroosiota ja muita odottamattomia pinnoitettujen betonirakenteiden vaurioita. Kaikkia malleja varten kerättiin dataa pitkältä aikaväliltä kolmesta eri kenttäkokeesta.

Karbonatisoitumista ennustavan mallin suorituskyky paljastui vertailussa paremmaksi kuin perinteisen menetelmän. Tutkimuksessa paljastui, että pehmittimen ja ilman koostumuksen vaikutukset karbonatisoitumiseen ovat kuuden tärkeimmän tekijän joukossa kahdestakymmenestäviidestä tutkitusta. Keskeisimmät betonin rakenteeseen vaikuttavista tekijöistä kloridirasituksen suhteen ovat soran raekoko, käytettyjen pehmittimien määrä ja laatu, sekä käytetyt sementiittilisämateriaalit. Hygrotermisen suorituskyvyn mallin havaittiin

ennustavan suorituskykyä hyvin. Integroitu hygrotermisen suorituskyvyn malli ja data-analyysimenetelmä tunnisti pinnan suojausmenetelmät, jotka suojaavat korroosiolta, kemiallisilta sekä roudan aiheuttamilta vaurioilta.

Kaikki tutkielmassa korroosion arviointiin kehitetyt menetelmät ovat luotettavia, robusteja sekä helposti toistettavia, mikä auttaa ennakoivien kunnossapitosuunnitelmien tekemisessä. Lisäksi tutkielmassa havaittujen merkittävien korroosiota aiheuttavien tekijöiden tunnistaminen auttaa yrityksiä optimoimaan sekoitussuhteita betoninvalmistuksessa niin, että tuloksena saatavat teräsbetonirakenteet kestävät entistä paremmin karbonatisoitumista sekä kloridirasitusta, samalla vähentäen rakennusten elinkaarikustannuksia.

Acknowledgements

The doctoral studies that led to this dissertation have been a long and challenging journey. I started my study at Department of Civil Engineering, Aalto University and finalized it at Department of Future Technologies, University of Turku. This work was made possible by financial support from various sources. I am grateful to the University of Turku Graduate School (UTUGS), Finnish Foundation for Technology Promotion (TES), Foundation for Aalto University Science and Technology, Auramo-Säätiö Foundation, Kerttu and Jukka Vuorinen Fund for providing me financial support that help me to fully concentrate on my research.

There are few people including colleagues and family members who have contributed to accomplish this journey. Firstly, I would like to express my deepest gratitude to my supervisors at University of Turku: Associate Professor Tapio Pahikkala, Professor Jukka Heikkonen and Professor Jouni Isoaho for their guidance and giving me the opportunity to finalize my doctoral study at the Department of Future Technologies. The doctoral degree would not have been possible to be realized without their support. Furthermore, I am grateful to Professor Jouni Isoaho for his time on following up closely all the official processes despite his busy schedules. Most of the research work was carried out within the Department of Civil Engineering at Aalto University. I am greatly thankful to D.Sc. (Tech.) Esko Sistonen for giving me the opportunity to start my research work, support in getting experimental data and more importantly for being my external supervisor at University of Turku. My appreciation also extended to Professor Jouni Punkki and D.Sc. (Tech.) Fahim Al-Neshawy for their kind assistance to all my requests at Aalto University.

I am also greatly thankful to the pre-examiners, Professor Mahmut Bilgehan and Associate Professor Marek Słoński, for reviewing the thesis. I would also like to thank Prof. Artūras Kaklauskas for his time and interest to this work as an opponent.

D.Sc. (Tech.) Antti Hakkala is warmly acknowledged for helping me in translating my research proposal and thesis abstract to Finnish language. It was not possible to secure some of the grants without his kind help. I am thankful to Dr. Mikhail Barash, Scientific Coordinator at TUCS, for his

kind assistance during the publication of this thesis. I am grateful to D.Sc. (Tech.) Khalid Latif for trying kindly to find solutions for the challenges I had encountered. I would also like to thank my family and friends who have encouraged me throughout the years.

Finally, my sincere gratitude with love goes to my wife Ethiopia. I am very grateful for her unconditional love, encouragement, and endurance during this long journey. She has stood by me throughout this journey and has made countless sacrifices for helping me get through the difficult times in the most positive way. She has been my inspiration and motivation for continuing to enhance my knowledge and move my research forward. Words cannot express my heartfelt appreciation and love for her infinite support, and for being most intellectually curious partner that I could hope for.

Turku, June 2020

Woubishet Zewdu Taffese

Contents

List of abbreviations and symbols

AEA	Air-entraining agents
BFS	Blast-furnace slag
CV	Cross validation
EDA	Exploratory data analysis
EN	European Standard
FA	Fly ash
HW	Highway
ITZ	Interfacial transition zone
LSBoost	Least-squares boosting
MAE	Mean-absolute error
MSE	Mean-square error
NARX	Nonlinear autoregressive with exogenous inputs
R	Correlation coefficient
RC	Reinforced concrete
RCM	Rapid chloride migration
RH	Relative humidity
RMSE	Root-mean-square error
SCC	Self-compacting concrete
T	Temperature
VI	Variable importance
w/b	Water- to-binder ratio
w/c	Water-to-cement ratio

List of publications

The work discussed in this doctoral dissertation is based on the synthesis of the following original publications.

Publications included in the thesis

1. Publication I

   Taffese, Woubishet Zewdu; Sistonen, Esko. 2017. Machine learning for durability and service-life assessment of reinforced concrete structures: Recent advances and future directions. Elsevier. Journal of Automation in Construction, volume 77, pages 1–14. ISSN 0926-5805. https://doi.org/10.1016/j.autcon.2017.01.016.

2. Publication II

   Taffese, Woubishet Zewdu; Sistonen, Esko; Puttonen, Jari. 2015. CaPrM: Carbonation prediction model for reinforced concrete using machine learning methods. Elsevier. Journal of Construction and Building Materials, volume 100, pages 70–82. ISSN 0950-0618. https://doi.org/10.1016/j.conbuildmat.2015.09.058.

3. Publication III

   Taffese, Woubishet Zewdu; Sistonen, Esko. 2017. Significance of chloride penetration controlling parameters in concrete: Ensemble methods. Elsevier. Journal of Construction and Building Materials, volume 139, pages 9–23. ISSN 0950-0618. https://doi.org/10.1016/j.conbuildmat.2017.02.014.

4. Publication IV

   Taffese, Woubishet Zewdu; Sistonen, Esko. 2016. Neural network based hygrothermal prediction for deterioration risk analysis of surface-protected concrete façade element. Elsevier. Journal of Construction and Building Materials, volume 113, pages 34–48. ISSN 0950-0618. https://doi.org/10.1016/j.conbuildmat.2016.03.029.

Publications not included in the thesis

The following publications are related to the research but are not appended in the thesis.

5. Publication V

   Taffese, Woubishet Zewdu; Nigussie, Ethiopia; Isoaho, Jouni. 2019. Internet of things based durability monitoring and assessment of reinforced concrete structures. Elsevier. Procedia Computer Science, volume 155, pages 672–679. ISSN 1877-0509. https://doi.org/10.1016/j.procs.2019.08.096.

6. Publication VI

   Taffese, Woubishet Zewdu; Al-Neshawy, Fahim; Sistonen, Esko; Ferreira, Miguel. 2015. Optimized neural network based carbonation prediction model, International Symposium on Non-Destructive Testing in Civil Engineering (NDT-CE), Berlin, Germany. pages 1074–1083.

7. Publication VII

   Taffese, Woubishet Zewdu; Sistonen, Esko; Puttonen, Jari. 2015. Prediction of concrete carbonation depth using decision tree. Proceedings of the 23rd European Symposium on Artificial Neural Networks, Computational Intelligence and Machine Learning (ESANN 2015), Bruges, Belgium. pages 415–420.

8. Publication VIII

   Taffese, Woubishet Zewdu; Sistonen, Esko. 2013. Service-life prediction of repaired concrete structure using concrete recasting method: State-of-the-art. Elsevier. Procedia Engineering, volume 57, pages 1138–1144, ISSN 1877-7058 https://doi.org/10.1016/j.proeng.2013.04.143.

9. Publication IX

   Taffese, Woubishet Taffese; Al-Neshawy, Fahim; Piironen, Jukka; Sistonen, Esko; Puttonen, Jari. 2013. Monitoring, evaluation and long-term forecasting of hygrothermal performance of thick-walled concrete structure. Proceedings of OECD/NEA WGIAGE Workshop on Nondestructive Evaluation of Thick-Walled Concrete Structures, Prague, Czech Republic. pages 121–143.

Chapter 1

Introduction

1.1 Background

Corrosion is one of the foremost critical problems affecting the durability of reinforced concrete (RC) structures throughout the world [1–3]. Several studies revealed that corrosion related maintenance and repair of RC structures cost multibillion USD per annum globally. Repairing of corrosion-induced damage in Western Europe alone causes the loss of 5 billion EUR annually [4]. Some developed countries even expend about 3.5% of their gross national product for corrosion associated damage and its control [5]. Even in repaired RC structures, continued corrosion of reinforcement bar accounts for 37% of the failure modes [6], causing costly repairs of repairs [6–8].

The process of corrosion in RC structures is divided into two general phases: initiation and propagation. In the initiation phase the aggressive substances, carbon dioxide (CO_2) and chloride ions (Cl^-), are transported through the concrete pores towards the surface of the reinforcement bar. Since concrete is alkaline with a pore solution pH of 12–13 that protects the embedded reinforcement bar from corrosion by forming a thin oxide layer on its surface. This layer deteriorates in the presence of Cl^- or due to the carbonation of concrete [9,10]. Carbonation is a physicochemical phenomenon induced naturally by the ingression of CO_2 into the concrete pores from the surrounding environment and reacts with hydrated cement. The propagation phase covers the time from the onset of reinforcement bar corrosion to structural failure. In this phase, the deterioration of reinforcement bar depends on the corrosion rate, which is mainly governed by two environmental agents: moisture and temperature. These agents control the corrosion rate through their effect on the electrochemical reactions [11,12].

Carbonation- and chloride-induced corrosion can diminish the cross-sectional area and the elongation capacity of the reinforcement bar. This causes severe cracking as well as reduction in the load-bearing capacity of

the structure. Cracked concrete could allow an additional entry of moisture, aggressive gasses and ions, aggravating reinforcement bar corrosion and concrete degradation. Subsequently, the strength, safety and serviceability of the RC structures will be declined.

In order to perform in-time and cost-effective maintenance and repair decisions, the initiation time of corrosion has to be reliably estimated. In practice, simplified Fick's second law based models are extensively applied for predicting carbonation depth and chloride concentration inside the concrete. Most of these models and the associated value of input parameters have been oversimplified, incomplete, and/or unsuitable for the prevailing conditions [13–15]. The use of these oversimplified models lacks the ability to capture the complex interactions among the involving parameters, causing suboptimal or even improper choice of design and maintenance strategies. A better understanding of the complex interacting parameters that controls the corrosion of reinforcement bar is a crucial step towards the development of reliable models. Indeed, examination of CO_2 and Cl^- transport in concrete is performed for several years to acquire a better understanding of various controlling parameters. Nevertheless, it is usually challenging to isolate the influences of particular parameters because other controlling parameters are also varying naturally at the same time [16,17]. Identifying the influential predictors using traditional statistical methods, such as linear regression method is unachievable since the penetration of these aggressive substances in field concrete is a highly complicated process involving several nonlinear interactions among the parameters. Determining powerful predictors based on linear regression method is only applicable for linear or nearly linear models. Hence, alternative approaches that are capable of managing multidimensional nonlinear parameters are necessary in order to determine the influential predictors reliably.

The conventional carbonation depth and chloride concentration prediction models were established based on short-term tests. It has been proven from many experimental data that these simplified models, especially those developed to predict chloride profile, can only characterize the chloride penetration under the exposure conditions for a short period of time close to the conditions for which the input parameters of the model were deduced [18]. There is no a straightforward method that can be

applied for the translation of short-term field data into values that can express the long-term performance of concrete structures exposed to field environment. Fortunately, several long-term field data are nowadays available from real structures and specimens made with several mix compositions exposed to carbonation and chloride environment. With the advancement of nondestructive technologies for monitoring of corrosion controlling parameters in concrete structure, the availability of field data subjected to different exposure conditions will increase significantly. Huge efforts are being made in the past in other industries to establish powerful data-driven methods that can be utilized to perform accurate predictions and extract useful information. Thus, in construction industry, examining the possibilities of predicting corrosion controlling parameters using readily available long-term field data as well as translating them into useful knowledge is essential.

In Finland, corrosion-induced damage on prefabricated RC façade is projected to be around 15 million m^2 per annum and will grow 2% each year [19]. It accounts for about 11–40% of the overall repair costs depending on the surface-finishing material types [20]. Substantial attempts have been made into devising cost-effective repair methods to control the rate of corrosion of reinforcement bar. Surface-protection system is one of the economical methods that are widely used to curb the corrosion rate by controlling the moisture of concrete [11,21]. The surface-protection system may have different degrees of protection against moisture even with identical generic chemical composition. They may even cause unintended damage to the structure since the compositions of the materials differ extensively [21]. Therefore, clear understanding of the hygrothermal performance of surface-protected concrete is essential since uncontrolled hygrothermal interaction may accelerate the corrosion of the embedded reinforcement bar. Certainly, hygrothermal transport phenomena in concrete and several other building materials are thoroughly understood and numerical models have already been established [22]. Though models to predict the hygrothermal behaviour of concrete have been suggested in the past, none has explicitly integrated diverse surface-protection materials and application procedures in their model. It is also challenging to provide satisfactory analytical methods to assess the performance of the protective measures since understanding the

interaction of various types of surface-protection systems with the substrate concrete in very dynamic environmental conditions is highly complex. In-service hygrothermal monitoring utilizing sensors is a better alternative for assessing the performance of surface-protected RC concrete elements. Using the sensor data, the hygrothermal interaction can be forecasted, which leads to understanding of the condition of corrosion. In addition, using the forecasted data and exploratory data analysis appropriate surface-protection system can be determined.

1.2 Research problem

The research problem of the dissertation is: *how to make valid, reliable, and robust corrosion assessment of RC structures through realization of the complex processes of carbonation, chloride ingress and hygrothermal interaction?* The research problem is approached through the following more detailed research questions:

Research question one: How to eliminate or mitigate the uncertainties observed in the traditional corrosion assessment methods?

Research question two: How to develop accurate carbonation depth prediction model that considers the complex parameter interactions? What are the predominant carbonation depth predictors?

Research question three: What are the significant parameters that describe the chloride concentration into concrete?

Research question four: How to predict the hygrothermal interaction inside surface-protected concrete while identifying the appropriate surface-protection system?

Each of the above research questions is answered in one of the annexed publications and each article contributes towards addressing the overall research problem. The logic on how the publications are interconnected in answering the research problem is illustrated in Figure 1.1. The first publication answers the research question one. This publication examines the recent advances and current practices of corrosions assessment of RC structures and recommends methods that mitigate the uncertainties observed in the conventional approaches. Research question two is addressed by Publication II, which presents the development of an optimized and integrated data-driven carbonation prediction model. It

also determines influential carbonation depth predicting parameters. Research question three is answered by Publication III. This publication evaluates the importance of variables that characterize the chloride concentration in concrete. The fourth publication provides answer for the research question four. It demonstrates how hygrothermal interaction inside surface-protected concrete can be predicted using data-driven models while identifying the appropriate surface-protection system.

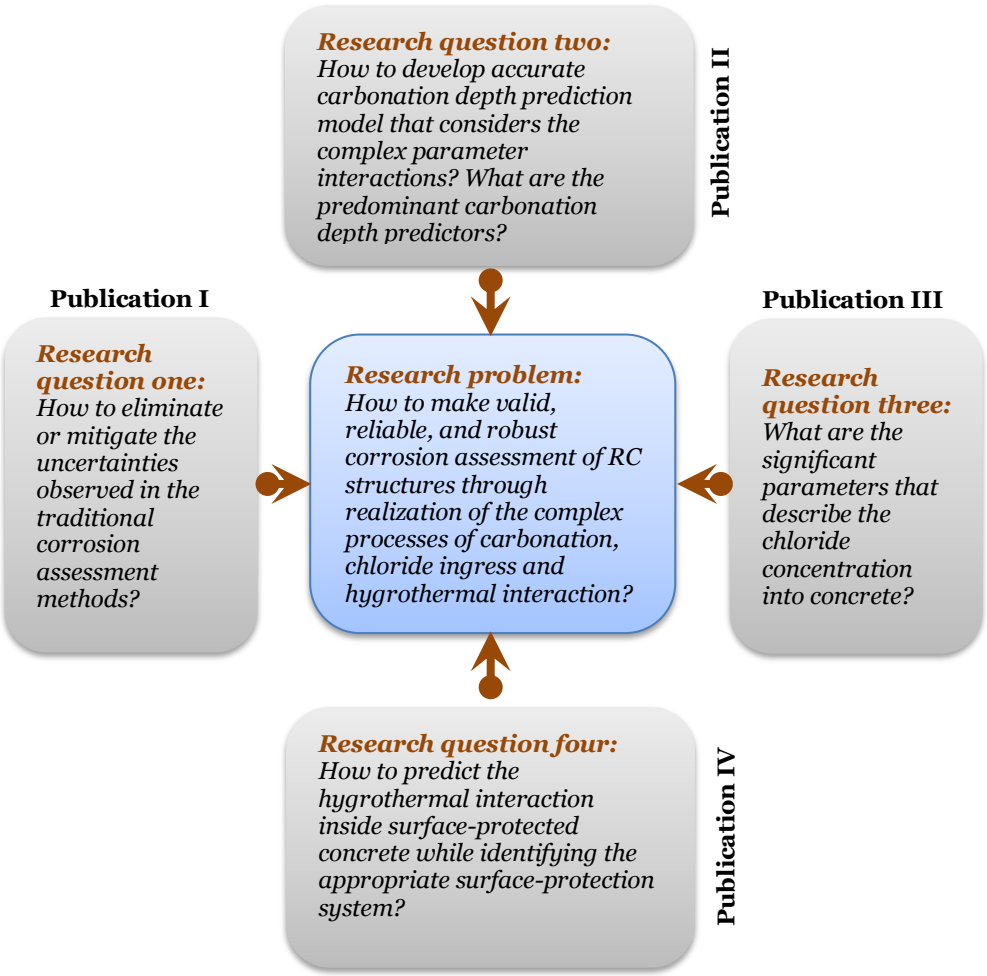

Figure 1.1. The logic on how the publications are interconnected in answering the research problem.

1.3 Aim and objectives of the research

The aim of this dissertation is *to provide a framework that enhances the assessment reliability of the corrosion controlling factors*. The framework is realized through the development of data-driven models that evaluate corrosion causing and accelerating factors. The objectives are: i) to reliably foresee the carbonation depth and to determine the influential predictors of carbonation depth; ii) to identify the significance of chloride penetration characterizing parameters; and iii) to evaluate the hygrothermal behaviour of surface-protected concrete elements.

A reliable prediction of carbonation depth, chloride profile and hygrothermal behaviour is instrumental for realizing optimal design and maintenance plans for RC structures. The determination of influential predictors will also yield scientific significance that could assist concrete researchers to design concrete mix that resist carbonation and chloride penetration. All these enable a considerable minimization in lifecycle costs, which in turn prevents economic loss.

1.4 Research methodology and dissertation structure

All the methods that are devised to assess corrosion causing and aggravating factors in this dissertation rely on machine learning algorithms and implemented using MATLAB programming language. The methods are utilized for developing data-driven models. As any data-driven models, the development process of these models primarily consists of data, data preprocessing and training. The experimental data employed for model development and testing are gathered from field experiments.

The thesis is divided into six chapters. Chapter Two presents the theoretical foundation of the thesis by focusing on corrosion causing and controlling factors as well as the limitations of the conventional carbonation and chloride profile prediction models. It also discusses the need for hygrothermal-behaviour prediction approaches for surface-protected concrete structures. The advantages of data-driven methods that mitigate the limitations of the conventional models and the fundamental concepts of the machine learning algorithms that are used in developing the data-driven models are discussed in the same chapter.

The materials and methods that are employed to address the research problem of the dissertation are discussed in Chapter Three. It presents the development process of data-driven models that predict carbonation depth, chloride profile and hygrothermal behaviour. As data-driven methodologies, the materials part of this chapter discusses the utilized experimental data for the development of carbonation, chloride and hygrothermal models in details.

The core results of the dissertation are presented in Chapter Four. It has four sections where each section answers the corresponding research questions. It presents the advantages of data-driven approaches in mitigating uncertainties that are observed in the conventional corrosion prediction methods. The performances of the developed models for carbonation depth prediction, and for determining significant predictors of carbonation depth and chloride concentration in concrete are discussed. The performance of the hygrothermal behaviour prediction model for surface-protected concrete element is also discussed in the same chapter.

Chapter Five presents the discussion of the research results in the context of theoretical and practical implications of the research as well as its reliability and validity. In addition, recommendations for further research are proposed in the same chapter. Finally, the conclusion of the dissertation is presented in Chapter Six.

1.5 Scope of the research

The scope of the dissertation is to examine and model corrosion causing and controlling factors by focusing on carbonation, chloride penetration and hygrothermal interaction. All the case structures or experiments in the dissertation represent natural Finnish climate. The hygrothermal, carbonation and chloride case structures are located in Vantaa, Espoo and Kotka, respectively. The environmental exposure classes for examination of carbonation, chloride ingress and hygrothermal are XC3 (moderate humidity), XD3 (cyclic wet and dry), and XF1 (moderate water saturation, without deicing agent), respectively. The maximum exposure time of the case structures is two, six, and seven years for hygrothermal, chloride, and carbonation investigation, respectively.

Chapter 2

Theoretical foundation

In this chapter, the corrosion process and factors that cause and control corrosion are presented. The limitations of the conventional corrosion assessment methods are also discussed. The fundamental principles of novel data-driven approach that are able to address the recognized limitations of the conventional methods are presented.

2.1 Corrosion process

Corrosion of reinforcement bar is an electrochemical process. The electrochemical potentials to generate the corrosion cells are induced in two mechanisms [9,10,12,23]: i) when two different types of metal are embedded in concrete or when there is a considerable dissimilarities in the surface characteristics of the reinforcement bar, and ii) when there is concentration differences in the dissolved ions at the vicinity of the reinforcement bar surface. As a result, in cases of mechanism (i), one of the two metals becomes anodic and the other cathodic. While, in case of mechanism (ii), some parts of the reinforcement bar begin to be anodic and the other part of the reinforcement bar becomes cathodic. The primary chemical changes occurring at the anodic and cathodic areas as well as the resulting rust formation are described by Equations (2.1) to (2.4). Furthermore, the corrosion of reinforcement bar in concrete as an electrochemical process is schematically illustrated in Figure 2.1.

At the anode, oxidation of iron occurs:

$$\mathrm{Fe} \rightarrow \mathrm{Fe}^{++} + 2\mathrm{e}^{-}. \tag{2.1}$$

At the cathode, reduction of atmospheric oxygen with water occurs:

$$\tfrac{1}{2}\mathrm{O}_2 + \mathrm{H}_2\mathrm{O} + 2\mathrm{e}^{-} \rightarrow 2(\mathrm{OH})^{-}. \tag{2.2}$$

When anodic and cathodic reaction products combine:

$$Fe^{++} + 2(OH)^{-} \rightarrow Fe(OH)_2. \quad (2.3)$$

Subsequent oxidation reaction results in the formation of rust:

$$FeO.(H_2O)_x. \quad (2.4)$$

The anodic and cathodic reaction is responsible for the formation of primary corrosion product of metal, $Fe(OH)_2$, but the action of O_2 and H_2O can yield other corrosion products with different colours [9,24,25]. Corrosion is often accompanied by a loss of reinforcement bar cross-sectional area and accumulation of corrosion products which invade a larger volume (usually 2 to 6 times) than the original reinforcement bar [9,11]. The corrosion product exerts substantial tensile stresses, causing cracking and spalling of the concrete cover. So, structural distress may gradually occur due to the bond loss between reinforcement bar and concrete or due to loss of reinforcement bar cross-sectional area [26,27].

The concrete cover provides both chemical and physical protections against corrosion of reinforcement bar. Chemical changes caused by the ingression of aggressive substances into concrete deteriorate the oxide layer at the surface of the reinforcement bar, causing initiation of

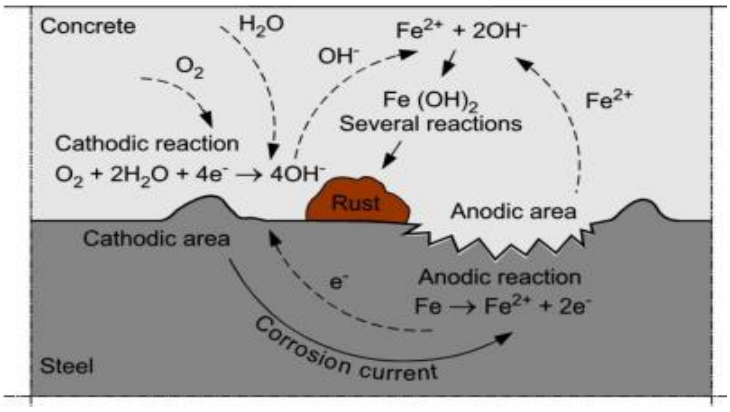

Figure 2.1. Schematic illustration of rebar corrosion in concrete as an electrochemical process [19].

corrosion. The concrete can also lose its protection capability due to cracking. Cracking of concrete let penetration of corrosion causing and accelerating agents, such as moisture, aggressive gasses, and ions to the vicinity of reinforcement bar surface.

2.2 Corrosion causing and controlling factors

Corrosion of reinforcement bar is typically triggered by the ingression of CO_2 and Cl^- into the concrete pores. Once the corrosion of reinforcement bar is initiated, the corrosion rate is mainly controlled by the environmental agents, which are moisture and temperature. Since the focus of the dissertation is on the above corrosion initiating and controlling factors, the process of carbonation, chloride ingression and hygrothermal interaction are discussed below.

2.2.1 Carbonation and chloride ingress

Normally, concrete is alkaline with a pore solution pH of 12–13 that passivizes the embedded reinforcement bar. The passivation of reinforcement bar is breakdown due to the existence of Cl^- or by the carbonation of the concrete [9–11]. Carbonation is a natural physicochemical process caused by the ingression of CO_2 from the neighbouring environment into the concrete through pores in the matrix where the CO_2 reacts with hydrated cement [28,29]. The chemical reaction of carbonation process is expressed in Equation (2.5). Calcium hydroxide ($Ca(OH)_2$) in contact with carbon dioxide (CO_2), in the presence of moisture, forms calcium carbonate ($CaCO_3$). This chemical reaction slowly lowers the alkalinity of the pore fluid from a pH value of about 13 to 9 [10,29–32]. Though the depletion of alkalinity caused by carbonation alters the chemical composition of concrete, its major consequence is that it destroys the passive oxide layer of reinforcement bar which ultimately initiates corrosion [10,28–35].

$$Ca(OH)_2 + CO_2 \xrightarrow{H_2O} CaCO_3 + H_2O. \quad (2.5)$$

The ingression of chloride ions is also the principal cause for corrosion of reinforcement bar in concrete. Similar to carbonation, the ingression of chloride ions does not normally cause damage to the concrete directly. Nevertheless, when the amount of chloride concentration at the reinforcement bar reaches a certain threshold, depassivation occurs that initiates corrosion [36–40]. Chloride ions exist in the cement paste surrounding the reinforcement bar react at anodic sites to form hydrochloric acid which obliterates the passive protection layer on the surface of reinforcement bar. The surface of the reinforcement bar then becomes activated locally to form the anode, while the passive surface forming the cathode, resulting corrosion initiation in the form of localized pitting [10,11,41]. Chloride attack is one of the primary threats for the durability of RC structures that are exposed to marine environment and deicing salts containing chloride [36–40]. The ingression of Cl^- is notable in countries at those latitudes where substantial amounts of deicing salts are spread on the roads to melt the ice during the winter. The melted ice slurry with intensely concentrated Cl^- from deicing salt splashes to RC structures by the moving vehicles. There is even a study that claim Cl^- from deicing salt is detected as high as 60^{th} floor of RC building structure located 1.9 km from a busy highway [42].

As presented above, the alkaline environment that shields the reinforcement bar is vulnerable to deterioration, either by carbonation or chloride attack. The penetration rate of these aggressive substances to breakdown the passive film is a function of the quality and the thickness of the concrete cover as well as the surrounding environment. Generally, the corrosion process of reinforcement bar in concrete is divided into two stages*:* initiation and propagation. In case of carbonation-induced corrosion, the corrosion initiation stage corresponds to the time required for the carbonation front to arrive at the surface of reinforcement bar. In chloride-induced corrosion, the corrosion initiation stage corresponds to the period for the Cl^- concentration to reach at a specific threshold level that damages the protective layer. Once the protective layer has broken, corrosion can onset and accelerate very fast in the presence of moisture and oxygen. The time taken from onset of corrosion to concrete failure is known as the propagation period. The initiation stage compared with the propagation period is long. It means that, if appropriate measures are not

timely taken, the period relative to the whole service life from the corrosion onset to the structural failure is short. Due to this fact, the corrosion initiation period has been often utilized to measure the service life of RC structures [43,44]. A schematic representation of the conceptual model of corrosion stages of reinforcement bar is presented in Figure 2.2.

The premature failures due to corrosion of reinforcement bar in RC structures are among the major challenges of civil infrastructures which causes huge economic losses. For instance, the annual total direct cost of chloride-induced corrosion in US highway bridges alone exceeds eight billion USD. The indirect costs caused by traffic delays and lost productivity are projected to be ten times more than the cost of corrosion associated maintenance, repair and rehabilitation [45,46]. Even if chloride-induced corrosion is normally more pernicious and more expensive to repair, carbonation-induced corrosion of reinforcement bar affects a wider range of RC structures at a larger scale. Thus, it is a critical problem in several parts of the world and presently two-thirds of RC structures are subjected to environmental situations that favour carbonation-induced corrosion [35,47] .

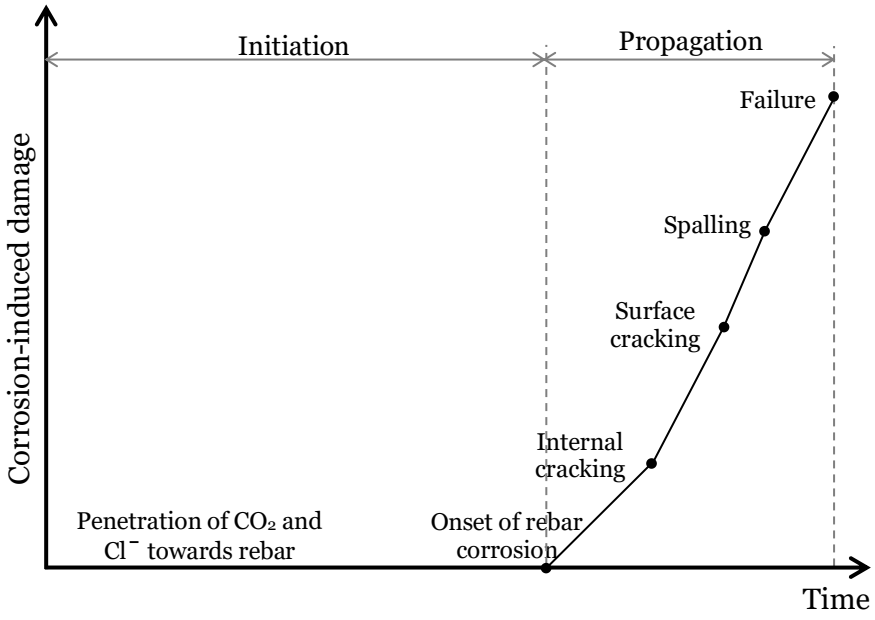

Figure 2.2. Corrosion of rebar in concrete structure: initiation and propagation periods (Publication I).

2.2.2 Hygrothermal behaviour

The amount of moisture within the concrete is the major factor that controls the corrosion rate through their influence on the electrochemical reactions at the reinforcement bar-concrete interface and ions transport between anodes and cathodes [11]. The surrounding temperature also governs the corrosion rate of reinforcement bar since it influences the electrochemical reactions and the amount of the moisture that the concrete retains [12]. For instance, the corrosion rate varies by more than a factor of ten in a regular seasonal temperature range of 5 to 30 °C [2,12,48]. Uncontrolled hygrothermal (moisture and temperature) can also cause other types of deterioration on concrete. In the presence of high moisture, some aggressive substances from internal or external sources can react with concrete ingredients leading to concrete damage [9,10,24,28]. For example, alkali reaction may take place when alkalis react with aggregates to form products that are deleterious to concrete. In low temperature, concrete may be damaged by freezing and thawing if the concrete pore system is filled with moisture and has reached a critical degree of saturation [28,49]. Hence, controlling the hygrothermal condition of RC structures is essential to prolong their service life.

The existence of a large number of RC structures that are subjected to corrosion of reinforcement bar and other deterioration mechanisms caused by uncontrolled hygrothermal interaction call for cost-effective maintenance measures. In the past few decades, substantial efforts have been put into devising economical methods to control the moisture penetration into RC structures. European Standard - EN 1504 proposes surface-protection systems to limit the amount of moisture content, and thus control the corrosion rate of reinforcement bar by increasing the concrete resistivity under rehabilitation principles P2 – *Moisture control of concrete* and P8 – *Increase of the electric resistivity of concrete* [21]. According to EN 1504, the surface-protection systems that can be applied for concrete are categorized into three groups: i) hydrophobic impregnation: produces a water-repellent surface with no pores filling effect; ii) impregnation: lessens the surface porosity with partial or full pores filling effect; and iii) coatings: forms a continuous protective film on the concrete surface.

The chemical compositions of commonly applied surface-protection materials to control the moisture penetration into concrete vary broadly. Due to this, the surface-coating systems may behave differently and even lead to unintentional damage to the concrete. It may also deliver dissimilar degrees of protection against moisture even for those surface-protection materials with similar generic chemical composition. All these facts make selection of suitable surface-protection system for a particular structure challenging.

In order to capture the hygrothermal behaviour inside surface-protected concrete members, details of the temporal change of properties of the applied coating materials under environmental and service conditions are necessary. Furthermore, a comprehensive understanding of the interaction of different surface-protection materials with the substrate concrete is indispensable. Some surface-treating materials penetrate into the pores of concrete and react with the hydration products of the concrete, but some other materials form a continuous layer at the surface of concrete. All these conditions create complexity on the hygrothermal behaviour assessment of surface-protected concrete.

2.3 Conventional corrosion assessment models

As discussed above, carbonation and chloride ion penetration into concrete cause initiation of corrosion of reinforcement bar. Reasonably accurate prediction of the depth of carbonation and concentration of chloride ions is crucial to optimize the design and maintenance programs for RC structures. In the past three decades, considerable attempts have been performed to develop durability models for RC structures subjected to environmental situations that favour carbonation- and chloride-induced corrosion. As a result, diverse models and input parameters have been established. The complexity degree of the proposed models differ from straightforward analytical models presuming uniaxial diffusion into concrete, to more complex numerical models which take the physical, chemical, and electrochemical processes of gases and ions transport into consideration [50–52]. Some of the adopted analytical models and the associated value of the input parameters have been suboptimal, incomplete, and/or unsuitable for the prevailing circumstances. Due to

these facts, the prediction outcomes of different models vary considerably even for concrete elements with the same mix proportions that are exposed to identical environmental conditions [13]. Though the complex scientific models yield rationally precise predictions, they lack user friendliness and require well-skilled professionals, making them appropriate only for research but not for practical applications. In practice, durability models in the form of simple analytical equations on the basis of Fick's second law of diffusion are widely applied to predict carbonation depth and chloride concentration in concrete.

Conventionally, the depth of carbonation is evaluated using a simplified version of Fick's second law of diffusion, Equation (2.6) [28,31,34,53,54]. This model obeys the square root law and is utilized to predict the depassivation time by extrapolating the carbonation depth measured at a certain time to the future.

$$x_c(t) = k\sqrt{t}, \tag{2.6}$$

where $x_c(t)$ is carbonation depth at the time t [mm], k is coefficient of carbonation [mm/year$^{0.5}$] and expressed as $\sqrt{\frac{2.D_{CO_2}(C_1-C_2)}{a}}$, where D_{CO_2} is diffusion coefficient for CO_2 through carbonated concrete [mm^2/year], C_1 is concentration of CO_2 for the surrounding environment [kg/m^3], C_2 is concentration of CO_2 at the carbonation front [kg/m^3], a is mass of CO_2 per unit volume of concrete required to carbonate all the available calcium hydroxide [kg/m^3], and t is the time of exposure to the atmosphere containing CO_2 [year].

The assumptions in Equation (2.6) are: i) diffusion coefficient for CO_2 through carbonated concrete is constant; ii) the amount of CO_2 required to neutralize alkalinity within a unit volume of concrete is invariant; and iii) CO_2 concentration varies linearly between fixed boundary values of C_1 at the external surface and C_2 at the carbonation front. To evaluate k, the carbonation depth of concrete should be determined in advance. It can be examined using concrete cores taken from existing structures or by performing an accelerated test in laboratory. Indeed, carbonation depth is often evaluated by carrying out an accelerated test using higher CO_2 concentration in a controlled environment since carbonation is a slow

process [55]. Then using the value of the laboratory measured depth of carbonation, the amount of the equivalent k and thus the depassivation time of the reinforcement bar is computed. This is a common approach even if the accelerated test may not precisely explain the natural carbonation process consistently [53]. Equation (2.6) is plausible as far as the three assumptions are fulfilled. However, the assumptions are invalid in reality. For instance, diffusion coefficient of CO_2 varies both temporally and spatially. The reason for these variability is that the diffusion of CO_2 in concrete depends on multiple factors, including concrete mix composition, curing conditions and the macro- and micro-environment to which the concrete is exposed [31,55,56]. Due to this, Equation (2.6) often fails to represent the actual condition of the concrete structures, leading to inaccurate carbonation depth prediction [28,56,57]. To minimize some of the uncertainties, analytical models which consider direct account of some of the carbonation controlling parameters have been proposed. For example, the model proposed in fib-MC2010 [58] and DuraCrete framework [59], that is given below in Equation (2.7).

$$x_c(t) = \sqrt{2\,.\,k_e\,.\,k_c\,.R_{NAC,0}^{-1}\,.\,C_a}\,.W(t).\sqrt{t}\,, \tag{2.7}$$

where $x_c(t)$ is carbonation depth at the time t [mm], t is exposure time [year], k_e is environmental function [-], k_c is execution transfer parameter [-], C_a is CO_2 concentration in the air [kg/m³], $W(t)$ is weather function [-], $R_{NAC,0}^{-1}$ is inverse effective carbonation resistance of concrete [(mm²/year)/(kg/m³)] which is determined at a certain time t_0 using the natural carbonation test.

As observed in Equation (2.7), the fib and DuraCrete model adopt Equation (2.6) by linking the carbonation coefficient with parameters of the concrete property and the environment condition. There are also other models which follow the same principle as Equation (2.7). Summarized list of those models can be found in [60]. The majority of the models incorporate limited carbonation controlling parameters. The linked parameters of these models, such as exposure condition, water-to-cement ratio (w/c), and compressive strength, have ordinarily been considered as random variables. Though air permeability of concrete relies largely on the

w/c, it is also governed by other parameters, e.g. mineral admixtures [61]. The combination of several assumptions and simplifications in the prevailing carbonation prediction models lead to a considerable uncertainty in their performance.

The chloride ion concentration in concrete is often estimated by adopting a simplified Fick's second law of diffusion based analytical formula described by Equation (2.8) [62].

$$C_x = C_i + (C_s - C_i)\left(1 - erf_{(x)}\left[\frac{x}{2\sqrt{D_{nss}t}}\right]\right), \tag{2.8}$$

where C_x is the Cl^- content measured at average depth x [m] after exposure time t [s][% by mass of concrete], C_s is the Cl^- content at the exposed surface [% by mass of concrete], C_i is the initial Cl^- content [% by mass of concrete], D_{nss} is the diffusion coefficient of Cl^- at nonsteady state [m^2/s], and $erf_{(x)}$ is the error function [-].

The foremost limitations of Equation (2.8) are [15,36,63,64]: i) the surface chloride content is invariant; ii) the nonsteady diffusion coefficient remains constant; and iii) the D_{nss} is assumed to be uninfluenced by different C_s. In real situation, C_s and D_{nss} cannot be recognized as constants. This is due to the fact that the transport properties of Cl^- depend on the amount of Cl^- concentration in the pore solution and the intrinsic permeability of the concrete. The Cl^- concentration amount varies due to the continuous chemical reaction of Cl^- with the dilute cement solution and the amount of diffused Cl^-. The concrete permeability property also varies during the cement hydration process with time. In another perspective, the change of the pore structure of concrete is governed by cement type, w/b, exposure time, type of admixtures, and exposure conditions. Due to these, both C_s and D_{nss} are temporally and spatially varying parameters [65,66]. It is also comprehended that the Cl^- is accumulated in the pore solution of concrete during chloride diffusion process. As the amount of Cl^- concentration increases, the mobility of free Cl^- slowly becomes weak, and thus lessens the magnitude of D_{nss}. This demonstrates that D_{nss} is a function of C_s and this makes the assumption (iii) in Equation (2.8) invalid. Moreover, in Equation (2.8), the error function equation takes only diffusion mechanism into consideration.

Nevertheless, the ingression of Cl^- into concrete involves a complex chemical and physical process that integrates diverse transport mechanisms besides diffusion, such as capillary sorption, and permeation. All these facts describe the reason behind the failure of Equation (2.8) to offer accurate predictions in several cases [64]. In fact, in order to undertake the time dependency of D_{nss} and the impact of other influential parameters some approaches have been suggested, e.g. fib-MC2010 [58] and DuraCrete framework [59]. Equation (2.9) is the most applied formula for estimating D_{nss}, but it also fails to eliminate the uncertainty fully because the input parameters exhibit substantial scatter.

$$D_{nss}(t) = k_e.\ k_t.\ k_c\ .D_0.\left(\frac{t_0}{t}\right)^n, \tag{2.9}$$

where k_e is environmental function [-], k_t is test method function [-], k_c is curing function [-], D_0 is experimentally determined chloride diffusion coefficient at time t_0 [m^2/s], t_0 is age of concrete at D_0 is measured [year], t is the exposure duration [year], and n is the age factor describing the time dependency of the diffusion coefficient [-].

The age factor in Equation (2.9) explains the time dependency of the diffusion coefficient based on the concrete mix composition. The magnitude of the age factor is often determined based on different concrete specimens subjected to various environments for relatively short period of time and reveals significant scatter. Several studies demonstrated that the age factor is the most sensitive parameter in Equation (2.9) [14,36,67,68]. A minimal change in its magnitude leads to a considerable uncertainty in the prediction of chloride concentration. The combination of all the above discussed assumptions causes considerable uncertainty in the prediction of Cl^- concentration in concrete which ultimately affects estimation of the time to onset corrosion of reinforcement bar or evaluation of the service life of the structure [15,69].

As elaborated above, the ingression rate of the aggressive substances (CO_2 and Cl^-) into the concrete pores is predominantly a function of concrete properties and environmental circumstances. In a given structure, the penetration rate of these substances cannot be constant and even they may alter in various parts of the structure. The presented

corrosion assessment methods in the form of analytical equations are no better than their underlying conceptual base. So, the estimation of corrosion onset utilizing Fick's law based analytical models is uncertain. In addition, the rapidly increasing use of combinations of supplementary cementitious materials and new technologies are another factors which make the traditional models incapable to precisely evaluate the corrosion initiation time [69–72]. Hence, developing novel methods that estimate the carbonation depth and chloride profile accurately are crucial to mitigate premature failure of RC structures caused by corrosion of reinforcement bar and the related costs.

The complexity of several interacting parameters which control the initiation of corrosion of reinforcement bar in concrete calls for researchers to question *how to eliminate or mitigate the uncertainties observed in the traditional corrosion assessment methods?* This is one of the research questions of this dissertation, research question one. Indeed, the oversimplified corrosion assessment methods can be integrated with a semi-probabilistic uncertainty model to enhance the accuracy as in the DuraCrete framework. Nonetheless, this approach cannot eliminate the associated uncertainty completely. Uncertainties can be mitigated by utilizing readily available long-term data or gathering more and more relevant data, and then modelling it using machine learning methods. Such data-driven models estimate without assumptions by mapping the variables of the input to the output that closely approximate the target instances. They do also have the ability of extracting useful knowledge from the data, thus contributing to a better understanding of the complex and nonlinear interaction of multiple parameters. Fortunately, there are readily available long-term field data obtained from real structures and specimens made with several mix compositions exposed to carbonation and chloride environment. The increment of the availability of more and more field data exposed to different exposure conditions is evident since nowadays real-time monitoring of several corrosion controlling parameters in concrete structure is achievable.

In another perspective, the broadly utilized Fick's law based carbonation depth and chloride profile prediction models rely on limited number of parameters. Certainly, exploration of CO_2 and Cl^- transport in concrete is conducted for several years to acquire a better understanding of the

influential predictors. In order to recognize the effect of different parameters, a large number of experiments must be carried out since the concrete microstructure is immensely complex and its transport properties are controlled by several interacting factors. However, it is generally challenging to isolate the effects of particular parameters since other governing parameters also vary naturally at the same time [16,17]. Hence, determining parameters that characterize the carbonation process and the chloride penetration in concrete as well as their interdependency is crucial in order to develop parsimonious and precise model. But identifying the significance of the parameters using the traditional statistical methods is impossible since the carbonation process and the chloride penetration in concrete is a complicated process governed by several nonlinear factors. All the limitations presented above can be mitigated by adopting various types of machine learning methods since they are capable of handling highly nonlinear variables with multiple interactions.

Unlike carbonation and chloride penetration assessment, hygrothermal transport phenomena through concrete are well understood and numerical models that can be used in practice have already been developed. A comprehensive review of hygrothermal simulation models is presented in [22]. Although hygrothermal prediction models for concrete are available, it is challenging to include the ever increasing of surface-protection material types and their application techniques in the models' library. It is a known fact that numerical models can yield accurate predictions of any process if and only if the actual material properties are well studied and utilized. In addition, hygrothermal interaction in surface-protected concrete elements involves multiple temporally varying complex interactions. Such a complex problem needs an approach where the most important features with the involved multiple interactions are modelled so that the behaviour of the system could be reasonably predicted. These features can be gathered through long-term in-service monitoring using appropriate sensors and predicting the hygrothermal behaviour from the gathered data using machine learning techniques is an attractive alternative. Furthermore, the gathered and the predicted data, with the help of exploratory data analysis technique, could assist to evaluate the performance of the applied protection materials while obtaining valid information regarding the real hygrothermal behaviour of the concrete.

2.4 Machine learning

Machine learning is a major subfield of artificial intelligence that deals with the design and implementation of algorithms to recognize complex patterns from data and make intelligent decisions [73–81]. Machine learning based models can be predictive to carryout prediction or descriptive to discover knowledge from data, or both without assuming a predetermined equation as a model [77,82,83]. Even if machine learning grew out of the quest for artificial intelligence, its scope and potential are more generic. It draws upon ideas from a diverse set of disciplines, including Probability and Statistics, Information Theory, Psychology and Neurobiology, Computational Complexity, Control Theory and Philosophy [80].

The design process of a machine learning model involves a number of choices, including the learning types, the target performance function to be learned, a representation of the target function and an algorithm (a sequence of instructions used for learning the target function). Based on the training conditions, machine learning is classified as supervised, unsupervised, semi-supervised and reinforcement learning [77,84]. The supervised and unsupervised learning are the most commonly implemented learning types in several area of applications [83].

Supervised learning: in this learning type, the training dataset comprises pairs of N input instance x and a desired output (target) value y: $\{x_i, y_i\}_{i=1}^{N}$. A supervised learning algorithm analyses the training data and generates an inferred function, which can be applied for mapping new instances. A best scenario will allow the algorithm to accurately estimate the target for unseen input instances. The process of learning from the training dataset can be thought of as a teacher supervising the learning process, hence the name *supervised learning*. The algorithm iteratively performs predictions on the training data and is rectified by the teacher. The learning process halts when the algorithm attains an acceptable performance level. Based on the nature of the target variable, supervised learning problem is categorized into two: *classification* and *regression*. Supervised learning problems where the target variable is defined as a finite set of discrete values are called *classification* whereas those in which the value of the target variable is continuous are referred to as *regression*.

Unsupervised learning: in this learning type, the training dataset consists of only N input instances $\{x_i\}_{i=1}^{N}$ and no corresponding target values. The goal of unsupervised learning is inferring a function to describe hidden structure from the unlabelled data. The most common unsupervised learning problem is clustering where the goal is to partition the training instances into subsets (clusters) so that the data in each cluster display a high level of proximity. Unlike supervised learning, there is no a teacher providing supervision as to how the instances should be handled. Also, there is no evaluation of the correctness of the structure that is output provided by the adopted relevant algorithm.

In order to perform predictions and/or discover new useful knowledge from data using machine learning methods, an algorithm that is capable of learning the target function from training data is required. The algorithms in machine learning implement different types of methods from various fields, such as, pattern recognition, data mining, statistics, and signal processing. This allows machine learning to undertake the synergy benefits from all these disciplines, and thus results in robust solutions that integrates various knowledge domains [81]. Some of the commonly adopted powerful algorithms that have been applied in supervised and unsupervised learning types are demonstrated in Figure 2.3. It can be observed that some algorithms operate under both supervised and unsupervised learning types to solve several diverse problems.

Supervised learning type is the focus of this dissertation since the research questions two, three and four deal with regression problems. Typically, regression types of problems are handled by developing a functional model which is the best predictor of y given input x employing a particular training data $D = \{y_i, x_i\}_1^N$ as expressed in Equation (2.10).

$$y = \hat{F}(x_1, x_2, \dots, x_n) = \hat{F}(X), \tag{2.10}$$

where y_i is the output variable, x_i is the input vector made of all the variable values for the i^{th} observation, n is the number of variables, and N is the number of instances.

A typical roadmap for building machine learning models is illustrated in Figure 2.4. It consists of the following three major steps:

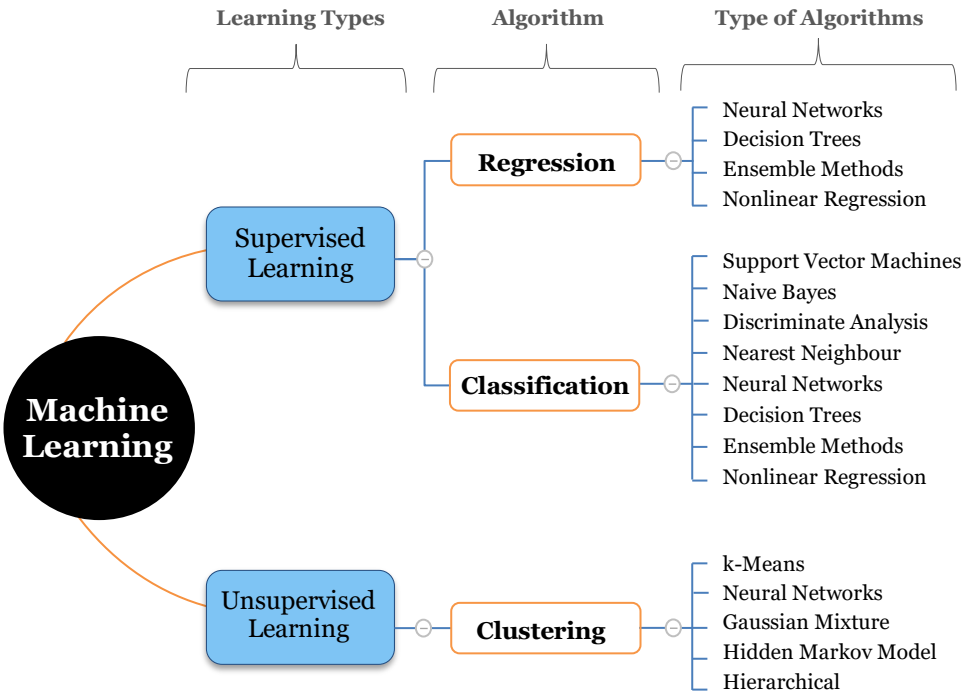

Figure 2.3. Commonly adopted machine learning algorithms (Publication I).

1. *Data preprocessing*: this step is the most critical one in machine learning applications since raw data usually comes in the form that is unsuited for the optimal performance of a learning algorithm. Due to this, the first step in data preprocessing activity is data cleaning. This activity includes replacing missed data, removing outliers, and smoothing noisy data. Data cleaning is often followed by integration of multiple data sources and data transformation to a specific range (normalization) and dimension reduction for optimal performance. Removing redundant features by compressing the features onto a lower dimensional subspace while holding most of the relevant information is also essential to make the learning process faster. In addition, in data preprocessing phase, the data is randomly divided into training and test set. The training set is applied to train and optimize the machine learning model, while the test set is used to assess the performance of the final model.

2. *Training and selecting a predictive model:* as presented earlier, there are a wide range of machine learning algorithms that have been developed to solve different problems. Each algorithm has different feature and the choice mainly depends on the types of the problem to be resolved and the available data. So, in this phase, at least a handful of different algorithms shall be trained in order to select the best performing one (a model that fitted well on the training dataset). The most commonly performance evaluating metric is the mean-square error (the mean of the squared difference between the target and its predicted value).
3. *Evaluating models and predicting unseen data instances:* the last step is dedicated to model assessment. The main issue that machine learning models face is how well they model the underlying data. The model can be too specific if it memorized the

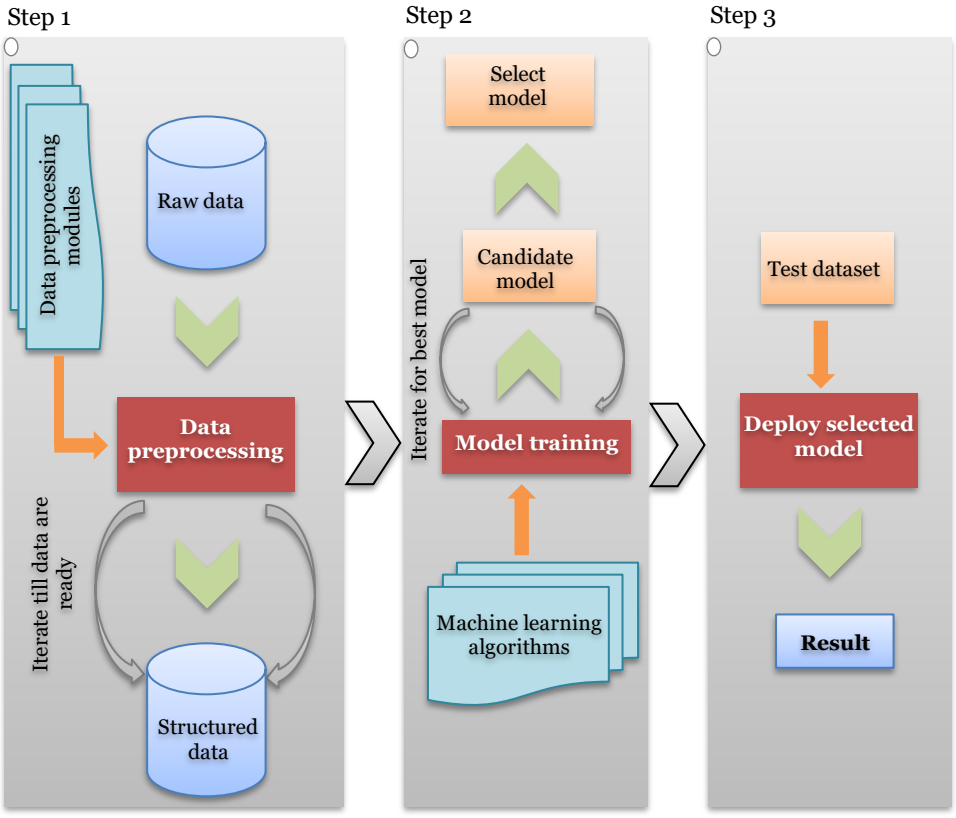

Figure 2.4. The fundamental steps of a typical machine learning workflow.

training dataset and unable to generalize to unseen examples. This means that the model *overfits* the data employed for training. The model can also be too generic if it is incapable to capture the relationship between the input instances and the target values. In another word, it *underfits* the training data. Both *overfitted and underfitted* models are useless for making valid predictions. Hence, the purpose of this step is to evaluate how well the model has generalized to new (unseen) data. To do so, the test dataset is applied. If the model performs well in the test data, it can be applied to predict new future data since it generalized the training dataset.

Machine learning is one of the most significant technological developments in recent history. There are a wide spectrum of successful practical applications of machine learning in different domains, such as, computational finance [85–87], image and speech processing [88–90], property valuation [91–93], computational biology [94–96], and energy production [97–99]. Although employing machine learning is becoming a regular practice in diverse engineering fields, its application for assessing durability of concrete is yet limited.

In this dissertation, supervised learning type is employed since estimation of carbonation depth, chloride ingress and hygrothermal performance are regression problems and the input and the target data are known in the training dataset. The adopted learning algorithms are neural network, decision tree, and boosted and bagged ensemble methods. The fundamental principles of these algorithms are discussed as follows.

2.4.1 Neural network

Neural network is a computational network inspired by biological neural networks which comprises partially or fully interconnected simple processing units called artificial neurons [100–102]. Each neuron processes data locally using similar concepts as learning in the brain. Neural network is ideal for supervised learning since the connections within the network can be systematically adjusted based on inputs and outputs. They are usually categorized based on their architecture (pattern of connections between the neurons) and the architecture is intimately

connected with the learning algorithm utilized to train the network. The common classification are: single-layer feedforward, multilayer feedforward, and recurrent networks [100]. Multilayer feedforward and recurrent networks were adopted in Publications II and IV to solve the research questions two and four, respectively. In this section, only the details of the utilized types of neural networks are discussed.

Multilayer feedforward architecture along with backpropagation training technique is broadly employed to solve complex nonlinear regression problems [103–106] and this approach is adopted in Publication II of the dissertation. This architecture often has three or more layers: input, hidden, and output layers. Figure 2.5 shows the architecture of a multilayer feedforward neural network (multilayer perceptron) with a single hidden layer. The first and the last layers are known as input and output layers, respectively. The intermediate layer is called hidden layer which assists to execute the necessary computations before conveying the input data to the output layer. This network can be seen as a nonlinear parametric function from a set of inputs, x_i , to a set of outputs, y_m. First, linear combinations of the weighted inputs are formed. This includes the additional external inputs provided to the network, which is known as bias, the neurons represented by blue colour in Figure 2.5. Biases have no effect on the performance of the network, but they increase the flexibility of the network

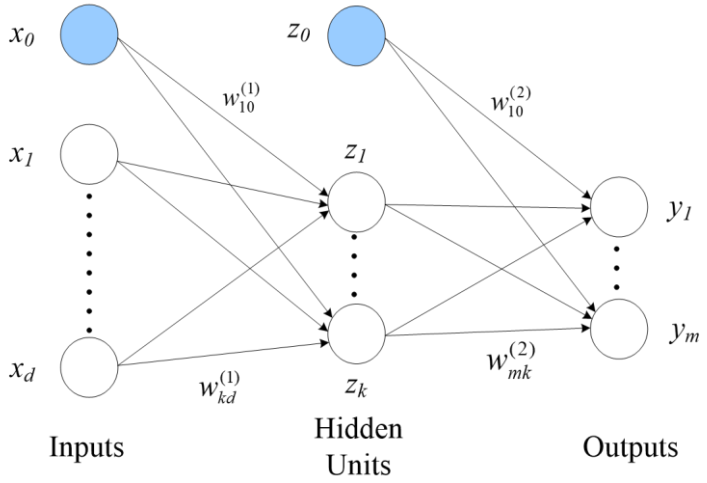

Figure 2.5. A multilayer feedforward neural network with a single hidden layer (Publication II).

to fit the data. After linear combinations, they are translated to new values using an activation function $\varphi(.)$, Equation (2.11) [105–107]. Then, the outputs of the first-hidden layer neurons are multiplied by the interconnection weights of the layer that connect them to neurons of the next layer as expressed by Equation (2.12). If the network has multiple hidden neurons, this activity continues until the output neurons compute the values of the output.

$$z_j = \varphi\left(\sum_i w_{ji}^{(1)} x_i\right), \tag{2.11}$$

$$y_m = \sum_j w_{mj}^{(2)} z_j, \tag{2.12}$$

where $w_{ji}^{(1)}$ and $w_{mj}^{(2)}$ are the weights of the network which are initially set to random values, and then adjusted during training by backpropagation using the response data.

The purpose of the activation function is to control the amplitude of the output of a neuron in terms of the induced local field v and break the linearity of a neural network, allowing it to learn more complex functions. Depending on the characteristics of the problems, various forms of activation functions can be defined [107]. The common ones are *linear*, *logistic* and *hyperbolic tangent* activation functions, which are expressed by Equations (2.13) to (2.15) and illustrated in Figure 2.6. The vertical and the horizontal axes represent the unit's output and its input, respectively. It can be noticed that the *hyperbolic tangent* function has the same form

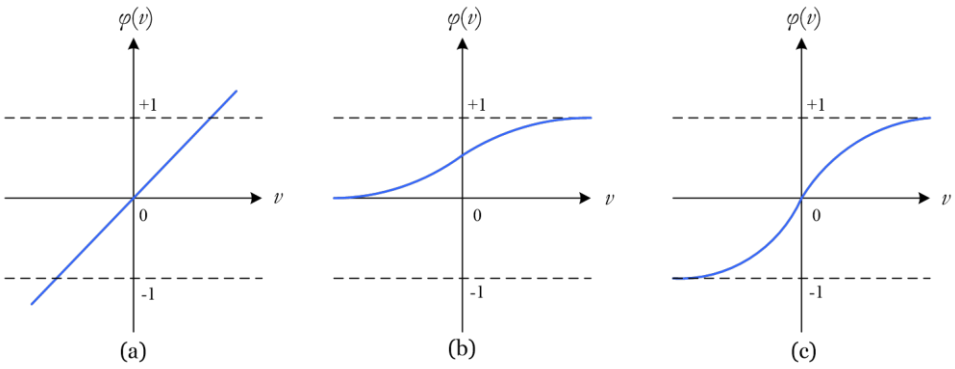

Figure 2.6. Activation functions (a) linear, (b) logistic, and (c) hyperbolic tangent.

as the *logistic*. However, the function *hyperbolic tangent* covers the range from [-1 1] whereas the *logistic* function covers from [0 1]. The *linear* function simply outputs a value proportional to the summed inputs. To build nonlinear models, the activation function of the network must be nonlinear and a single type of activation function is applied for neurons in the same layer.

Linear function: $$\varphi(v) = v. \quad (2.13)$$

Logistic function: $$\varphi(v) = \frac{1}{1+e^{-av}}. \quad (2.14)$$

Hyperbolic tangent function: $$(v) = \frac{e^{2v}-1}{e^{2v}+1}. \quad (2.15)$$

Recurrent neural network differentiates itself from a feedforward neural network by having arbitrary feedback connections, including neurons with self-feedback [100]. Self-feedback refers to a circumstance where the output of a neuron is fed back into its own input. The architectural layout of recurrent network takes many different forms depending on the kinds of time-series problems. The adopted subclass of recurrent network in Publication IV is called nonlinear autoregressive with exogenous inputs (NARX). It is one of the popular network and has high capability in capturing long-term dependencies since it uses the feedback derived from the output at explicit time lags as part of the input data [100,101]. The general architecture of the NARX network is illustrated in Figure 2.7. The network has a single input that is applied to a tapped-delay-line memory of q units. It has a unique output that is fed back to the input through another tapped-delay-line memory also of q units. The values of these two tapped-delay-line memories are utilized to feed the input layer of the multilayer perceptron. The present input value of the network is represented by $u(n)$, and the respective output value of the network is expressed by $\hat{y}(n+1)$. This mean that the output is ahead of the fed-back input by one-time unit. So, the data window supplied to the input layer of the multilayer perceptron can be denoted as follows:

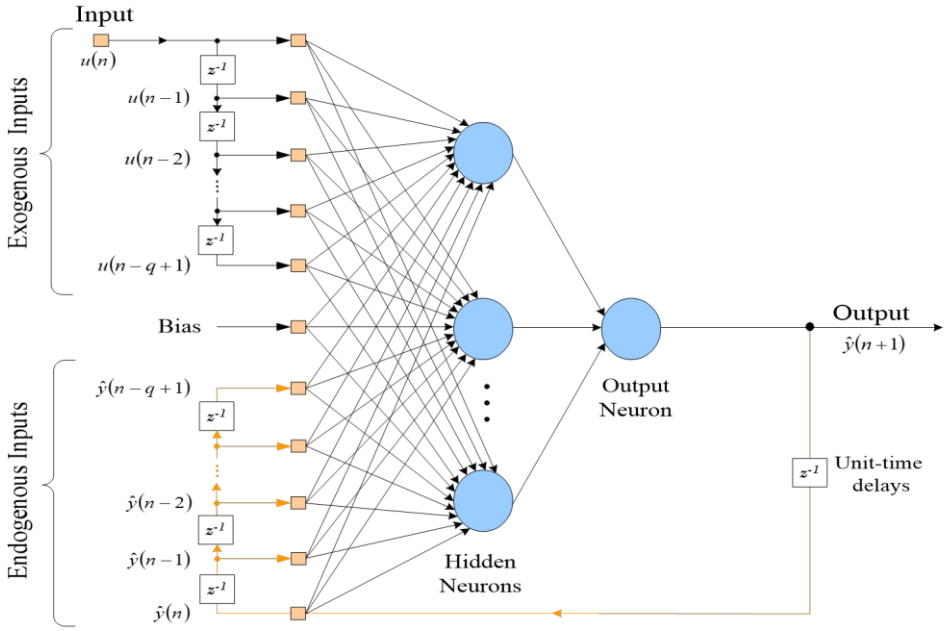

Figure 2.7. NARX network with ***q*** delayed inputs (Publication IV).

- Present and past input values, $u(n)$, $u(n-1)$,..., $u(n-q+1)$, which denote exogenous inputs. This input values comes from other sources (outside the network), and
- Delayed output values, $\hat{y}(n)$, $\hat{y}(n-1)$,..., $\hat{y}(n-q+1)$, on which the network output $\hat{y}(n+1)$ is regressed and represents the value of the endogenous variables.

The dynamic behaviour of the NARX network is expressed by Equation (2.16).

$$\hat{y}(n+1) = F\big(\hat{y}(n), \dots, \hat{y}(n-q+1);\ u(n), \dots, u(n-q+1)\big). \tag{2.16}$$

2.4.2 Decision tree

Decision tree is a nonparametric hierarchical data structure which implements the divide-and-conquer strategy. Decision tree model comprises nodes, branches, and leaves. Nodes correspond to domain regions that need to be decompounded into smaller regions by splitting. Leaves represent domain regions where additional splits cannot be

implemented. Branches connect to descendant nodes or leaves in proportion to specific split outcomes. Splits are determined by some relational circumstances on the basis of the selected instances that may have two or more outcomes. A split can be formally characterized by a test function $t : X \rightarrow R_t$ that maps instances into split outcomes. A separate outgoing branch is associated with each possible outcome of a node's split. The relationship between the parent node and its descendant nodes, theoretically characterized by the branches linking the former to the latter, does not often have to be unambiguously delineated in the data structure of the decision tree. If a split's outcome can be explicitly ascertained for any attainable instance, then it does partition the domain into disjoint subsets, in proportion to the outgoing branches. Hence, it is easy to realize that each node n of a decision tree complies with a region (subset) of the domain (Equation 2.17) determined by the sequence of splits $t_1, t_2, \dots, t_k$ and their outcomes $r_1, r_2, \dots, r_k$ occurring on the path from the root to the node [108].

$$X_n = \{x \in X | t_1(x) = r_1 \wedge t_2(x) = r_2 \wedge \cdots \wedge t_k(x) = r_k\}. \quad (2.17)$$

Decision tree is fast learner with high degree of interpretability and handles complex nonlinear problems with a large number of observations and input variables by reducing them into manageable levels and recursively applies the same approach to the sub problems [109–111]. The power of this procedure arises from the potential to divide the instance space into subspaces and each subspace is fitted with varied models [77,110]. A decision tree that is applied for examining regression problems can be referred as a regression tree. The basic structure of a regression tree is shown in Figure 2.8. The left subfigure denotes the data points and their partitions while the right subfigure illustrates structure of the corresponding regression tree. As it can be observed from Figure 2.8, regression tree is composed of decision and leaf nodes. A test function is applied at each decision node and the branches are labelled with discrete outcomes of the function. This test procedure starts at the root and recursively carried out until leaf nodes are found. The value at the leaf node is the output [77]. Regression tree is one of the integrated learning

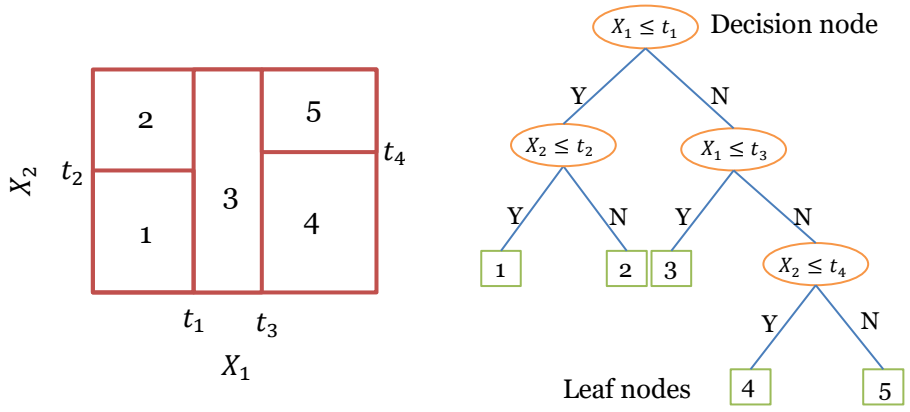

Figure 2.8. Example of a dataset and its corresponding regression tree (Publication III).

algorithms that are developed in Publication II to predict carbonation depth.

2.4.3 Ensemble method

The idea of an ensemble method is to build a powerful predictive model by aggregating multiple machine learning models, each of which solves the same original task [76,77,109,112,113]. Normally, generating multiple models utilizing different datasets without integrating them into an ensemble and directly choosing one of them that performs best does not deliver a functional solution. Ensemble methods are applicable to the two foremost predictive modelling tasks, classification and regression. In both cases, ensemble method provides significant improvement over a single model at the expense of investing more computation time due to building multiple models. To utilize this potential for superior predictive power, suitable techniques for building of base models (models used as inputs for ensemble methods) and aggregation are needed [108]. The base models often generated using machine learning algorithms. Model aggregation comprises integration of base models $m_1, m_2, \dots, m_k$ into an ensemble model $\acute{M}$ by building a prediction combination strategy that compute $\acute{M}(x)$ based on $m_1(x), m_2(x), \dots, m_k(x)$ for arbitrary $x \in X$. The amalgamated model $\acute{M}$ is represented by all of its base models and the strategy applied

for integrating their predictions. Depending on the types of base models as well as the applied integration methods, various ensemble methods can be formed.

Though there are several ensemble models in the machine learning literature, there are two models that use decision tree learners as a base model and have proven to be effective on solving regression problems for a wide range of datasets. These ensemble models are: bagging and boosting decision trees [76,90,108]. Both types of models are integrated in the developed carbonation depth prediction model presented in Publication II of the dissertation. Boosting decision tree is adopted in Publication III to answer the research question three.

Bagging decision tree

In bagging decision tree, the base models are created using the training datasets. Multiple randomly drawn bootstrapped samples from the original data form the training datasets. This procedure is performed a number of times until a large subset of training datasets are formed and the same samples can be extracted more than once. On average, every formed bootstrapped training dataset hold $N\left(1-\frac{1}{e}\right) \approx 0.63N$ instances, where N is the total number of samples in the original training dataset. The left-out instances in the training dataset are known as out-of-bag observations. The final output of the bagging ensemble model is the average of the projected output of the individual base models, thereby reducing its variance (tendency to learn random things) and provide higher stability [77,90,109,114]. The performance of the ensemble model is evaluated using the out-of-bag observations. In bagging decision tree, the base model fits the training data $D = \{(x_1, y_1), (x_2, y_2), \dots, (x_N, y_N)\}$, obtaining the tree's prediction $\hat{f}(x)$ at input vector x. Bagging averages this prediction over a wide array of bootstrap samples. For each bootstrap sample $D^{*t}, t = 1,2, \dots, T$, the model provides prediction $\hat{f}^{*t}(x)$. The bagged estimate is the mean prediction at x from T trees as described by Equation (2.18).

$$\hat{f}_{bag}(x) = \frac{1}{T}\sum_{t=1}^{T} \hat{f}^{*t}(x). \tag{2.18}$$

Bagging decision tree, with several base models, provides better prediction over a single model. Unlike the base models, overfitting will not occur in this ensemble method since the integration of the base models cancel it out effectively. Bagging decision tree often builds deep trees. Due to this bagging decision tree is time consuming and memory intensive, which in turn leads to slow predictions.

Boosting decision tree

Boosting can be described as an improvement of bagging that comprises multiple base models by shifting the focus toward instances that experience difficulty in prediction [90,108,114]. The shift of focus is mainly addressed by instance weighting. In contrast to bagging, boosting decision tree build simple tree models in a serial manner with advancement from one tree model to the other and combining them to boost the model accuracy. Each tree is grown from a training dataset $D = \{(x_1, y_1), (x_2, y_2), \dots, (x_N, y_N)\}$, using information from previously grown trees. A relevant algorithm can be applied to fit the sample training datasets $D^{(t)}, t = 1,2, \dots, T$, utilizing a sequence of varying weights $w^{(1)}, w^{(2)}, \dots, w^{(T)}$, yielding the tree's predictions $\hat{f}^{(1)}(x), \hat{f}^{(2)}(x), \dots, \hat{f}^{(T)}(x)$ for each input vector x and their corresponding weight vector w. The weight vector is normally started by applying an initial weight $w^{(1)}$ and continually adjusted in every generated base model depending on observed residuals. The weight is increased for observations in which the base model yields high residuals (poor predictions) and decreased for cases in which the model provides low residuals (good predictions). The output of the boosted decision tree can be expressed by Equation (2.19), where $\{\propto_t\}_{t=1}^{T}$ are the linear combination coefficients.

$$\hat{f}_{boost}(x) = \sum_{t=1}^{T} \propto_t \hat{f}^{(t)}(x). \tag{2.19}$$

Various types of strategies for adjustment instance weight and model weighting can be applied to create boosting ensemble method. For instance, it is possible to apply residuals of previous models as target function values for generation of subsequent base model rather than instance weighting. This allows the regression algorithm to counteract

limitation of the previous models instead of optimizing its training performance.

In boosting decision tree, each tree model can only deliver reasonably good predictions on some instances, and therefore more and more trees are built to enhance the performance iteratively. Unlike bagging, boosted ensemble models utilize shallow trees which make them usually smaller in terms of memory, and making prediction faster.

2.5 Machine learning based variable importance measure

Variable importance measure allows insight into the importance of the variables employed in the training dataset. Generally, there are three major categories of variable selection methods: filter, wrapper and embedded [111,115]. Filter methods are independent of the learning algorithms and relies only on the intrinsic characteristic of the data. These methods, compared to wrapper methods, are less computationally intensive. Wrapper methods demand a prespecified learning algorithm and based on the selected algorithm the performance of each variable is used as the measure for determining the final subset of variables. These methods are computationally intensive but yield better accuracy compared to filter methods. Embedded methods include the process of variable selection as part of the model development process. These methods combine the advantages of the filter and the wrapper methods, in terms of low computational costs and an adequate accuracy.

The ensemble methods (bagging and boosting decision trees) discussed above can perform an embedded variable selection. Both bagging and boosting decision trees are applied in Publication II. Both models were used to evaluate the importance of the input variables in predicting the carbonation depth. Ensemble method based on bagging decision tree is also implemented in Publication III in order to examine the importance of variables that describe the chloride penetration into concrete.

Variable importance measure based on permutation is one of the advanced and reliable embedded selection methods. As the name indicated, the variable importance (VI) measure based on this method is obtained by randomly permute the j^{th} predictor variable x_j (on each

decision tree in the ensemble) with some permutation φ_j among the training dataset. Then evaluate the out-of-bag error on this perturbed dataset. The importance score for the j^{th} variable is computed by averaging the difference in out-of-bag error before and after the permutation over all the trees. The score is normalized by the standard deviation of these differences. Variables which induce large values for this score are ranked as more critical than variables which generate small values. This process is expressed mathematically in Equations (2.20) to (2.22) [116].

Let $\bar{\beta}^{(t)}$ be the out-of-bag instance for a tree t, with $t \in \{1, 2, \dots, T\}$. Then the importance of variable x_j in tree t is described by Equation (2.20).

$$VI^{(t)}(x_j) = \frac{\sum_{i \epsilon \bar{\beta}^{(t)}} I\left(y_i = \hat{y}_i^{(t)}\right)}{|\bar{\beta}^{(t)}|} - \frac{\sum_{i \epsilon \bar{\beta}^{(t)}} I\left(y_i = \hat{y}_{i,\varphi_j}^{(t)}\right)}{|\bar{\beta}^{(t)}|}, \tag{2.20}$$

where $\hat{y}_i^{(t)} = f^{(t)}(x_i)$ and $\hat{y}_{i,\varphi_j}^{(t)} = f^{(t)}\left(x_{i,\varphi_j}\right)$ is predicted value for i^{th} instance before and after permuting its value of variable x_j, respectively. By definition, $VI^{(t)}(x_j) = 0$, if variable x_j is not in tree t.

The measure of variable importance for each variable is determined as the average importance over all the trees, Equation (2.21).

$$VI(x_j) = \frac{\sum_{t=1}^{T} VI^{(t)}(x_j)}{T}. \tag{2.21}$$

The standardized variable importance is evaluated by applying Equation (2.22). As expressed in Equation (2.22), the individual importance measures $VI^{(t)}(x_j)$ are computed from T samples which are extracted from the original dataset. Thus, if every individual measure of variable importance $VI^{(t)}(x_j)$ has standard deviation σ, the average importance measure from T replications has standard error $\sigma/\sqrt{T}$.

$$\widetilde{VI}(x_j) = \frac{VI(x_j)}{\frac{\sigma}{\sqrt{T}}}. \tag{2.22}$$

Permutation based variable importance measure is applied in this dissertation to answer the research question three. Another technique has also been applied to evaluate the importance of variables in predicting the

carbonation depth in order to answer second part of the research question two. This is due to the fact that variable importance measure based on permutation is impracticable for boosting decision tree, which is one of the ensemble methods employed in answering research question two. Details of the implemented method for measuring variable importance in case of boosting decision tree are presented in Section 3.4.4.

Chapter 3

Materials and methods

In this chapter, the utilized materials and the developed methods for assessing corrosion causing and controlling factors are discussed. The materials used in Publications II, III, and IV are presented since Publication I is based on a thorough literature review. In Publication I, materials from secondary sources, which include books, conference, and journal articles are used. The purpose of this publication is to examine the capability of machine learning methods in addressing the limitations of classical corrosion assessment models. As the focus of this dissertation is on data-driven corrosion assessment methods, the materials for Publications II, III, and IV are experimental data obtained from three different case structures.

All the methods developed in this dissertation rely on machine learning approach and implemented using MATLAB programming language. All the proposed methods to answer the research questions two, three and four of the dissertation are discussed in detail. The methods are utilized for developing data-driven models to assess corrosion causing and aggravating factors. The assessment includes predictions of carbonation depth, chloride profile and hygrothermal performance. In addition, the methods are used to discover influential predictors of carbonation depth and chloride concentration. As any data-driven models, the development process of these models primarily consists of data, data preprocessing and training. The experimental data and all the involved activities associated with model development process are presented in this chapter.

3.1 Concrete specimens for carbonation field test

The experimental data for carbonation study were obtained from concrete specimens that were prepared for Finnish DuraInt-project. The specimens have diverse mix compositions that represent the current prevalent industrial concrete mixes in Finland. This project was carried out jointly

by Aalto University and VTT Technical Research Centre of Finland. The data were based on 23 concrete specimens. All the specimens were casted in steel moulds of size 100 x 100 x 500 mm^3 and demoulded after 24 hours. Then they were immersed into water for seven days and cured in a controlled environment (21 °C temperature and 60% relative humidity). The specimens were sheltered and kept on wooden racks at about the age of 28 days in Espoo, southern Finland in order to simulate as sheltered concrete structures that are exposed to natural conditions (exposure class, XC3 (moderate humidity) as shown in Figure 3.1. The annual average CO_2 concentration, temperature, and relative humidity at the storage of specimens are 375 ppm, 6 °C and 79%, respectively.

The carbonation front depths of the concrete specimens, from all sides, in a freshly broken surface of 100 x 100 mm^2 were measured at the age of 268, 770, 1825 and 2585 days. The carbonation depths were examined by spraying a pH indicator solution of phenolphthalein. The average of the carbonation depths measured from the four sides of each concrete specimen was considered as the representative value.

Accelerated carbonation tests were also carried out at the age of 28 and 56 days for the same concrete mixes. It was executed by exposing the concrete specimens to be carbonated in a climatic control test chamber

Figure 3.1. Sheltered concrete specimens for carbonation field test (Publication II).

which was filled with 1% of CO_2 and kept in a room with RH 60% and temperature 21 °C. The carbonation depths were measured by applying 1% phenolphthalein in ethanol solution. Carbonation fronts of two groups of concrete specimens after 56 days in the accelerated carbonation chamber is shown in Figure 3.2. Surface areas with a pink colour indicate the pH is above nine and are the non-carbonated part. The carbonated part of the specimens is the area where the colour of the concrete is unchanged.

3.2 Concrete specimens for chloride field test

The experimental data for chloride assessment were also acquired from concrete specimens of Finnish DuraInt-project. Though the data for both carbonation and chloride were obtained from the same project, the specimens for each case have dissimilar concrete mixes. The two cases were exposed to different field environments. Assessment of chloride penetration was performed using data acquired from concrete specimens with 18 dissimilar mix proportions. The specimens were casted in wooden moulds of size 300 x 300 x 500 mm^3 in upright position to perform chloride test in the field. Surface treatments (impregnation, form lining, copper mortar) were applied on some of the specimens of DuraInt-project

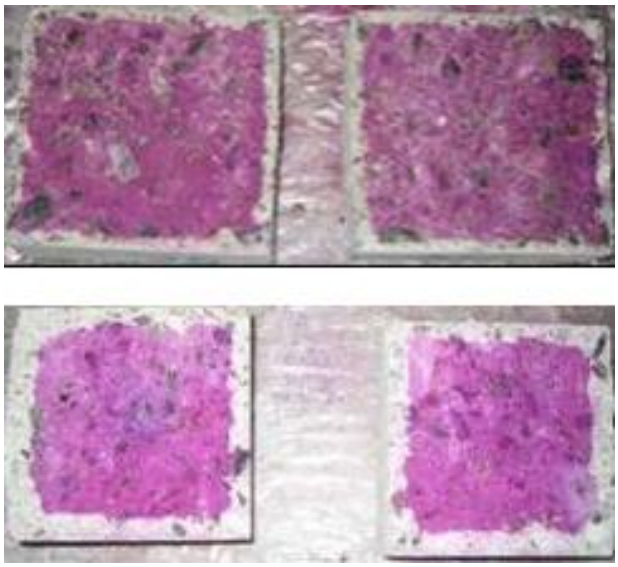

Figure 3.2. Carbonation fronts of two groups of concrete specimens after 56 days in a climatic control chamber (Publication II).

to examine their effect on chloride ingression. The concrete specimens were placed on the roadside at Kotka, Finland and Borås, Sweden. In this dissertation, the experimental data employed for chloride penetration assessment were taken from concrete specimens without surface treatment that were placed on the side of highway 7 (HW 7) at Kotka, representing exposure class XD3 (cyclic wet and dry). The reason for this is that the number of surface-treated concrete specimens with dissimilar concrete mix was few. In addition, all of them were not situated on the side of the thaw-salted road of HW 7 for long period of time. The geographical location of Kotka is illustrated in the map in Figure 3.3.

The amount of deicing salt (NaCl) that spread on HW7 from 2007 – 2013 (the considered period of experimental data) was about 0.99 kg/m^2 with an average of 102 salting instances. The daily average number of vehicles riding on HW 7 was estimated about 27,000 of which about 13% are heavy vehicles. The concrete specimens were placed in an array at a distance of 4.5 m, 6 m, 8 m, and 10 m from the HW 7 lane. All the specimens were placed on wooden stands which were installed on a gravel bed in order to avoid the probable water suction through the lower surfaces of the specimens. Field maintenance was performed in regular manner in order to assure that the surfaces of the specimens were exposed to splash water and water vapour. The chloride concentrations in concrete specimens were

Figure 3.3. Map of Finland and Kotka where the concrete specimens for chloride field tests are located (Publication III).

evaluated after one, three, and six years of exposure in the field environment. The chloride profile analyses were executed by extracting cylinder cores with size of (ø 100 mm, height >100 mm) from the concrete specimens. Dust samples were collected from the cored cylinders using a profile grinding technique at different depths. The examined depths of chloride range from 0.5 mm to 26 mm with increments of diverse orders. In addition, the nonsteady-state chloride diffusion coefficient (D_{nssm}) of all the specimens was examined by the rapid chloride migration (RCM) test in laboratory. In order to conduct this lab test, concrete cylinder specimens (three for each mix categories) with size of (ø 98 mm, height = 250 mm) were produced. The specimens were sliced at a thickness of 50 mm to form specimens size of (ø 98 mm, height = 50 mm) in accordance with NT Build 492 [117].

3.3 Case structure for hygrothermal measurement

The experimental data for hygrothermal performance assessment were gathered from a six-storey building with surface-protected prefabricated RC sandwich panels. The building was constructed in 1972 and is located in the city of Vantaa, Finland. The exterior wall of the building is sandwich-type panels where the thermal insulation lies between two RC panels. They are connected to each other by steel trusses. The finishing type of the concrete façade members were brushed and coated. The average thickness of the outermost layers of the concrete panels is 53 mm with surface area of 7.84 m^2 (2.82 m width and 2.78 m height). This type of prefabricated RC sandwich panels were, and still are, predominantly utilized in Finnish multi-storey residential buildings [19,118–120].

Previously coated six concrete façade members from the southeast side of the case building were selected for hygrothermal behaviour investigation. The old coating from the outermost layer of the façade elements was removed using sand-water blasting method. Among the designated six concrete façade members, five of them were repaired with surface-protection systems after performing all the essential surface preparations. The applied surface treatments are labelled as S1, S2, S4, S5, and S6 as illustrated in Figure 3.4. The cleaned but the uncoated façade

element is labelled as S3 and used as a reference. The surface treatments that were applied on the outermost layer of the façade elements can be categorized into two: cementitious and organic coatings. The S1 and S2 façade elements were treated with cementitious materials, whereas S4, S5, and S6 were coated with organic coating materials obtained from different Finnish companies. Cementitious coatings form a broad class that ranges from true cement-based coatings of a few to 10 mm thick. While, organic coatings form a continuous polymeric film on the concrete surface with a thickness ranging from 100 to 300 μm [11]. According to European Standard EN 1504, all the applied surface treatments in the concrete façade elements are able to limit the moisture content and to increase the concrete resistivity under rehabilitation principles P2 and P8, respectively. The types of the surface treatments applied in the five concrete façade members with the application methods are listed in Table 3.1.

The hygrothermal conditions of the ambient and inside the outermost surface-protected RC panels were measured using relative humidity/temperature probes. One probe for each concrete façade element was installed to measure the inner relative humidity and

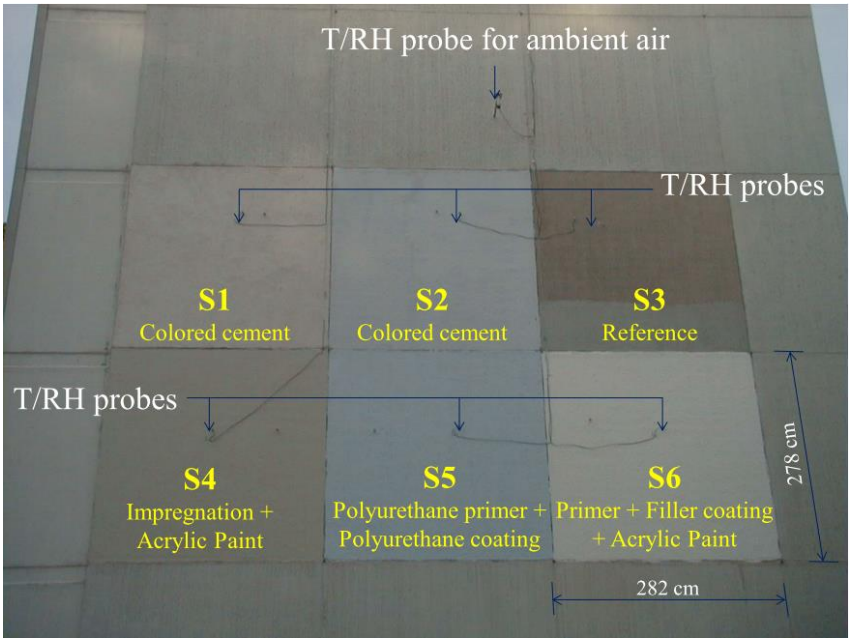

Figure 3.4. Concrete façade elements of the case structure for hygrothermal behaviour measurement (Publication IV).

Table 3.1. Concrete façade elements: treatment types and application methods (Publication IV).

Façade labels	Treatment types	Application methods
S1	Coloured cement coating	1 x trowel
S2	Coloured cement coating	2 x brush
S4	Impregnation	1 x roller
	Acrylic Paint	2 x roller
S5	Polyurethane primer	1 x brush
	Polyurethane coating	2 x brush
S6	Primer	1 x roller
	Filler coating	1 x roller
	Acrylic Paint	2 x roller

temperature, whereas one probe was mounted on the surface of a façade for ambient measurement. In order to mount the inner probes, holes were bored to a depth of about 40 mm at an approximate angle of 45° at the central area of the concrete façade members. Schematic representation of the mounted probe is illustrated in Figure 3.5. The cables of the probes were connected to a data logger to record the hygrothermal measurements. The ambient and the inner hygrothermal conditions were recorded with a regular time interval of half an hour for 719 days. Before installing the probes, they were calibrated using two-point calibration technique in

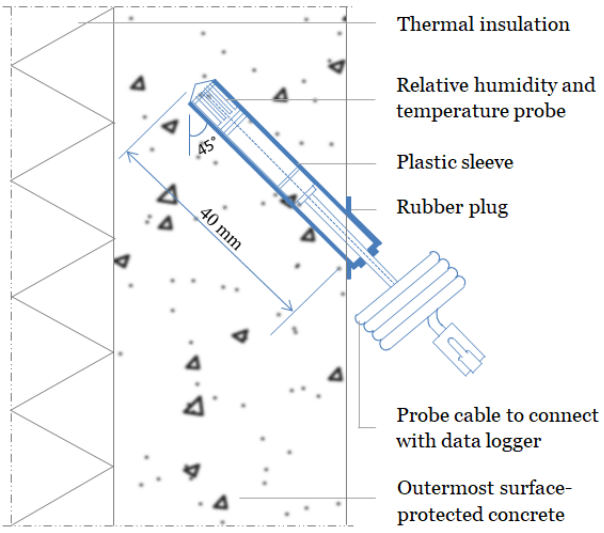

Figure 3.5. Schematic representation of the installed probe on concrete façade elements (Publication IV).

accordance with the manufacturer's guide. The same calibration technique was also followed every six months after the installation of the probes.

3.4 Model development for carbonation depth prediction

The development process of the carbonation depth prediction model, CaPrM, is presented in this section. CaPrM is designed by integrating four machine learning algorithms: neural network, decision tree, bagged and boosted decision trees. The overall CaPrM development process is shown in Figure 3.6. The initial task of the model development process is importing gathered experimental raw data that comprises parameters which describe the concrete mix ingredients, the concrete properties, the curing and field exposure conditions as well as the depth of carbonation measured at different ages. Then the execution of basic data exploration and data preprocessing follows. In any machine learning based methods, data often needs to be cleaned during preprocessing stage before they are processed further since unclean data may produce misleading results. For example, there may be incorrect or missed values in the training dataset and these values need to be rectified so that the model can analyse the data appropriately. Preprocessing phase could also include other tasks, such as data encoding and normalization.

After successful data preparation, the next stage is splitting the data into training, validation, and test subsets. The training data comprise the values of the input and the target parameters in order to learn a general rule that maps inputs to the desired output. The employed learning algorithms to train the data in the CaPrM were neural network, decision tree, bagged and boosted decision trees. These learning algorithms are commonly utilized to solve complex nonlinear regression problems efficiently, and thus making it suitable for carbonation depth prediction. The novelty of the proposed method lies in its ability to integrate the above four powerful learning methods and advanced optimization techniques. Each integrated algorithm learns from the training data and make predictions. Some of the employed machine learning methods requires the user to adjust certain controlling parameters in order to optimize their performance. The adjustment is carried out by evaluating the performance using validation dataset in case of neural network and cross-validation (subset of the

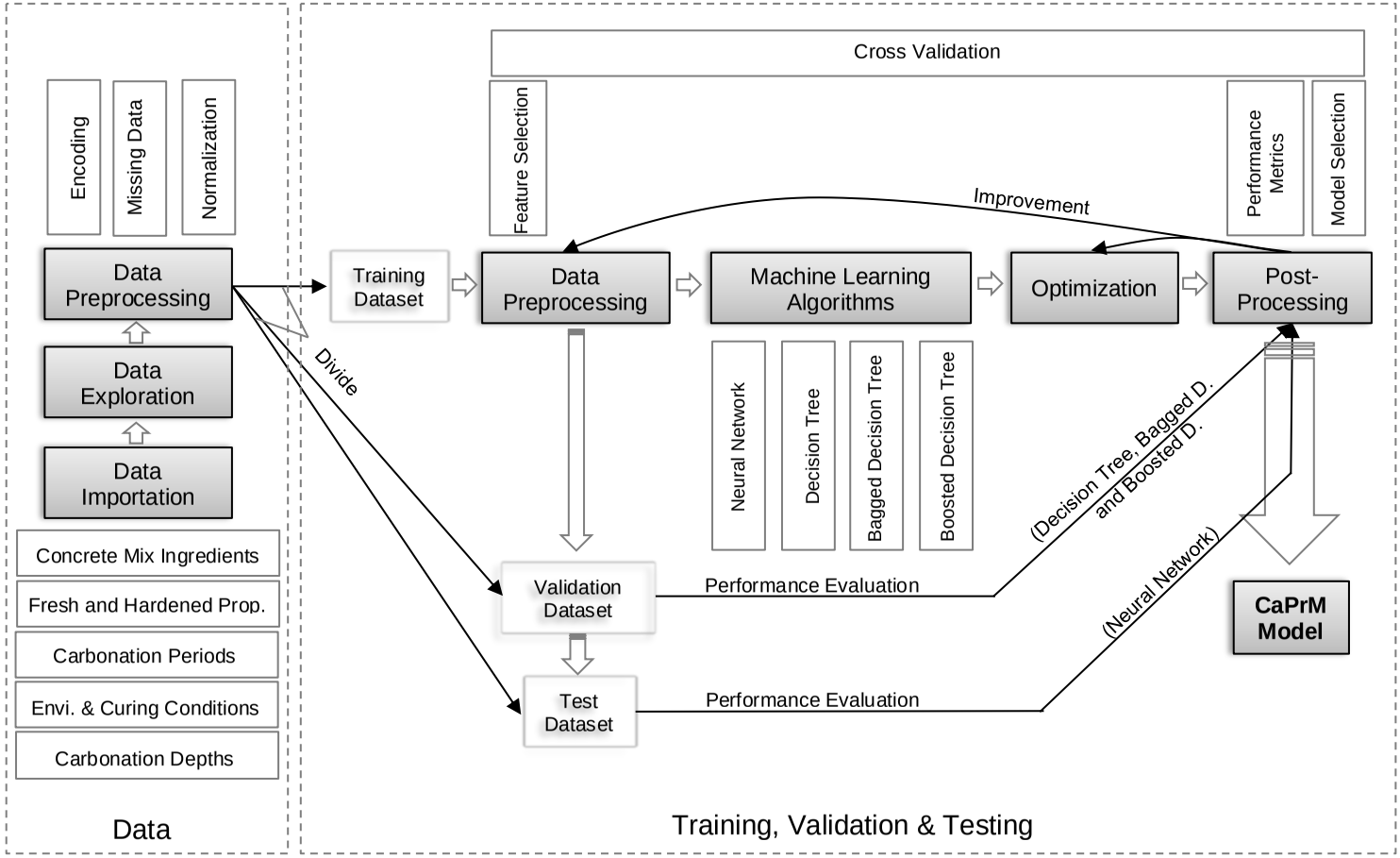

Figure 3.6. Development process of the CaPrM (Publication II).

training set) for decision tree based learning methods. After performing successful training and the necessary parameter adjustment, the prediction ability of the proposed carbonation depth prediction method is evaluated using a test dataset that are different from the training dataset. The integration of the four learning algorithms provides the opportunity to select the best performing learning methods among the four choices, by comparing the test error matrix, since there is no a single machine learning technique that performs optimal all the time. The incorporated ensemble methods enable selection of the influential carbonation predictors among the considered parameters. The major tasks involved in the development process are represented by grey coloured rectangular boxes.

3.4.1 Data for CaPrM

The experimental data employed in the CaPrM entail information regarding the concrete mix ingredients, the fresh and hardened concrete properties, the carbonation periods, the environmental and curing conditions, as well as the carbonation depths. The details of the data are given in Table 3.2. A total of six kinds of cements, based on the categorization of EN 197-1 [121], were utilized. These are Portland cement (CEM I 42,5 N-SR, CEM I 52,5 N and CEM I 52,5 R), Portland limestone cement (CEM II/A-LL 42,5 R), Portland composite cement (CEM II/A-M(S-LL) 42,5 N) and Portland slag cement (CEM II/B-S 42,5 N). Portland limestone cement (partially replaced with pulverized blast-furnace slag (BFS) or fly ash (FA)) was also utilized to produce few of the concrete specimens. The water-to-binder ratio (w/b) of the data ranges from 0.40 to 0.60. Every concrete mixture employs one type of plasticizer obtained from three producers, *VB-Parmix*, *Glenium G 51* or *Teho-Parmix*. An air-entraining agent (called either *Ilma-Parmix* or *Mischöl)* was introduced in each concrete mix type. Normally concrete admixtures are broadly classified into subcategories based on their chemical nature. Today, diverse type of plasticizers and air-entraining agents are available on the market from different sources. The performance of the chemical admixtures obtained from different sources are less uniform even if they are under the same subcategory or even with identical chemical compositions [122,123], causing difficulty to standardized them [28]. Due

to this fact, the type of plasticizers and air-entraining agents applied for producing the concrete specimens are classified based on their brand names. It can be seen from Table 3.2 that the fresh concrete properties consist of test results of slump, slump flow of self-compacting concrete and air content. Tests that define the hardened concrete properties contain compressive strength and accelerated carbonation depth. The compressive strength of the concrete specimens was performed at the age of 28 days. The accelerated carbonation depth was tested at the age of 28 and 56 days.

It can be observed from Table 3.2 that there are 26 variables representing the employed data. Parameters numbered from 1 to 25 were used as input parameters and the last parameter, natural carbonation depth, which was measured at various age was designated as a target variable. The input variables comprise continuous and nominal data types, whereas the target variable entails only continuous data type. In Table 3.2, continuous variables are represented as C and nominal data types as N. Continuous variables are real numbers, such as results of quantitative measurements. Nominal variables are non-numeric and descriptive data types.

3.4.2 Data preprocessing for CaPrM

Data preprocessing is an essential step in the development process of any machine learning based methods. It often includes data encoding, missing data processing, data normalization and data partitioning. In the CaPrM development process the following data preprocessing tasks were executed.

Data encoding

Not all machine learning methods process heterogeneous data types (continuous and nominal). For instance, decision trees support both continuous and nominal data types without any problem, but neural network lacks the ability to process nominal data types. Hence, in the CaPrM all the non-numeric variables need to be encoded as numerical variables since one of the integrated learning methods is neural network. To do this, the most commonly applied encoding technique “1-of-N” was applied. The encoded variables are listed in Table 3.3.

Table 3.2. Description of variables employed in the carbonation dataset (C: continuous and N: nominal) adopted from Publication II.

Variables category	No.	Variable subcategory	Description	Unit	Type and range	Short name
Concrete mix ingredients	1	Binder types	CEM I 42,5 N – SR	-	N:***	Cem. types
			CEM I 52,5 N	-		
			CEM I 52,5 R	-		
			CEM II/A-LL 42,5 R	-		
			CEM II/A-M(S-LL) 42,5 N	-		
			CEM II/B-S 42,5 N	-		
			CEM II/A-LL 42,5 R & blast-furnace slag			
			CEM II/A-LL 42,5 R & fly ash			
	2	Water-to-binder ratio		-	C:0.37 to 0.60	w/b
	3	Cement content		[kg/m³]	C:217.22 to 451	Cement
	4	Blast-furnace slag content		[kg/m³]	C: 0 to 217.22	BFS
	5	Fly ash content		[kg/m³]	C: 0 to 106	FA
	6	Silica fume content		[kg/m³]	C: 0 to 0	SF
	7	Total effective water		[kg/m³]	C: 153.60 to 185	Total eff. water
	8	Aggregate content	Total aggregate	[kg/m³]	C: 1706 to 1895	Total Agg.
	9		Aggregate < 0.125mm	[%]*	C: 2.40 to 6.70	Agg. <0.125mm
	10		Aggregate < 0.250mm	[%]*	C: 6.60 to 15.80	Agg. <0.250mm
	11		Aggregate < 4mm	[%]*	C: 36.30 to 53.20	Agg. <4mm
	12	Product name of plasticizers	Glenium G 51	-	N:***	Plas. pro. name
			Teho-Parmix	-		
			VB-Parmix	-		
	13	Plasticizers content		[%]**	C: 0 to 3.05	Plasticizers
	14	Product name of air-entraining agents	Ilma-Parmix	-	N:***	AEA pro. name
			Mischöl	-		
	15	Air-entraining agents content		[%]**	C: 0 to 0.06	Air-ent. agents
Fresh concrete properties	16	Basic properties	Slump value	[mm]	C: 0 to 180	Slump
	17		SCC Slump-flow/T_{50}	[mm/s]	C: 0 to 750	Slump-flow/T_{50}

	18		Air content	[%]	C: 2.60 to 7.30	Air cont.
Curing and field conditions	19	Curing conditions	uncontrolled	-	N:***	Curing cond.
			controlled	-		
			wet	-		
	20	Field conditions	Temperature	[°C]	C: 6****	Temp.
	21		Relative humidity	[%]	C: 79****	RH
	22		CO_2 concentration	[ppm]	C: 375****	CO_2 conc.
Hardened concrete properties	23	Mechanical property	Compressive strength	[MPa]	C: 32.80 to 58.50	Comp. str.
	24	Durability properties	Accelerated carbonation depth	[mm]	C: 1.58 to 7.90	Acc. carb. dep.
	25		Age of the concrete at carbonation testing	[days]	C: 268 to 2585	Carb. period
Carbonation depth	26	Natural Carbonation depth		[mm]	C: 0.10 to 6.40	Nat. carb. dep.

*compared with the total aggregate, ** compared with the total binder materials, ***described in Table 3.3, ****yearly average

Table 3.3. 1-of-N encoding for non-numeric variables of the carbonation data (Publication II).

Binder materials		Curing conditions, product names of plasticizers and air-entraining agents		
Nominal input variables	Encoded output	Nominal input variables		Encoded output
CEM I 42,5 N – SR	[10000000]	Curing cond.	Uncontrolled	[100]
CEM I 52,5 N	[01000000]		Controlled	[010]
CEM I 52,5 R	[00100000]		Wet	[001]
CEM II/A-LL 42,5 R	[00010000]	Plasticizers	Glenium G 51	[100]
CEM II/A-M(S-LL) 42,5 N	[00001000]		Teho-Parmix	[010]
CEM II/B-S 42,5 N	[00000100]		VB-Parmix	[001]
CEM II/A-LL 42,5 R & BFS	[00000010]	Air-ent. agents	Ilma-Parmix	[10]
CEM II/A-LL 42,5 R & FA	[00000001]		Mischöl	[01]

Data normalization

Normalization of the data before processing them in the neural network is a standard practice. It puts different variables on a common scale and is highly essential especially if the variables are in divergent scales. All the input and target variables are normalized using the formula presented in Equation (3.1) [124].

$$y = (y_{max} - y_{min}) * \frac{(x - x_{min})}{(x_{max} - x_{min})} + y_{min}, \quad (3.1)$$

where y is the normalized value of the variable; y_{max} is the maximum value of the normalization range, (+1); y_{min} is the minimum value of the normalization range, (-1); x is the original inputs or target variables; x_{max} is the maximum value for variable x; and x_{min} is the minimum value for variable x. If $x_{max} = x_{min}$ or if either x_{max} or x_{min} are non-finite, then $y = x$ and no change occurs. After normalization, the values of the inputs and target fall in the interval [-1, 1].

Missing data

In any data driven based models, data quality plays a vital role in controlling the performance of the model. The amount of missing data less than 1% is generally considered trivial and 1–5% is manageable. Nevertheless, 5–15% requires advanced methods to correct it and more than 15% may severely impact any kind of interpretation [125]. Fortunately, all the gathered experimental data in the CaPrM are complete, though the Finnish DuraInt-project has missing values for some of the variables.

Data partitioning

The data employed in the CaPrM (92 instances and 26 features) were divided into training, validation, and test subsets for the neural network learning algorithm. The training dataset are utilized for computing the gradient and updating the network weights and biases. The validation dataset is used to halt the training when the generalization process stops improving, and thus avoiding overfitting. The purpose of the test dataset is to evaluate the predictive performance of the developed model. The training, validation, and test dataset represented 60%, 20% and 20% of the original data, respectively. Unlike neural network, the data for the decision tree was partitioned into training and test subsets by applying *K*-fold cross-validation technique. In case of limited data, *K*-fold cross-validation method is the best alternative in order to attain an unbiased estimate of the system performance, which in turn enhance the generalization ability of the model without overfitting [77]. In *K*-fold cross-validation, the training data is arbitrarily divided into *K* subsets with roughly identical sizes. One of the *K* subsets is applied as a test dataset for evaluating the model and the remaining (*K-1*) subsets as a training dataset. In total, *K* models are fit and *K* validation statistics are obtained. The predictive accuracy evaluations from the *K*-folds are averaged to provide a measure of the overall predictive performance of the model. Algorithm 1 presents the procedure of *K*-fold cross validation. In case of bagging decision tree, the training and test subset was formed based on the embedded sampling

Algorithm 1: *K-fold cross validation*

Input: Training dataset $D = \{(x_i, y_i), i = 1, \dots, N\}$, where $y \in \mathbb{R}$

Output: Cross-validation estimate of prediction error, $CV(\hat{f})$

1: let randomly partition D to K roughly equal-sized parts

2: for the k^{th} part $k = 1, \dots, K$, fit the model to $K - 1$ parts of the training data D

3: do the above for the k^{th} part and combine the K estimates of the prediction error

Let $k: \{1, \dots, n\} \rightarrow \{1, \dots, K\}$ denote the indexing function that reveals the partition to which observation i is assigned by the randomization. Then the prediction error of the cross-validation estimate is given by:

$$CV(\hat{f}) = \frac{1}{K}\sum_{k=1}^{K} L\left(y_i, \hat{f}^{-k(i)}(x_i)\right)$$

where $\hat{f}^{-k}(x)$ denote the function fitted with the k^{th} part of the data removed.

Table 3.4. Type of algorithms, data size, and data partitioning applied in the CaPrM modelling process.

Applied algorithms	Instances	Features	Data partitioning
Neural network	92	26	60/20/20
Decision tree	92	26	10-fold cross validation
Bagging decision tree	92	26	63/37
Boosting decision tree	92	26	70/30

procedure that underline in the method as presented in Section 2.4.3. In case of boosting decision tree, the original data were partitioned into training and test subset, covering 70% and 30% respectively. Using the training dataset, decision trees were grown sequentially until optimal size of the boosting ensemble is defined by cross validation. The applied data partitioning in the CaPrM modelling process is presented in Table 3.4 along with data size and type of algorithms.

3.4.3 Training for CaPrM

The adopted training algorithm in case of neural network is the fastest backpropagation algorithm that updates weight and bias values according to Levenberg-Marquardt optimization [126]. This algorithm computes the error contribution of each neuron after a batch of training data is processed. The error computed at the output is distributed back through the network layers in order to adjust the weight of each neuron. So, the network can learn the internal representations that allow mapping of the 25 input variables to the output (carbonation depth measured at different exposure times).

The Levenberg-Marquardt algorithm was formulated to approach second-order training speed without computing the Hessian matrix [127,128]. When the performance function has the form of a sum of squares, then the Hessian matrix can be estimated and described by Equation (3.2).

$$H = J^T J. \tag{3.2}$$

The gradient can be computed and expressed by Equation (3.3).

$$g = J^T e, \tag{3.3}$$

where J is the Jacobian matrix that holds first derivatives of the network errors with respect to the weights and biases, and e is a vector of network errors.

The Levenberg–Marquardt algorithm uses this approximation to the Hessian matrix in the Newton-like update, Equation (3.4).

$$x_{k+1} = x_k - [J^T J + \mu I]^{-1} J^T e, \tag{3.4}$$

where scalar parameter μ will ensure that matrix inversion will always yield a result.

Levenberg–Marquardt algorithm is effective and firmly suggested for neural network training [127,128]. This algorithm is fast when training neural networks measured on sum-of-squared error since it is tailored for such type of functions. Indeed, for large networks, it requires a huge memory as the Hessian matrix inversion needs to be computed every time for weight updating and there may be several updates in each iteration. So, the speed gained by second-order approximation may be completely lost [128].

The fundamental architecture of the neural network model integrated in the CaPrM is identical with Figure 2.5. It has three layers: an input, a hidden and an output layer. The optimal number of neurons in the hidden layer was determined based on the generalization error after performing a number of trainings. The activation functions allocated for the hidden layer was hyperbolic tangent transfer function. This function generates outputs between -1 and 1 as the input of the neuron goes from negative to positive infinity. Linear transfer activation function was assigned to the output layer of the network since nonlinear activation function may distort the predicted output. It transfers the neuron's output by simply returning the value passed to it. The input layer did not have an activation function as their role is to transfer the inputs to the hidden layer. Detail of the applied transfer functions are presented in Section 2.4.1. The learning rate of 0.1 was applied during the model training to update the weights and biases. The updates are obtained by multiplying the learning rate with the negative gradient. The larger the learning rate is the bigger the step, and thus the algorithm becomes unstable. A learning rate that is too small require more training to converge since steps towards finding optimal parameter values which minimize the loss function are tiny. The applied

learning rate yields small generalization error with reasonable computational time.

Validation dataset is utilized to stop the network training early if its performance on this dataset fails to improve. Generally, the validation error (the error on the validation dataset) will decrease during the initial training phase. But it will typically begin to increase when the network begins to overfit the data as illustrated in Figure 3.7. When the validation error rises, the training is halted and the weights that were generated at the minimum validation error are utilized in the network. This approach usually gives the best generalization. The test dataset does not have any effect on network training, but it is used to evaluate the generalization of the network further. The training and the test performance of the network is discussed in Section 4.2. A MATLAB built-in function, `trainlm`, was applied to train the neural network part of the CaPrM using the training dataset presented in Section 3.4.1.

Decision tree is one of the integrated learning methods in the CaPrM. A MATLAB function, `fitrtree`, was applied to grow a regression tree. In a similar way presented in Section 2.4.2, this function builds a tree that yields the best prediction of the outcome for the training dataset. It partitioned the feature space into a set of rectangles recursively, and then fit a simple model in each one. This process recursively repeated until it fulfils stopping criteria. The applied function is able to grow deep decision

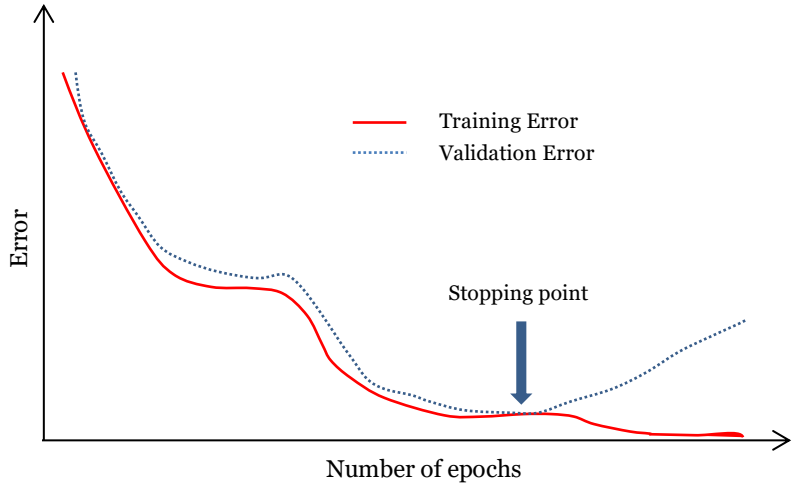

Figure 3.7. Illustration of training and validation errors as a function of epochs (training cycles).

trees by assigning the following three default values as stopping criteria: i) $N-1$ for maximal number of decision split, where N is the sample size of the training dataset, ii) one for minimum number of leaf node observations, and iii) ten for minimum number of branch node observations. The model developer can change the default values when building a regression tree in order to control its depth. In the CaPrM, the default three stopping criteria were implemented for fitting the tree using a training dataset which entails information regarding the concrete mix ingredients, the fresh and hardened concrete properties, the carbonation periods, the environmental and curing conditions, as well as the carbonation depths.

The developed decision tree was cross validated to yield accurate prediction for new dataset since this method mitigates overfitting by testing for out-of-sample performance as part of tree building. Ten-fold cross validation was applied to evaluate the tree model as it has been the most common in machine learning based modelling practices. In fact, studies show that ten is the optimal number of folds that optimizes the time it takes to finalize the test while minimizing the bias and variance associated with the validation process [129]. Ten-fold cross validation randomly partitioned the training dataset into ten parts and trains ten new trees, each one on nine parts of the data. It then tests the predictive accuracy of each new tree on the data excluded in training of the corresponding tree. The mean square of the validation error was considered to evaluate the prediction performance of the developed decision tree. The generalization ability of the model was also examined using a test (previously unseen) dataset. The overall performance of the model is presented in Section 4.2.

Bagging and boosting decision trees are the two ensemble methods that are integrated in the CaPrM. As discussed in Section 2.4.3, the fundamental principle of an ensemble method is to aggregate multiple base models in order to enhance the prediction performance of a model. A MATLAB function, `fitensemble`, was used to build both bagging and boosting decision trees. This function returns a trained ensemble tree model that comprises the results of an ensemble of multiple decision tree based models. The development procedure of the base trees for both ensemble methods is the same as of the decision tree presented above. The main differences between the two methods are on sampling of the training

dataset and the aggregation method of the trees. The pseudocode of the bagging decision tree is shown in Algorithm 2. It starts by defining the number of regression trees T to be built. It then randomly draws multiple bootstrap samples from the original training dataset to create new training datasets D^{*t} in order to build T number of regression trees. Generally, a large number of trees will result in better accuracy but making it computationally expensive. In order to identify the optimal tree size, the bagging decision tree was trained using 300 trees and its MSE was computed using the out-of-bag instances. Then the out-of-bag error was evaluated with respect to the number of trees. The optimal number of trees that yield the lowest MSE was 150 trees. Using the newly formed training dataset, the bagging decision tree built an ensemble of 150 trees for predicting carbonation depth as a function of the multidimensional input variables. The performance of the developed bagging decision tree in predicting the carbonation depth was evaluated using the test dataset. The test outcomes of the model are presented in Section 4.2.

The boosted decision tree generally learned the training dataset $D = \{(x_i, y_i), i = 1, \dots, N\}$ in sequence with improvement from one model to the next. As discussed in Section 2.4.3, there are several types of boosting ensemble methods. CaPrM adopted LSBoost (least-squares boosting) algorithm to minimize the cross-validated mean-square error of the ensemble. The applied LSBoost algorithm is summarized in Algorithm 3. It begins from the null model with residuals $r_i = y_i$ for all i in the training dataset. Then it fit a decision tree to the residuals from the model instead

Algorithm 2: *Bagging*

Input: Training dataset $D = \{(x_i, y_i), i = 1, \dots, N\}$, where $y \in \mathbb{R}$

Output: Bagged decision tree

1: let T be a total number of regression trees
2: **for** $t = 1, 2, \dots, T$ **do**
3: create bootstrap samples D^{*t} with equal number of intsances from a dataset D
4: fit a tree $\hat{f}^{*t}(x)$ to the bootstrap sample D^{*t}
5: **end for**

Output the bagged model

6: $\hat{f}_{bag}(x) = \frac{1}{T}\sum_{t=1}^{T} \hat{f}^{*t}(x)$

Algorithm 3: *LSBoost*

Input: Training dataset $D = \{(x_i, y_i), i = 1, \dots, N\}$, where $y \in \mathbb{R}$

Output: Boosted decision tree, $\hat{f}_{LS\ Boost}(x)$

1: let T be a total number of regression trees and λ is the learning rate
2: initialize $\hat{f}(x) = 0$ and $r_i = y_i$ for all i in the training data set
3: **for** $t = 1, 2, \dots, T$ **do**
4: fit a tree $\hat{f}^t$ with d splits ($d + 1$ terminal nodels) to the training data (x, r)
5: update $\hat{f}$ by adding in a shrunken version of the new tree: $\hat{f}(x) \leftarrow \hat{f}(x) + \lambda \hat{f}^t(x)$
6: update the residuals: $r_i \leftarrow r_i - \lambda \hat{f}^t(x_i)$
7: **end for**

Output the boosted model

8: $\hat{f}_{LS\ Boost}(x) = \hat{f}(x) = \sum_{t=1}^{t} \lambda \hat{f}^t(x)$

of the outcome y. Sequentially, the algorithm updates the residuals by adding the newly generated decision tree into the fitted function. Each of these trees can be small to a certain extent by controlling the parameter d in the algorithm. By fitting small trees to the residuals, the $\hat{f}$ will be slowly boosted in areas where the performance is weak. The shrinkage parameter (learning rate) λ slows down the learning process further. For a small value of λ, the iteration number needed to attain a certain training error increase. In the CaPrM, the assigned learning rate was 0.1 and the number of trees was 150. Finally, the 150 tree models are combined to form a strong ensemble model. The prediction ability of the boosted decision tree was evaluated using a test dataset. The test results are presented in detail in Chapter Four.

3.4.4 Measuring importance of carbonation predictors

Besides predicting the depth of carbonation, the developed ensemble methods were applied to evaluate the importance of the input variables in estimating the carbonation depth. There are several ways to measure the importance of variables. Variable importance measurement by permuting out-of-bag observations (discussed in Section 2.4.3) is one of the commonly used methods. Nevertheless, in CaPrM another technique was applied since the described method is impracticable for boosting decision tree model. To measure the variable importance, `predictorImportance`

function in MATLAB was applied for both bagging and boosting ensemble methods. This function averages the predictive measure of association for all input variables (predictors) over all trees in the ensemble. The predictive association measure is a value that shows the resemblance between decision rules that split observations. Among all viable decision splits that are compared to the best split (identified by growing the tree), the optimal surrogate decision split (that uses a correlated predictor variable and split criterion) provides the maximum predictive association measure. The second-best surrogate split yields the second-largest predictive association measure.

Assume x_j and x_k are input variables j and k, respectively, and $j \neq k$. At node t, the predictive association measure, ξ_{jk}, between the best split $x_j < u$ and a surrogate split $x_k < v$ is described by Equation (3.5).

$$\xi_{jk} = \frac{\min(P_L, P_R) - \left(1 - P_{L_j L_k} - P_{R_j R_k}\right)}{\min(P_L, P_R)}, \tag{3.5}$$

where P_L is the proportion of observations in the left child of node t, such that $x_j < u$; P_R is the proportion of observations in the right child of node t, such that $x_j \geq u$; $P_{L_j L_k}$ is the proportion of observations at the left child node t, such that $x_j < u$ and $x_k < v$; $P_{R_j R_k}$ is the proportion of observations at right child node t, such that $x_j \geq u$ and $x_k \geq u$; ξ_{jk} is a value in $(-\infty, 1]$. If $\xi_{jk} > 0$, then $x_k < v$ is a worthwhile surrogate split for $x_j < u$. Note: observations with missing values for x_j or x_k do not provide to the proportion computation.

The computed estimates of variable importance for the bagging and boosting decision trees are presented in Section 4.2. Every input variable employed in the training dataset to foresee the carbonation depth has one value. Variables that have obtained high value mean that they are important for the ensemble.

3.5 Model development for chloride profile prediction

In this section, the development process of chloride profile prediction model based on ensemble method is discussed. The ultimate purpose of the model is to determine the variables that are describe best the

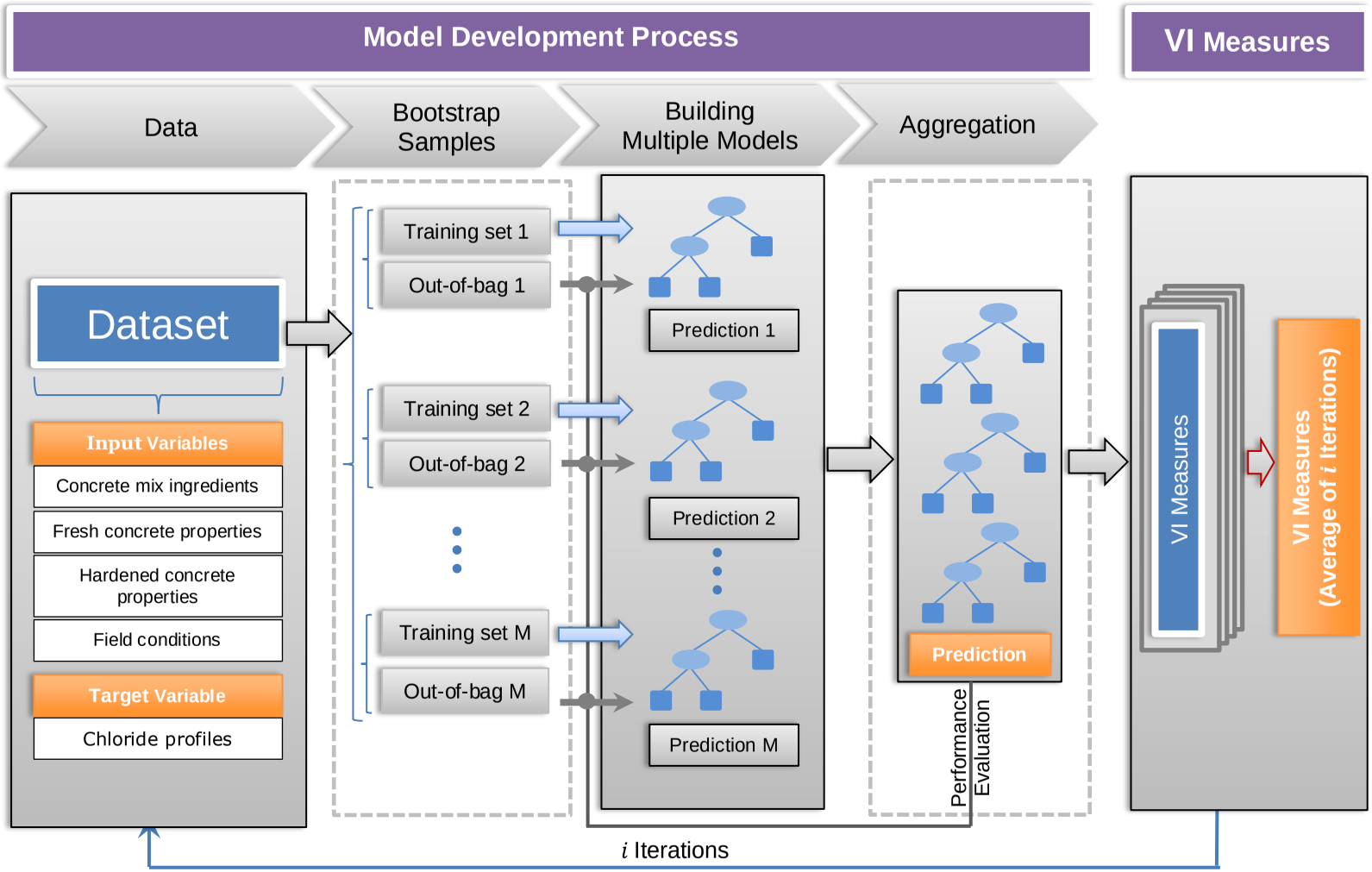

Figure 3.8. Chloride ingress prediction model development process and VI measures (Publication III).

penetration of chloride into concrete. The model development process has four main steps: i) data, ii) bootstrap samples, iii) building multiple models, and iv) aggregation as shown in Figure 3.8. As any machine learning based model, the first step of the model development process is importing the experimental data. Though executing data preprocessing tasks is a standard practice, they were not performed during this model development process. This is due to the fact that the adopted ensemble method does not require data encoding and normalization. In addition, there are no missed values in the employed data that call for handling of missing values. The next step of the model development process is data partitioning to train and validate the model. The training sets are formed by drawing multiple bootstrap instances randomly from the dataset using bagging method. On average, each training set consists of about 63% of the original dataset. Any remaining samples (out-of-bag observations) after bootstrapping from the dataset are applied to evaluate the performance of the model training. The third step is building multiple chloride profile prediction models by utilizing the bootstrapped samples. The final step is aggregation of the models output in order to form an ensemble model. This is carried out by combining the predicted output of each model as discussed in Section 2.4.3. Once the ensemble model is created, the variable importance (VI) measures were carried out in order to determine the significance of chloride penetration controlling parameters in concrete. The whole process was iterated i times to attain reliable results and then the average of these results become the VI measures.

3.5.1 Data for chloride prediction model

The data employed in the model entail information regarding the concrete mix ingredients, the fresh and hardened concrete properties, the field conditions and the chloride profiles measured at various exposure times. The details of the data are given in Table 3.5. A total of five types of cements, in accordance with the classification of EN 197-1 [56], were utilized to produce the concrete specimens. These are Portland cement (CEM I 42,5 N-SR and CEM I 52,5 R), Portland limestone cement (CEM II/A-LL 42,5 R), Portland composite cement (CEM II/A-M(S-LL) 42,5 N) and Portland slag cement (CEM II/B-S 42,5 N). Similar to the data utilized for carbonation depth prediction, few of the specimens adopted here were

also produced using Portland limestone cement partially substituted with BFS or FA. The same types of plasticizers and air-entraining agents as in carbonation were also employed and classified based on their brand names for the same reason. The w/b ratio of the data spans from 0.38 to 0.51.

The data for the fresh concrete properties comprise test results of slump, density, and air content. Hardened concrete properties contain laboratory test results of pore volume, density (wet and dry), air void, compressive strength, carbonation diffusion coefficient and chloride migration coefficient. The test results of the pore volume provide information about the porosity of the concrete at early hardening phase. This property was tested at the same age with the wet and dry density which is at about the age of two days. The air void of the hardened concrete specimens was evaluated by thin-section analysis. The compressive strength was tested at the age of 28 days. The carbonation diffusion coefficient was computed after determining the carbonation depth of the concrete specimens at the age of 28 days. The chloride diffusion coefficient was examined at the age of three months.

The total number of variables employed in the data is 33. Variables numbered from 1 to 32 were assigned as input variables and the last variable (chloride profile of each specimen) was allocated as a target variable. The input variables encompass continuous and nominal data types whereas the target variable comprises only continuous data type. The continuous and the nominal data types are designated as C and N in Table 3.5, respectively.

3.5.2 Training of chloride prediction model

Bagging decision tree was developed to examine the importance of chloride penetration predicting parameters in concrete. The fundamental building process of bagging decision tree is described in Algorithm 2 (Section 3.4.3). Similar to CaPrM, the ensemble model was built in MATLAB but using a function known as `TreeBagger`. Ensembles created using `TreeBagger` algorithm have more functionality than those constructed with `fitensemble`. Both functions grow decision trees in the ensemble using bootstrap samples of the data, but the former selects a random subset of variables at each decision split and every tree involves several splits. Due to this, the ensemble method generated using `TreeBagger` function some-

Table 3.5. Description of variables employed in the chloride dataset (C: continuous and N: nominal, Publication III).

Variables category	No.	Variable subcategories	Description	Units	Types and range	Short name
Concrete mix ingredients	1	Binder types	CEM I 42,5 N – SR	-	N: (1 = CEM I 42,5 N – SR, 2 = CEM I 52,5 R, 3 = CEM II/A-LL 42,5 R, 4 = CEM II/A-M(S-LL) 42,5 N, 5 = CEM II/B-S 42,5 N, 6 = CEM II/A-LL 42,5 R & blast-furnace slag, 7 = CEM II/A-LL 42,5 R & fly ash)	Bind. types
			CEM I 52,5 R	-		
			CEM II/A-LL 42,5 R	-		
			CEM II/A-M(S-LL) 42,5 N	-		
			CEM II/B-S 42,5 N	-		
			CEM II/A-LL 42,5 R & blast-furnace slag	-		
			CEM II/A-LL 42,5 R & fly ash	-		
	2	Water to binder ratio		-	C: 0.37 to 0.51	w/b
	3	Cement content		[kg/m³]	C: 217.22 to 451	Cement
	4	Blast-furnace slag content		[kg/m³]	C: 0 to 217.22	BFS
	5	Fly ash content		[kg/m³]	C: 0 to 106	FA
	6	Total effective water		[kg/m³]	C: 159.50 to 180.40	Total eff. water
	7	Aggregate content	Total aggregate	[kg/m³]	C: 1706 to 1895	Total Agg.
	8		Aggregate < 0.125 mm	[%]*	C: 2.40 to 4.50	Agg. <0.125 mm
	9		Aggregate < 0.250 mm	[%]*	C: 6.60 to 11.40	Agg. <0.250 mm
	10		Aggregate < 4 mm	[%]*	C: 36.30 to 52.50	Agg. <4 mm
	11	Product name of plasticizers	Glenium G 51	-	N: (1 = Glenium G 51, 2 = Teho-Parmix, 3 = VB-Parmix)	Plas. pro. name
			Teho-Parmix	-		
			VB-Parmix	-		
	12	Plasticizers content		[%]**	C: 0.60 to 2.54	Plasticizers
	13	Product name of air-entraining agents	Ilma-Parmix	-	N: (1 = Ilma-Parmix, 2 = Mischöl)	AEA pro. name
			Mischöl	-		
	14	Air-entraining agents content		[%]**	C: 0.01 to 0.06	Air-ent. agents
Fresh concrete properties	15	Basic properties	Slump	[mm]	C: 40 to 180	Slump
	16		Density	[kg/m³]	C: 2287 to 2395	Density
	17		Air content	[%]	C: 3.40 to 6.90	Air cont.
	18	Pore volumes and density	Air pores	[%]	C: 3.55 to 6.99	Air pores

Hardened concrete properties	19		Total porosity	[%]	C: 17.52 to 20.39	T. porosity
	20		Capillary + gel porosity	[%]	C: 12.87 to 14.68	C+G porosity
	21		Density (wet)	[kg/m^3]	C: 2502 to 2581	Density (w)
	22		Density (dry)	[kg/m^3]	C: 2354 to 2427	Density (d)
	23	Thin section results	Total air pores	[%]	C: 1.90 to 5.90	T. air pores
	24		Air pores <0.800 mm	[%]	C: 0.80 to 4.60	AP <0.800 mm
	25		Air pores <0.300 mm	[%]	C: 0.60 to 3.50	AP <0.300 mm
	26		Specific surface	[mm^2/mm^3]	C: 12.80 to 36.50	S. surface
	27		Spacing factor (< 0.800 mm pores)	[mm]	C: 0.18 to 0.51	SF < 0.800 mm
	28	Mechanical property	Compressive strength	[MPa]	C: 38 to 58.50	Comp. str.
	29	Durability properties	Accelerated carbonation coefficient	[mm/d$^{0.5}$]	C: 1.58 to 3.96	k_{acc}
	30		Chloride migration coefficient	[m^2/s]	C: 1.40 to 15.09x10^{-12}	D_{nssm}
Field conditions	31	Field conditions	Exposure time	[year]	C: 1 to 6	Expo. time
	32		Distance from highway lane	[m]	C: 4.50 to 10	Dis. from HW
Chloride profiles	33	Chloride profiles	Chloride concentration at various depth	[%]***	C: 0 to 0.10	Chloride profile

*compared with the total aggregate, **compared with the total binder materials, *** by weight of concrete

times referred as random forest algorithm. The basic development step of random forest algorithm is summarized in Algorithm 4. In this dissertation, the developed ensemble method referred as bagging decision tree instead of random forest.

The first step for development of a powerful bagging decision tree is determining a suitable leaf size for each decision tree in the ensemble. In fact, the default minimal leaf size of the adopted algorithm to build bagging decision trees is five. Trees grown with this value are usually very deep and optimal for determining the predictive power of an ensemble. Bagging decision trees grown with larger leaves may not lose their predictive power while reducing training and prediction time as well as memory usage. Due to these facts, it is necessary to find the optimal leaf size. This can be attained by building ensemble trees employing the training dataset with dissimilar leaf sizes and rational number of trees. Then assess which of the tree configuration option offers the least mean-square error (MSE). To determine the suitable leaf size, ensemble trees with tree size of 100 and leaf sizes of 5, 10, 20, 50 and 100 were built. For each ensemble trees, the out-of-bag predictions were computed by averaging over predictions from

Algorithm 4: *Random forest*

Input: Data $D = \{(x_i, y_i), i = 1, \dots, N\}$, where $y \in \mathbb{R}$

Output: Random forest (Bagged decision tree)

let T and B be a total number of regression trees and nodes, respectively
for $t = 1, 2, \dots, T$ **do**
    create a bootstrap sample D^{*t} with equal number of intsances from a dataset D
    grow a random-frost tree T_t to the bootstrapped data until the minimum node size is reached
    for $b = 1, \dots, B$ **do**
        select m variables at random from the p variables
        choose the best split among the m variables
        split the node into two daughter nodes
    end for
end for

Output the random forest

$\hat{f}_{rf}(x) = \frac{1}{T}\sum_{t=1}^{T} T_t(x)$

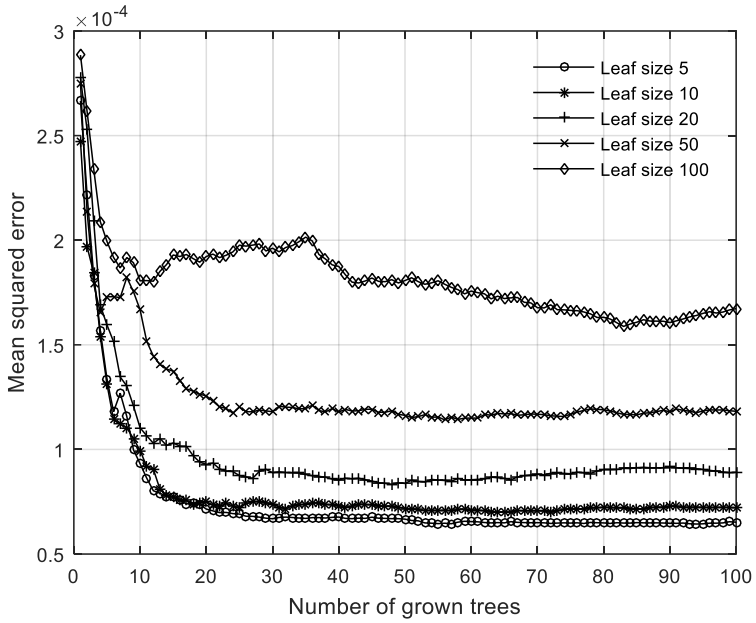

Figure 3.9. Mean-square errors to determine optimal tree and leaf sizes for chloride profile prediction model (Publication III).

all trees in the corresponding ensembles. Then the MSEs of each ensemble trees were computed by averaging the squared difference between the predicted responses of the out-of-bag and the target responses. The MSEs obtained by the ensemble methods for the examined leaf and tree sizes are shown in Figure 3.9. Even if the errors for leaf size five and ten are comparable as can be seen from Figure 3.9, leaf size five provides the lowest MSE. Therefore, to carryout effective model training the leaf and the tree sizes were designated as five and 100, respectively. Using the identified configuration, trees were grown for each bootstrap replica and train each tree in the ensemble. The bootstrap replicas comprise information about the concrete's mix ingredients, the fresh and hardened concrete properties, the field conditions as well as the chloride profiles measured at different ages.

3.5.3 Measuring importance of chloride predictors

The objective of the variable importance analysis is to determine the degree of significance of each variable which are embedded in the dataset

in predicting the chloride concentration in concrete. It was discussed above that the ensemble decision trees of CaPrM built using `fitensemble` algorithm had applied a function, `predictorImportance`, to examine how influential the input variables in predicting the carbonation depth. Its equivalent for `TreeBagger` algorithm is a function called `OOBPermutedVarDeltaError`. This function gives a numeric array of size (1-by-number of variables) consisting of significance measure for each input variable. This was executed by arbitrarily permuting out-of-bag data across a single variable at a time and predicting the increase in the out-of-bag error due to the permutation. This measure was computed for each tree in the ensemble then averaged them and the averaged value was divided by the standard deviation over the whole ensemble. This process was reiterated ten times since this number of iterations offered stable outcome with rational computational time. The ultimate variable importance measure for each variable was evaluated by averaging the results of the ten iterations. The higher the value of the variable importance measure the greater the significance of the variable in predicting the chloride concentration in concrete. The process of out-of-bag variable importance measurement by permutation is already discussed in detail in Section 2.4.3 and summarized by Algorithm 5.

In order to evaluate the significance of variables from various perspectives, ten bagged decision tree based chloride profile prediction models were developed by following the same procedure presented above. Based on the parameters in their input dataset, the ten models were categorised into two groups: Model A and Model B. The details of the classifications of the ten models are presented in Table 3.6. Model A utilized all parameters presented in Table 3.5 except chloride profiles as input parameters. Model B employed input parameters representing only concrete mix ingredients, field exposure conditions, and chloride migration coefficients. The purpose of Model B was to study the importance of fresh and hardened concrete tests in predicting the chloride profile. In both model categories, the target dataset was the chloride profile. Each group was further divided into three scenarios to analyse the parameter's significance by excluding the influence of the exposure time and distance from highway. The number of instances and features

Algorithm 5: *Out-of-bag VI measure by permutation*

Input: Data $D = \{(x_i, y_i), i = 1, \dots, N\}$, where $y \in \mathbb{R}$

Output: Out-of-bag VI measure

Let D^{*t} the bootstrap samples and p is the number of predictors in the training dataset.

for $t = 1, 2, \dots, T$ **do**
  identify the out-of-bag instances for a tree t, $\bar{\beta}^{(t)} \subseteq \{1, \dots, p\}$
  estimate the out-of-bag error $\hat{y}^{(t)}$
  for each predictor variable x_j, $j \in \bar{\beta}^{(t)}$
    randomly permute the instances of x_j
    estimate the model error, $\hat{y}_{\varphi j}^{(t)}$, using the out-of-bag instances containing the permuted values of x_j
    take the difference $\hat{y}_j^{(t)} = \hat{y}_{\varphi j}^{(t)} - \hat{y}^{(t)}$// Predictor variables not split when growing tree t are attributed a difference of 0.//
    for each predictor variable in the training dataset, D^{*t}
      compute the mean, $\bar{y}_j$ of the differences over the learners, $j = 1, \dots, p$
      standard deviations, σ_j of the differences over the learners, $j = 1, \dots, p$
    end for
  end for
end for

Output out-of-bag VI measure for x_j

$\widetilde{VI}(x_j) = \frac{\bar{y}_j}{\sigma_j}$

considered in each model is different and presented in Table 3.7 along with the adopted type of algorithm and data partitioning.

The first scenario (A.1 and B.1) takes into account all the respective variables of Models A and B as described above. The second scenario (A.2 and B.2) is identical with scenario one except the employed chloride profiles comes only from the specimens located at 4.5 m. The intention of this scenario is to avoid the distance effect on predicting the chloride profile and concentrate on the influence of other parameters. The focus of the third scenario is to eliminate the influence of the exposure time by considering the chloride profile measured at a specific exposure time. Under this scenario, there are three models in each model group (A.3(i),

Table 3.6. Details of the ten models developed for chloride profile prediction (Publication III).

Scenario	Model A			Model B			Description
	Model name	Input variables category	No. of variables	Model name	Input variables category	No. of variables	
1	**A.1**	All variables*	33	**B.1**	All concrete mix ingredients*, field conditions* and D_{nssm}	18	Entails data at which the chloride profiles measured on all specimens at different ages.
2	**A.2**	All variables* except dis. from HW	32	**B.2**	All concrete mix ingredients*, expo. time and D_{nssm}	17	Consists of data at which the chloride profiles measured on specimens only located at 4.5 m away from HW 7.
3	**A.3(i)**	All variables* except expo. time	32	**B.3(i)**	All concrete mix ingredients*, dis. from HW and D_{nssm}	17	Entails data of specimens at which the chloride profiles measured at one year of exposure.
	A.3(ii)			**B.3(ii)**			Ditto but at three years of exposure.
	A.3(iii)			**B.3(iii)**			Ditto but at six years of exposure.

Table 3.7. Type of algorithm, data size, and data partitioning used to build chloride profile prediction models.

Applied algorithms	Model types	Instances	Features	Data partitioning
Bagged decision tree	Model A.1 and B.1	522	33	63/37
	Model A.2 and B.2	345	32	63/37
	Model A.3(i) and B.1(i)	215	32	63/37
	Model A.3(ii) and B.2(ii)	120	32	63/37
	Model A.3(iii) and B.2(iii)	189	32	63/37

A.3(ii), A.3(iii) and B.3(i), B.3(ii), B.3(iii)) since the chloride concentration in the concrete specimens were analysed at three different exposure times (one, three, and six years). All these models employed the chloride profiles measured at the depth of 0.5 mm, 1.5 mm, 3 mm, and 5 mm since the amount of chloride was examined in all concrete specimens at these depths. Each model was run ten iterations and the final variable importance measure was evaluated by averaging the results of the ten iterations. The findings are presented in Section 4.3 in detail.

3.6 Model development for hygrothermal prediction

The development process of the hygrothermal prediction model is discussed in this section and illustrated in Figure 3.10. The rectangular boxes coloured in grey in the figure represent the major tasks of the modelling procedure. As in any other data-driven models, the initial step was importing the monitored hygrothermal data. The data comprise the hygrothermal measurements of the ambient and the inner surface-protected concrete façade elements. After importing the data, data exploration was executed in order to comprehend and visualize the principal characteristics of the dataset. This activity is usually carried out by utilizing customized visual analytical tools. Data preprocessing was the next essential step and this task needs to be carried out before the data being processed further. Data preprocessing, especially in neural network based models, could also involve other tasks as discussed in Section 3.4.2. The next important step after data preprocessing was data partitioning in which the data were divided into training, validation, and test sets. The training dataset is a set of hygrothermal data that are utilized to train the adopted neural network algorithm (Nonlinear autoregressive with

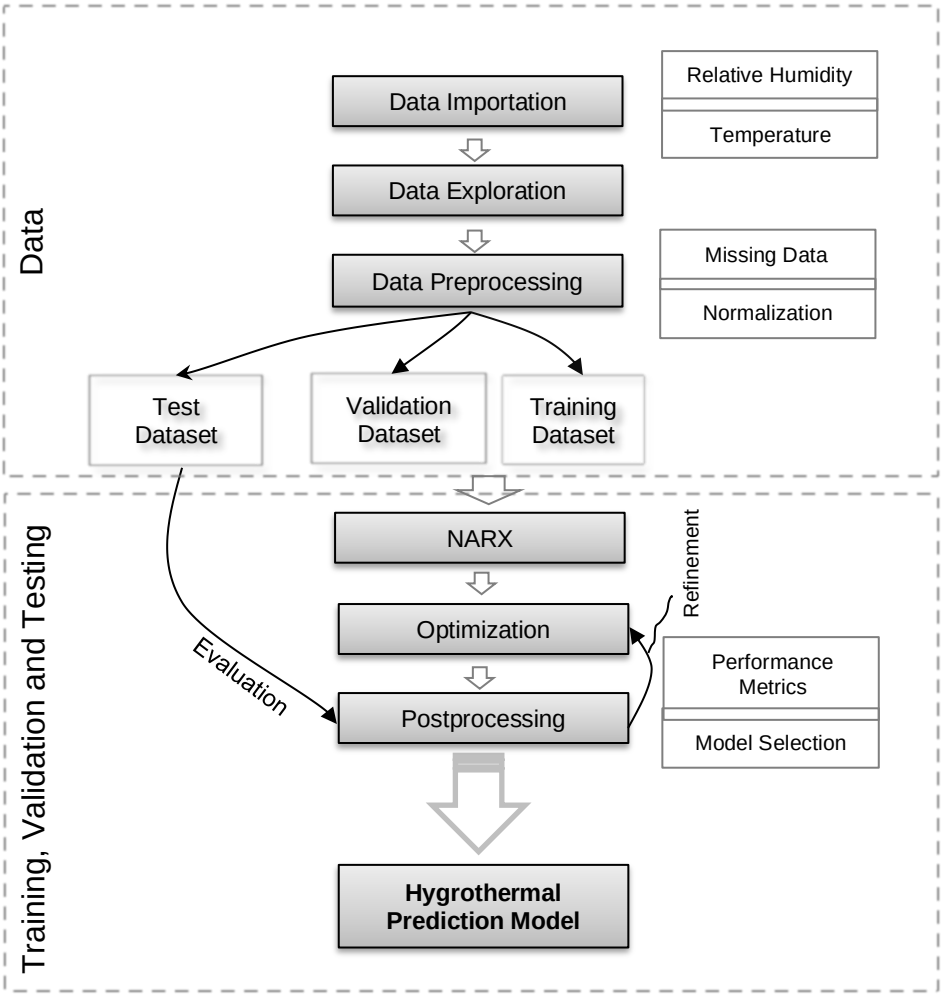

Figure 3.10. Hygrothermal prediction model development process (Publication IV).

external input, NARX). The purpose of the validation dataset is to assist the network to halt training when the generalization process stops improving and thus preventing overfitting. The test dataset was utilized to evaluate the performance of the developed neural network based hygrothermal prediction model.

3.6.1 Data and its preprocessing for hygrothermal model

The data employed in the hygrothermal prediction model entail four variables: ambient relative humidity, ambient temperature, inner relative

Table 3.8. Type of algorithm, data size, and data partitioning applied to build hygrothermal prediction model.

Applied algorithm	Façade element	Algorithms	Instances	Features	Data partitioning
NARX	S1	Relative Humidity	719	2	75/15/10
		Temperature	719	2	75/15/10
	S2	Relative Humidity	719	2	75/15/10
		Temperature	719	2	75/15/10
	S4	Relative Humidity	719	2	75/15/10
		Temperature	719	2	75/15/10
	S5	Relative Humidity	719	2	75/15/10
		Temperature	719	2	75/15/10
	S6	Relative Humidity	719	2	75/15/10
		Temperature	719	2	75/15/10

humidity, and inner temperature. The data were gathered from two years of in-service monitoring of the concrete façade elements in the case structure. The data were recorded with a regular time interval of half an hour. The ambient relative humidity and temperature were designated as the input variables. The target variables were the values of the relative humidity and the temperature measured inside the concrete façade members. Both temperature and relative humidity values are numeric, and units used for them were °C and %, respectively. The size of the data utilized to predict the hygrothermal behaviour inside each concrete façade element is given in Table 3.8.

During the hygrothermal modelling process, data encoding was unrequired since the utilized data entail only numerical variables. The applied data normalization and data partitioning procedure were exactly the same as the procedure presented in Section 3.4.2. All the data were normalized by transforming the values of the input and the target variables in the interval [-1, 1]. The data (size of 719 instances and two features) were also randomly divided into three clusters: training, validation, and test datasets which hold 75%, 15% and 10% of the dataset, respectively. Missing data processing was carried out since about 6% of the monitored hygrothermal data were missed for successive days at particular times from every surface-protected façade element. To substitute the missing data and eliminate the noise from the monitored hygrothermal data, a moving average filter technique was applied. This method smooths and replaces the missing data with the average of the neighbouring data points defined within the span [130] and is expressed by Equation (3.6).

$$x_s(i) = \frac{1}{2M+1}\big(x(i+M) + x(i+M-1) + \cdots + x(i-M)\big), \tag{3.6}$$

where $x_s(i)$ is the smoothed value for the i^{th} data point, M is the number of neighboring data points on either side of $x_s(i)$, and $2M + 1$ is the span.

3.6.2 Training of hygrothermal prediction model

The model training process was carried out using a function `narxnet` in MATLAB. This function builds a NARX network with the default hyperbolic and linear transfer functions in the hidden and output layers, respectively. The hyperbolic activation function produces outputs in the range between -1 and 1 whereas the linear transfer function computes the neurons output by simply transferring the value given to it. As discussed in Section 2.4.1, the NARX network has generally two inputs. In case of the considered NARX network, one of the inputs is from the monitored hygrothermal data (e.g. ambient temperature/relative humidity), and the other input is a feedback connection obtained from the output of the model (e.g. predicted inner temperature/relative humidity). For each of these inputs, there is a tapped-delay-line memory to store previous values. In order to complete the architecture of NARX network, the number of tapped-delay-line memories and hidden neurons should also be assigned. The default number of the tapped-delay-line memories and hidden neurons for `narxnet` function is 2 and 10, respectively. These default values were employed for creation of the initial NARX network that predicts the hygrothermal performance inside surface-treated concrete element. Then the network was tested with other values and all training performances were compared. The comparison is necessary to identify the optimal number of hidden neurons and the tapped-delay-line memories that yield the best performance. The determined optimal values were utilized in the model as the final configuration of the model. The basic graphical representation of the designed NARX network for modelling the hygrothermal behaviour of the case structure is identical with Figure 2.7.

After the configuration of the NARX network was completed, the next task was inputting the preprocessed hygrothermal data for model training. Since the network contains tapped-delay-lines, it is vital to fill initial values

on the delay-line memories of the inputs and the outputs of the network. This was carried out by applying a command, `preparets`, which automatically shifts the input and the target time series as many steps as required to fill the initial delay states. This function also reformats the input and the target data whenever the network is redesigned with different numbers of delays. After the training data is ready, the network was trained using a Levenberg-Marquardt algorithm. It is a fast, powerful, and widely applied algorithm to solve several types of problems. Details of this algorithm are already discussed in Section 3.4.3.

The performance of the network training was evaluated using the validation dataset for different networks with varying number of tapped-delay-line memories and hidden layer neurons. After performing several trainings, tapped-delay-line memories of two and hidden layer neurons of ten were identified as the optimal ones that provide the least generalization errors. Tapped-delay-line memories of two units mean that the output of the designed network, $\hat{y}(n+1)$, is fed back to the input of the network through delays, $\hat{y}(n)$, and $\hat{y}(n-1)$ as the output of the network is a function of these delays. The training performance of the developed NARX model to predict the relative humidity in concrete façade element S4 is illustrated, as an example, in Figure 3.11. It can be clearly observed that the network has been trained smoothly and any overfitting/underfitting has not been occurred. The best validation performance is obtained at nine epochs (full training cycles on the training dataset) with MSE of 1.05. The MSE of test dataset (which was randomly generated) is 1.16. After successful training, the performance of the model in evaluating the hygrothermal behaviour inside all surface-treated concrete façade elements were tested using the last 90 days of the data, which were not utilized during the model trainings as well as validation processes. The details of the training performance and the prediction ability of the developed hygrothermal prediction models on the last 90 days for all façade elements are presented in Section 4.4.

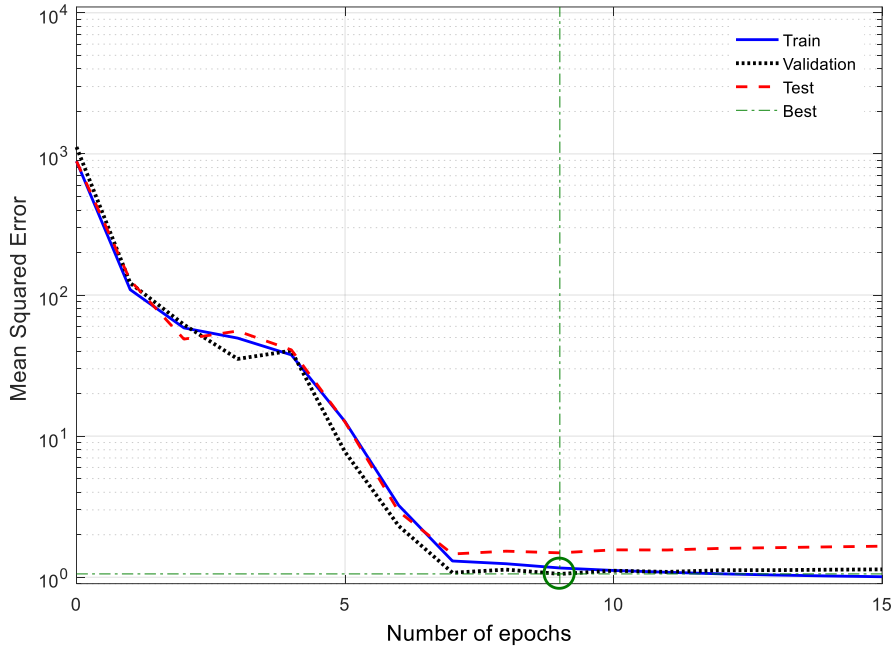

Figure 3.11. Validation performance of the trained NARX model that employs relative humidity data obtained from the ambient and inside S4.

3.7 Exploratory data analysis development for visualization

In this section, the development process of exploratory data analysis (EDA) technique is presented. Its primary aim is to visualize the condition of corrosion and other deterioration mechanisms caused unintentionally by the implemented surface-protection systems in a more realistic manner. EDA is an essential step in any data-driven modelling process, and it is often applied after data collection and preprocessing, where the data is merely visualized, plotted, and manipulated without any presumption. It assists to assess the data quality and build optimal models. EDA is not only guide for building a useful model but also assist to understand the output of the model.

The data image technique was applied for visualizing the status of corrosion, frost and chemical attacks in surface-protected concrete façade elements using the hygrothermal data. MATLAB programing language was

used for displaying these images employing `imagesc` function. This function uses x and y values to specify the data size in respective directions, and then generates an image with dataset to scaled values with direct or indexed colours to indicate the magnitude of each variable for each observation. As the hygrothermal data were monitored with a regular interval of short time and comprise missed values, producing and visualization of the status of corrosion, frost and chemical attacks in the concrete elements is not a straightforward task. The following fundamental steps were carried out.

Step 1: smooth the data to reduce irregularities of the monitored/predicted time-series hygrothermal data to deliver a clearer view of the true underlying behaviour.

Step 2: translate the data to status of corrosion, frost and chemical attacks by utilizing predefined conventions.

Step 3: display the image by applying the `imagesc` function and add a colour scale to the image.

Step 4: define the coordinates of the missed values in concrete façade elements which comprise the missed data.

Step 5: represent the missed data using the coordinates defined in step 4.

The visualized conditions of corrosion, frost, and chemical attacks of surface-protected concrete façade elements of the case structure are presented and analysed in Section 4.4.

Chapter 4

Results

This chapter presents the main results of the dissertation. The presentation of the results is organised into four sections based on the four research questions. Each section presents the core results of one of the research questions that are discussed in Chapter One.

4.1 Need for data-driven approaches

Publication I answers the research question of "*how to eliminate or mitigate the uncertainties observed in the traditional corrosion assessment methods?*". To answer this question, Publication I concentrates on: i) examining the limitations of the conventional corrosion assessment methods, and ii) reviewing the recent advances and future directions on the concrete durability assessment. The focus in this section is on the findings of (ii) as the first task has already been discussed in Section 2.3.

The findings of Publication I revealed that there had been few attempts to predict the carbonation depth and the chloride concentration in concrete using machine learning methods. The few proposed carbonation depth prediction modes are listed in Table 4.1. The majority of these works were based on short-term tests which were aimed to characterize the carbonation resistance of concrete at laboratory. They also consider few parameters, missing some of the important ones that describe the microstructure of concrete. The model proposed in [131] take into account 39 input parameters, but some of them do not describe the condition well. This is due to the fact that the data were collected from concrete specimens exposed to natural environment located in different exposure conditions. The data were acquired from 88 literatures. All works, except those executed by the author of this dissertation [132–134], failed to perform a certain crucial data optimization steps during the model development process. Without following these steps, some parameters may become

Table 4.1. Data-driven models that are proposed for carbonation depth prediction.

Work	Main learning algorithm type	Exposure environment		Exposure duration		No. of input parameters	Data optimization
		Lab	Field	Long	Short		
[161]	Neural Network	X	✓	✓	X	6	X
[131]	Neural network	X	✓	✓	X	39	X
[162]	Neural network	✓	X	X	✓	5	X
[163]	Adaptive neuro-fuzzy inference system	X	✓	✓	X	6	X
[132]	Neural network	✓	X	X	✓	15	✓
[164]	Neural network	✓	X	X	✓	3	X
[133]	Decision tree Bagged decision tree	✓	X	X	✓	15	✓
This work [134]	Neural network Decision tree Bagged decision tree Boosted decision tree	X	✓	✓	X	25	✓

X = not applicable, ✓= applicable, Short < 52 weeks, Long ≥ 52 weeks

irrelevant and/or redundant for representing the carbonation process, which ultimately reduces the performance of the model.

Similar to the carbonation depth prediction models, the existing machine learning based chloride concentration prediction models largely employ data generated from accelerated laboratory tests as seen in Table 4.2. These models were applied to characterize the chloride permeability of concrete. The purpose of the models was to reduce or fully substitute the rapid chloride penetration test since its experimental determination in laboratory is usually resource and time consuming. Except [135], all the related work failed to perform data optimization techniques. Unlike the existing works, the model developed in this dissertation is based on long-term field tests, taken into account 32 input parameters and performed data optimization technique. The main purpose of the developed model is to determine the influential parameters that predict the chloride profile of concrete besides making chloride profile prediction.

In both carbonation and chloride cases, the majority of the existing models have adopted neural network algorithm. Unlike these works, the developed models in this dissertation employs neural network and other learning algorithms including decision trees and ensemble methods. Examining the ability of various machine learning algorithms for prediction of the corrosion causing factors is essential in order to identify

Table 4.2. Data-driven models proposed for evaluating chloride penetration (directly or indirectly).

Work	Problem type	Main learning algorithm type	Exposure environment		Exposure duration		No. of input parameter	Data optimization
			Lab	Field	Long	Short		
[165]	Permeability	Neural network	✓	X	✓	X	5	X
[166]	Permeability	Neural network	✓	X	X	✓	6	X
[135]	Permeability	Support vector regression	✓	X	X	✓	7	✓
[45]	Permeability	Neural network	✓	X	X	✓	2 - 6	X
[167]	Permeability	Neural network Adaptive neuro-fuzzy inference system	✓	X	X	✓	4	X
[168]	Permeability	Neural network	✓	✓	X	✓	6	X
[169]	Diffusion coefficient	Neural network	✓	X	X	✓	7	X
[170]	Diffusion coefficient	Neural network	✓	X	X	✓	4	X
[171]	Diffusion coefficient	Neural network	✓	X	X	✓	8	X
[54]	Diffusion coefficient	Neural network	✓	X	X	✓	8	X
This work [172]	Influential predictors	Bagged decision tree	X	✓	✓	X	32	✓

X = not applicable, ✓= applicable, Short < 52 weeks, Long ≥ 52 weeks

the algorithm that performs best. This is due to the fact that the relative prediction power of any machine learning algorithms primarily depends on the details of the considered problems. Without experimenting, it is impossible to identify the powerful algorithms that excel a given problem.

The previous attempts to predict carbonation depth and chloride concentration using data-driven models are encouraging but a lot of improvements have to be carried out. The shortcomings of the previous works can be summarized as follows. First of all, the majority of the models have employed few data to train the models which are acquired from short-term tests. Secondly, the models missed some important input parameters that describe the carbonation and the chloride ingress process. Thirdly, most of them adopted only one type of learning algorithm. Fourthly, the few models that considered several parameters failed to perform certain crucial data optimization steps during the model development process. The performance of the proposed machine learning based carbonation depth and chloride profile prediction models can be improved

considerably by addressing the above shortcomings, which is the contribution of Publications II and III of the dissertation.

The results of Publication I also demonstrated that machine learning will be a core to the next generation corrosion assessment method due to the emerging use of wireless sensors for monitoring RC structures. Today, there are several studies which show the applicability of wireless sensors for monitoring RC structures spanning from earlier-age parameters to environmental situations that can initiate or accelerate corrosion of reinforcement bar [136–140]. Monitoring of various parameters without extracting knowledge or inference from the monitored data is pointless. So, the integration of machine learning and wireless monitoring will form a principal component in the inspection, assessment, and management of RC structures. Eventually, it will bring a paradigm shift in durability assessment of RC structures. The future recommended layout of aging management method for RC structures is shown in Figure 4.1. As seen in the figure, the sensors that are integrated in the structure will continuously deliver real-time data regarding the temporal and spatial changes of the monitored parameters that control corrosion of reinforcement bar or other deterioration mechanisms. The sensors data will be transferred to a cloud storage that gives substantial benefit because data from various streams can be accessed and shared with Internet connectivity from anywhere. Such a monitoring system can be seen as a reliable nondestructive technique that provides valuable in-service data without the participation of inspection crews on the field. This approach will be more cost effective than performing periodic field testing in the long term, considering the cost of labour, the costs to the users, and their safety [141,142]. Condition assessment and prediction of the structure can be executed remotely and rapidly without the need for empirical models. The prediction enables a more realistic condition assessment of a structure and accurately timed maintenance measures, which in turn reduces the associated costs considerably. Moreover, the proposed system can learn the synergic effect of different deterioration mechanisms and discover new useful knowledge using data of several parameters monitored by various sensors. The discovered knowledge will assist engineers to come up with optimal solutions that improve the durability of RC structures as well as to define proactive maintenance plan.

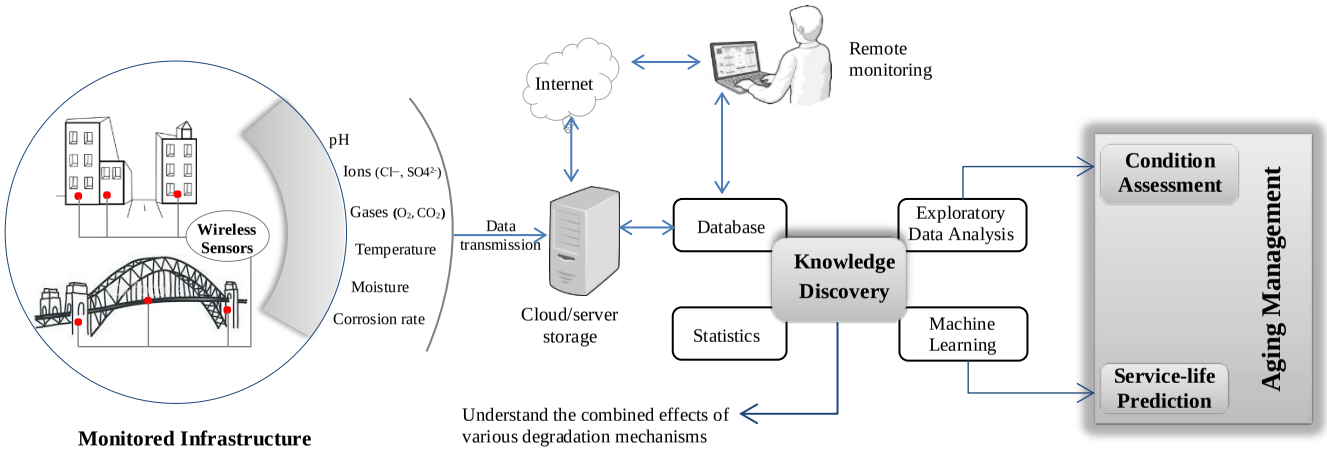

Figure 4.1. Overview of next generation preferred condition assessment method for RC structures (Publication I).

4.2 Carbonation depth prediction

The development process of the carbonation depth prediction model (CaPrM) has been discussed in Section 3.4 and in this section the performance result of CaPrM is presented. This section is arranged into three subsections. The first subsection elaborates the performance of the developed carbonation prediction model and its validity. The second subsection presents the set of influential variables that describe the carbonation depth. The comparison of CaPrM versus traditional carbonation prediction model is presented in the last subsection. These three subsections answer the research question two of the dissertation, *"how to develop accurate carbonation depth prediction model that considers the complex parameter interactions? What are the predominant carbonation depth predictors?"*.

4.2.1 CaPrM performance

CaPrM was trained using a dataset generated from concrete specimens that are exposed to natural carbonation for long term at field environment. The training dataset comprise information regarding the concrete mix ingredients, the fresh and hardened concrete properties, the carbonation periods, the environmental and curing conditions, as well as the carbonation depths. The training performance of CaPrM is illustrated in Figure 4.2, demonstrating the measured versus the predicted carbonation depth of all the integrated learning algorithms. The coefficient of correlation (R-values) were applied to examine the training accuracy of each learning algorithms. This parameter indicates how well the integrated learning algorithms regress the carbonation depth on the input variables. It can be observed from Figure 4.2 that the R-values of all of the four utilized learning algorithms surpass 0.90. This confirms that all the integrated machine learning methods track the real carbonation depth competently during the model training phase. Observably, neural network has attained the best learning performance (R=0.97), followed by decision tree (R=95), boosted decision tree (R=0.94), and bagged decision tree (R=0.91). It can also be noticed that, except neural network, all the learning algorithms exhibit a slight tendency to underestimate the depth

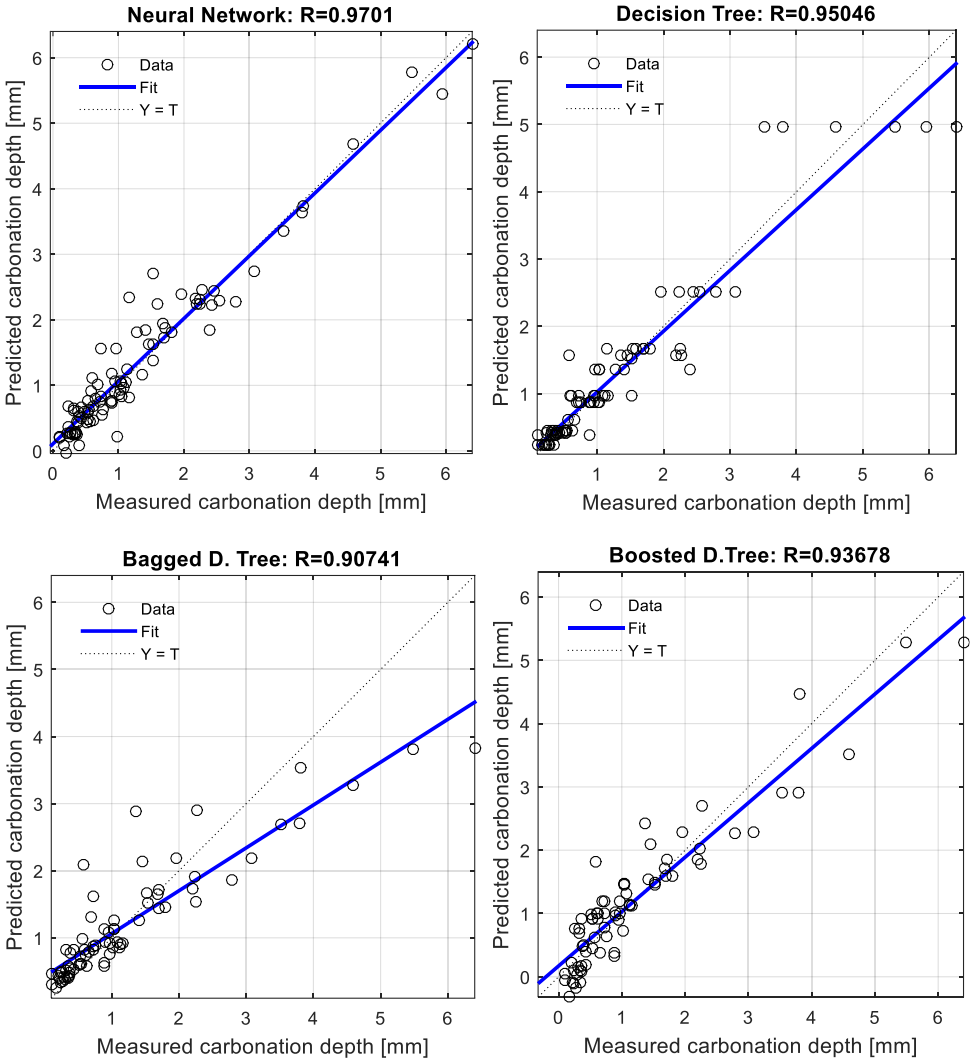

Figure 4.2. Training performance of the CaPrM. Y and T are predicted and measured, respectively (Publication II).

of carbonation when the carbonation depth is large. The reason is the available number of large carbonation depths in the training dataset was few. For example, measurements of carbonation depth above 3 mm represent only about 9% of the total observation. The lack of sufficient number of data in the training dataset causes for the underestimation in this range.

As any machine learning model, the validity of the developed model should be evaluated using a test dataset which is extracted from the

original data but different from training dataset. The purpose is to test the real performance of the model since data-driven models may introduce error due to high bias and variance. High bias can cause the learning algorithm to miss the relevant association between the input and the target variables, resulting *underfitting*. High variance can cause the learning algorithm to model the random noise in the training dataset rather than the desired outputs and causing *overfitting* [82]. These can make a prediction model unstable and therefore unsuitable for solving real-world applications. Hence, the optimal data-driven models should have the best trade-off between the bias and the variance. This is often controlled by altering the model's capacity (ability to fit a wide variety of functions).

The training and test error of all the integrated learning algorithms in the CaPrM were checked to detect any overfitting and/or underfitting. Overfitting occurs when the difference between the error of training and test is far too high. Underfitting happens when the model is unable to acquire a sufficiently low error value on the training dataset. To detect overfitting and/or underfitting, the following error measurements were carried out: mean-square error (MSE), root-mean-square error (RMSE), and mean-absolute error (MAE). The MAE, also called the absolute loss, is an average of the absolute residuals/errors (the difference between the predicted and the actual value) and measured in the same units as the data. MSE is the mean of the squared difference between the target and the predicted value. It is the most widely employed loss function for regression models. RMSE is simply the square root of the MSE. Sometime RMSE is preferable than MSE because understanding of error values of MSE is difficult due to the squaring effect, particularly, if the target value represents quantities in unit of measurements. RMSE retains the original units as MAE. The MSE, RMSE, and MAE are calculated using Equations (4.1), (4.2), and (4.3), respectively.

$$MSE = \frac{1}{n}\sum_{i=1}^{n}\left(Y_i - \hat{Y}_i\right)^2, \tag{4.1}$$

$$RMSE = \sqrt{\frac{1}{N}\sum_{i=1}^{N}\left(Y_i - \hat{Y}_i\right)^2}, \tag{4.2}$$

$$MAE = \frac{1}{N}\sum_{i=1}^{N}\left|Y_i - \hat{Y}_i\right|, \quad (4.3)$$

where $\hat{Y}_i$ is the predicted output value, Y_i is the measured target value, and N is the number of observations.

The performance evaluation using the above statistical measures confirm that all the integrated learning algorithms predict the carbonation depth with rationally low error on previously unseen data. Average of ten round statistical performance indicators (MSE, MAE, and RMSE) of all the learning methods are given in Table 4.3. The difference between the training and the test errors of all the integrated learning algorithms is small, confirming the generalization ability of the CaPrM. The lower the statistical errors in training and testing phases are the superior the performance of the model. It can be easily noticed from Table 4.3 that the neural network algorithm outperformed all the other models. The MSE of the neural network algorithm is the lowest both in training and testing stages compared to the other integrated learning algorithms. For instance, the MSE of the boosted decision tree is increased by 9% in the model training phase while by 10% in the testing phase. This demonstrates that the neural network algorithm integrated in the CaPrM has a balanced trade-off between bias and variance errors, confirming its high learning and generalization abilities. Among decision tree based algorithms, boosted decision tree has a high generalization ability with errors at training phase (MSE=0.21, MAE=0.23 and RMSE=0.46) and testing phase (MSE=0.26, MAE=0.31, and RMSE=0.51). Though, MAE of the decision tree is slightly less than the bagged decision tree, its MSE value revealed that it has relatively weak generalization ability. Indeed, these

Table 4.3. Average of ten round statistical performance measurements for CaPrM.

Dataset	Learning method	Training error			Test error		
		MSE	MAE	RMSE	MSE	MAE	RMSE
After variable selection	Neural network	0.1895	0.1962	0.4353	0.2417	0.2860	0.4916
	Decision tree	0.3696	0.2436	0.6079	0.4189	0.3232	0.6473
	Bagged decision tree	0.2820	0.2498	0.5310	0.3770	0.3415	0.6140
	Boosted decision tree	0.2068	0.2326	0.4548	0.2649	0.3061	0.5147
Before variable selection	Neural network	0.3664	0.2624	0.6053	0.3522	0.3860	0.5935
	Decision tree	0.4106	0.3325	0.6408	0.5295	0.4491	0.7276
	Bagged decision tree	0.3998	0.3298	0.6323	0.4907	0.4391	0.7005
	Boosted decision tree	0.3371	0.3094	0.5806	0.3749	0.4116	0.6123

results are valid only for the utilized particular dataset. The performance of each learning algorithms may vary if a different data were employed. This would not be a problem in CaPrM since it always provides the opportunity to select the best performing one by comparing the validation errors of the four integrated learning algorithms.

The performance evaluations discussed above are after integrating the variable selection technique. The statistical measures before incorporation of variable selection method in the model development process were also evaluated and presented in Table 4.3. The motive for evaluating results of both approaches was to demonstrate the importance of implementing variable selection methods in enhancing the prediction ability of the model. According to the statistical measures, incorporation of variable selection technique in modelling process improved the prediction ability of all the integrated learning algorithms in CaPrM considerably. It can be observed from Table 4.3 that after implementing variable selection the MSE of the neural network was reduced by a factor of about 1.5 followed by boosted decision tree with 1.4 reduction factor. Similarly, the MSE of the standalone decision tree and the bagged decision tree have decreased by 26% and 30%, respectively. This proofs that integration of variable selection methods in CaPrM modelling process leads to its prediction performance enhancement.

The test residuals (the difference between the actual and the predicted carbonation depths) of the four integrated models are computed and their distributions are visualized with boxplot in Figure 4.3. The median of the residuals is represented by a red line within the blue box that covers the middle 50% (25^{th}–75^{th} percentiles) of the residuals. The whiskers go down to the smallest and up to the largest values. Residuals greater than 1.5 box lengths above the whiskers are outliers and designated by a red plus sign. It can be clearly seen from Figure 4.3 that the median of residuals of the neural network is about in the middle of the box and distributed around zero. In another word, the residuals have a constant variance pattern and normally distributed. This confirms that the neural network based carbonation prediction model is accurate on average for all tested data. The median of the residuals of decision tree and bagged decision tree are almost zero. The medians of bagged and boosted decision trees are closer to the first quartile than to the third quartile. This indicates that the

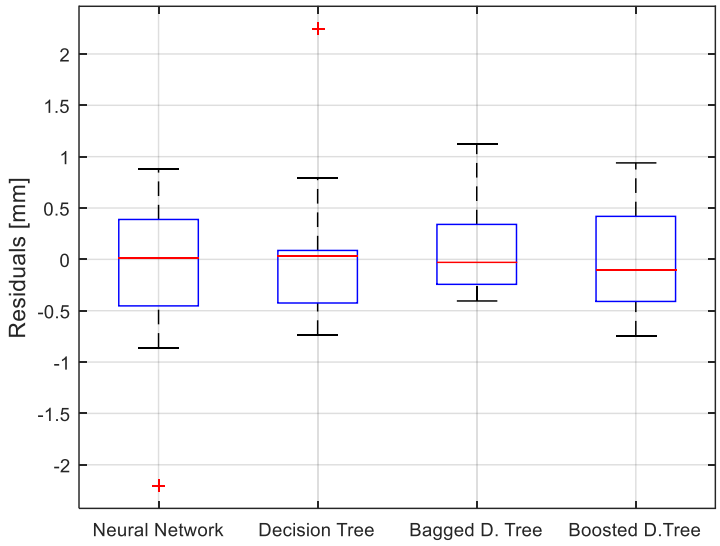

Figure 4.3. Boxplot of residuals of the CaPrM model (Publication II).

distributions of the residuals are slightly skewed to the right. Generally, the boxplot of the residuals of a single run test validates that all the integrated models learn the nonlinear relation of the input variables and are able to predict the carbonation depth with high accuracy.

4.2.2 Carbonation depth predictors

The second part of the research question two aims to determine the predominant carbonation depth predictors. Discovering the most informative set of variables that describe the carbonation depth is vital in order to develop efficient and parsimonious carbonation depth prediction model. To determine the influential variables, the predictive power of all the utilized input parameters of the dataset was examined using the ensemble methods (bagged and boosted decision trees). These methods provide variable importance weight, which are computed by aggregating the weights over the trees in the ensemble. Variables with a higher importance score are indicative of their significance in predicting carbonation depth. The importance score of all the considered input parameters that were deduced from the bagged and boosted decision trees are shown in Figure 4.4. It can be clearly noticed from the figure that accelerated carbonation depth, w/b and compressive strength are the

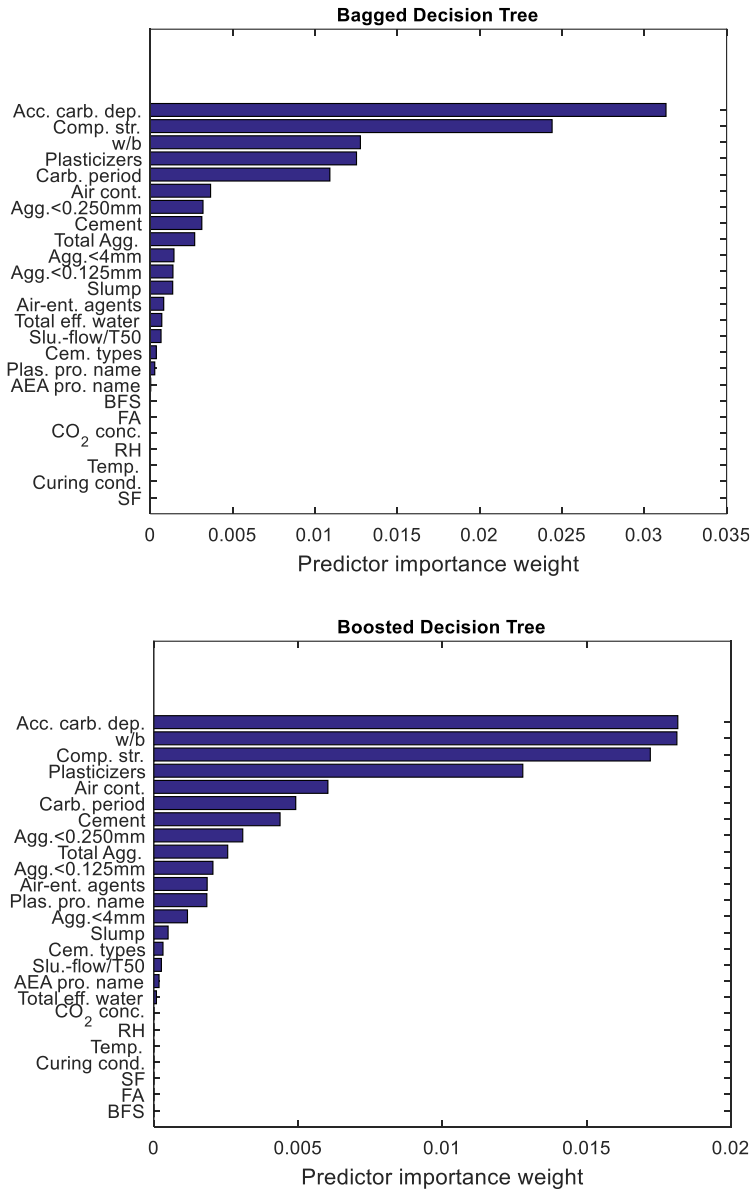

Figure 4.4. Measures of carbonation predictor parameters (Publication II).

topmost three predicting parameters of carbonation depth for the considered data. These determined top three carbonation predictors are well-known parameters and they have already been considered in several empirical models. It is known that cement types affect the carbonation process, but it was not identified as influential parameter by the models.

This does not mean that this variable is uninformative. It only means that this variable was unpicked by the ensemble trees since other variables encode the same information. For instance, cement types are already described by both w/b and compressive strength. The compressive strength of concrete is not only affected by the w/b and cement types but also by other factors such as aggregate size distribution. Hence, compressive strength describes the carbonation process better than the combination of individual parameters that influence the strength of concrete.

Next to the top three parameters, the amount of plasticizers, the air content, and the carbonation period are the predominant carbonation depth predictors. This is an interesting finding since the identified parameters, except the carbonation period, are overlooked in various conventional models. In fact, there are few studies that demonstrate the effect of different types of plasticizers in improving the carbonation resistance of concrete through their influence on the pore structure and the morphology of the hydrated product [143,144]. Other studies show the impact of air content on carbonation process by conducting experiment on air-entrained concrete [145,146]. According to the studies, air-entraining admixtures increase the carbonation resistance of concrete. Those studies were made on concrete specimens of different mix compositions exposed to indoor and outdoor environments. Though air-entraining admixture is one of the influential factors that control the carbonation process, it was not identified as among the top predictors. This is due to the fact that the effect of the air-entraining admixtures is already explained by the air content of the concrete. So, this describes the reason for air content of the concrete being identified as among the top carbonation predictor. The significance of aggregate size distribution in predicting the carbonation depth is noticeable in Figure 4.4, although it is not among the top six descriptors. The reason is that it controls the air permeability of gases. The finding of aggregate size distribution as influential predictor is supported by earlier research [30,147]. This parameter is also missed in several conventional models.

The importance measure does not identify some known significant parameters, such as supplementary cementitious materials, curing, and environmental conditions. In case of supplementary cementitious

materials, the reason is that they have already been expressed by w/b and the combination of other variables, for example, accelerated carbonation depth, comprehensive strength, and air content. The use of similar curing and environmental conditions for all concrete specimens was the reason for these parameters to be unidentified by the model. It can be observed from Figure 4.4 that the ranks provided by both learning methods, bagged and boosted decision trees, are fairly similar. Cumulatively, about 87% of the total influence is attributed by the top six significant parameters in both models.

4.2.3 Comparison of CaPrM and conventional models

The prediction performance of the CaPrM was compared with the conventional Fick's second law based carbonation depth prediction model. To execute a fair comparison, the natural carbonation coefficient for each concrete type was determined and employed in the conventional model given in Equation (2.6). The natural carbonation coefficient of each concrete type was computed using the carbonation depth measured at the age of 268 days. Using this coefficient in Equation (2.6), the carbonation depths at the ages of 770, 1825 and 2585 days were predicted. Then the performance of the model was evaluated by analysing the mean-square error difference between the computed and the measured carbonation depths. The MSE of the conventional model was 0.51, which is larger than the MSE of the CaPrM as can be seen from Table 4.3. The error difference is significant, about two-fold compared with the MSE of neural network and boosted decision tree. The MAE of the conventional model was 0.50, which is more than 1.7 times the MAE of the neural network of the CaPrM.

The residual distribution of the traditional model is presented in Figure 4.5 since the error statistics alone do not deliver sufficient information regarding their distribution. This figure comprises two plots (a boxplot and a histogram plot). These two plots are essential to check the normality of the residual distribution. It can be observed from the boxplot that the residuals median of the traditional carbonation prediction model is higher than any of the integrated models in the CaPrM (illustrated in Figures 4.3 and 4.5). The whisker of the conventional carbonation prediction model ranges from -1 to 1.76 which is greater than from all integrated models in

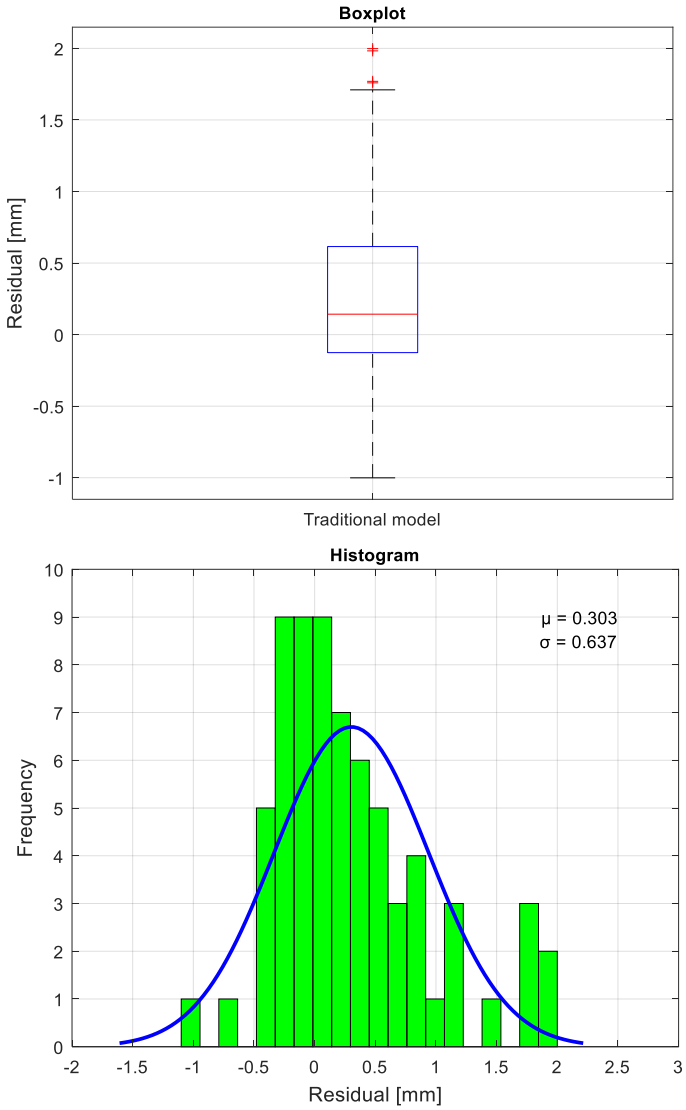

Figure 4.5. Residual of the conventional carbonation model: as a boxplot and histogram with a distribution fit.

the CaPrM. This demonstrated that the number of underestimate and overestimate predictions of the carbonation depth by the traditional model is considerably higher than the CaPrM. The histogram plot shows the histogram of the residuals with the best-fitting normal curve. It can be noticed that the shape of the histogram is asymmetric and skewed to the right direction. The estimated mean (μ) and standard deviation (σ) of the fitted normal distribution curve is 0.30 and 0.64, respectively. Unlike the

conventional model, the residual distribution of the neural network of the CaPrM is more closely resembles a symmetric normal distribution as can be seen in Figure 4.3. This shows that mean of the error is close to zero. All these facts confirmed the superiority of the CaPrM over the conventional model.

Though the traditional carbonation depth prediction model based on Fick's second law of diffusion is commonly applied, it is unable to provide accurate predictions as presented above. The main reason for this is that the dependence between concrete carbonation and its conditioning factors is inherently complex and time dependent. So, it is impossible or too complex to describe them mathematically. In the presence of readily available data, machine learning algorithms can characterize the carbonation process very well since it has the ability to learn the complex interrelation among the governing factors. Unlike the conventional model, machine learning based models are able to discover patterns that never been observed before.

4.3 Significance of chloride penetration controlling parameters

The third publication answers the research question three of the thesis, *"what are the significant parameters that describe the chloride concentration into concrete?"*. The influential parameters that describe the chloride profile were determined and evaluated using the developed chloride profile prediction model that was discussed in Section 3.5. The model is developed using bagging decision trees and employed long-term field experimental data that are acquired from the Finnish DuraInt-project. Ten models were established by utilizing diverse input dataset. In order to examine the importance of fresh and hardened concrete tests in predicting the chloride profile, the ten models were categorized into two groups: Model A and Model B. That is, Model A utilizes all the input variables whereas Model B excludes the fresh and hardened concrete test variables except chloride migration coefficient, D_{nssm}. The reason for keeping D_{nssm} in the dataset is that this parameter is considered as one of the best indicators of the resistance of the concrete to chloride ion ingression. Each group was further divided into three scenarios

employing: i) all the input variables, ii) all the input variables except distance from highway, and iii) all the input variables except exposure time. The model classification details can be referred from Table 3.6.

4.3.1 Chloride profile predictors using all variables

In this scenario, the training dataset consists of all the respective input parameters of the Models A and B. The parameter importance measures for both Models (A.1 and B.1) were performed and shown in Figure 4.6. It can be clearly seen from Figure 4.6 that the distance from highway is the primary parameter which controls the chloride profile in both models. This is the anticipated outcome since the quantity of chlorides splashed on the concrete surfaces heavily depends on the distance between the highway lane and the specimens. The nearer the distance the higher is the amount of the splashed chlorides. Next to distance from highway, compressive strength, cement content, total effective water, binder types, and exposure time are the five influential predictors in Model A.1. Even if this model comprises numerous parameters from fresh and hardened concrete properties, the discovered influential chloride profile predictors are from concrete mix ingredients. This demonstrated that the influence of advanced laboratory tests performed at early age is impotent in predicting the chloride profile holistically.

In the case of Model B.1, the significant parameters next to distance from highway are cement content, total effective water, binder types, exposure time, and w/b ratio. In both models, supplementary cementitious materials have the lowest influence in predicting the chloride concentration in concrete. Indeed, it is renowned that supplementary cementitious materials are mainly utilized to boost the resistance of concrete against chloride permeability because they can reduce the size of large pores and capillaries. However, they were not recognized as a significant chloride profile predictor since their types and quantities are already described by the binder types and w/b, respectively. The type of air-entraining agents is also appeared to be powerless for predicting the chloride concentration in concrete as confirmed by the results of Model A.1 and B.1. This parameter was classified based on their production name (due to the same reason mentioned in Section 3.4.1), and thus it appeared

as “AEA pro. name” in Figure 4.6. Though, the types of chemical admixtures generally influence the pore structure of concrete, the finding of this study confirmed that the air-entraining agent types (unlike type of plasticizers) do not affect the chloride permeability property of concrete. The utilized air-entraining agents in this dissertation were produced from either fatty acid soap or vinsol resin. So, it is worth to mention that this finding is only valid for the employed type of air-entraining agents, mix composition and exposure conditions. Other types of air-entraining agents may behave differently in concrete specimens exposed to the same or different environments.

In this scenario, the chloride migration coefficient (D_{nssm}) is recognized as a trivial parameter in predicting the chloride profile. The reason for this is that the chloride transport properties rely on the intrinsic permeability of the concrete, which is varying with time throughout the cement hydration process as well as based on the amount of chloride concentration

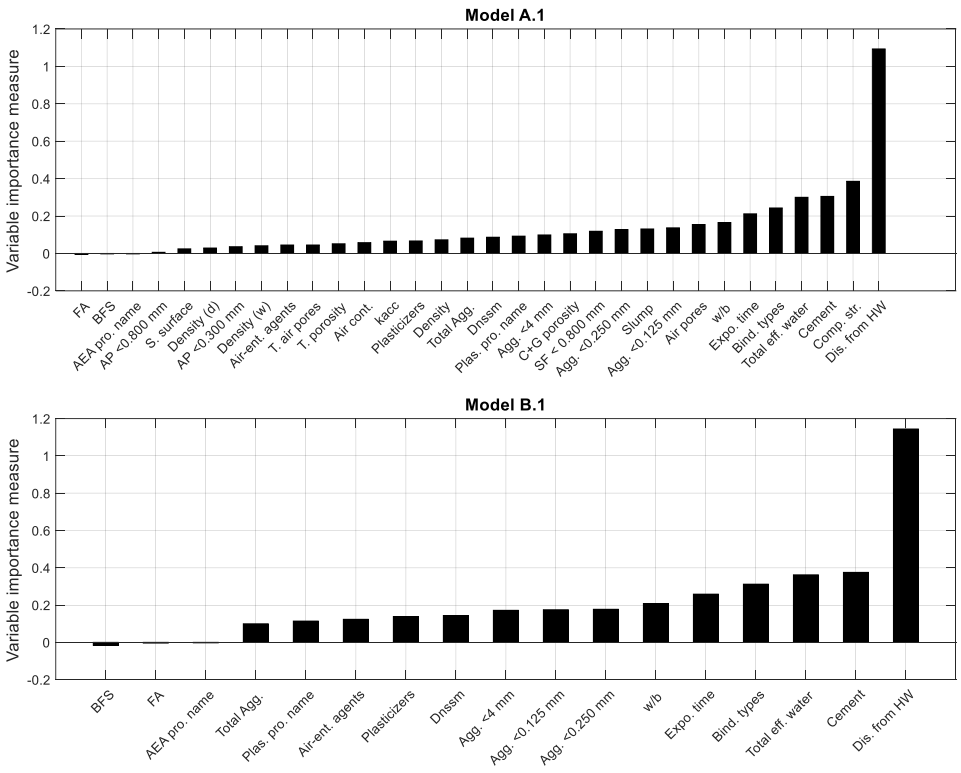

Figure 4.6. Variable importance measures of chloride profile for scenario one (Publication III).

in the pore solution. Additionally, the incorporation of chloride profiles quantified from specimens composed of various binder types and located at various distances with different exposure times diminish the significance of D_{nssm} in predicting concentration of chloride in concrete. Though D_{nssm} is the most widely adopted parameter to evaluate the resistance of concrete against chloride ingress, discovering it as an insignificant predictor is not a new phenomenon. There is a study based on long-term experiment that corroborates the inability of D_{nssm} obtained from accelerated lab test in characterizing the long-term chloride permeability of concrete exposed to real environmental conditions [148]. The power of D_{nssm} in describing the resistance of concrete against chloride ingress is evaluated in Section 4.3.2 and 4.3.3 by excluding the parameter distance from highway and exposure time, respectively.

4.3.2 Chloride profile predictors at fixed distance

In order to examine the significance of parameters independent of specimen's distance from highway, the chloride profile measured only at 4.5 m and all the respective input parameters of this scenario were employed in the dataset of Models A.2 and B.2. The choice of this distance is due to the presence of higher number of specimens at this distance, acquiring more chloride profile in the dataset. The top six most significant chloride profile predictors determined in this scenario are illustrated in Figure 4.7. It can be observed that the exposure time is the foremost powerful predictor of chloride concentration in concrete for Models A.2 and B.2 with importance measure of 0.43 and 0.44, respectively. The discovered six topmost significant chloride profile predictors have about 77% and 85% of the collective contributions to the ensemble Models A.2 and B.2, respectively. These are substantial percentage of contributions given the fact that the number of utilized input parameters for Model A.2 was 31 whereas for Model B.2 was 16. The variable importance measures of each corresponding parameters of the two models are comparable as can be seen from their rank in Figure 4.7. The importance variable measures of the top six significant chloride profile predictors with their percentile contribution for both models are presented in Table 4.4. As it can be noticed from Table 4.4, the exposure time has a relative

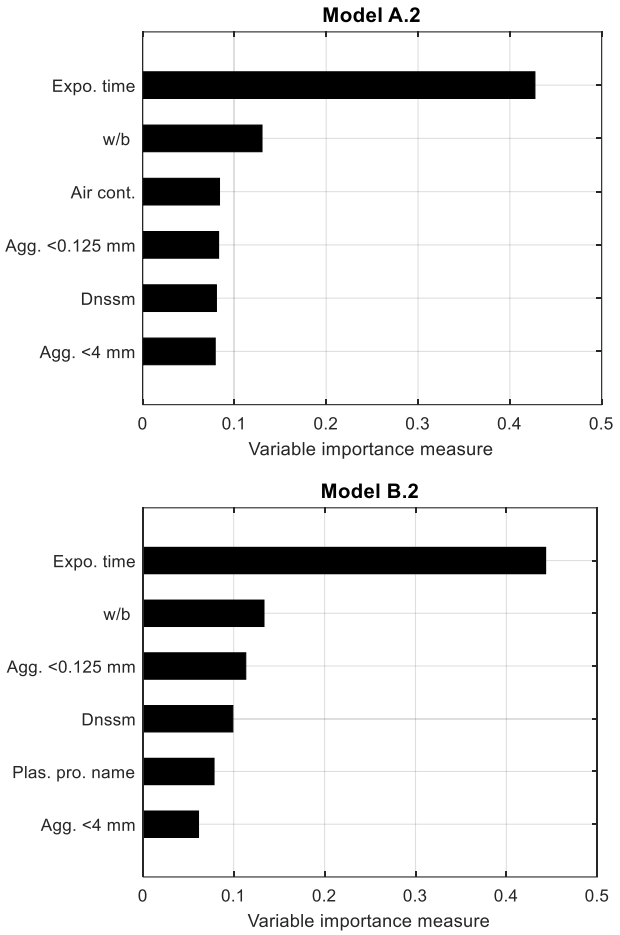

Figure 4.7. Variable importance measures of chloride profile for scenario two (Publication III).

contribution of 40.8% in Model B.2. The w/b parameter with a 12.3% contribution is the second leading variable. Aggregate <0.125 mm is the third predominant parameter that had 10.4% contributions to the chloride profile prediction. Cumulatively, 63.5% of the total influence is attributed by these three significant parameters. The D_{nssm}, plasticizers type, and aggregate <4 mm parameters are the next significant variables which represent 9.1%, 7.2% and 5.6% of contributions in predicting the amount of chloride concentration in concrete, respectively.

Unlike scenario one, the variable importance analysis demonstrated that the chloride migration coefficient (D_{nssm}) is among the six significant

Table 4.4. Importance measure of influential variables and their percentile contribution for Models A.2 and B.2 (Publication III).

Model A.2			**Model B.2**		
Variable name	VI measures [-]	Contribution [%]*	Variable name	VI measures [-]	Contribution [%]*
Expo. Time	0.4273	37.62	Expo. time	0.4431	40.78
w/b	0.1300	11.45	w/b	0.1333	12.27
Air cont.	0.0837	7.37	Agg. <0.125 mm	0.1133	10.43
Agg. <0.125 mm	0.0828	7.29	D_{nssm}	0.0991	9.12
D_{nssm}	0.0804	7.08	Plas. pro. Name	0.0784	7.22
Agg. <4 mm	0.0790	6.96	Agg. <4 mm	0.0613	5.64

*compared with the total contributions of all input variables utilized in respective models.

chloride concentration predictors in both models. The most probable reason for this is that the distance from highway lane is fixed, and thus the amount of the splashed surface chloride is identical for all the specimens included in the models. Despite the same amount of splashed surface chloride, the amount of chloride concentrations in the concrete specimens varies because of the continuous chemical reaction of chlorides with the dilute cement solution. Thus, discovering the D_{nssm} as a significant predictor confirms that it is a function of the amount of chloride at the concrete surface. The other laboratory test which is identified as a powerful chloride profile predictor by Model A.2 is the air content. Discovering the air content as a potential chloride profile predictor by Model A.2 out of the considered 16 types of fresh and hardened concrete tests is an interesting finding. The air content test was carried out on fresh concrete using pressure method in accordance with EN 12350-7 [149]. All the concrete specimens considered in this study employ air-entraining admixtures. The discovery of the air content as a powerful predictor indirectly represents the air-entraining admixtures since the air content is largely controlled by this admixture. Though the purpose of this admixture is to improve the resistance of the concrete against frost attack, it also influences the chloride ingress into the concrete. Even if very little research has been performed on understanding the effect of air-entraining admixtures on chloride transport, there is a study which demonstrates their power in controlling the transport processes of gases and ions into the concrete [150]. The finding of only air content as influential predictor out of the considered 16 types of fresh and hardened concrete tests demonstrates that several advanced laboratory tests executed at early age are

insignificant in predicting the chloride concentration in concrete in this scenario.

Among the parameters that describe the concrete mix ingredients, w/b and aggregate size distribution appeared to be the leading influential predictors of chloride penetration into the concrete pores. The reason for this is that w/b and aggregates govern the pore structure of the cement paste and thus influence the chloride ion transport properties. It is a well-known fact that chloride transportation in concrete through aggregates is trivial since aggregates that are used to produce concrete are generally dense. Nonetheless, at the interfacial transition zone (ITZ) where the cement paste in the vicinity of aggregate surface exhibits lower cement content and higher porosity compared with the cement paste in areas far away from the aggregate. The ITZ covers a considerable portion of the total cement paste volume and governed by the aggregate size distribution [16,151]. This may explain why aggregate size distribution influences the chloride transport property of concrete. Parameters that describe the concrete mix ingredients such as the type of cement, the supplementary cementitious materials, and the chemical admixtures are not discovered as powerful predictors by Model A.2. This is due to the fact that their effect is already explained by the air content since this test is predominantly governed by the type and amount of cement, the supplementary cementitious materials, and the chemical admixtures.

It can be observed that the type of plasticizers is determined as a significant predictor by Model B.2. This model considers only parameters from concrete mix ingredients and D_{nssm}. The identified parameter (type of plasticizers) is appeared as “plas. pro. name” in Figure 4.7 since product name of concrete admixtures were applied to classify them. The plasticizers applied in the concrete mix were based on Polycarboxylate, Melaminsulfonate or Polycarboxsylate Ether. The discovery of type of plasticizers as a predominant chloride profile predictor is an interesting finding. This parameter is not considered in the conventional chloride concertation prediction models. Indeed, there are several studies which demonstrated that plasticizers alter the pore characteristics of the hardened concrete. But the effect of type of plasticizers on chloride permeability is still insufficiently studied. There is a study based on short-term test that confirm the same finding [152].

4.3.3 Chloride profile predictors at three different ages

The intention of this scenario is to examine the effect of the input parameters in characterizing the chloride profile at particular exposure times. The determined top six parameters that describe well the penetration of chloride into concrete at various years of exposure are illustrated in Figure 4.8. Similar to scenario one, distance from highway is the leading significant parameter in both models, Model A.3 and B.3. In fact, this is the anticipated result as the chloride profile is highly dependent on the amount of chloride at the concrete surface. Next to distance from highway, the compressive strength, the total effective water and the cement content are the three powerful chloride profile predictors identified by Model A.3 at one, three, and six years of exposure. It is well understood that the chloride permeability of concrete depends predominantly on the porosity and interconnectivity of the pore system in the concrete. The above identified three parameters directly/indirectly govern the porosity and interconnectivity of the pore system, and thus their selection as chloride profile indicators are evident. The amount of the total effective water and cement are also identified as powerful predictors of chloride profile by Model B.3 at all age groups. The influence of these two parameters in describing the chloride permeability is recognized by numerous studies and used in conventional models. They are commonly represented as water-to-cement ratio (w/c). In all models, the w/b ratio was employed as one of the training input parameters but not as w/c since different type of supplementary cementitious materials, including blast-furnace slag and fly ash were utilized to produce some of the concrete specimens. Identifying the w/b as one of the influential predictors indirectly demonstrates that the supplementary cementitious materials are powerful in predicting the chloride concentration in concrete. As the number of occurrences of blast-furnace slag and fly ash are limited in the original dataset, the model recognized the cement amount and the total effective water as more powerful chloride profile predictors than the w/b.

It can be noticed from Model A.3 (i) that the amount of plasticizers and the binder types are among the influential chloride profile predictors for concrete specimens. When the exposure time is increased from one to three and six years, the power of plasticizers as a predictor to evaluate the

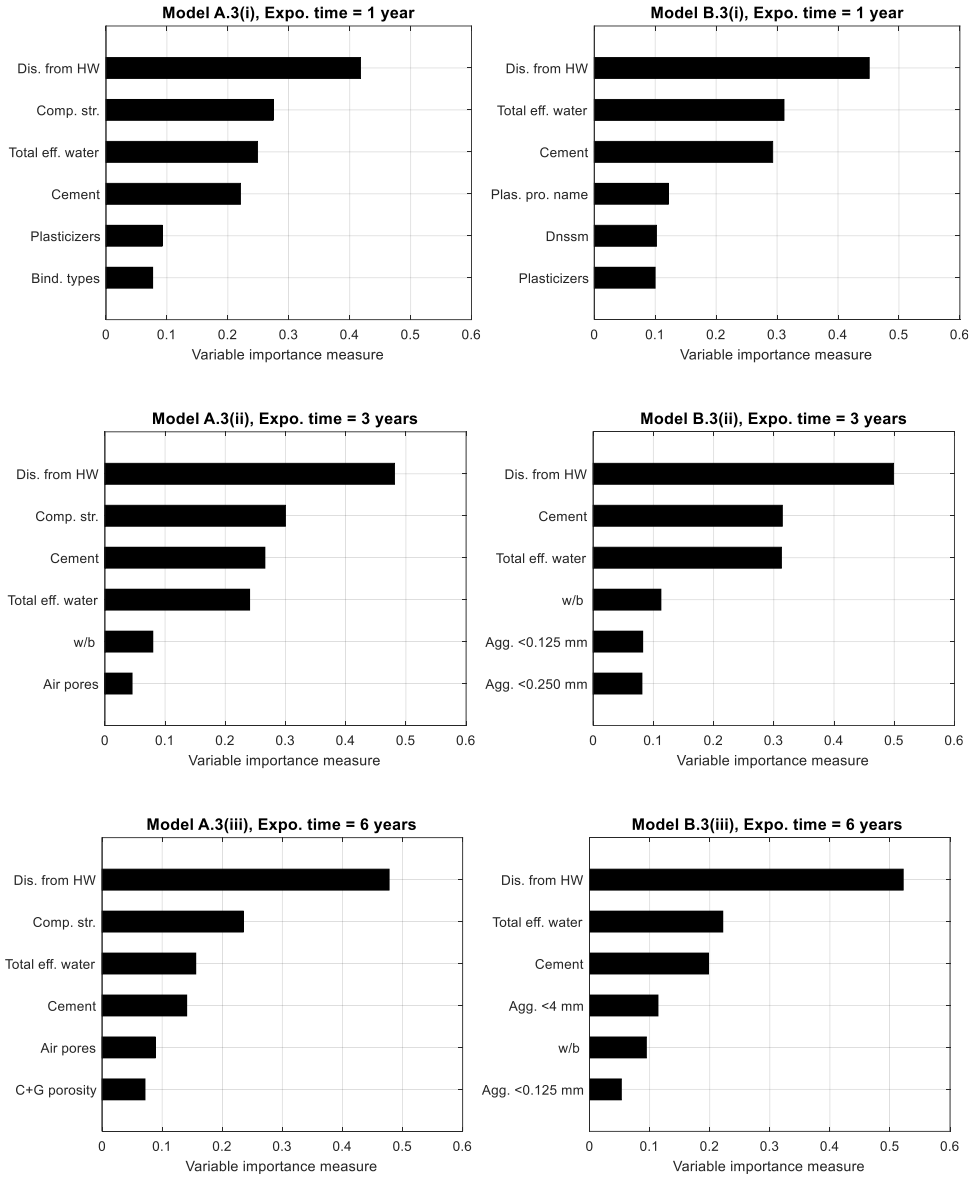

Figure 4.8. Variable importance measures of chloride profile for scenario three (Publication III).

chloride resistance of concrete has vanished. In case of Model A.3 (ii) and A.3 (iii), air pores as well as capillary and gel porosity from concrete properties are determined as significant predictors. Though these two models have considered 18 types of fresh and hardened concrete properties, only those that describe the strength and the air void of the

hardened concrete were discovered as influential chloride profile predictors. The chloride migration coefficient which is commonly used as an indicator of chloride permeability of concrete is not among the identified influential predictors.

The variable importance measure of Model B.3 revealed that the amount and type of plasticizers and the D_{nssm} are among the influential descriptor of the chloride profile at one-year exposure than older ages. The supplementary cementitious materials appeared to be more informative for describing chloride ingress into concrete pores at three and six years of exposure but not at earlier age. The utilization of supplementary cementitious materials in concrete alters the kinetics of hydration. This change modifies the microstructure of the concrete, and thus changing its long-term durability properties [153–155]. This reason explains why the supplementary cementitious materials characterize the chloride concentration at older ages. As in supplementary cementitious materials, the importance of the aggregate size distribution in predicting the chloride profile also appeared to be less significant at the age of one year. For example, three predictors representing aggregate size distribution (Agg. <0.125 mm, Agg. <0.250 mm, and Agg. <4 mm) got importance ranks of 11^{th}, 12^{th} and 13^{th}, respectively in Model B.3(i). Whereas they got 5^{th}, 6^{th} and 9^{th} in Model B.3(ii), and 4^{th}, 6^{th} and 8^{th} in Model B.3(iii). Some of the parameters are not shown in Figure 4.8 since it consists only the top six predictors due to readability reason. These three aggregate size distributions contribute about 7%, 13%, and 15% in predicting the chloride penetration at the age of one, three, and six years, respectively. This can be described by the alteration of the ITZ properties over time.

The significance measure of the aggregate size distribution and the aggregate content on concrete exposed to deicing environment at specific exposure times that are determined by the developed model is illustrated in Figure 4.9. In Model A.3 (utilizes all input parameters), it can be observed that the contribution of the aggregate size distribution in describing the ingression of chloride ions into concrete has increased with exposure time. In Model B.3 (employs all parameters from concrete mix ingredients, distance from highway and D_{nssm}), the influence of the aggregate size distribution is insignificant at earlier age than exposure time of three and six years. However, the reverse phenomenon has been

observed in case of aggregate content in both models with even negative importance measure at later age. This demonstrates that after some years of exposure, aggregate content does not have a predictive power to determine the chloride concentration in concrete. There are studies that concluded the aggregate content influences the chloride penetration into concrete but not the aggregate size distribution [16,17]. But they come up with this finding by validating the model with mortars exposed to chloride for short term, three weeks and 15 months. The evaluation at one-year exposure time in Figure 4.9 also shows aggregate content influences the chloride penetration more than the aggregate size distribution, but it is the opposite at three and six years of exposure. In addition to the aggregate size distribution, findings of Publication III revealed that utilization of supplementary cementitious materials in concrete production plays a role in characterizing the chloride penetration into concrete at later age. Hence, all these confirm that generalizing results that are acquired from short-term laboratory/field examination is inappropriate.

In another perspective, the findings of this scenario confirmed that D_{nssm} derived from the chloride profile at early age is not always describing the chloride profile of concrete. Though this property is widely applied as a durability indicator, it appeared to be impotent to describe the chloride permeability of concrete in the case of Model A of this scenario where a range of fresh and hardened concrete properties were considered for training the model. But the D_{nssm} becomes a significant descriptor at the age of one year in the case of Model B of this scenario where only the concrete mix ingredients and the D_{nssm} were considered for the model training. This proofs that best indicators of chloride permeability of concrete determined from short-term experiment are not always powerful predictors. Similar to scenario two, the aggregate size distribution, the amount and type of plasticizers and the supplementary cementitious materials were discovered as best indicators of chloride profile of concrete. These parameters are missed in the conventional chloride concentration prediction models.

Overall, distance from highway, compressive strength, total effective water and cement content are the top four best predictors of chloride profile in all age groups identified by Model A.3. These parameters, except compressive strength, are also among the top three influential predictors

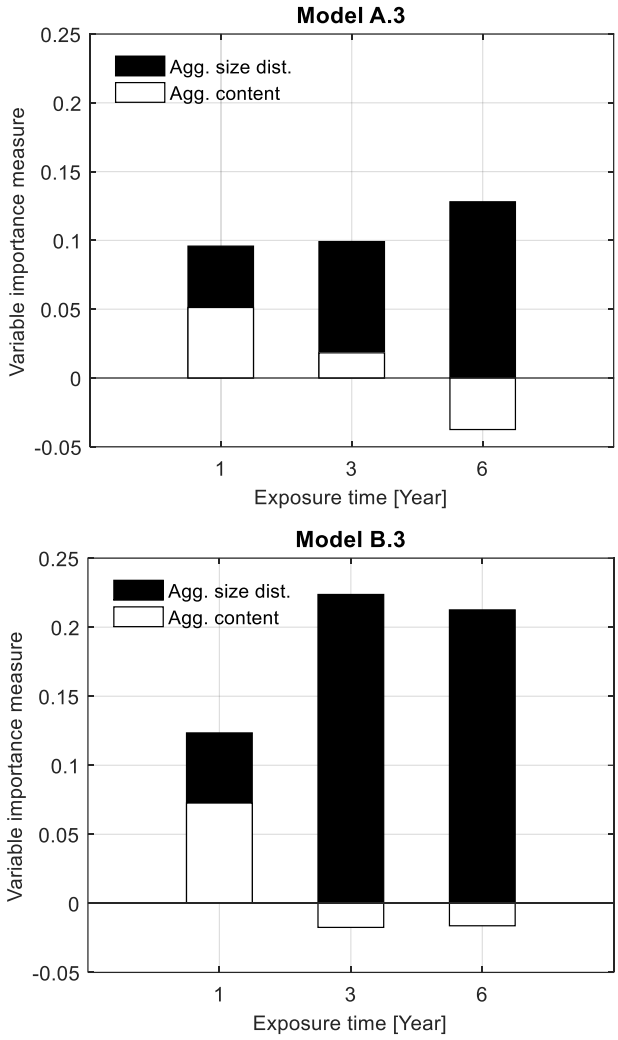

Figure 4.9. Significance measure of aggregate size distribution and aggregate content with respect to exposure time in Models A.3 and B.3 (Publication III).

of chloride ingress in all age groups in case of Model B.3. The remaining significant predictors identified by each model are varying at each exposure time. Indeed, it is well known that transport of chloride ions into concrete pores decreases with exposure time due to the change in microstructure. Even depending on the exposure condition, the chloride ions may leach out from the concrete pores, which in turn lessen the chloride concentration. For instance, 45% of the cases utilized in this scenario showed that the chloride profiles measured at one year of

exposure is larger than those after three years of exposure. Similarly, 39% of the concretes exposed to six years had lower chloride concentration than those exposed only for three years. Even, 35% of the cases revealed that the chloride profile after six years of exposure is lower than those after only one year of exposure. This may explain why some of the discovered predictors are varying at different exposure time and the complexity of chloride profile predictions.

4.3.4 Evaluating prediction power of the influential parameters

The contribution of the determined top six influential parameters in predicting the chloride penetration in all the above three scenarios was evaluated using unseen data. The evaluation was carried out using the respective models of the scenarios by employing three input data categories. In the first category, the inputs were all parameters presented in Table 3.5. The second category entails the top six significant parameters that were determined by the ensemble method in their respective models. In the third category, the most widely utilized parameters in the classical models (cement content, total effective water, chloride migration coefficient, exposure time and distance from highway lane) were employed. The contributions of the parameters considered in the three categories were evaluated using the MSE of the ten models. The MSEs of the models for all the three categories are given in Table 4.5. These MSE values are average of ten iterations. It can be recognized from Table 4.5 that the MSEs of all models which consider the top six significant parameters (second category) is smaller compared with the first category. The decrement in MSEs is noticeably large except in case of Models A.2 and B.2. This result demonstrates that the use of several parameters does not warrant accurate predictions. It is also recognized that the MSEs of all models with top six influential parameters is smaller than the MSEs of the third category except Models A.2 and A.3(i). For example, 19% reduction in MSE is perceived in Model B.3(iii) of the second category compared to that of the third category. In the same model, the second category achieved 34% less MSE than the first category. This proofs that data-driven models that take into account the influential parameters have the ability to provide a more accurate chloride-profile prediction.

Table 4.5. Chloride profile prediction models' error on the three categories (Publication III).

Model names	Mean-square error		
	Category 1	Category 2	Category 3
A.1	1.43E-04	1.21E-04	1.37E-04
B.1	1.37E-04	1.18E-04	1.35E-04
A.2	1.70E-04	1.64E-04	1.58E-04
B.2	1.60E-04	1.52E-04	1.59E-04
A.3(i)	8.66E-05	7.29E-05	6.93E-05
A.3(ii)	2.31E-04	1.62E-04	1.67E-04
A.3(iii)	4.10E-04	3.01E-04	3.36E-04
B.3(i)	8.66E-05	7.26E-05	7.80E-05
B.3(ii)	2.30E-04	1.62E-04	1.69E-04
B.3(iii)	3.75E-04	2.80E-04	3.33E-04

4.4 Hygrothermal behaviour prediction

In this section, the results of Publication IV which answers the research question four, "*how to predict the hygrothermal interaction inside surface-protected concrete while identifying the appropriate surface-protection system?",* are discussed. As presented in Section 3.6, the surface-protection systems were applied on the five outermost layer of the façade elements of the case structure and labelled as S1, S2, S4, S5, and S6. S1 and S2 are coated with cementitious materials, whereas S4, S5, and S6 are treated with organic coating materials that are obtained from different manufacturers.

The hygrothermal prediction model was developed by utilizing two years of the monitored data. The training performance of the model for predicting the relative humidity and temperature inside all surface-protected concrete façade members are illustrated in Figure 4.10 and Figure 4.11, respectively. It is clearly seen from Figure 4.10 that the performance of the applied surface treatments in controlling the relative humidity is varying. The relative humidity in S1 and S2 is largely above 90% and 80% respectively, whereas in S5 and S6 it is above 70%. The relative humidity in S4 is mostly in the range between 60% and 100%. The temperature interaction in all façade members are almost in the same range as seen in Figure 4.11. It can also be observed that the correlation coefficients (R-values) for the prediction of the inner relative humidity and

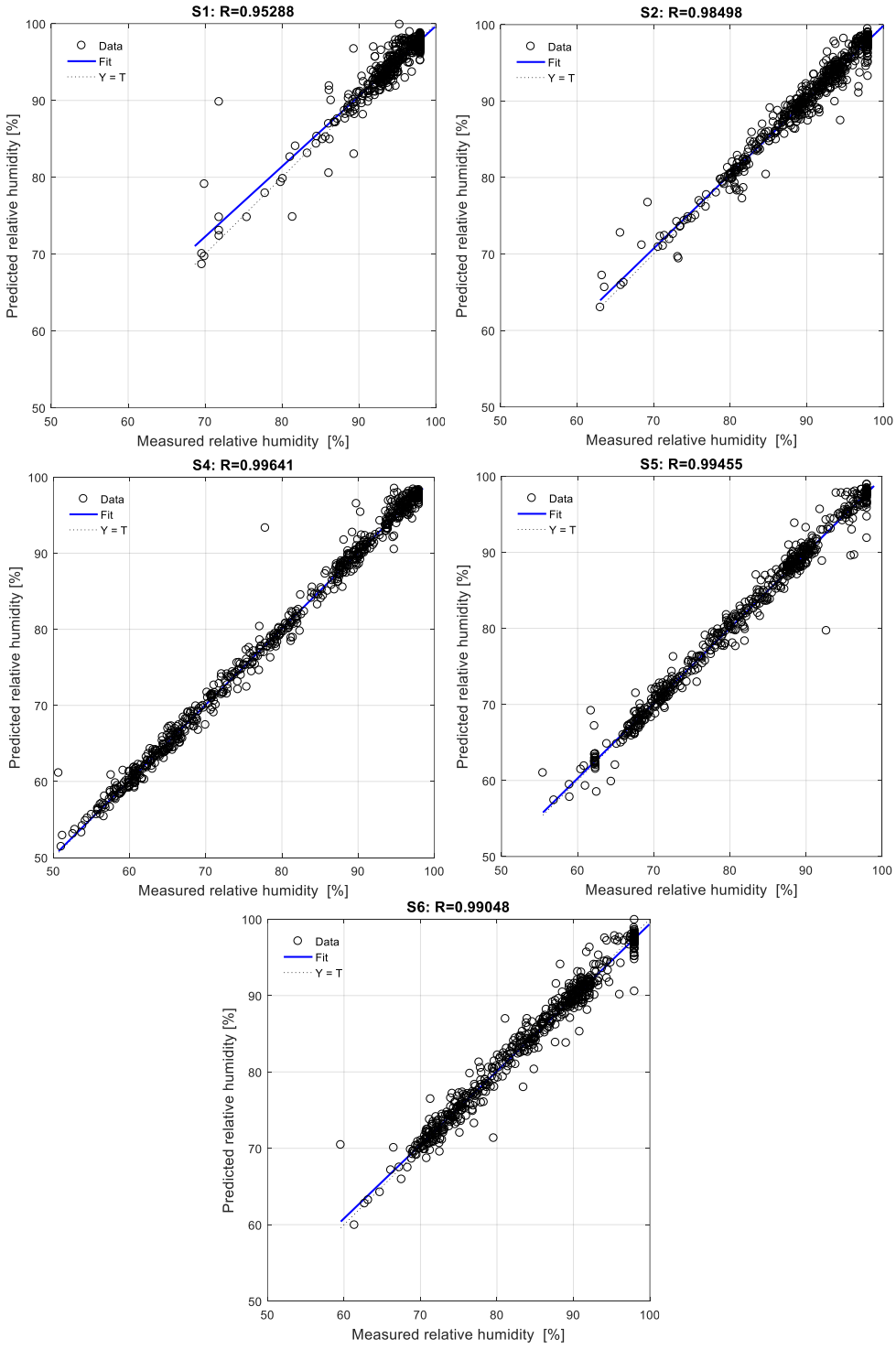

Figure 4.10. Training performance of hygrothermal model: inner relative humidity. Y and T are predicted and measured, respectively.

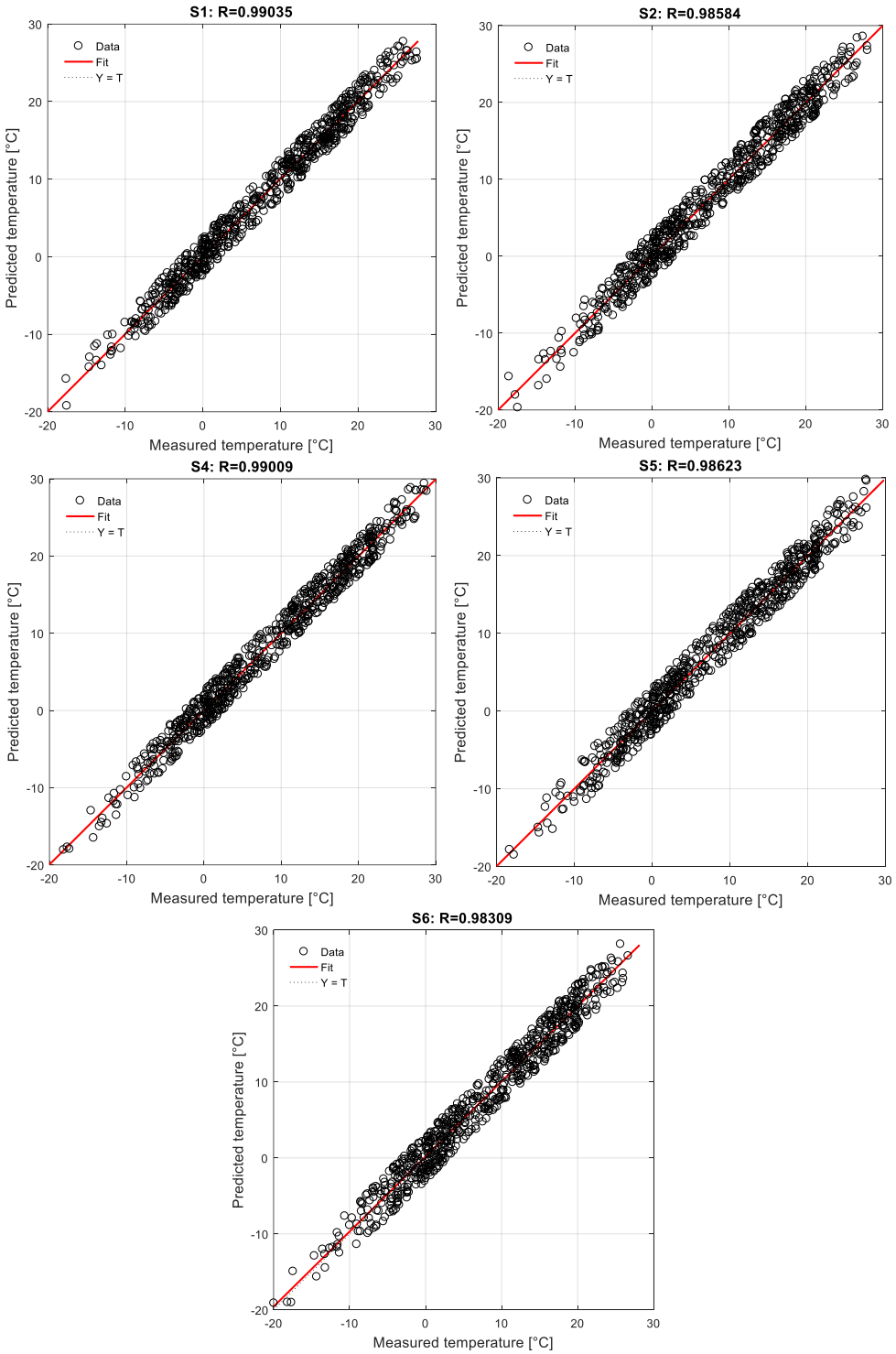

Figure 4.11. Training performance of hygrothermal model: inner temperature. Y and T are predicted and measured, respectively.

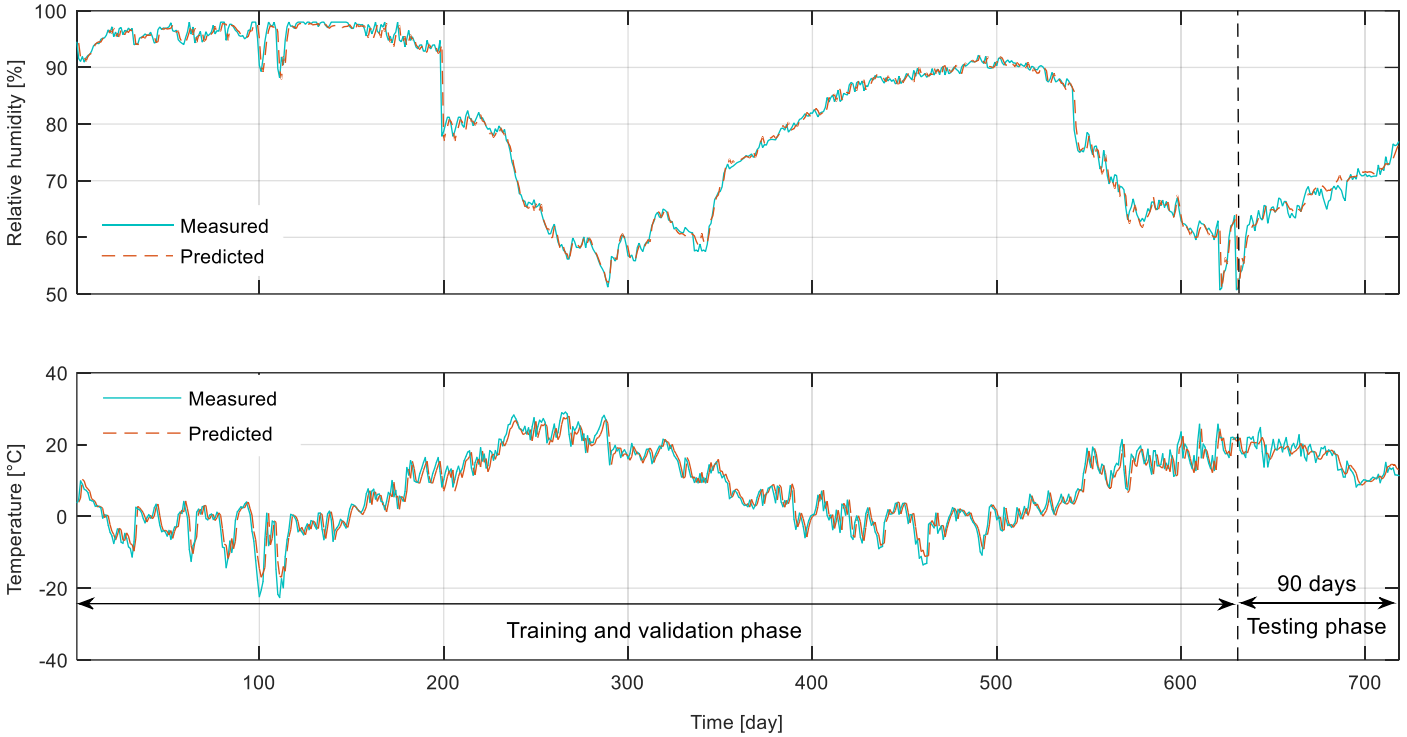

Figure 4.12. Predicted hygrothermal performance of the façade element S4 (Publication IV).

temperature for all façade elements are close to one. This demonstrates that the developed model, during the training phase, track effectively the actual measured relative humidity and temperature inside the surface-protected concrete façade members.

The validity of any successfully trained machine learning based model is evaluated based on their generalization capability. Such a model should be able to perform well when it is presented with unseen data within the range of the input parameters that are utilized during the model training phase. The performance of the developed hygrothermal models in predicting the inner hygrothermal behaviour were tested using the unseen datasets of the ambient relative humidity and temperature which covers the measurements of the last 90 days. The measured and the predicted relative humidity and temperature in concrete façade element S4 is illustrated in Figure 4.12. It can be seen that the predicted relative humidity and temperature are almost similar with the actual ones. The MSE of the predicted inner relative humidity and temperature were 7.89 and 2.44, respectively. The MAE of the predicted relative humidity and temperature were 4.04 and 0.89, respectively. As the MAE value has the same unit as the data, the average errors of the relative humidity and the temperature are about ±4% and ±0.89 °C, respectively. The MSEs and MAEs of the temperature are smaller than the relative humidity since the ambient temperature does not fluctuate extensively unlike the ambient relative humidity. Overall, the test results confirmed that the developed model predicts the hygrothermal behaviour inside surface-protected concrete façade element with rationally low error despite some missing data in the training dataset.

The test errors of the developed hygrothermal models for each concrete façade elements are presented in Table 4.6. These values are the average of ten statistical measures for each façade element. Although the model development principles are identical, each model was optimized for each façade elements because their hygrothermal behaviours are dissimilar due to the difference in the applied surface-protection materials and methods. The lower the value of the error statistics (MSE, RMSE, and MAE) is the better the prediction accuracy of the model. The small MSE values of the predicted relative humidity and temperature confirm that the developed model has high generalization capability. It can be observed from Table

Table 4.6. Statistical performance measurement of the developed hygrothermal prediction model on test dataset (Publication IV).

Façade element	MSE		MAE		RMSE	
	Relative humidity	Temperature	Relative humidity	Temperature	Relative humidity	Temperature
S1	3.5074	2.8867	5.0236	0.7265	1.8728	1.6990
S2	4.3062	2.7960	4.4686	0.7756	2.0751	1.6721
S4	5.8039	2.8320	3.9995	0.8875	2.4091	1.6829
S5	4.0053	2.5812	4.1923	0.8125	2.0013	1.6066
S6	3.9371	2.5936	4.4386	0.6289	1.9842	1.6105

4.6 that the MSE, MAE and RMSE of the temperature are smaller compared to their corresponding values of the relative humidity. The MSE and RMSE of the temperature are almost equal for all façade members. Though the error measures for each façade elements are different, the error values are generally low which proof the suitability of the developed model for examining the hygrothermal performance in surface-protected concrete façade elements.

The developed data-driven hygrothermal prediction models were able to learn the hygrothermal interrelation inside surface-protected concrete façade elements using data obtained from sensors and perform fairly accurate prediction without the need for other mathematical solutions. The prediction allows to perform a pragmatic evaluation of the case structure in order to make rationally accurate schedule for maintenance measures, which in turn lessens the associated costs remarkably. With the availability of long period of measured hygrothermal data, the performance of the developed models adaptively enhances and thus able to generate more long-term predictions. In addition, increasing the number and types of the monitored structures that are situated in different locations results in getting more divers data that help to make the model results to be applicable for a wide range of cases.

4.4.1 Corrosion status of façade elements

In order to determine the protection performance of the applied surface-treatment systems against corrosion of reinforcement bar, the correlation between the hygrothermal and the corrosion rate is needed. The corrosion rate of the embedded reinforcement bar can be computed using Equation (4.4) [156–158].

$$r = C_T r_o, \tag{4.4}$$

where r is the rate of corrosion [µm/year], C_T is the temperature coefficient, and r_o is the rate of corrosion at +20 °C [µm/year]. C_T and r_o are time-variant variables which are dependent on the temperature and relative humidity inside the concrete, respectively. For carbonated concrete, C_T and r_o can be described by Equations (4.5) to (4.7) [156,158].

$$C_T = 1.6 \cdot 10^{-7}(30 + T)^4, \tag{4.5}$$

$$r_o = 190 \cdot (RH)^{26} \text{ when } RH \leq 0.95, \tag{4.6}$$

$$r_o = 2000 \cdot (1 - RH)^2 \text{ when } RH > 0.95, \tag{4.7}$$

where T is the inner temperature [°C] and RH is the inner relative humidity [%] of the pore structure.

The corrosion rate was computed by employing the measured and the predicted hygrothermal data only for the last one year of the data. The computed corrosion rate values are translated to corrosion status based on the classification (passive, low, moderate, and high) as given in Table 4.7, [159,160]. The corrosion state of the last one year is visualized by utilizing the developed exploratory data analysis technique (Section 3.7) and it is illustrated in Figure 4.13. The developed data exploratory method helps to easily visualize the corrosion status of the façade elements throughout the year. The unidentified amount of the corrosion rate due to the malfunction of the hygrothermal probes in the reference concrete façade member is left blank in the figure (white colour). It can be noticed from Figure 4.13 that the state of corrosion analysed using the monitored and the predicted data is almost identical. In both situations, the corrosion status for the concrete façade members S4, S5, and S6 is low and passive, whereas for S1, S2, and

Table 4.7. Classification of corrosion status.

Corrosion rate [µm/year]	State of corrosion
< 1	Passive
1- 5	Low
5-10	Moderate
>10	High

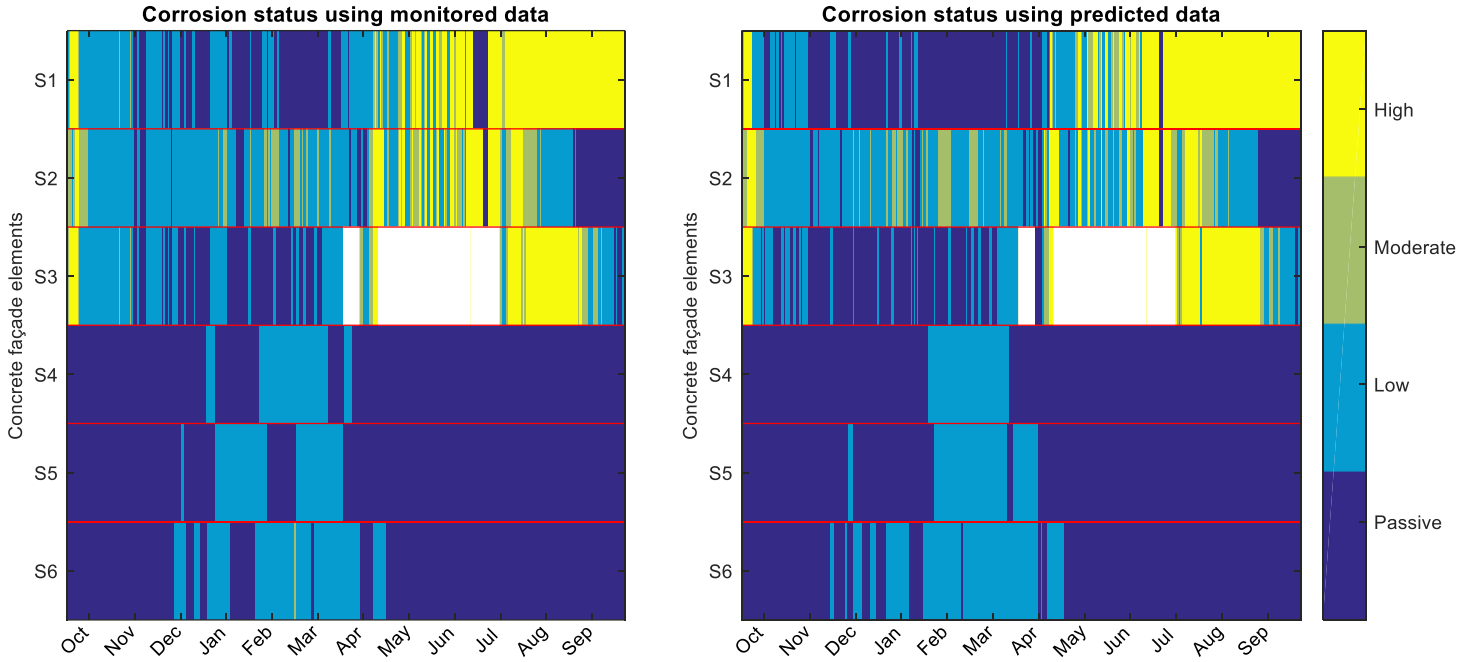

Figure 4.13. Corrosion statuses of the concrete façade elements (Publication IV).

S3 it ranges from passive to high. Among all the façade elements, S1 and S2 provide poor protection against the progression of corrosion. Even if the surface of both façade elements were coated by the same materials from different manufacturers, the coating applied on façade element S1 offers the poorest protection. This reveals that not only the type of the coating materials but also their source and/or application technique has influence on the protection performance of the coating. It can also be observed that the corrosion status is varying within a short period of time in façade elements S1 and S2. This demonstrates that corrosion rate prediction based on the traditional instantaneous electrochemical measurement may under or overestimates its value. Hence, implementation of a long-term hygrothermal monitoring and modelling strategy is essential.

4.4.2 Status of frost and chemical attacks

As discussed in Section 2.2.2, surface-protection systems are commonly applied on the surface of RC structures to protect the corrosion of reinforcement bar since they act as a physical barrier preventing the penetration of moisture. Nevertheless, some of the applied surface-protection systems may cause other type of deteriorations unintentionally. Due to this, the effectiveness of the surface-protection systems was evaluated by considering the effect of moisture on frost and chemical attacks. To analyse these attacks, four risk levels were defined (insignificant, slight, medium, and high) as in [28] and presented in Table 4.8.

The sensitivity of the surface-treated concrete façade elements for frost and chemical attacks on the second year was analysed using the monitored and the predicted data based on the defined risk levels. It is visualized

Table 4.8. Risk level classification of frost and chemical attacks.

Effective relative humidity	Risk levels	
	Frost attack	Chmical attack
Very low (RH < 45%)	Insignificant	Insignificant
Low (RH = 45-65%)	Insignificant	Insignificant
Medium (RH = 65-85%)	Insignificant	Insignificant
High (RH = 85-98%)	Medium	Slight
Saturated (RH > 98%)	High	High

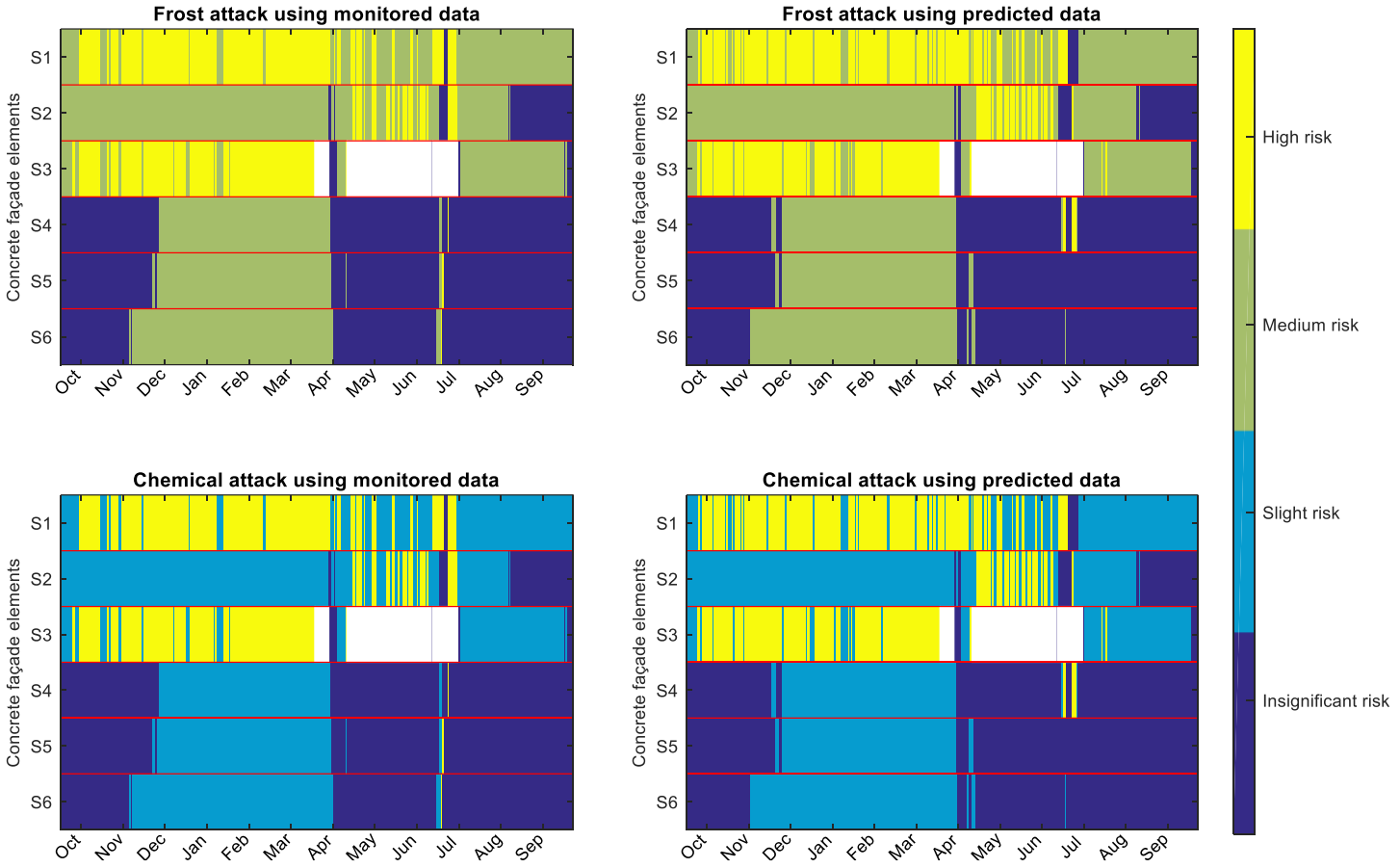

Figure 4.14. Statuses of frost and chemical attacks of concrete façade elements (Publication IV).

using the developed exploratory data analysis method and illustrated in Figure 4.14. The unknown deterioration risk levels caused by the failure of the hygrothermal probes in the reference façade element is left blank and represented in the figure by white colour. It can be noticed from Figure 4.14 that the sensitivity differences between the monitored and the predicted data are inconsiderable for both type of attacks. Organic coatings outperform the cementitious ones in protecting the concrete elements against frost and chemical attacks while hindering the rate of corrosion. The cementitious coatings applied on the surface of S1 and S2 façade elements are ineffective in defending the concrete against frost and chemical attacks. Coating applied on surface of S1 is less protective than S2. This confirmed that the coating application techniques and their source influence the performance of the surface treatment in protecting against corrosion as well as frost and chemical attacks.

Chapter 5

Discussion

This chapter presents the implications of the dissertation findings as well as the reliability and validity of the undertaken research. It also discusses recommendation for future research directions. The discussion of theoretical and practical implications of the research to the scientific community, society and companies is necessary in order to facilitate the transfer of the discovered knowledge and methodologies. Assuring the reliability and validity of the research is vital in order to confirm the credibility of the findings of this dissertation.

5.1 Theoretical implications

As discussed in Chapter Two, the conventional models that predict the carbonation depth and the chloride concentration in concrete rely on limited parameters. Clear understanding of the significance of all involving parameters that describe the carbonation process and the penetration of chloride ions into concrete is critical in order to develop reliable and reasonably precise prediction models. The research results of this dissertation have established methods for prediction of carbonation depth and the ingression of chloride ions into concrete as well as measuring of parameters significance. These methods are based on machine learning techniques.

The findings based on the developed method of parameters significance measure revealed that accelerated carbonation depth, w/b and compressive strength are the three foremost powerful predictors of the carbonation depth. These are well recognized parameters and have been considered in the conventional models. The next three determined carbonation depth predictors are the amount of plasticizers, the carbonation period, and the air content. This is an interesting finding since these parameters, except the carbonation period, are overlooked in various conventional models. This finding is supported by the previous works [143,144]. These earlier researches claimed that different types of

plasticizers govern the carbonation resistance of concrete through their influence on the pore structure and the morphology of the hydrated product. The research results of this dissertation also highlight the importance of air-entraining admixtures in characterising the carbonation process. Though the main purpose of air-entraining admixtures is to improve the resistance of the concrete against frost attack, it also affects the carbonation process. In fact, the discovered parameter by the CaPrM was the air content. This parameter can explain the effect of air-entraining admixtures as they heavily controlled it. The finding of air-entraining admixtures as influential descriptor is complemented by earlier researches [145,146]. These researches were made on concrete specimens of different mix compositions exposed to indoor and outdoor environments. They pointed out that the air-entraining admixtures increase the carbonation resistance of concrete.

The discovered topmost powerful predictors of chloride penetration representing the mix composition of the concrete are cement content, amount of total effective water, aggregate size distribution, supplementary cementitious materials, amount and type of plasticizers. The cement content and the amount of total effective water (usually designated in the form of water-to-cement ratio, w/c) are taken into consideration in numerous traditional chloride concentration prediction models. Nevertheless, the aggregate size distribution is not considered in the conventional models and its role in describing chloride penetration into concrete is often controversial. There are earlier researches that concluded the aggregate content influences the chloride penetration into concrete but not the aggregate size distribution [16,17]. But they come up with this finding by validating the model with mortars exposed to chloride environment for short term, three weeks and 15 months. Indeed, the findings of this dissertation agree with [16,17] for the case of one year exposure but contradicting them at older ages (three and six years). In addition to the aggregate size distribution, the findings of this research revealed that utilization of supplementary cementitious materials in concrete production plays a role in characterizing the chloride penetration into concrete at later age. Contrary to the aggregate size distribution, the amount and type of plasticizers describe the chloride profile of concrete at one-year exposure than older age. All these findings confirm that

generalizing results that are acquired from short-term laboratory/field examination is inappropriate.

The dissertation discovered the amount and type of plasticizers as a predominant descriptor of the chloride profile. This parameter is not considered in the conventional chloride concertation prediction models. Indeed, there are several studies which demonstrated that plasticizers alter the pore characteristics of the hardened concrete. However, the effect of the type of plasticizers on chloride permeability is still insufficiently studied. The finding of the type of plasticizers as influential predictor of chloride profile is supported by previous study in [152]. The findings of this dissertation also showed that the air-entraining admixture influences the chloride ingress into the concrete. This parameter is not taken into an account by the conventional models. Even if very few researches have been performed on understanding the effect of air-entraining admixtures on chloride transport, the research in [150] is in line with the above finding.

Among several advanced fresh and hardened concrete properties, the compressive strength was determined as an influential descriptor of chloride concentration in concrete. This is not a new finding and it has been considered by several conventional models as a predictor. Next to this parameter, D_{nssm} was discovered as a predominant chloride profile predictor. The significance of this predictor is higher at earlier age than exposure time of three and six years. In scenario where a range of fresh and hardened concrete properties were considered, the findings revealed that the prediction power of D_{nssm} to describe the chloride profile has diminished. Other few properties that describe the pore volume of the concrete (air content, air pores as well as capillary and gel porosity) characterize the chloride concentration better than $D_{nssm.}$ All these facts demonstrate that several advanced laboratory tests executed at early age are insignificant in predicting the chloride concentration in concrete. In addition, the nonsteady-state chloride diffusion coefficient derived from the chloride profile at early age is not always describing the chloride profile of concrete.

All the above findings have important theoretical implications. The results of the developed data-driven models proof their ability in isolating the effect of particular parameters out of several interdependent complex corrosion causing parameters. Understanding the contribution of

parameters in predicting the carbonation depth and the chloride penetration could help researchers to focus their research on concrete materials that can resist well carbonation and chloride ingression. In addition, discovering the optimal influential parameters that best predict the carbonation depth and the chloride profile is critical in order to develop parsimonious and accurate model. In another perspective, the results of this dissertation serve as a show case for researchers to conduct similar scientific research on other concrete deterioration mechanisms by adopting data-driven models.

5.2 Practical implications

The penetrations of CO_2 and Cl^- into concrete are the predominant factors that initiate corrosion of reinforcement bar. Accurate estimations of the carbonation depth and the chloride concentration in concrete are crucial to make realistic decisions regarding the maintenance plan of RC structures. Establishing analytical models that fully represent the carbonation process and the chloride ingression is challenging. This is due to the complex nature of the degradation mechanisms as well as the availability of a wide variety of concrete mix types and exposure conditions. In another perspective, once the corrosion initiates, the rate of corrosion is primarily governed by the hygrothermal interaction through their influence on the electrochemical reactions. In this dissertation, data-driven models that evaluate the carbonation depth, chloride profile and hygrothermal behaviour were developed.

The carbonation depth and chloride profile prediction models were able to discover new influential parameters which were missed in the conventional models. The discovered useful knowledge could assist companies to produce concrete that has the ability to resist against carbonation and/or chloride attack. Using the developed models, the material engineer/concrete designer can evaluate the performance of the newly designed concrete against carbonation and chloride penetration. Both models can be applied to evaluate the depth of carbonation and the chloride profile anywhere as far as there is a readily available input data to train them. All these facts have huge economical implication to the society

since the models assist in designing optimal concrete mixes and defining proactive maintenance plan, which in turn minimize the lifecycle costs.

The developed data-driven hygrothermal model is a practical approach to evaluate the performance of surface-protection systems. This model along with the exploratory data analysis technique allows a more realistic evaluation of corrosion condition and other deterioration mechanisms caused unintentionally by the implemented surface-protection systems. In practice, this evaluation result helps the engineer/owner in choosing appropriate surface-protection system for the RC structure under consideration. As in any data-driven models, longer-term prediction becomes achievable when the amount of training data increases. This helps in determining the deterioration of the surface-protection materials well in advance, leading to proactive maintenance which ultimately saves the lifecycle costs substantially.

All the developed data-driven models are robust and reproducible with no or little effort by anyone who already has data or can acquire monitoring systems to collect data. The models with long-term data can be used to carryout corrosion assessment of structures accurately, which in turn enable to perform timed maintenance measures. Indeed, as presented in Section 4.1, with the advancement of sensing technologies, infrastructure of the next generation will integrate the physical infrastructures with cyber infrastructures which comprise wireless sensors, networks and computing devices. There is no doubt that data-driven based models presented in this dissertation will be the integral components of tomorrow's cyber-physical infrastructure systems. So, the developed models will play a substantial role in making proactive decisions and/or preparing short- and long-term plans to manage RC structures efficiently.

5.3 Reliability and validity

The reliability and validity of the research undertaken in this dissertation have been confirmed. All the findings of this research were deduced using the developed data-driven prediction models of carbonation depth, chloride penetration, and hygrothermal interaction. The validity of all the models was verified with unseen data and the verification outcomes have

proofed their high accuracy prediction capability. The reliability of all the models was validated by using different unseen/test dataset and analysing the residuals. Detail verification procedures of all the developed models are presented in Chapter Four. The resulting residuals of all the models fell within the acceptable range and demonstrated the high generalization ability of the models. To ensure the stability of the models that are developed to determine the significance of parameters, the whole processes were reiterated ten times and the average of the ten outputs were taken as a final result. Though, the averaged values were taken into consideration, the difference among the ten outcomes were insignificant. All these facts confirm that the research outcomes of this dissertation are reliable and valid.

Lack of spatially dispersed experimental data can be seen as limitations of this dissertation. The models that were developed to examine the significance of parameters in predicting chloride profile employ data obtained from concrete specimens which were located at Kotka, Finland. These specimens were placed in identical altitude and experience similar multi-deterioration actions throughout the field experiment period. Due to this, factors describing the boundary conditions of the concrete specimens, the amount and frequency of sprinkled deicing salt in the highway, the climatic situations, the altitude where the concrete specimens placed, the amount of carbon dioxide in the environment and the traffic density, are the same. It is obvious that these parameters play a significant role on the chloride penetration, and thus incorporating data from different field experiments could help to measure the importance of these factors. The same is also true in the case of the CaPrM. All the concrete specimens employed as input data for the CaPrM were placed at Espoo, Finland. The curing conditions and methods as well as the environmental situations for all concrete specimens were identical. Due to this, it was impossible to measure the importance of these parameters in predicting the carbonation depth. The data utilized in the hygrothermal model were also gathered from surface-protected concrete façade of a building situated in Vantaa, Finland. Except the applied coating materials and their application methods, all the conditions that govern the hygrothermal performance such as the concrete mix composition, the depth of concrete cover, and the curing condition of the concrete panels were identical. This

was the reason for considering only the hygrothermal data for model training. It would have been interesting if these parameters were different and able to evaluate their effect on predicting the hygrothermal performance of surface-protected concrete panels. In addition, the data come from a single structure, lacking consideration of different environmental conditions. This limits the application of the model results in a wide range of cases.

5.4 Recommendations for future research

In this thesis, the addressed degradation mechanisms that cause and control the corrosion of reinforcement bar are carbonation, chloride penetration and hygrothermal interaction. These degradation mechanisms were dealt separately using data obtained from three different case structures, one for each deterioration mechanism. In fact, the chloride penetration study was carried out using concrete specimens exposed to deicing salts as well as freezing and thawing. But the effect of freeze-thaw cycling was not separately studied due to lack of spatially disperse concrete specimens in the training dataset. In reality, all the described degradation mechanisms affect the corrosion of reinforcement bar simultaneously or consequently. It is a well-known fact that the influence of the synergic deterioration progresses faster and severe than the effect caused by any single degradation process. With the advancement of durability sensors, it will soon be practical to simultaneously monitor all the parameters which describe the degradation mechanisms in a single concrete element. In the future, it is highly recommended to monitor all corrosion causing and controlling mechanisms simultaneously in a single concrete element in both laboratory and field environments. In addition, data should be collected from spatially dispersed RC structures. Once data are available, it is possible to follow the same modelling approaches that were presented in this dissertation and the significance of various parameters involved in the synergic deterioration mechanisms on corrosion of reinforcement bar can be understood. After determining the influence of several complex interacting parameters on corrosion of reinforcement bar, more reliable and valid model can be established in order to assess the corrosion of reinforcement bar. This assessment helps

to define proactive maintenance plan that enable reduction of lifecycle costs. The discovered knowledge could also assist researchers and designers working in concrete durability to produce concrete that resist well these deterioration mechanisms.

Chapter 6

Conclusions

In this dissertation a data-driven framework for evaluating corrosion causing and accelerating factors in concrete structures is presented. The framework was realized through the developed data-driven carbonation depth, chloride profile and hygrothermal performance prediction models. By utilizing these models i) better prediction accuracy for all the models has been achieved; ii) previously overlooked influential carbonation and chloride predicting parameters have been discovered; iii) it has been discovered that the influence of some of the chloride profile predicting parameters vary significantly based on exposure time, and iv) efficient surface-protection materials that protect concrete façade elements from corrosion as well as chemical and frost attacks have been determined.

The thesis demonstrated that estimation of corrosion onset utilizing conventionally applied corrosion assessment methods in the form of analytical equations is uncertain since they are formulated by considering several simplifications and assumptions. The developed data-driven models mitigate uncertainties by mapping inputs (multiple complex corrosion controlling parameters) to the output that closely approximate the desired output values. The mapping was performed through learning algorithms that are capable of handling highly nonlinear interacting parameters with rational computational time. This allows evaluating all the influential parameters as a group rather than individually, which in turn ensures the reliability of the prediction since imperative dependencies are not overlooked.

The performance comparison of the developed carbonation depth prediction model with the conventional one confirmed the prediction superiority of the developed data-driven carbonation model. The error difference between the two was significant. The conventional one has about two-fold more MSE than the developed data-driven carbonation model. The performance analysis of the developed data-driven hygrothermal model revealed its prediction capability with low error. This data-driven approach is a better alternative method since understanding

the interaction of different surface-protection systems with the substrate concrete is a highly complex process. The integrated exploratory data analysis technique with the hygrothermal model had eased the challenge of selecting appropriate surface-protection materials that protect effectively from corrosion as well as chemical and frost attacks.

The developed carbonation depth and chloride profile prediction models discovered the best predictors of carbonation depth and chloride ingression by measuring the significance of all the considered input parameters. Among the input parameters, the amount of plasticizers and the air content are the most predominant carbonation depth predictors. These two parameters are overlooked in various conventional models despite few studies that demonstrate the effect of plasticizers in improving the carbonation resistance of concrete. In case of chloride penetration, the aggregate size distribution, the amount and type of plasticizers, and the supplementary cementitious materials are among the discovered influential predictors. These parameters are missed in the conventional chloride concentration prediction models. This finding corroborates that several advanced laboratory tests (except those describe the air-void characteristics of concrete) executed at early age are insignificant in predicting chloride concentration in concrete. This proofs that best predictors of chloride permeability of concrete determined from short-term experiment are not always powerful predictors in long term. By employing the determined influential parameters, the MSE of the chloride profile prediction was decreased by up to 19% compared to the results that employ only conventionally agreed variables. This improvement in MSE confirmed that the developed data-driven models have the capability of determining optimal subset of influential variables that best predict the chloride profile. In addition, the parameters importance measure revealed that the effects of supplementary cementitious materials are more pronounced at a later age, whereas chloride migration coefficient influences at earlier age. It also demonstrated that several of the early-age fresh and hardened concrete property tests are insignificant in describing the chloride ingression into concrete. This proofs that evaluation of long-term chloride transport into concrete using short-term tests is unrealistic.

Understanding the influential predictors help companies to produce optimized concrete mix that is able to resist carbonation and chloride

penetration and thus enable reduction of lifecycle costs. The same models can be applied to evaluate the performance of the newly designed concrete against carbonation and chloride penetration if they are exposed to similar conditions that are used in training the models. In addition, discovering the optimal influential parameters that best predict the carbonation depth and chloride profile assists researchers to develop efficient and parsimonious corrosion assessment models as well as focus their research on concrete materials that can resist well these deteriorations. Furthermore, the results of this dissertation serve as a show case for researchers to conduct similar scientific researches on other concrete deterioration mechanisms by developing data-driven models.

The developed models play substantial roles in making proactive decisions and/or preparing short- and long-term plans to manage RC structures efficiently. All the developed corrosion assessment models are robust and reproducible with no or little effort by anyone who already has data or can acquire monitoring systems to gather data. The prediction results of the models adaptively adjust depending on the input data (the composition of the case structure and exposure conditions). With the advancement of sensing technologies, the next generation infrastructure will have sensing systems integrated into them, making data driven based condition assessments the primary choice. Therefore, the presented data-driven framework will be one of the key components for smart aging management of RC structures.

References

[1] B. Yu, L. Yang, M. Wu, B. Li, Practical model for predicting corrosion rate of steel reinforcement in concrete structures, Constr. Build. Mater. 54 (2014) 385–401. https://doi.org/10.1016/j.conbuildmat.2013.12.046.

[2] M. El-Reedy, Steel-reinforced concrete structures: assessment and repair of corrosion, CRC Press, Boca Raton, FL, 2008. https://doi.org/10.1201/9781420054316.

[3] Y. Zhou, B. Gencturk, K. Willam, A. Attar, Carbonation-induced and chloride-induced corrosion in reinforced concrete structures, Mater. Civ. Eng. 27 (2015) 04014245(17). https://doi.org/10.1061/(ASCE)MT.1943-5533.0001209.

[4] G. Markeset, S. Rostam, O. Klinghoffer, Guide for the use of stainless steel reinforcement in concrete structures, Oslo, 2006.

[5] J.R. Mackechnie, M.G. Alexander, Repair principles for corrosion-damaged reinforced concrete structures, Department of Civil Engineering, University of Cape Town, 2001.

[6] S.L. Matthews, J.R. Morlidge, Performance based rehabilitation of reinforced concrete structures, in: M.G. Alexander, H.-D. Beushausen, F. Dehn, P. Moyo (Eds.), Concr. Repair, Rehabil. Retrofit. II 2nd Int. Conf. Concr. Repair, Rehabil. Retrofit. ICCRRR-2, CRC Press, Leiden, 2008: pp. 277–278. https://doi.org/10.1201/9781439828403.ch100.

[7] A.M. Vaysburd, P.H. Emmons, B. Bissonnette, Concrete repair: research and practice – the critical dimension, in: M.G. Alexander, H.-D. Beushausen, F. Dehn, P. Moyo (Eds.), Concr. Repair, Rehabil. Retrofit. II 2nd Int. Conf. Concr. Repair, Rehabil. Retrofit. ICCRRR-2, CRC Press, Leiden, 2008: pp. 275–276. https://doi.org/10.1201/9781439828403.ch99.

[8] W.Z. Taffese, E. Sistonen, Service life prediction of repaired structures using concrete recasting method: state-of-the-art, Procedia Eng. 57 (2013) 1138–1144. https://doi.org/10.1016/j.proeng.2013.04.143.

[9] P.K. Mehta, P.J.M. Monteiro, Concrete: microstructure, properties, and materials, 3rd ed., McGraw-Hill, New York, 2006. https://doi.org/10.1036/0071462899.

[10] A.M. Neville, J.J. Brooks, Concrete technology, 2nd ed., Prentice Hall, Harlow, 2010.

[11] L. Bertolini, B. Elsener, P. Pedeferri, R.B. Polde, Corrosion of steel in concrete: prevention, diagnosis, repair, Wiley-VCH Verlag GmbH & Co. KGaA, Weinheim, 2004. https://doi.org/10.1002/3527603379.

[12] F. Hunkeler, Corrosion in reinforced concrete: processes and mechanisms, in: H. Böhni (Ed.), Corros. Reinf. Concr. Struct., CRC Press,

Boca Raton, 2005: pp. 1–45.

[13] F. Papworth, A whole of life approach to concrete durability—the CIA concrete durability series, in: F. Dehn, H.-D. Beushausen, M.G. Alexander, P. Moyo (Eds.), Concr. Repair, Rehabil. Retrofit. IV Proc. 4th Int. Conf. Concr. Repair, Rehabil. Retrofit., CRC Press, Leiden, 2015: pp. 213–219. https://doi.org/10.1201/b18972-30.

[14] T. Luping, J. Gulikers, On the mathematics of time-dependent apparent chloride diffusion coefficient in concrete, Cem. Concr. Res. 37 (2007) 589–595. https://doi.org/10.1016/j.cemconres.2007.01.006.

[15] J. Marchand, E. Samson, Predicting the service-life of concrete structures – Limitations of simplified models, Cem. Concr. Compos. 31 (2009) 515–521. https://doi.org/10.1016/j.cemconcomp.2009.01.007.

[16] J. Zheng, H.S. Wong, N.R. Buenfeld, Assessing the influence of ITZ on the steady-state chloride diffusivity of concrete using a numerical model, Cem. Concr. Res. 39 (2009) 805–813. https://doi.org/10.1016/j.cemconres.2009.06.002.

[17] S.D. Abyaneh, H.S. Wong, N.R. Buenfeld, Modelling the diffusivity of mortar and concrete using a three-dimensional mesostructure with several aggregate shapes, Comput. Mater. Sci. 78 (2013) 63–73. https://doi.org/10.1016/j.commatsci.2013.05.024.

[18] L. Tang, U. Peter, B. Dimitrios, Durability and service life prediction of reinforced concrete structures, J. Chinese Ceram. Soc. 43 (2015) 1408–1419. https://doi.org/10.14062/j.issn.0454-5648.2015.10.11.

[19] J. Lahdensivu, Durability properties and actual deterioration of Finnish concrete facades and balconies, Tampere University of Technology, 2012.

[20] A. Köliö, M. Honkanen, J. Lahdensivu, M. Vippola, M. Pentti, Corrosion products of carbonation induced corrosion in existing reinforced concrete facades, Cem. Concr. Res. 78 (2015) 200–207. https://doi.org/10.1016/j.cemconres.2015.07.009.

[21] Dansk Standard, Repair of concrete structures to EN 1504, Elsevier Butterworth-Heinemann, Oxford, 2004.

[22] A. Janssens, M. Woloszyn, C. Rode, A. Sasic-Kalagasidis, M. De Paepe, From EMPD to CFD – overview of different approaches for Heat Air and Moisture modeling in IEA Annex 41, in: C. Rode, H. Hens, H. Janssen (Eds.), Proc. IEA ECBCS Annex 41 Closing Semin., Technical University of Denmark, Department of Civil Engineering, Copenhagen, 2008: pp. 9–20.

[23] S. Ahmad, Reinforcement corrosion in concrete structures, its monitoring and service life prediction–a review, Cem. Concr. Compos. 25 (2003) 459–471. https://doi.org/10.1016/S0958-9465(02)00086-0.

[24] Z. Li, Advanced concrete technology, John Wiley & Sons, Inc., Hoboken, 2011. https://doi.org/10.1002/9780470950067.

[25] P.R. Roberge, Corrosion engineering: principles and practice, McGraw-Hill, New York, 2008. https://doi.org/10.1036/0071482431.

[26] G.K. Glass, Deterioration of steel reinforced concrete, in: I. Milne, R.O. Ritchie, B. Karihaloo (Eds.), Compr. Struct. Integr., Volume 6, Elsevier Ltd, 2003: pp. 321–350. https://doi.org/10.1016/B0-08-043749-4/06140-1.

[27] T. Pan, L. Wang, Finite-element analysis of chemical transport and reinforcement corrosion-induced cracking in variably saturated heterogeneous concrete, J. Eng. Mech. 137 (2011) 334–345. https://doi.org/10.1061/(ASCE)EM.1943-7889.0000232#sthash.k8XKi23x.dpuf.

[28] fib (International Federation for Structural Concrete), Structural concrete: textbook on behaviour, design and performance, Volume 1, fib, Lausanne, 2009.

[29] B. Lagerblad, Carbon dioxide uptake during concrete life cycle – State of the art, 2005.

[30] Q. Huang, Z. Jiang, W. Zhang, X. Gu, X. Dou, Numerical analysis of the effect of coarse aggregate distribution on concrete carbonation, Constr. Build. Mater. 37 (2012) 27–35. https://doi.org/10.1016/j.conbuildmat.2012.06.074.

[31] K.Y. Ann, S.W. Pack, J.P. Hwang, H.W. Song, S.H. Kim, Service life prediction of a concrete bridge structure subjected to carbonation, Constr. Build. Mater. 24 (2010) 1494–1501. https://doi.org/10.1016/j.conbuildmat.2010.01.023.

[32] X.-Y. Wang, H.-S. Lee, A model for predicting the carbonation depth of concrete containing low-calcium fly ash, Constr. Build. Mater. 23 (2009) 725–733. https://doi.org/10.1016/j.conbuildmat.2008.02.019.

[33] E. Sistonen, Service life of hot-dip galvanised reinforcement bars in carbonated and chloride-contaminated concrete, Helsinki University of Technology, 2009.

[34] C.L. Page, Corrosion and protection of reinforcing steel in concrete, in: C.L. Page, M.M. Page (Eds.), Durab. Concr. Cem. Compos., Woodhead Publishing Ltd, Cambridge, U.K, 2007: pp. 136–186.

[35] A. Köliö, T.A. Pakkala, J. Lahdensivu, M. Kiviste, Durability demands related to carbonation induced corrosion for Finnish concrete buildings in changing climate, Eng. Struct. 62–63 (2014) 42–52. https://doi.org/10.1016/j.engstruct.2014.01.032.

[36] L. Tang, L.-O. Nilsson, P.A.M. Basheer, Resistance of concrete to chloride ingress: testing and modelling, CRC Press, Boca Raton, FL, 2012. https://doi.org/10.1201/b12603.

[37] T.S. Nguyen, S. Lorente, M. Carcasses, Effect of the environment temperature on the chloride diffusion through CEM-I and CEM-V

mortars: An experimental study, Constr. Build. Mater. 23 (2009) 795–803. https://doi.org/10.1016/j.conbuildmat.2008.03.004.

[38] H. Ye, X. Jin, C. Fu, N. Jin, Y. Xu, T. Huang, Chloride penetration in concrete exposed to cyclic drying-wetting and carbonation, Constr. Build. Mater. 112 (2016) 457–463. https://doi.org/10.1016/j.conbuildmat.2016.02.194.

[39] X. Zhu, G. Zi, Z. Cao, X. Cheng, Combined effect of carbonation and chloride ingress in concrete, Constr. Build. Mater. 110 (2016) 369–380. https://doi.org/10.1016/j.conbuildmat.2016.02.034.

[40] M. Torres-Luque, E. Bastidas-Arteaga, F. Schoefs, M. Sánchez-Silva, J.F. Osma, Non-destructive methods for measuring chloride ingress into concrete: State-of-the-art and future challenges, Constr. Build. Mater. 68 (2014) 68–81. https://doi.org/10.1016/j.conbuildmat.2014.06.009.

[41] V. Zivica, Corrosion of reinforcement induced by environment containing chloride and carbon dioxide, Bull. Mater. Sci. 26 (2003) 605–608. https://doi.org/10.1007/BF02704323.

[42] C. Houska, Deicing salt – Recognizing the corrosion threat, (2009) 1–11.

[43] C.G. Nogueira, E.D. Leonel, Probabilistic models applied to safety assessment of reinforced concrete structures subjected to chloride ingress, Eng. Fail. Anal. 31 (2013) 76–89. https://doi.org/10.1016/j.engfailanal.2013.01.023.

[44] J. Zhang, Z. Lounis, Nonlinear relationships between parameters of simplified diffusion-based model for service life design of concrete structures exposed to chlorides, Cem. Concr. Compos. 31 (2009) 591–600. https://doi.org/10.1016/j.cemconcomp.2009.05.008.

[45] N. Ghafoori, M. Najimi, J. Sobhani, M.A. Aqel, Predicting rapid chloride permeability of self-consolidating concrete: A comparative study on statistical and neural network models, Constr. Build. Mater. 44 (2013) 381–390. https://doi.org/10.1016/j.conbuildmat.2013.03.039.

[46] X. Shi, L. Fay, Z. Yang, T.A. Nguyen, Y. Liu, Corrosion of deicers to metals in transportation infrastructure: Introduction and recent developments, Corros. Rev. 27 (2011) 23–52. https://doi.org/10.1515/CORRREV.2009.27.1-2.23.

[47] R. Neves, F.A. Branco, J. De Brito, A method for the use of accelerated carbonation tests in durability design, Constr. Build. Mater. 36 (2012) 585–591. https://doi.org/10.1016/j.conbuildmat.2012.06.028.

[48] R. Akid, Corrosion of engineering materials, in: J.K. Wessel (Ed.), Handb. Adv. Mater. Enabling New Des., John Wiley & Sons, Inc., Hoboken, 2004: pp. 487–542. https://doi.org/10.1002/0471465186.ch11.

[49] W. Li, M. Pour-Ghaz, J. Castro, J. Weiss, Water absorption and critical degree of saturation relating to freeze-thaw damage in concrete pavement joints, Mater. Civ. Eng. 24 (2012) 299–307.

https://doi.org/10.1061/(ASCE)MT.1943-5533.0000383.

[50] Y. Hosokawa, K. Yamada, B. Johannesson, L.-O. Nilsson, Development of a multi-species mass transport model for concrete with account to thermodynamic phase equilibriums, Mater. Struct. 44 (2011) 1577–1592. https://doi.org/10.1617/s11527-011-9720-2.

[51] K. Henchi, E. Samson, F. Chapdelaine, J. Marchand, Advanced finite-element predictive model for the service life prediction of concrete infrastructures in support of asset management and decision-making, in: L. Soibelman, B. Akinci (Eds.), Proc. 2007 Int. Work. Comput. Civ. Eng., American Society of Civil Engineers, Reston, 2007: pp. 870–880. https://doi.org/10.1061/40937(261)103.

[52] E. Bastidas-Arteaga, A. Chateauneuf, M. Sánchez-Silva, P. Bressolette, F. Schoefs, A comprehensive probabilistic model of chloride ingress in unsaturated concrete, Eng. Struct. 33 (2011) 720–730. https://doi.org/10.1016/j.engstruct.2010.11.008.

[53] O.P. Kari, J. Puttonen, E. Skantz, Reactive transport modelling of long-term carbonation, Cem. Concr. Compos. 52 (2014) 42–53. https://doi.org/10.1016/j.cemconcomp.2014.05.003.

[54] H.-W. Song, S.-J. Kwon, Evaluation of chloride penetration in high performance concrete using neural network algorithm and micro pore structure, Cem. Concr. Res. 39 (2009) 814–824. https://doi.org/10.1016/j.cemconres.2009.05.013.

[55] P. Schiessl, S. Lay, Influence of concrete composition, in: H. Böhni (Ed.), Corros. Reinf. Concr. Struct., Woodhead Publishing Limited, Cambridge, U.K, 2005: pp. 91–134.

[56] R. Neves, F. Branco, J. De Brito, Field assessment of the relationship between natural and accelerated concrete carbonation resistance, Cem. Concr. Compos. 41 (2013) 9–15. https://doi.org/10.1016/j.cemconcomp.2013.04.006.

[57] fib (International Federation for Structural Concrete), Code-type models for concrete behaviour: state-of-the-art report, fib, Lausanne, 2013.

[58] fib (International Federation for Structural Concrete), fib model code for concrete structures 2010, Ernst & Sohn, Berlin, 2013.

[59] DuraCrete, DuraCrete final technical report: probabilistic performance based durability design of concrete structures, 2000.

[60] J.P. Broomfield, Corrosion of steel in concrete: understanding, investigation and repair, Second, Taylor & Francis, New York, NY, 2007.

[61] S.O. Folagbade, Effects of supplemetary cementitious materials on the air permeability of concrete, Mater. Eng. Struct. 4 (2017) 51–61.

[62] O.P. Kari, J. Puttonen, Simulation of concrete deterioration in Finnish rock cavern conditions for final disposal of nuclear waste, Ann. Nucl. Energy. 72 (2014) 20–30.

https://doi.org/10.1016/j.anucene.2014.04.035.

[63] B. Saassouh, Z. Lounis, Probabilistic modeling of chloride-ianduced corrosion in concrete structures using first- and second-order reliability methods, Cem. Concr. Compos. 34 (2012) 1082–1093. https://doi.org/10.1016/j.cemconcomp.2012.05.001.

[64] C. Andrade, R. D'Andrea, N. Rebolledo, Chloride ion penetration in concrete: The reaction factor in the electrical resistivity model, Cem. Concr. Compos. 47 (2014) 41–46. https://doi.org/10.1016/j.cemconcomp.2013.09.022.

[65] G. Morcous, Z. Lounis, Prediction of onset of corrosion in concrete bridge decks using neural networks and case-based reasoning, Comput. Civ. Infrastruct. Eng. 20 (2005) 108–117. https://doi.org/10.1111/j.1467-8667.2005.00380.x.

[66] Y.-M. Sun, T.-P. Chang, M.-T. Liang, Kirchhoff transformation analysis for determining time/depth dependent chloride diffusion coefficient in concrete, J. Mater. Sci. 43 (2008) 1429–1437. https://doi.org/10.1007/s10853-007-2304-4.

[67] L. Tang, A. Lindvall, Validation of models for prediction of chloride ingress in concrete exposed in de-icing salt road environment, Int. J. Struct. Eng. 4 (2013) 86–99. https://doi.org/10.1504/IJSTRUCTE.2013.050766.

[68] G. Markeset, O. Skjølsvold, Time dependent chloride diffusion coefficient - field studies of concrete exposed to marine environment in Norway, in: K. van Breugel, G. Ye, Y. Yuan (Eds.), 2nd Int. Symp. Serv. Life Des. Infrastructures, RILEM Publications SARL, 2010: pp. 83–90.

[69] J.C. Walraven, Design for service life: how should it be implemented in future codes, in: M.G. Alexander, H.-D. Beushausen, F. Dehn, P. Moyo (Eds.), Concr. Repair, Rehabil. Retrofit. II 2nd Int. Conf. Concr. Repair, Rehabil. Retrofit. ICCRRR-2, CRC Press, Leiden, 2008: pp. 3–10. https://doi.org/10.1201/9781439828403.sec1.

[70] M. Marks, D. Jozwiak-Niedzwiedzka, M.A. Glinicki, Application of machine learning for prediction of concrete resistance to migration of chlorides, in: A.M. Brandt, J. Olek, I.H. Marshall (Eds.), Proc. Int. Symp. "Brittle Matrix Compos. 9," Woodhead Publishing Ltd. and Institute of Fundamental Technological Research, Warsaw, 2009: pp. 227–236.

[71] F. Papworth, A whole of life approach to concrete durability—the CIA concrete durability series, in: F. Dehn, H.-D. Beushausen, M.G. Alexander, P. Moyo (Eds.), Concr. Repair, Rehabil. Retrofit. IV 4th Int. Conf. Concr. Repair, Rehabil. Retrofit. ICCRRR-4, CRC Press, Leiden, 2015: pp. 213–219. https://doi.org/10.1201/b18972-30.

[72] S.W. Tang, Y. Yao, C. Andrade, Z.J. Li, Recent durability studies on concrete structure, Cem. Concr. Res. 78 (2015) 143–154. https://doi.org/10.1016/j.cemconres.2015.05.021.

[73] R. Bekkerman, M. Bilenko, J. Langford, Scaling up machine learning: introduction, in: R. Bekkerman, M. Bilenko, J. Langford (Eds.), Scaling up Mach. Learn. Parallel Distrib. Approaches, Cambridge University Press, New York, 2012: pp. 1–22.

[74] V. Cherkassky, F. Mulier, Learning from data: concepts, theory, and methods, 2nd ed., John Wiley & Sons, Inc., Hoboken, NJ, 2007.

[75] J. Han, M. Kamber, J. Pei, Data mining: concepts and techniques, Morgan Kaufmann, Waltham, MA, 2012.

[76] I.H. Witten, E. Frank, M.A. Hall, Data mining: practical machine learning tools and techniques, Morgan Kaufmann, Burlington, MA, 2011.

[77] E. Alpaydin, Introduction to machine learning, 2nd ed., MIT press, Cambridge, MA, 2010. https://doi.org/10.1017/S0269888910000056.

[78] Y. Reich, Machine learning techniques for civil engineering problems, Microcomput. Civ. Eng. 12 (1997) 295–310. https://doi.org/10.1111/0885-9507.00065.

[79] V.M. Karbhari, L.S.-W. Lee, Vibration-based damage detection techniques for structural health monitoring of civil infrastructure systems, in: V.M. Karbhari, F. Ansari (Eds.), Struct. Heal. Monit. Civ. Infrastruct. Syst., Woodhead Publishing Limited, Cambridge, U.K, 2009: pp. 177–212.

[80] T. Mitchell, Machine learning, McGraw Hill, 1997.

[81] M. Kanevski, V. Timonin, A. Pozdnukhov, Machine learning for spatial environmental data: theory, applications, and software, EPFL Press, Lausanne, 2009. https://doi.org/10.1201/9781439808085.

[82] S. Marsland, Machine learning: an algorithmic perspective, Chapman and Hall/CRC, Boca Raton, FL, 2009.

[83] K.P. Murphy, Machine learning: a probabilistic perspective, Machine learning: a probabilistic perspective, Cambridge, MA, 2012.

[84] M. Ivanović, M. Radovanović, Modern machine learning techniques and their applications, in: A. Hussain, M. Ivanović (Eds.), Electron. Commun. Networks IV Proc. 4th Int. Conf. Electron. Commun. Networks, CRC Press, Leiden, 2015: pp. 833–846. https://doi.org/10.1201/b18592-153.

[85] T. Harris, Credit scoring using the clustered support vector machine, Expert Syst. Appl. 42 (2015) 741–750. https://doi.org/10.1016/j.eswa.2014.08.029.

[86] A. Takeda, T. Kanamori, Using financial risk measures for analyzing generalization performance of machine learning models, Neural Networks. 57 (2014) 29–38. https://doi.org/10.1016/j.neunet.2014.05.006.

[87] M.J. Kim, D.K. Kang, Ensemble with neural networks for bankruptcy prediction, Expert Syst. Appl. 37 (2010) 3373–3379.

https://doi.org/10.1016/j.eswa.2009.10.012.

[88] K. Di, W. Li, Z. Yue, Y. Sun, Y. Liu, A machine learning approach to crater detection from topographic data, Adv. Sp. Res. 54 (2014) 2419–2429. https://doi.org/10.1016/j.asr.2014.08.018.

[89] G. Dede, M.H. Sazlı, Speech recognition with artificial neural networks, Digit. Signal Process. 20 (2010) 763–768. https://doi.org/10.1016/j.dsp.2009.10.004.

[90] W.W. Hsieh, Machine learning methods in the environmental sciences: neural networks and kernels, Cambridge University Press, Cambridge, 2009. https://doi.org/10.1017/CBO9780511627217.

[91] W.Z. Taffese, Case-based reasoning and neural networks for real estate valuation, in: V. Devedžic (Ed.), Proc. 25th IASTED Int. Multi-Conference Artif. Intell. Appl., ACTA Press, Anaheim, CA, 2007: pp. 84–89.

[92] B. Park, J.K. Bae, Using machine learning algorithms for housing price prediction: The case of Fairfax County, Virginia housing data, Expert Syst. Appl. 42 (2015) 2928–2934. https://doi.org/10.1016/j.eswa.2014.11.040.

[93] W.Z. Taffese, A survey on application of artificial intelligence in real estate industry, in: M.Y. Hamid, A. Chekima, G. Sainarayanan, N. Prabhakaran, P. Anthony, F. Wong, J.A. Dargham, J.T.T. Wei, K.T.T. Kin (Eds.), Proc. Third Int. Conf. Artif. Intell. Eng. Technol., Universiti Malaysia Sabah, Kota Kinabalu, 2006: pp. 710–715.

[94] A. Lavecchia, Machine-learning approaches in drug discovery: methods and applications, Drug Discov. Today. 20 (2015) 318–331. https://doi.org/10.1016/j.drudis.2014.10.012.

[95] G. Wang, K.-M. Lam, Z. Deng, K.-S. Choi, Prediction of mortality after radical cystectomy for bladder cancer by machine learning techniques, Comput. Biol. Med. 63 (2015) 124–132. https://doi.org/10.1016/j.compbiomed.2015.05.015.

[96] D. Che, Q. Liu, K. Rasheed, X. Tao, Decision tree and ensemble learning algorithms with their applications in bioinformatics, in: H.R. Arabnia, Q.-N. Tran (Eds.), Softw. Tools Algorithms Biol. Syst., Springer-Verlag, New York, 2011: pp. 191–199. https://doi.org/10.1007/978-1-4419-7046-6.

[97] A. Vaughan, S. V. Bohac, Real-time, adaptive machine learning for non-stationary, near chaotic gasoline engine combustion time series, Neural Networks. 70 (2015) 18–26. https://doi.org/10.1016/j.neunet.2015.04.007.

[98] S. Jurado, À. Nebot, F. Mugica, N. Avellan, Hybrid methodologies for electricity load forecasting: Entropy-based feature selection with machine learning and soft computing techniques, Energy. 86 (2015) 276–291. https://doi.org/10.1016/j.energy.2015.04.039.

[99] A. Kialashaki, J.R. Reisel, Development and validation of artificial neural network models of the energy demand in the industrial sector of the United States, Energy. 76 (2014) 749–760. https://doi.org/10.1016/j.energy.2014.08.072.

[100] S. Haykin, Neural networks and learning machines, 3rd ed., Pearson Education, Inc., Upper Saddle River, 2009.

[101] S. Samarasinghe, Neural networks for applied sciences and engineering: from fundamentals to complex pattern recognition, Auerbach Publications, Boca Raton, 2006. https://doi.org/10.1201/9781420013061.fmatt.

[102] S.T. Skias, Background of the verification and validation of neural networks, in: B.J. Taylor (Ed.), Methods Proced. Verif. Valid. Artif. Neural Networks, Springer Science+Business Media, Inc., New York, 2006: pp. 1–12. https://doi.org/10.1007/0-387-29485-6_1.

[103] K. Vinaykumar, V. Ravi, C. Mahil, Software cost estimation using soft computing approaches, in: E.S. Olivas, J.D.M. Guerrero, M.M. Sober, J.R.M. Benedito, A.J.S. López (Eds.), Handb. Res. Mach. Learn. Appl. Trends Algorithms, Methods, Tech., IGI Global, Hershey, 2010: pp. 499–518. https://doi.org/10.4018/978-1-60566-766-9.ch024.

[104] B.J. Taylor, Methods and procedures for the verification and validation of artificial neural networks, Springer Science & Business Media, New York, 2006. https://doi.org/10.1007/0-387-29485-6.

[105] J. Wu, S. Coggeshall, Foundations of predictive analytics, CRC Press, Boca Raton, 2012.

[106] G. Dreyfus, Neural networks: methodology and applications, Springer-Verlag, Berlin, 2005. https://doi.org/10.1007/3-540-28847-3.

[107] S. Haykin, Neural networks: a comprehensive foundation, Pearson Education Pte. Ltd., Singapore, 1999.

[108] P. Cichosz, Data mining algorithms: explained using R, John Wiley & Sons, Ltd, 2015. https://doi.org/10.1002/9781118950951.

[109] C.D. Sutton, Classification and regression trees, bagging, and boosting, in: C.R. Rao, E.J. Wegman, J.L. Solka (Eds.), Handb. Stat. Data Min. Data Vis., Elsevier B.V., Amsterdam, 2005: pp. 303–330. https://doi.org/10.1016/S0169-7161(04)24001-9.

[110] J. Gama, Knowledge discovery from data streams, Chapman and Hall/CRC, Boca Raton, 2010. https://doi.org/10.1201/EBK1439826119-c1.

[111] E. Tuv, A. Borisov, G. Runger, K. Torkkola, Feature selection with ensembles, artificial variables, and redundancy elimination, J. Mach. Learn. Res. 10 (2009) 1341–1366. https://doi.org/10.1145/1577069.1755828.

[112] L. Rokach, O. Maimon, Data mining with decision trees: theory and

applications, World Scientific Publishing Co. Pte. Ltd., Singapore, 2008.

[113] G. Seni, J.F. Elder, Ensemble methods in data mining: improving accuracy through combining predictions, Morgan & Claypool, 2010. https://doi.org/10.2200/S00240ED1V01Y200912DMK002.

[114] M.R. Berthold, C. Borgelt, F. Höppner, F. Klawonn, Guide to intelligent data analysis: how to intelligently make sense of real data, Springer-Verlag, London, 2010. https://doi.org/10.1007/978-1-84882-260-3.

[115] U. Stańczyk, Feature evaluation by filter, wrapper, and embedded approaches, in: U. Stańczyk, L.C. Jain (Eds.), Featur. Sel. Data Pattern Recognit., Springer-Verlag, Berlin, 2015: pp. 29–44. https://doi.org/10.1007/978-3-662-45620-0.

[116] C. Strobl, Statistical issues in machine learning: Towards reliable split selection and variable importance measures, Ludwig-Maximilians-Universität München, 2008.

[117] NT Build 492, Concrete, mortar and cement-based repair materials: Chloride migration coefficient from non-steady-state migration experiments, 1999.

[118] J. Mattila, On the durability of cement-based patch repairs on Finnish concrete facades and balconies, Tampere University of Technology, 2003.

[119] T.A. Pakkala, A. Köliö, J. Lahdensivu, M. Kiviste, Durability demands related to frost attack for Finnish concrete buildings in changing climate, Build. Environ. 82 (2014) 27–41. https://doi.org/10.1016/j.buildenv.2014.07.028.

[120] F. Al-Neshawy, Computerised prediction of the deterioration of concrete building facades caused by moisture and changes in temperature, Aalto University, 2013.

[121] 197-1 EN, Cement - Part 1: Composition, specifications and conformity criteria for common cements, Eur. Comm. Stand. (2003).

[122] M. Barfield, N. Ghafoori, Air-entrained self-consolidating concrete: A study of admixture sources, Constr. Build. Mater. 26 (2012) 490–496. https://doi.org/10.1016/j.conbuildmat.2011.06.049.

[123] S. Chandra, J. Björnström, Influence of cement and superplasticizers type and dosage on the fluidity of cement mortars—Part I, Cem. Concr. Res. 32 (2002) 1605–1611. https://doi.org/10.1016/S0008-8846(02)00839-6.

[124] M.H. Beale, M.T. Hagan, H.B. Demuth, Neural network toolbox™: user's guide, The MathWorks, Inc., 2015.

[125] E. Acuña, C. Rodriguez, The treatment of missing values and its effect in the classifier accuracy, in: D. Banks, F. McMorris R., P. Arabie, W. Gaul (Eds.), Classif. Clust. Data Min. Appl., Springer Berlin Heidelberg, Berlin, 2004: pp. 639–647. https://doi.org/10.1007/978-3-642-17103-1_60.

[126] G.H. Nguyen, A. Bouzerdoum, S.L. Phung, Efficient supervised learning

with reduced training exemplars, in: IEEE Int. Jt. Conf. Neural Networks, IJCNN 2008, IEEE, Hong Kong, 2008: pp. 2981–2987. https://doi.org/10.1109/IJCNN.2008.4634217.

[127] M.H. Beale, M.T. Hagan, H.B. Demuth, Neural network toolbox™: user's guide, Natick, 2013.

[128] H. Yu, B.M. Wilamowski, Levenberg–marquardt training, in: B.M. Wilamowski, J.D. Irwin (Eds.), Intell. Syst., 2nd ed., CRC Press, Boca Raton, FL, 2011: pp. 12–1–12–16. https://doi.org/10.1201/b10604-15.

[129] D.L. Olson, D. Delen, Advanced data mining techniques, Springer-Verlag Berlin Heidelberg, 2008. https://doi.org/10.1007/978-3-540-76917-0.

[130] MathWorks, Curve fitting toolbox™: user's guide, The MathWorks, Inc., 2015.

[131] N.R. Buenfeld, N.M. Hassanein, A.J. Jones, An artificial neural network for predicting carbonation depth in concrete structures, in: I. Flood, N. Kartam (Eds.), Artif. Neural Networks Civ. Eng. Adv. Featur. Appl., American Society of Civil Engineers, Reston, VA, 1998: pp. 77–117.

[132] W.Z. Taffese, F. Al-Neshawy, E. Sistonen, M. Ferreira, Optimized neural network based carbonation prediction model, Int. Symp. Non-Destructive Test. Civ. Eng. (2015) 1074–1083.

[133] W.Z. Taffese, E. Sistonen, J. Puttonen, Prediction of concrete carbonation depth using decision trees, 23rd Eur. Symp. Artif. Neural Networks, Comput. Intell. Mach. Learn. (2015).

[134] W.Z. Taffese, E. Sistonen, J. Puttonen, CaPrM: Carbonation prediction model for reinforced concrete using machine learning methods, Constr. Build. Mater. 100 (2015) 70–82. https://doi.org/10.1016/j.conbuildmat.2015.09.058.

[135] S.S. Gilan, H.B. Jovein, A.A. Ramezanianpour, Hybrid support vector regression – Particle swarm optimization for prediction of compressive strength and RCPT of concretes containing metakaolin, Constr. Build. Mater. 34 (2012) 321–329. https://doi.org/10.1016/j.conbuildmat.2012.02.038.

[136] N. Barroca, L.M. Borges, F.J. Velez, F. Monteiro, M. Górski, J. Castro-Gomes, Wireless sensor networks for temperature and humidity monitoring within concrete structures, Constr. Build. Mater. 40 (2013) 1156–1166. https://doi.org/10.1016/j.conbuildmat.2012.11.087.

[137] G. Qiao, G. Sun, Y. Hong, T. Liu, X. Guan, Corrosion in reinforced concrete panels: wireless monitoring and wavelet-based analysis, Sensors. 14 (2014) 3395–3407. https://doi.org/10.3390/s140203395.

[138] F. Michelis, Wireless nano sensors for embedded durability monitoring in concrete, IFSTTAR - Institut Français des Sciences et Technologies des Transports, 2015.

[139] Q. Yang, L.H. Zhu, J.J. He, Z.F. Yan, R. Ren, Research on wireless remote

monitoring system of the durability for large concrete structures, Adv. Mater. Res. 368–373 (2012) 2194–2199. https://doi.org/10.4028/www.scientific.net/AMR.368-373.2194.

[140] W.Z. Taffese, E. Nigussie, J. Isoaho, Internet of things based durability monitoring and assessment of reinforced concrete structures, Procedia Comput. Sci. 155 (2019) 672–679. https://doi.org/10.1016/j.procs.2019.08.096.

[141] W.J. McCarter, Ø. Vennesland, Sensor systems for use in reinforced concrete structures, Constr. Build. Mater. 18 (2004) 351–358. https://doi.org/10.1016/j.conbuildmat.2004.03.008.

[142] D. Cusson, Z. Lounis, L. Daigle, Durability monitoring for improved service life predictions of concrete bridge decks in corrosive environments, Comput. Civ. Infrastruct. Eng. 26 (2011) 524–541. https://doi.org/10.1111/j.1467-8667.2010.00710.x.

[143] J. Cui, Effect of chemical admixture on durability of concrete, Chem. Eng. Trans. 55 (2016) 439–444. https://doi.org/10.3303/CET1655074.

[144] C. Shi, T. He, G. Zhang, X. Wang, Y. Hu, Effects of superplasticizers on carbonation resistance of concrete, Constr. Build. Mater. 108 (2016) 48–55. https://doi.org/10.1016/j.conbuildmat.2016.01.037.

[145] H. Quan, H. Kasami, Experimental study on durability improvement of fly ash concrete with durability improving admixture, Sci. World J. 2014 (2014) 11 pages. https://doi.org/10.1155/2014/818103.

[146] R. Rixom, N. Mailvaganam, Chemical admixtures for concrete, 3rd ed., E & FN Spon, New York, 1999.

[147] H. Zhao, W. Sun, X. Wu, B. Gao, The effect of coarse aggregate gradation on the properties of self-compacting concrete, Mater. Des. 40 (2012) 109–116. https://doi.org/10.1016/j.matdes.2012.03.035.

[148] J. Gulikers, Pitfalls and practical implications in durability design of reinforced concrete structures, in: C. Andrade, J. Gulikers (Eds.), Adv. Model. Concr. Serv. Life, RILEM Book, Springer, Dordrecht, 2012: pp. 11–20. https://doi.org/10.1007/978-94-007-2703-8_2.

[149] SFS-EN 12350-7, Testing fresh concrete. Part 7: Air content. Pressure methods, 2000.

[150] G. Lomboy, K. Wang, Effects of strength, permeability, and air void parameters on freezing-thawing resistance of concrete with and without air entrainment, J. ASTM Int. 6 (2010) 135–154. https://doi.org/10.1520/JAI102454.

[151] S. Caré, Influence of aggregates on chloride diffusion coefficient into mortar, Cem. Concr. Res. 33 (2003) 1021–1028. https://doi.org/10.1016/S0008-8846(03)00009-7.

[152] H. Huang, C. Qian, F. Zhao, J. Qu, J. Guo, M. Danzinger, Improvement on microstructure of concrete by polycarboxylate superplasticizer (PCE)

and its influence on durability of concrete, Constr. Build. Mater. 110 (2016) 293–299. https://doi.org/10.1016/j.conbuildmat.2016.02.041.

[153] E.M.J. Berodier, Impact of the supplementary cementitious materials on the kinetics and microstructural development of cement hydration, École polytechnique fédérale de Lausanne, EPFL, 2015.

[154] B. Lothenbach, K. Scrivener, R.D. Hooton, Supplementary cementitious materials, Cem. Concr. Res. 41 (2011) 1244–1256. https://doi.org/10.1016/j.cemconres.2010.12.001.

[155] M.C.G. Juenger, R. Siddique, Recent advances in understanding the role of supplementary cementitious materials in concrete, Cem. Concr. Res. 78 (2015) 71–80. https://doi.org/10.1016/j.cemconres.2015.03.018.

[156] K. Jolkkonen, S. Huovinen, Influence of coatings on the service life of concrete sandwich-facades, Espoo, 2000.

[157] A. Sarja, E. Vesikari, Durability design of concrete structures: report of RILEM technical committee 130-CSL, E & FN Spon, London, 1996.

[158] Finnish Association of Civil Engineers, RIL 183-4.9-1995. Service Life of Construction Materials and Structures. Methods of Appraisal. 4.9: Service Life Design of Concrete Structures., Finnish Association of Civil Engineers (RIL), Vantaa, 1995.

[159] C. Andrade, I. Martínez, Techniques for measuring the corrosion rate (polarization resistance) and the corrosion potential of reinforced concrete structures, in: C. Maierhofer, H.-W. Reinhardt, G. Dobmann (Eds.), Non-Destructive Eval. Reinf. Concr. Struct. Non-Destructive Test. Methods, Woodhead Publishing Limited, Cambridg, 2010: pp. 284–316. https://doi.org/10.1533/9781845699604.2.284.

[160] N.J. Carino, Methods to evaluate corrosion of reinforcement, in: V.M. Malhotra, N.J. Carino (Eds.), Handb. Nondestruct. Test. Concr., 2nd ed., CRC Press, Boca Raton, 2004: p. 384.

[161] Y. Kellouche, B. Boukhatem, M. Ghrici, A. Tagnit-Hamou, Exploring the major factors affecting fly-ash concrete carbonation using artificial neural network, Neural Comput. Appl. (2017) 1–20. https://doi.org/10.1007/s00521-017-3052-2.

[162] C. Lu, R. Liu, Predicting carbonation depth of prestressed concrete under different stress states using artificial neural network, Adv. Artif. Neural Syst. 2009 (2009) 1–8. https://doi.org/10.1155/2009/193139.

[163] H.-C. Cho, H. Ju, J.-Y. Oh, K.J. Lee, K.W. Hahm, K.S. Kim, Estimation of concrete carbonation depth considering multiple influencing factors on the deterioration of durability for reinforced concrete structures, Adv. Mater. Sci. Eng. 2016 (2016) 1–18. https://doi.org/10.1155/2016/4814609.

[164] D. Luo, D. Niu, Z. Dong, Application of neural network for concrete carbonation depth prediction, in: J. Olek, J. Weiss (Eds.), Proc. 4th Int.

Conf. Durab. Concr. Struct., Purdue University Press, West Lafayette, IN, 2014: pp. 66–71. https://doi.org/10.5703/1288284315384.

[165] J. Peng, Z. Li, B. Ma, Neural network analysis of chloride diffusion in concrete, J. Mater. Civ. Eng. 14 (2002) 327–333. https://doi.org/10.1061/(ASCE)0899-1561(2002)14:4(327).

[166] S. Inthata, W. Kowtanapanich, R. Cheerarot, Prediction of chloride permeability of concretes containing ground pozzolans by artificial neural networks, Mater. Struct. 46 (2013) 1707–1721. https://doi.org/10.1617/s11527-012-0009-x.

[167] A.R. Boğa, M. Öztürk, İ.B. Topçu, Using ANN and ANFIS to predict the mechanical and chloride permeability properties of concrete containing GGBFS and CNI, Compos. Part B Eng. 45 (2013) 688–696. https://doi.org/10.1016/j.compositesb.2012.05.054.

[168] H. Yasarer, Y.M. Najjar, Characterizing the permeability of Kansas concrete mixes used in PCC pavements, Int. J. Geomech. 14 (2014) 04014017(8). https://doi.org/10.1061/(ASCE)GM.1943-5622.0000362.

[169] Y.-Y. Kim, B.-J. Lee, S.-J. Kwon, Evaluation technique of chloride penetration using apparent diffusion coefficient and neural network algorithm, Adv. Mater. Sci. Eng. Article ID (2014) 13 pages. https://doi.org/10.1155/2014/647243.

[170] O.A. Hodhod, H.I. Ahmed, Developing an artificial neural network model to evaluate chloride diffusivity in high performance concrete, HBRC. 9 (2013) 15–21. https://doi.org/10.1016/j.hbrcj.2013.04.001.

[171] R. Parichatprecha, P. Nimityongskul, Analysis of durability of high performance concrete using artificial neural networks, Constr. Build. Mater. 23 (2009) 910–917. https://doi.org/10.1016/j.conbuildmat.2008.04.015.

[172] W.Z. Taffese, E. Sistonen, Significance of chloride penetration controlling parameters in concrete: Ensemble methods, Constr. Build. Mater. 139 (2017) 9–23. https://doi.org/10.1016/j.conbuildmat.2017.02.014.

Publications

Publication I

Taffese, Woubishet Zewdu; Sistonen, Esko. 2017. Machine learning for durability and service-life assessment of reinforced concrete structures: Recent advances and future directions. Journal of Automation in Construction, volume 77, pages 1–14. ISSN 0926-5805. https://doi.org/10.1016/j.autcon.2017.01.016.

Automation in Construction 77 (2017) 1–14

Contents lists available at ScienceDirect

Automation in Construction

journal homepage: www.elsevier.com/locate/autcon

Review

Machine learning for durability and service-life assessment of reinforced concrete structures: Recent advances and future directions

Woubishet Zewdu Taffese *, Esko Sistonen

Department of Civil and Structural Engineering, Aalto University, P. O. Box 12100, FI-00076 Aalto, Finland

ARTICLE INFO

Article history:
Received 29 August 2016
Received in revised form 21 October 2016
Accepted 18 January 2017
Available online xxxx

Keywords:
Reinforced concrete
Corrosion
Durability
Service life
Machine learning
Modelling
Carbonation
Chloride

ABSTRACT

Accurate service-life prediction of structures is vital for taking appropriate measures in a time- and cost-effective manner. However, the conventional prediction models rely on simplified assumptions, leading to inaccurate estimations. The paper reviews the capability of machine learning in addressing the limitations of classical prediction models. This is due to its ability to capture the complex physical and chemical process of the deterioration mechanism. The paper also presents previous researches that proposed the applicability of machine learning in assisting durability assessment of reinforced concrete structures. The advantages of employing machine learning for durability and service-life assessment of reinforced concrete structures are also discussed in detail. The growing trend of collecting more and more in-service data using wireless sensors facilitates the use of machine learning for durability and service-life assessment. The paper concludes by recommending the future directions based on examination of recent advances and current practices in this specific area.

Contents

1. Introduction

The durability and service life of the reinforced concrete (RC) structures are one of the foremost problems faced by the construction industry for the past few decades. Degradation of RC structures induced by corrosion causes severe problem all over the globe [1–8]. It has been reported that corrosion associated maintenance and repair of RC structures cost multibillion USD per annum. Repairing of corrosion-induced damage in Western Europe alone costs 5 billion EUR annually [9]. Surprisingly, for corrosion related damage and control, some developed countries spend nearly 3.5% of their gross national product (GNP) [10].

* Corresponding author.
E-mail address: woubishet.taffese@aalto.fi (W.Z. Taffese).

http://dx.doi.org/10.1016/j.autcon.2017.01.016
0926-5805/

In another perspective, continued corrosion of reinforcement bar (rebar) is also the most prevalent form of deterioration in repaired RC structures, which accounts for 37% of the failure modes [11–13]. This leads to costly and time consuming repairs of repairs.

Clear understanding of the concrete performance is critical in order to estimate the durability and the service life of a structure. Most of the time, performance of concrete is assessed under the influence of single deterioration mechanism. However, in reality, several complex degradation mechanisms affecting the performance of concrete can act simultaneously or consequently [14,15]. The effect of the synergic degradation mechanisms is more faster and severe than the effect of any single action participating in the deterioration process [16–18]. Measuring the influence of the combined degradation mechanisms in laboratory and translating the results to an actual structure is impracticable. Moreover, concrete performance investigation either in laboratory or in field often tends to be time consuming and costly (directly and indirectly) [19]. For instance, conventional in-service inspection and maintenance programs of highway structures cause traffic delay which accounts for between 15%–40% of the construction costs [20]. Hence, cost-effective reliable prognosis of the concrete performance while in service, from economy and safety perspective, is prerequisites of life-cycle management of RC structures.

The implementation of durability monitoring systems in RC structures could allow identifying deterioration at an early stage. The accessibility of short- and long-term data with spatial and temporal resolution from the monitoring system is a critical underlying necessity for better durability assessment of RC structures. Data collected from the monitoring system have to be analysed efficiently in order to use them for estimation of the remaining service life of a structure. Indeed, data on their own are pointless unless either knowledge or an inference is extracted out from them. Machine learning can be implemented to analyse the monitored complex data and it can deliver more accurate results that can guide better decisions even in real-time without human intervention, e.g., fault diagnosis [21], and tsunami early warning system [22]. Machine learning techniques have been used extensively for a broad range of applications and its employment in civil engineering is not new. Currently, machine learning technique has a broad application prospects in the field of civil engineering to solve complex practical problems.

The objectives of this paper are threefold: (i) to present the current practice on durability assessment focusing on penetration of aggressive substances into concrete causing corrosion of rebar; (ii) to discuss the role of machine learning techniques in improving the accuracy of durability and service-life assessments; and (iii) to give an insight on the future direction of durability monitoring and service-life prediction of RC structures.

The structure of the paper is as follows. In Section 2, the conditions causing corrosion of rebar in RC structures are presented. The conventional models which are used to evaluate the durability and the remaining service life of RC structure along with their limitations are also discussed in the same section. The fundamental knowledge on machine learning is provided in Section 3. In Section 4, the application of machine learning techniques, in two specific areas, in the field of civil engineering is discussed. In Section 5, the current practices of machine learning techniques in durability and service-life assessment as well as durability monitoring systems are presented. The future direction of durability monitoring and service-life prediction approach is also explained in the same section. Finally, conclusion is presented in Section 6.

2. Durability and service life of RC structures

Corrosion of rebar in concrete is typically triggered by ingression of either carbon dioxide (CO_2) or chloride ions (Cl^-) into the concrete pores. Naturally, concrete is alkaline with a pore solution pH of 12–13 that passivizes embedded rebar. The passivation of rebar is deteriorated by the occurrence of Cl^- or by the carbonation of concrete [23–25]. Carbonation is a physicochemical phenomenon induced naturally by the ingression of CO_2 into the concrete pores from the surrounding environment and reacts with hydrated cement [26,27]. Both carbonation- and chloride-induced corrosion of rebar may diminish its cross-sectional area, degrade its elongation ability and cause serious cracks to the concrete, which in turn reduces the load-bearing capacity of the structure considerably. Cracked concrete could offer more ready access to moisture and aggressive gases and ions such as oxygen (O_2), CO_2 and Cl^- leading to aggravated rebar corrosion and degradation of concrete. Consequently, the serviceability, strength, safety and service life of concrete structures will be diminished [6–8,28]. Although chloride-induced corrosion of rebar is normally more harmful and costly to repair, carbonation-induced corrosion of rebar may attack a broader area of RC structures at a bigger scale. It is estimated that about two-thirds of the total concrete structures are exposed to favourable environmental situations for carbonation-induced corrosion [29,30].

The deterioration process of RC structure caused by corrosion can be divided into two phases: initiation and propagation. In case of carbonation-induced corrosion, the corrosion initiation phase corresponds to the diffusion of CO_2 gas into concrete while the rebar remains passivated. In chloride-induced corrosion, the corrosion initiation phase corresponds to the process of Cl^- penetrating into concrete. The propagation period covers the time from the onset of rebar corrosion to structural failure. This period is relatively short compared with corrosion initiation stage. Due to these, the duration of the initial stage has been regularly used to specify the durability and service life of RC structures [31,32]. The conceptual model of rebar corrosion process illustrating the initiation and propagation phases is shown in Fig. 1.

2.1. Deterioration models

Deterioration models are crucial for accurately predicting the performance of concrete and thus to make effective decision regarding maintenance and rehabilitation of RC structures. In the past three decades, considerable attempts have been made to develop durability models for RC structures exposed to environmental conditions that favour for carbonation- and chloride-induced corrosion. Accordingly, various models and input parameters have been established. The complexity level of the developed models vary from simple analytical models assuming uniaxial diffusion into concrete, to more sophisticated numerical models which considers the physical, chemical, and electrochemical processes of gas and ion transport [33–36]. Some of the applied analytical models and the related value of input parameters have been incorrect, incomplete, and/or unsuitable for the prevailing conditions. Due to these facts, the prediction results differ substantially even for the same concrete matrix exposed in identical conditions [37]. Though the complex scientific models provide reasonably accurate predictions, they lack user friendliness and demand highly skilled professional making them suitable only for research, but not for practical design applications. In practice, empirical deterioration models in the form of simple analytical equations on the basis of Fick's second law of diffusion are commonly adopted to model penetration of CO_2 and Cl^- into concrete.

2.1.1. Carbonation model

Concrete carbonation has been recognized as one of the major cause of early deterioration, serviceability loss and safety of RC structures. It is an essential index of durability. The classic carbonation depth prediction model deduced from Fick's second law of diffusion is shown in Eq. (1) [26,38–41]. This model obeys the square root law and can be applied to foresee the depassivation time by extrapolating the carbonation depth measured at a certain time to the future.

$$x_c(t) = k\sqrt{t}, \tag{1}$$

where $x_c(t)$ is carbonation depth at the time t in [mm], k is carbonation coefficient [mm/year$^{0.5}$] which is equivalent to $\sqrt{\frac{2.D_{CO_2}(C_1-C_2)}{a}}$, D_{CO_2} is

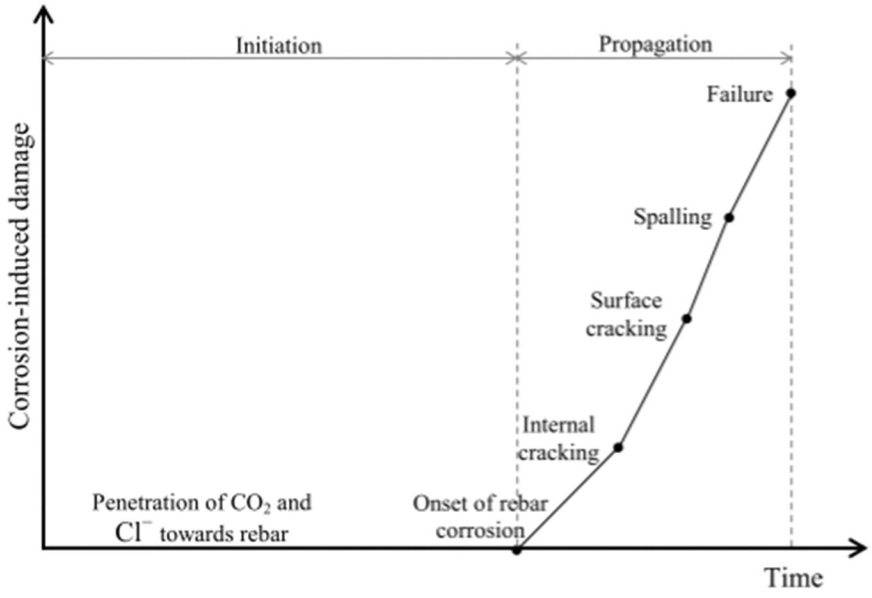

Fig. 1. Conceptual model of rebar corrosion process.

diffusion coefficient for CO_2 through carbonated concrete [mm^2/year], C_1 is CO_2 concentration in the surrounding environment [kg/m^3], C_2 is CO_2 concentration at the carbonation front [kg/m^3], a is mass of CO_2 per unit volume of concrete needed to carbonate all the available calcium hydroxide [kg/m^3], and t is exposure time to the atmosphere holding carbon dioxide [year].

2.1.2. Chloride model

Prediction of chloride profile is a necessary procedure since chloride attack affects the remaining service life of RC structures. Through the years several models have been developed to predict chloride concentration inside the concrete. Despite the availability of numerous models, empirical models are most commonly utilized to estimate the chloride profile in concrete. Eq. (2) is an empirical formula based on Fick's second law of diffusion applied to evaluate long-term chloride penetration in concrete [42]

$$C_x = C_i + (C_s - C_i)\left(1 - erf_{(x)}\left[\frac{x}{2\sqrt{D_{nss}t}}\right]\right), \quad (2)$$

where C_x is the Cl^- content measured at average depth x [m] after exposure time t [s][% by mass of concrete], C_s is the computed Cl^- content at the exposed surface [% by mass of concrete], C_i is the initial Cl^- content [% by mass of concrete], D_{nss} is the diffusion coefficient of Cl^- at non-steady state [m^2/s], and $erf_{(x)}$ is the error function [−].

2.2. Modelling uncertainty

The initiation period of carbonation-induced corrosion is the total time needed for the carbonation front to arrive at a depth of the concrete cover. If the carbonation coefficient k and the concrete cover thickness are known, the initiation time can be calculated using simplified Fick's law based formula, Eq. (1). The assumptions in Eq. (1) are: (i) diffusion coefficient for CO_2 through carbonated concrete is constant; (ii) amount of CO_2 required to neutralize alkalinity within a unit volume of concrete is invariant; and (iii) CO_2 concentration varies linearly between fixed boundary values of C_1 at the external surface and C_2 at the carbonation front. To determine k, the concrete carbonation depth must be measured in advance either by measuring the carbonation depth of an existing structure or by carrying out an accelerated test. Indeed, carbonation is usually examined by executing an accelerated test using higher CO_2 concentration in a controlled environment since the process is slow [43]. Then, using the measured carbonation depth the equivalent k, and thus the time of depassivation of the rebar, can be computed. This approach is commonly adopted though the accelerated test may not always explain the natural carbonation process precisely [39]. Eq. (1) is plausible as far as the three assumptions are fulfilled but CO_2 diffusion coefficient varies both temporally and spatially. The reason for these variability is that the diffusion of CO_2 relies on many parameters, such as CO_2 concentration, concrete composition, curing and environmental conditions [38,43,44]. Due to this, Eq. (1) usually fails to represent the real state of the concrete structures, which in turn leads to incorrect carbonation depth prediction [26,44,45]. To minimize some of the assumptions, empirical models have been suggested which take into direct account the influence of some factors that govern the rate of carbonation e.g. the model proposed in fib-MC2010 [46] and DuraCrete framework [47], Eq. (3)

$$x_c(t) = \sqrt{2.k_e.\ k_c.R_{NAC,0}^{-1}.C_s}.W(t).\sqrt{t}, \quad (3)$$

where $x_c(t)$ is carbonation depth at the time t in [mm], t is time in [year], k_e is environmental function [−], k_c is execution transfer parameter [−], C_s is CO_2 concentration in the air in [kg/m^3], $W(t)$ is weather function [−], $R_{NAC,0}^{-1}$ is inverse effective carbonation resistance of concrete in [(mm^2/year) / (kg/m^3)] which is determined at a certain time t_0 using the natural carbonation test NAC in [(mm^2/year) / (kg/m^3)].

As seen in Eq. (3), the fib and DuraCrete models adopt Eq. (1) by linking the coefficient of carbonation with factors of the concrete material and the environment. There are also other models which follow the same principle. The linked parameters have normally been regarded as random variables which define the concrete properties that dominate the ingress rate of CO_2, such as exposure, water to binder ratio (w/b), and compressive strength. The physical-chemical phenomena related with transport of CO_2 through the concrete are largely controlled by its permeability. Even though the permeability coefficient of concrete depends mainly on the w/b, it is also influenced by other parameters such as aggregate distribution, age, curing condition, and the inclusion of chemical or mineral admixtures. The majority of the enhanced models do not include all such governing factors which control the carbonation process. Integrating two or more of these models does not also solve the problem either. The combination of several simplifications and assumptions in the prevailing models for carbonation prediction lead to a substantial uncertainty in their performance.

In engineering practice, the penetration of Cl^- into concrete is often evaluated by adopting a simplified empirical formula based on Fick's second law of diffusion described by Eq. (2). This equation has downsides that make the Cl^- prediction into concrete uncertain. The foremost limitations of Eq. (2) are the following assumptions [28,48–50]: (i) the surface chloride content (C_s) remains constant; (ii) the non-steady diffusion coefficient (D_{nss}) is invariant; and (iii) value of D_{nss} cannot be compared for different C_s. Nevertheless, in real condition, C_s and D_{nss} cannot be recognized as constants. This is due to the transport properties of Cl^- relying on the intrinsic permeability of the concrete and the amount of Cl^- concentration in the pore solution. The permeability is changing during the process of cement hydration with time. The amount of Cl^- concentration varies due to the continuous chemical reaction of Cl^- with the dilute cement solution and the amount of diffused Cl^-. In another perspective, the alteration of capillary pore structure of concrete is controlled by cement type, w/b, age, type of admixtures, and exposure condition. Due to these, both C_s and D_{nss} are varying with time and space [51,52]. It is also recognized that the Cl^- is accumulated in the concrete pore solution during the chloride diffusion process. As the amount of Cl^- concentration rises, the mobility of free Cl^- gradually becomes weak which in turn diminishes the value of D_{nss}. This shows that D_{nss} is a function of C_s and the assumption (iii) considered in Eq. (2) is invalid. In addition, in Eq. (2), the error function equation considers only diffusion mechanism. However, the penetration of Cl^- into concrete involves a complex physical and chemical process that combines various transport mechanisms other than diffusion such as capillary sorption, and permeation. All these facts explain why Eq. (2) model fail to deliver accurate predictions in several instances [50]. Indeed, in order to address the time dependency of D_{nss} and effect of other influential factors some approaches have been proposed e.g. in fib-MC2010 [46] and DuraCrete framework [47]. The most common one is expressed by Eq. (4). This model also fails to eliminate the uncertainty fully since the input variables exhibit considerable scatter. The combination of all the presented assumptions causes a substantial uncertainty in the output of the model, specifically the time to corrosion initiation or estimation of the remaining service life [49,53]. This uncertainty could have severe outturn regarding insufficient design, planning of inspection and maintenance, and thus shortens the service life of the structure and increases the lifecycle cost.

$$D_{nss}(t) = k_e.k_t.k_c.D_0.\left(\frac{t_0}{t}\right)^n, \quad (4)$$

where k_e is environmental function [−], k_c is test method function [−], k_c is curing function [−], D_0 is experimentally determined chloride diffusion coefficient at time t_0 [m^2/s], t_0 is age of concrete at D_0 is measured [year], t is the exposure duration [year], and n is the age factor describing the time dependency of the diffusion coefficient [−].

As discussed above, penetration rate of CO_2 and Cl^- into the concrete structure is mainly a function of concrete properties and environmental conditions. In real structure, the ingress rate of these substances cannot be constant and even they may change in different parts of a single element. So, depassivation of the rebar caused by carbonation and/or chloride attack is enormously complex. The empirical degradation models in the form of analytical equations presented in Section 2.1.1 and 2.1.2 are no better than their underlying conceptual base. Thus, durability estimation using Fick's law based empirical models are uncertain. In fact, such simple empirical deterioration models can be integrated with a semi-probabilistic uncertainty model to improve the reliability as included in the DuraCrete framework. However, this approach cannot eliminate the associated uncertainty fully. Uncertainty can be eliminated by gathering more and more accurate data and analysing it using machine learning techniques. This methods estimate without uncertainty or assumptions and continuously learn from the observed data in order to improve their accuracy score.

3. Machine learning

Machine learning is a major subfield in artificial intelligence that deals with the design and development of algorithms to identify complex patterns from experimental data, without assuming a pre-established equation as a model, and make decisions intelligently [54–62]. Machine learning based models can be either predictive to perform predictions or descriptive to gain knowledge from data, or both [58,63,64]. Although machine learning grew out of the quest for artificial intelligence, its scope and potential is much more general. It encompasses thoughts from a various set of disciplines, including Information Theory, Probability and Statistics, Psychology and Neurobiology, Control Computational Complexity, Theory and Philosophy [61].

Developing a machine learning model involves a small number of design choices: (i) the type of training experience; (ii) the target function to be learned; (iii) a representation of the target function; and (iv) an algorithm for learning the target function from training instances. Depending on the resources of training, machine learning is categorized as supervised, unsupervised, semi-supervised and reinforcement learning [58,65]. The supervised and unsupervised learning are the most widely adopted types of machine learning in several fields of application, including engineering [64].

Supervised learning: starting from a training database that contains input instances and desired outputs, its goal is to build a function (or model) to precisely predict the unknown target output of future instances. The key characteristic of supervised learning is the existence of a "*teacher*" and the training input-output data. If the goal is to predict continuous target variables, the task is known as *regression*. But, if the goal is to predict discrete target variables, the task is said to be *classification*.

Unsupervised learning: starting from a training database that involves input instances, its goal is to divide the training examples into clusters so that the data in every cluster demonstrate a high level of proximity. Unlike supervised learning, the labels for the data are unavailable in unsupervised learning.

In machine learning methods, an algorithm has to be developed to solve problems. The algorithms in machine learning adopt various methods from various fields, for example, pattern recognition, data mining, statistics and signal processing. This enables machine learning to take advantage of the synergy from all these fields, which in turn leads to robust solutions that use different domains of knowledge [62]. Some of the most influential algorithms that have been widely used in supervised and unsupervised learning types are illustrated in Fig. 2. It can also be noted that some of the algorithm types operate under different learning types to solve various problems.

Nowadays, there are a wide spectrum of successful practical applications of machine learning in different domains such as: computational finance [66–68], image and speech processing [69–71], property valuation [72–74], hydrology [75–78], computational biology [79–82], and energy production [83–85]. Although employing machine learning is becoming popular in several fields of engineering, its implementation in durability and service-life assessment of RC structures is yet limited.

4. Application of machine learning techniques in civil engineering

Over the past few decades, machine learning techniques have been adopted for modelling the real-world problems because of their enormous capacity to capture interrelationships among data pairs of input and output which are nonlinear, unknown or complex to formulate. Though the application of machine learning in service-life assessment of concrete is limited, it has been in use in other civil engineering problems. The first uses of machine learning techniques, three decades ago, comprises testing of various prevailing methods on easy problems (e.g. knowledge acquisition to conceptual design of steel members [86], management tool development to control structural safety [87]). The selection of machine learning algorithms during that time mainly

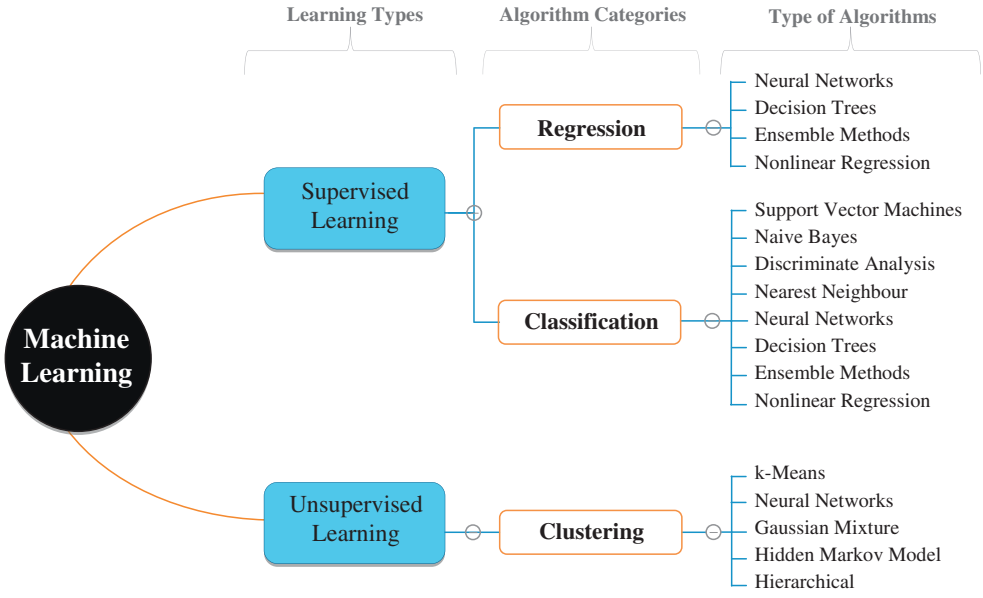

Fig. 2. Machine learning types with commonly adopted algorithms.

was based on their obtainability but not their applicability to the target problem [59]. Due to this, the applied problem representation was a simplification controlled by the inadequacy of the obtainable machine learning algorithms. Then slowly, complex problems were taken into consideration. Among the applications, structural health monitoring and evaluation of concrete properties and mix design are the most common ones. In this section, the implementations of machine learning methods in these two applications are discussed.

4.1. Structural health monitoring (SHM)

Structural damage caused by operation and environment is an inevitable process for civil structures. Early identification of damage in a structure by means of SHM system is imperative in order to ensure public safety and reliability of in-service structures while avoiding economic losses [88–91]. It involves monitoring of a structure over time using dynamic response measurements spaced at regular intervals of time, extraction of damage-sensitive features and statistical examination of the extracted features to learn the current health status of the system.

SHM system has been increasingly used in several structures, mainly long-span bridges, large dams and tall buildings, enabling smooth shift from time-based to condition-based maintenance. Several researches have been carried out in this field of interest recently, either in model-driven or data-driven approaches [89,92]. In SHM, a classic model-driven approach uses a numerical model (often based on finite element analysis (FEA)) of the structure which relates discrepancies between measured data and the data produced by the model to identify a damage. This approach is computationally expensive due to an iterative analysis of a computer simulation model [90]. In addition, a numerical model may not accessible all the time in practice and does not precisely capture the exact performances (e.g. materials, geometry and boundary conditions) of the real structure invariably [93]. Accordingly, the results obtained from FEA are often not accurate enough for a precise assessment of structural health. Unlike a model-driven approach, a data-driven approach creates a model by learning from measured data and then performs a comparison between the model and measured responses in order to identify damage. This approach adopts methods in pattern recognition, or more generally, in machine learning [89]. The recent advances in sensing techniques, internet technologies, and wireless communications are increasingly facilitating and allowing practical deployment of large and dense sensor networks for SHM. These make data-driven approach well convenient for early damage detection in a continuous and real-time manner [90].

The implementation of machine learning methods to detect structural damage is often observed under the categorization of supervised learning, where data from healthy and damaged conditions were needed. Single machine learning algorithms such as neural network (NN), support vector machine (SVM), support vector regression (SVR), and genetic algorithm (GA) are attractive ones for detection of structural damage because of their robustness and efficacy in dealing with inadequate information, uncertainty, and noise [89,94–96]. Hybrid methods such as multi-objective genetic algorithm (MOGA), neuro-fuzzy (NF) and wavelet neural network (WNN) [97–99] have also been proposed for different problems in SHM area. Table 1 reveals the usability of several types of machine learning algorithms in evaluating the structural health and dam behaviour. The performance comparisons of all studies revealed that machine learning based models outperforms the model-driven approach and found to be satisfactorily accurate.

4.2. Concrete properties and mix design

Mechanical properties of concrete, such as compressive strength, elastic modulus, splitting tensile and shear strength are taken into consideration in designing concrete structures. Compressive strength of concrete can be predicted using empirical formula in the form of linear or non-linear regression equations in order to save time and costs [111–114]. Measurement of elastic modulus is complicated and time consuming. Due to this, it is often acquired from the stress–strain relations of concrete under compression [115–117]. Indeed, several national building codes adopt empirical formulas that correlate the elastic modulus with compressive strength, including American Concrete Institute (ACI) [118] and Comité Euro-International du Béton (CEB) [119]. Similar to modulus of elasticity, splitting tensile of concrete is often estimated through the compressive strength due to the complexity, cost and time-consuming nature of the test. Empirical regression models derived from experimental data is also used to evaluate shear strength of RC element [120]. The conventional empirical models to evaluate the mechanical properties of concrete were formulated by a fixed equation based on a limited experimental data and factors. They are effective just for explaining their own experimental outcomes applied for their calibration. If the original data is altered, then it is a must to update the model coefficients and the form of the equation. Thus, the

Table 1
Reported application of machine learning techniques in structural health monitoring.

Researchers	Problem types	Case structures	Algorithms
Hao and Xia [100]	Detection and/or identification of structural damage	One-span steel portal frame and aluminium cantilever beam	Genetic algorithm
Chou and Ghaboussi [94]		Truss bridges	
Yan et al. [101]		Beams on ocean platform	Neural network
Yun et al. [102]		Steel frame structure	
Lee et al. [103]		Simple beam and multi-girder bridge	
Cha and Buyukozturk [97]		Steel structure	Multi-objective genetic algorithm
Satpal et al. [104]		Aluminium beams	Support vector machines
Yan et al. [101]		Beams on ocean platform	
Feng et al. [96]	Identification of structural parameters	Concrete highway bridge	Neural network
Soyoz and Feng [105]		Concrete bridge	
Karimi et al. [106]		Concrete dam	
González and Zapico [107]	Seismic damage identification	Buildings with steel moment-frame structure	Neural network
Mata [108]	Dam behaviour assessment	Concrete dam	Neural network
Kao and Loh [109]			
Ranković et al. [110]			Support vector regression
Su and Wen [99]			Wavelet neural network
Ranković et al. [98]			Neuro-fuzzy

conventional models may be unsuitable for determining mechanical properties of new concrete because the correlation between constituents and concrete characteristics for some concrete types are highly nonlinear [112–114,121–123]. Furthermore, it is challenging to come up with a universally agreed mathematical model. Dry shrinkage is another key property of concrete and its value has great importance for assessing the ability for long-term operation of concrete structures. In the past five decades, several empirical equations for shrinkage estimation were proposed in different codes such as ACI [124], CEB [125]. However, it is difficult to get accurate results using these formulas in some cases because dry shrinkage is influenced by numerous factors associated with the concrete composition, the size of specimen, the quality of its constituents, and the environmental conditions [126].

Concrete mix design is the process of determining appropriate constituents and their relative quantities in order to produce a concrete that meets the desired strength, workability and durability as minimal cost as possible. Conventional algorithms of concrete mix proportion are merely form on a generalization of preceding practice which is often obtainable as empirical formulas or as tables. Because of the uncertainty of concrete constituents (e.g. chemical and mineral admixtures, cement, and fine and coarse aggregates), the conventional algorithms of concrete mix proportion are a trial and error exercise, which results in additional costs, and time [127].

Developing accurate and reliable models to evaluate the concrete properties and mix design can optimize costs and time by delivering engineers with crucial data. The potential of machine learning algorithms have been harnessed for modelling such properties in order to overcome the drawbacks of traditional empirical regression models. A number of single or hybrid machine learning algorithms have been used to develop accurate and effective models for predicting concrete properties and mix design of various concrete types including fibre–reinforced polymer (FRP) concrete. Table 2 presents list of studies which demonstrates the applicability of machine learning methods in designing mix proportions and evaluating concrete properties. The studies adopt various machine learning algorithms, such as neural network (NN), genetic programing (GP), fuzzy logic (FL), support vector machine (SVM), adaptive network-based fuzzy inference system (ANFIS), and fuzzy inference system (FIS). All these studies concluded that machine learning techniques are powerful tool to evaluate concrete properties without being influenced by data complexity, incoherence, or incompleteness. They are also a better option for selecting suitable material proportions for the desired strength and rheology of concrete mixes. This leads to ecological and economical mix design process by reducing the number of trial mixes.

5. Recent advances and future directions in durability and service-life assessment

Deterioration of the RC structures caused by corrosion of rebar has been mainly assessed using the carbonation and/or chloride empirical models developed from experimental data. Such models limit the ability to predict accurately the time taken for depassivation of rebar since the penetration of CO_2 and Cl^- into concrete are governed by several parameters that are complex to describe mathematically. The penetration of these aggressive substances into concrete structures are controlled by several factors including material properties, casting method, workability, curing conditions, and the macro- and micro-environment to which the RC structure is exposed. In addition, the rapidly growing use of blended supplementary cementitious materials and new technologies are another factors which make the conventional empirical models incapable of accurate evaluation of the time to onset of rebar corrosion [53,144–146]. These limitations of the empirical models are the reasons for failing to attain conditions for optimized choice of suitable design, planning of inspection and maintenance that will assure an extended service life.

5.1. Recent advances

Models should be able to consider most of the influential parameters which govern the deterioration mechanisms in order to accurately predict the extent of deterioration and/or the remaining service life of a structure. Certainly, developing empirical carbonation and/or chloride models which fully address the controlling factors is challenging because the concrete behaviour is a function of several factors that are burdensome to express mathematically. Hence, developing machine learning based prediction model that can learn from the existing long-term in-service data is an attractive alternative. In the rest of this subsection, the current direct or indirect application of machine learning methods in assisting the evaluation of carbonation depth and chloride penetration is discussed.

Buenfeld et al. [147] adopted NN to predict carbonation depth based on large amount of data, around 6600, drawn from various literatures. The proposed model employ 39 input parameters describing the cement compositions, supplementary cementitious materials, concrete mix proportions, accelerated test conditioning, curing condition, and exposed environment regime and conditions. The performance of the model was tested with data obtained from 20 research papers. The prediction for real structures were found to be as accurate as for naturally exposed specimens. Lu and Liu [148] proposed two NN based models,

Table 2
Reported application of machine learning in concrete mix design and properties.

Researchers	Problem types	Types of concrete	Algorithms
Uysal and Tanyildizi [128]	Prediction of compressive strength	Self-compacting	Neural network
Prasad et al. [129]			
Siddique et al. [130]			
Prasad et al. [129]		High performance	Neural network
Cheng et al. [111]			Hybrid of FL, SVM & GA
Dantas et al. [131]		Concrete with construction and demolishing (C&D) waste	Neural network
Duan et al. [132]			
Naderpour et al. [133]		FRP reinforced	Neural network
Nazari and Sanjayan [134]		Geopolymers	Support vector machine
Nazari and Shadi [135]	Prediction of splitting tensile strength	High performance	Neural network, genetic programing
Sarıdemir [136]		Various	Genetic programing
Ahmadi-Nedushan [137]	Prediction of elastic modulus	Normal and high strength	Adaptive network-based fuzzy inference system
Demir [138]			Neural network
Yan and Shi [117]			Support vector machine
Demir and Korkmaz [123]		High strength	Fuzzy logic
Lee and Lee [139]	Prediction of shear strength	FRP reinforced	Neural network
Bashir and Ashour [140]			
Nasrollahzadeh and Basiri [141]			Fuzzy inference system
Mansour et al. [120]		Reinforced	Neural network
Bal and Buyle-Bodin [126]	Prediction of drying shrinkage	Various	Neural network
Mermerdaş and Arbili [142]		Concretes incorporate silica fume & fly ash	
Ji et al. [127]	Concrete mix design	Normal and high strength	Neural network
Khan [143]		High performance	

back-propagation neural network (BPNN) and the radial basis function neural network (RBFNN), to predict the carbonation depth of prestressed concrete. Data for training and testing were generated by conducting an accelerated carbonation test in the laboratory. The input parameters considered the stress level of concrete, w/b, cement to fine aggregate ratio, cement to coarse aggregate ratio and exposure time. The model verification test demonstrated that both the proposed NN based models had a high prediction and generalization capability in evaluation of carbonation depth. Taffese et al. [149] developed NN based carbonation depth prediction model. It employed a total of 15 input variables which characterize the concrete mix ingredients and the exposure time. Unlike several models, the authors incorporated variable selection methods to choose most appropriate parameters, and eliminate unrelated and/or redundant ones from the original input experimental data to create robust learning models. The performance assessment of the model demonstrated that it foresees reasonably well with enhanced generalization capability. Xiang [150] suggested SVM to predict the concrete carbonation depth. Real historical data which entails water to cement ratio, cement content and exposure time were assigned as input variables. The prediction performance was compared with those from NN modelling and it is noted that the SVM has higher precision and generalization capability. Zhitao et al. [151] also adopted SVM to predict concrete carbonation depth. They employed the same input parameters which were considered by Xiang's study. The prediction ability of SVM model was compared with BPNN model. The result showed that both models are effective in evaluating carbonation depth and SVM has higher prediction capability than BPNN. There are also other studies which demonstrate the applicability of machine learning in predicting carbonation depth [152–154]. These models are mainly based on neural network algorithm and consider limited subset of influential variables which controls the carbonation process. For instance, Bu et al. [152] developed DE-BP (Differential Evolution-Back Propagation) neural network based model. This model is a hybrid of differential evolution algorithm and back propagation neural network. The training data comprises parameters of w/b, cement content and exposure time (age). The authors tested the accuracy of the model using experimental data. The test result confirmed that the hybrid DE-BP neural network model provides high prediction accuracy. Luo et al. [153] proposed BPNN which is optimized by the particle swarm optimization (PSO) to predict the carbonation depth. The input data used to train the model involves three parameters which are water to cement ratio, cement content and relative humidity. The performance examination of the model revealed that the model has a good ability in predicting carbonation depth with a faster convergence. Liu et al. [154] studied the prediction ability of RBFNN and BPNNN model in predicting concrete carbonation depth using three factors as input. The authors concluded that both models predict the carbonation front with high accuracy and RBFNN has superior prediction ability than BPNN.

Taffese et al. [155] adopted three decision tree based learning algorithms (regression tree, bagged and reduced bagged ensemble regression tree) to predict the carbonation depth. Experimental data from laboratory tests were used to develop the model. The model employed 15 influential input parameters consisting of concrete mixture ingredients and the carbonation depth. The model performance test revealed that the ensemble methods predict the carbonation depth with reasonably lower error than the regression tree. Among the ensemble methods, reduced bagged ensemble regression tree has superior performance with relatively better generalization capability. Besides predicting the carbonation depth, the bagged ensemble regression tree discovered important variables that influenced the carbonation process. The influences of these variables on the carbonation process were not well known previously. The same authors, in another work, [156] developed an optimized and integrated carbonation prediction model (named CaPrM) by adopting four machine learning techniques. CaPrM is developed using experimental data gathered from concrete specimens kept in sheltered natural environment for about seven years. CaPrM utilized 25 input variables which entail information regarding the ingredients used to produce the concrete specimens, fresh and hardened properties of the concrete. The integrated learning methods are NN, decision tree and ensemble methods (bagged and boosted decision trees). The integration of the four algorithms provides the opportunity to select the best performing learning methods since their relative performance alters when a condition varies. The prediction capability assessment of CaPrM revealed that all the integrated machine learning techniques estimate the depth of carbonation with minimal error. In addition, CaPrM helped to identify other influential parameters which were disregarded in the prevailing empirical models and to rank the parameters according to their importance in the carbonation process.

Peng et al. [157] proposed a NN with cascade-correlation architecture to predict the chloride profiles diffused through concrete pores.

The input data comprises of five parameters which are cement content, fly ash, calcium nitrite solution, microsilica, and exposure time. The prediction ability of the suggested model was tested using unseen experimental data. The test result demonstrated that, in both steady and unsteady, the prediction outcomes are in good agreement with the experimental results. Inthata et al. [158] predicted chloride penetration by applying NN algorithm. The utilized experimental data covers normal and high strength concrete specimens which contain ground pozzolans such as fly ash, bottom ash and rice husk ash. Six parameters were assigned as input parameters in which five of them describe the concrete mix design (w/b, percent replacement, testing ages, pozzolans types, and aggregate to cement ratio) and one of them is a compressive strength. The assigned target parameters were chloride penetration which was obtained from rapid chloride penetration test (RCPT) and chloride depth. The RCPT is a method to evaluate the chloride permeability of concrete on the basis of the electric charge passing through them. The model were tested and compared with linear and non-linear regression techniques. The comparison result revealed that the presented NN based model have superior capability to predict chloride penetration and depth than linear and non-linear regression methods. Gilan et al. [159] developed a hybrid support vector regression (SVR) – particle swarm optimization (PSO) model to predict the chloride permeability of concrete containing metakaolin (MK). A total of 25 different concrete mix proportions were prepared to generate the training-testing database. The model employed eight input parameters consisting of cement content, MK type, amount of MK, coarse aggregate content, fine aggregate content, amount of water, exposure time and value of surface resistivity. The total charge passed through the concrete specimens was assessed and utilized to determine the chloride permeability of each concrete. In their work, a sequential forward feature selection technique was employed to attain a parsimonious model with precise prediction outcomes by selecting only a subset of variables. The performance of the proposed hybrid model was compared with ANFIS model. The comparison results showed that the SVR-PSO model has strong potential to predict chloride permeability with high degree of precision and robustness. Ghafoori et al. [160] studied the prediction ability of NN in predicting chloride permeability of self-consolidating concretes based on their mix compositions which includes binder content, w/b, coarse aggregate content, fine aggregate content, amount of air-entraining admixture and high range water reducer. Various models were established by altering the number of parameters and mixtures assigned to training and testing. The performances of the models were compared with those from linear and nonlinear regression models. The test results demonstrated that NN models have higher prediction ability than models obtained by linear and nonlinear regressions, especially when testing evaluations were selected from the boundaries of mix compositions. Boğa et al. [161] presented NN and ANFIS model for prediction of chloride permeability of concrete. In their study, concrete specimens comprising only ground granulated blast furnace slag (GGBFS), calcium nitrite-based corrosion inhibitor (CNI) and a combination of these constituents in different ratios were utilized. The proposed models employed curing types, curing time, and ratio of GGBFS and CNI as input parameters and chloride permeability obtained from RCPT as a target variable. The test evaluation revealed that both models predict the chloride permeability with reasonably low error. Yasarer and Najjar [162] developed BPNN based chloride permeability prediction model to reduce or fully substitute the rapid chloride penetration test. This is due to the fact that, unlike conventional approaches, determination of chloride permeability using machine learning techniques is time and cost effective because its experimental determination in laboratory is often time and recourse consuming. The authors employed data obtained from Kansas Department of Transportation. These data are either prepared in the laboratory or gathered from field. Six input parameters were assigned, which are oven dry weight, saturated surface dry weight, weight in water, curing time, specific gravity, and percentage of water absorbed. The total charge passed through the concrete sample was set as a target parameter. These parameters are not well considered in other studies. The performance evaluation of the model proved that NN is an efficient method to develop accurate chloride permeability prediction model. The model was compared with their counterpart regression-based models and it showed that NN model has outperformed them.

Song and Kwon [41] adopted BPNN to estimate chloride diffusion coefficient which is a decisive factor for quantification of chloride profile in concrete element. The employed training data entails eight input variables. Seven of them are components from concrete mix design and the remaining one is the exposure time. They verified the performance of the proposed model by comparing with the experimental results. The verification test revealed that the proposed NN based chloride diffusion coefficient prediction model yields high precision. The authors also argued that the model has an advantage of applicability to different concrete mix design. Kim et al. [163] were also able to accurately predict diffusion coefficient of chloride using NN algorithm. They considered seven mix components: w/b, content of cement, ground granulated blast furnace slag (GGBFS), fly ash (FA), silica fume (SF), sand, and coarse aggregate as input parameters. The chloride profiles based on the diffusion coefficient from NN were compared with test results which were kept in submerged condition for six months. The proposed model revealed that NN can assist to reasonably predict chloride penetration in the concrete. Lizarazo-Marriaga and Claisse [164] presented NN based method to determine the chloride diffusion coefficient for concrete. The method employed measurement of the electrical properties of concrete as input variables. The prediction accuracy of the proposed methodology was evaluated by comparing with the experimental data. The comparison of the results demonstrated that the employed NN methodology can yield precise concrete diffusivity values. Hodhod and Ahmed [165] developed a model using BPNN by considering w/b, cement content, FA and slag content as well as curing age as input parameters. The prediction accuracy of the proposed model was compared with the experimental results. The verification outcome demonstrated that the proposed model has high accuracy for predicting the chloride diffusion coefficient and confirms that NN based models are practical and beneficial. Tarighat and Erfanimanesh [166] employed NN to predict chloride diffusion coefficient for concrete. The proposed model utilized four input parameters including type of aggregates, w/b, binder content, and condensed SF to cementitious materials ratio. The prediction ability of the model was tested using experimental data and it is found that the model has ability to predict chloride diffusion coefficient accurately. Delnavaz et al. [167] suggested NN based chloride diffusion coefficient prediction method. It employed input parameters encompass w/b, SF content and exposure condition of the specimens. The specimens were exposed to simulated marine environments including atmospheric, submerged, and tidal zone. The target parameter was chloride diffusion coefficient. The performance evaluation of the proposed model confirmed that the proposed model has the capability to predict the chloride diffusion coefficient with high precision. Mazer and Geimba de Lima [168] proposed fuzzy logic based chloride diffusion coefficient prediction model. Parameters of the concrete mix design and the environment were considered in the model development. The performance examination showed that the model has a good capability in estimating the diffusion coefficient of chlorides.

There are also successful applications of machine learning for coupled transport processes in concrete (e.g. CO_2 and Cl^-). The purposes of the applications are mainly to evaluate the penetration rate of the aggressive substances and to investigate factors governing their transport. For instance, Cho et al. [169] proposed ANFIS based model to predict carbonation depth of RC member. The data utilized for the model training were obtained from field inspections of nine buildings which reflect the effect of the combined deterioration, including carbonation diffusion coefficient, surface chloride ion concentration, chloride diffusion coefficient, compressive strength, and crack width. The performance evaluation revealed that the proposed model estimate

the carbonation depths with high accuracy. Delnavaz and Ramezanianpour [170] adopted NN to examine the association between concrete mix design and chloride diffusion coefficients in carbonated and non-carbonated concretes. The model employed w/b, SF content, rapid chloride ion permeability test value and capillary absorption coefficient as input variables. The chloride diffusion coefficient was assigned as a target parameter. With the help of the proposed model, the authors were able to draw relationships between chloride diffusion coefficients and concrete mix design in carbonated and non-carbonated concretes. Marks et al. [171,172] utilized J48 algorithm to describe the relation between concrete mix composition and the chloride resistance which was examined by rapid chloride permeability test. The model was trained using data which describes the concrete mix design and chloride permeability in order to induce rules. Based on the generated rules they were able to effectively classify plain and modified concretes as good, acceptable and unacceptable resistance to chloride penetration. Parichatprecha and Nimityongskul [173] adopted NN algorithm to investigate the effect of water and cement content, w/b, and the replacement of FA and SF on the chloride permeability of high performance concrete (HPC). The proposed model was trained and tested by employing data obtained from experiments and previous researches. The test results indicated that the proposed model is reliable and accurate. Using the NN based simulating model they were able to determine the optimum cement content for designing durable HPC. They also recognized that increasing the amount of SF results in diminishing the chloride permeability to a greater degree than FA. In addition, their study presented how NN can be utilized to beneficially predict chloride permeability across a broad range of concrete mix parameters of HPC.

The use of machine learning in predicting carbonation depth and chloride profile in the models discussed above is encouraging, though majority of the models have adopted only NN algorithms. Studying other learning methods is necessary to achieve optimal accuracies since it is impossible to identify machine learning algorithms that perform exceptionally well for a certain problem in advance unless otherwise tested. Relative power of any machine learning based models greatly relies on the details of the considered problems. A single model (e.g. NN) may achieve greatest results on problems of particular data, but may not be true for a different data. Unlike the conventional models, machine learning based models are capable to address nearly all the governing factors which control the ingress CO_2 and Cl^- into concrete pores. This permits to assess all the governing factors as a cluster rather than separately and thus ensures the prediction reliability because crucial dependencies will not be disregarded. In another perspective, identifying the degree of influence of each parameter which controls the degradation mechanisms in traditional approach is unachievable because of the availability of several unknown aspects. On the other hand, the machine learning approaches can reflect the inherent relationships among all parameters since they have capabilities to handle complex patterns from a large data.

5.2. Future directions

As seen in the above subsection, the advantages of machine learning in assessing durability and service life of RC structures is evident. It is already recognized that machine learning has an essential and encouraging role in the aging management of RC structures. The performance of machine learning depends on the amount of data and inclusion of sufficient parameters in the data. To gather these data, monitoring systems are needed. The advancement of monitoring systems and machine learning algorithms adopted in assessing concrete properties and structural health is illustrated in Fig. 3. It can be observed that in 1990s wired sensors have been deployed to assess performance of structures. Wired monitoring systems entail high-priced communication cables to be mounted and maintained periodically. Due to the associated high costs, wired monitoring systems are not broadly implemented [174]. With the improvements in wireless sensor networks, in 2000s, the attainment of inexpensive wireless structure monitoring systems have become practicable. Recently, there are a rising number of studies demonstrating the use of wireless sensors for monitoring RC structures. The systems can be adopted to monitor parameters covering from earlier-age to environmental condition that can result in concrete degradation [175]. Durability monitoring based on wireless sensors can transform the way of inspecting structures to a rapid, remote, automated, and objective manner. They can be considered as a reliable non-destructive in-service monitoring system that delivers data about real-time ingress profile of substances. In addition, in long term, continuous remote monitoring using wireless sensors can be more economical than conducting periodic field experimenting, taking the labour cost, safety of users and the costs to the users into consideration [176,177]. More recently, smart wireless sensor provide a promising alternative to the traditional sensor systems. It is small in size and equipped with an independent on-board microprocessor with reliable wireless communication technology. Hence, there is no doubt that, wireless sensors gradually would become an integral part of aging management of RC structures.

The deployment of embedded sensors to monitor concrete properties had been demonstrated by several researchers [176,178]. Today, there are more than fifty different types of sensors for monitoring of structural changes, rebar corrosion, concrete chemistry, moisture and temperature state [175,179]. To mention few relevant cases, there are a wide range of studies that employed sensors for monitoring corrosion of rebar and/or aggressive substances causing corrosion [180–183]. Likewise, sensor-based monitoring systems to assess parameters that are controlled by the ambient environment, such as relative humidity and temperature, have been widely used in RC structures [175,184–187]. Monitoring of these parameters will provide crucial information about the extent of deteriorations, such as rebar corrosion, carbonation, freeze–thaw cycles and alkali–aggregate reaction [188]. Generally, monitoring RC structures allows a more informed performance assessment of the concrete and an early-warning indicator of incipient problems. It would also provide valuable data that can be used to calibrate the existing service-life prediction models, and thus better estimation. Moreover, the utilization of data from monitoring systems in combination with empirical models for service-life prediction leads to extra savings in lifecycle costs since planning and scheduling of maintenance programs can be optimized further [175–179].

Already, one way or another, data-driven prognostics based on embedded sensors and historical experimental data had been applied by combining with empirical model to predict the service life of RC structures. Though these approaches improve the performance prediction, they still rely on the empirical formula which has limitations (as discussed in Section 2.2). Since there was no long-term data from parameters that mainly controls the deterioration mechanisms, integrating the output obtained from the machine learning algorithms with the conventional models was inevitable. In future, durability and service-life assessment of RC structure will rely only on data obtained from continuous monitoring through various wireless sensors and machine learning. Machine learning techniques are powerful for extracting insights and developing predictive models from large data. Moreover, as illustrated in Fig. 3, the adopted machine learning algorithms for SHM as well as evaluation of concrete properties and mix design are increasing. This indicates that machine learning is already becoming a prevalent alternative approach in aging management of RC structures.

The integration of wireless sensors and machine learning tools to evaluate the performance and service life of structures will form an imperative component in the inspection, evaluation and management of RC structures. The evaluation can be done remotely and rapidly by installing sensors at different locations, transmitting the sensor data wirelessly and analysing the data using machine learning techniques. All these are done without the involvement of inspection crews to the site. Layout of the future preferred aging management method for RC structures is illustrated in Fig. 4. As seen in the layout figure, the employed sensors in the structure will provide information about the

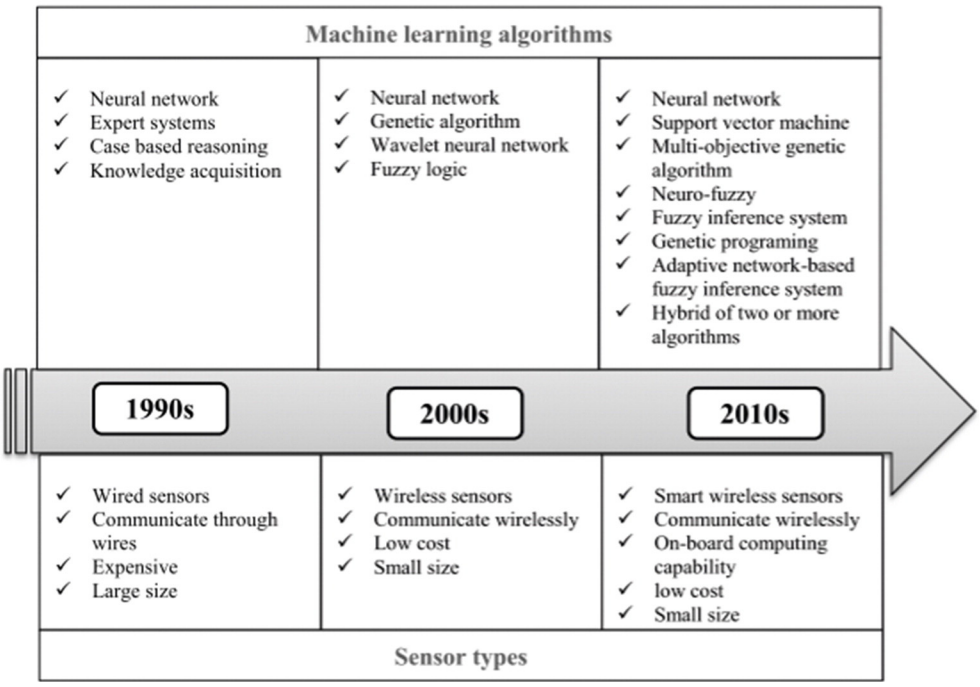

Fig. 3. Advancement of sensors and machine learning algorithms adopted in assessing concrete properties and structural health.

spatial distribution and temporal changes of the degradation governing parameters. The sensors data will be transmitted to a cloud-based storage server. It has a great advantage since, with the help of Internet connectivity, diverse streams of data can be displayed, retrieved and shared from any place. Condition assessment of the structure can be carried out by adopting explanatory data analysis remotely. Machine learning can learn the complex interrelation among factors obtained from the sensors data and perform prediction without the need for empirical model. The prediction allows for a more reasonable method to a pragmatic evaluation of the service life of a structure and accurately scheduled repair measures, and thus lessens the costs of maintenance remarkably. As the quantity of obtainable data for learning grows, the performance of machine learning based models adaptively enhances generating more reliable predictions. In addition, the use of different sensors enables the machine learning to learn the combined effect of various deterioration mechanisms. In fact, measuring the impact of the combined deterioration mechanisms in laboratory and converting the outcomes to real structure is unattainable. Hence, the integration of sensors and machine learning techniques would substitute the traditional performance assessment methods the latter often consider the influence of single deterioration mechanism. It also plays a significant role in extracting previously unknown knowledge. The discovered knowledge will assist to come up with optimal solutions that improve the durability of the structure.

6. Conclusions

This paper established the importance and applicability of machine learning for durability and service life assessment of RC structures by closely analysing its capability in addressing the limitations of the commonly used empirical models. Machine learning algorithms can learn the complex interrelation among prominent parameters that control the degradation mechanisms and perform service-life prediction accurately in real time without the need for empirical model. The paper also reviewed previously demonstrated application of machine learning methods for SHM as well as concrete properties and mix design. In addition, the recently proposed machine learning application for assisting durability assessment of RC structures are also presented. Due to the

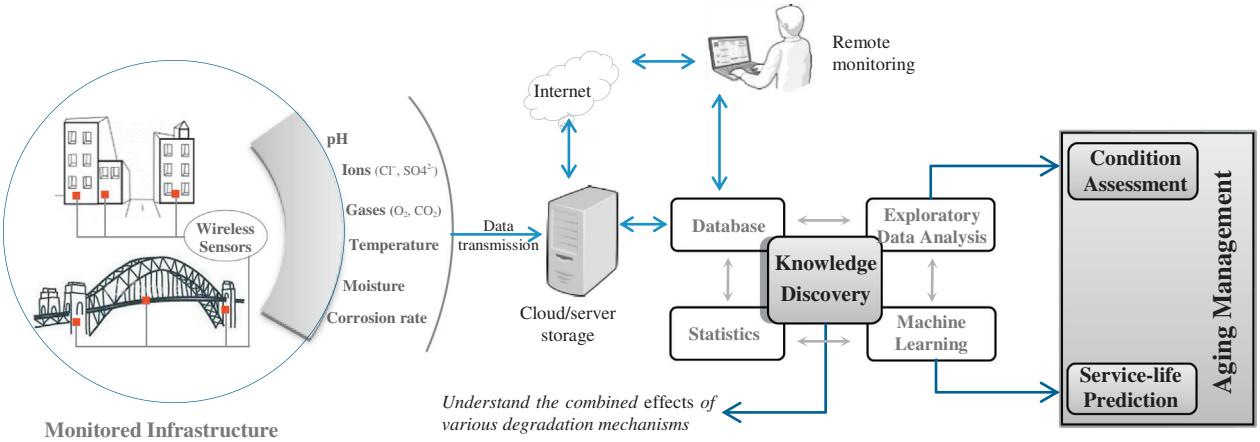

Fig. 4. Layout of the future preferred condition assessment and service-life prediction methods for RC structures.

emerging use of wireless sensors for continuous monitoring of structures, machine learning based models would likely be the future preferred non-destructive and reliable durability assessment method, bringing a paradigm shift in service-life prediction. This approach helps to accurately plan repair measures and thus enables a substantial reduction in maintenance and lifecycle costs. Furthermore, machine learning based models have the ability to learn the synergic effect of several degradation mechanisms using data obtained from various sensors, enabling them to find hidden insights. The discovered knowledge will assist the experts to optimize the concrete mix to produce durable concrete and optimal repairing methods. This work can be extended further by considering all aspects of machine learning methods in applications of several civil engineering areas.

References

[1] ACI (American Concrete Institute), Protection of Metals in Concrete Against Corrosion, ACI 222R-01, 2001.
[2] G.K. Glass, Reinforcement corrosion, in: J. Newman, B.S. Choo (Eds.), Adv. Concr. Technol. 2 Concr. Prop, Elsevier L, Butterworth-Heinemann, Oxford 2003, pp. 8/1–9/27.
[3] Z. Wang, Q. Zeng, L. Wang, Y. Yao, K. Li, Corrosion of rebar in concrete under cyclic freeze–thaw and chloride salt action, Constr. Build. Mater. 53 (2014) 40–47, http://dx.doi.org/10.1016/j.conbuildmat.2013.11.063.
[4] B. Pradhan, Corrosion behavior of steel reinforcement in concrete exposed to composite chloride–sulfate environment, Constr. Build. Mater. 72 (2014) 398–410, http://dx.doi.org/10.1016/j.conbuildmat.2014.09.026.
[5] E. Sistonen, Service Life of Hot-dip Galvanised Reinforcement Bars in Carbonated and Chloride-contaminated Concrete, Helsinki University of Technology, 2009 (http://urn.fi/URN:ISBN:978-952-248-168-9).
[6] B. Yu, L. Yang, M. Wu, B. Li, Practical model for predicting corrosion rate of steel reinforcement in concrete structures, Constr. Build. Mater. 54 (2014) 385–401, http://dx.doi.org/10.1016/j.conbuildmat.2013.12.046.
[7] M. El-Reedy, Steel-reinforced Concrete Structures: Assessment and Repair of Corrosion, CRC Press, Boca Raton, FL, 2008http://dx.doi.org/10.1201/9781420054316.
[8] Y. Zhou, B. Gencturk, K. Willam, A. Attar, Carbonation-induced and chloride-induced corrosion in reinforced concrete structures, Mater. Civ. Eng. 27 (2015), 04014245. http://dx.doi.org/10.1061/(ASCE)MT.1943-5533.0001209.
[9] G. Markeset, S. Rostam, O. Klinghoffer, Guide for the Use of Stainless Steel Reinforcement in Concrete Structures, Oslo, 2006.
[10] J.R. Mackechnie, M.G. Alexander, Repair Principles for Corrosion-damaged Reinforced Concrete Structures, Department of Civil Engineering, University of Cape Town, 2001.
[11] S.L. Matthews, J.R. Morlidge, Performance based rehabilitation of reinforced concrete structures, in: M.G. Alexander, H.-D. Beushausen, F. Dehn, P. Moyo (Eds.), Concr. Repair, Rehabil. Retrofit. II 2nd Int. Conf. Concr. Repair, Rehabil. Retrofit. ICCRRR-2, CRC Press, Leiden 2008, pp. 277–278, http://dx.doi.org/10.1201/9781439828403.ch100.
[12] W.Z. Taffese, E. Sistonen, Service life prediction of repaired structures using concrete recasting method: state-of-the-art, Procedia Eng. 57 (2013) 1138–1144, http://dx.doi.org/10.1016/j.proeng.2013.04.143.
[13] B. Bissonnette, P.H. Emmons, A.M. Vaysburd, Concrete repair: research and practice – the critical dimension, in: M.G. Alexander, H.-D. Beushausen, F. Dehn, P. Moyo (Eds.), Concr. Repair, Rehabil. Retrofit. II 2nd Int. Conf. Concr. Repair, Rehabil. Retrofit. ICCRRR-2, CRC Press, Leiden 2008, pp. 275–276, http://dx.doi.org/10.1201/9781439828403.ch99.
[14] A. Holst, H. Budelmann, H.-J. Wichmann, Improved sensor concepts for durability monitoring of reinforced concrete structures, in: F.-K. Chang (Ed.), Proc. 8th Int. Work. Struct. Heal. Monit. (IWSHM 2011), DEStech Publications, Inc., Lancaster 2011, pp. 1472–1479.
[15] ACI (American Concrete Institute), Service-life Prediction—State-of-the-art Report, ACI 365.1R-00, 2000 43.
[16] F.H. Wittmann, T. Zhao, F. Jiang, X. Wan, Influence of combined actions on durability and service life of reinforced concrete structures exposed to aggressive environment, Restor. Build. Monum. 18 (2014) 105–112, http://dx.doi.org/10.1515/rbm-2012-6510.
[17] A. Costa, J. Appleton, Concrete carbonation and chloride penetration in a marine environment, Concr. Sci. Eng. 3 (2001) 242–249.
[18] M.G. Grantham, Understanding defects, testing and inspection, in: M.G. Grantham (Ed.), Concr. Repair a Pract. Guid, CRC Press, Boca Raton, FL 2011, pp. 1–55.
[19] W. McCarter, T. Chrisp, G. Starrs, A. Adamson, E. Owens, P. Basheer, et al., Developments in performance monitoring of concrete exposed to extreme environments, Infrastruct. Syst. 18 (2012) 167–175, http://dx.doi.org/10.1061/(ASCE)IS.1943-555X.0000089.
[20] W. McCarter, T. Chrisp, G. Starrs, N. Holmes, L. Basheer, M. Basheer, et al., Developments in monitoring techniques for durability assessment of cover-zone concrete, 2nd Int. Conf. Durab. Concr. Struct, Hokkaido University Press, Sapporo 2010, pp. 137–146.
[21] P.K. Wong, Z. Yang, C.M. Vong, J. Zhong, Real-time fault diagnosis for gas turbine generator systems using extreme learning machine, Neurocomputing 128 (2014) 249–257, http://dx.doi.org/10.1016/j.neucom.2013.03.059.
[22] I.E. Mulia, T. Asano, A. Nagayama, Real-time forecasting of near-field tsunami waveforms at coastal areas using a regularized extreme learning machine, Coast. Eng. 109 (2016) 1–8, http://dx.doi.org/10.1016/j.coastaleng.2015.11.010.
[23] L. Bertolini, B. Elsener, P. Pedeferri, R.B. Polde, Corrosion of Steel in Concrete: Prevention, Diagnosis, Repair, Wiley-VCH Verlag GmbH & Co. KGaA, Weinheim, 2004http://dx.doi.org/10.1002/3527603379.
[24] A.M. Neville, J.J. Brooks, Concrete Technology, second ed. Prentice Hall, Harlow, 2010.
[25] P.K. Mehta, P.J.M. Monteiro, Concrete: Microstructure, Properties, and Materials, third ed. McGraw-Hill, New York, 2006http://dx.doi.org/10.1036/0071462899.
[26] fib (International Federation for Structural Concrete), Structural Concrete: Textbook on Behaviour, Design and Performance, fib, Lausanne, 2009.
[27] B. Lagerblad, Carbon Dioxide Uptake During Concrete Life Cycle – State of the Art, 2005.
[28] B. Saassouh, Z. Lounis, Probabilistic modeling of chloride-induced corrosion in concrete structures using first- and second-order reliability methods, Cem. Concr. Compos. 34 (2012) 1082–1093, http://dx.doi.org/10.1016/j.cemconcomp.2012.05.001.
[29] R. Neves, F.A. Branco, J. De Brito, A method for the use of accelerated carbonation tests in durability design, Constr. Build. Mater. 36 (2012) 585–591, http://dx.doi.org/10.1016/j.conbuildmat.2012.06.028.
[30] A. Köliö, T.A. Pakkala, J. Lahdensivu, M. Kiviste, Durability demands related to carbonation induced corrosion for Finnish concrete buildings in changing climate, Eng. Struct. 62–63 (2014) 42–52, http://dx.doi.org/10.1016/j.engstruct.2014.01.032.
[31] C.G. Nogueira, E.D. Leonel, Probabilistic models applied to safety assessment of reinforced concrete structures subjected to chloride ingress, Eng. Fail. Anal. 31 (2013) 76–89, http://dx.doi.org/10.1016/j.engfailanal.2013.01.023.
[32] J. Zhang, Z. Lounis, Nonlinear relationships between parameters of simplified diffusion-based model for service life design of concrete structures exposed to chlorides, Cem. Concr. Compos. 31 (2009) 591–600, http://dx.doi.org/10.1016/j.cemconcomp.2009.05.008.
[33] Y. Hosokawa, K. Yamada, B. Johannesson, L.-O. Nilsson, Development of a multi-species mass transport model for concrete with account to thermodynamic phase equilibriums, Mater. Struct. 44 (2011) 1577–1592, http://dx.doi.org/10.1617/s11527-011-9720-2.
[34] K. Henchi, E. Samson, F. Chapdelaine, J. Marchand, Advanced finite-element predictive model for the service life prediction of concrete infrastructures in support of asset management and decision-making, in: L. Soibelman, B. Akinci (Eds.), Proc. 2007 Int. Work. Comput. Civ. Eng, American Society of Civil Engineers, Reston 2007, pp. 870–880, http://dx.doi.org/10.1061/40937(261)103.
[35] E. Bastidas-Arteaga, A. Chateauneuf, M. Sánchez-Silva, P. Bressolette, F. Schoefs, A comprehensive probabilistic model of chloride ingress in unsaturated concrete, Eng. Struct. 33 (2011) 720–730, http://dx.doi.org/10.1016/j.engstruct.2010.11.008.
[36] O.-P. Kari, Long-term Ageing of Concrete Structures in Finnish Rock Caverns as Application Facilities for Low- and Intermediate-level Nuclear Waste, Aalto University, 2015 (http://urn.fi/URN:ISBN:978-952-60-6052-1).
[37] F. Papworth, A whole of life approach to concrete durability—the CIA concrete durability series, in: F. Dehn, H.-D. Beushausen, M.G. Alexander, P. Moyo (Eds.), Concr. Repair, Rehabil. Retrofit. IV Proc. 4th Int. Conf. Concr. Repair, Rehabil. Retrofit, CRC Press, Leiden 2015, pp. 213–219, http://dx.doi.org/10.1201/b18972-30.
[38] K.Y. Ann, S.W. Pack, J.P. Hwang, H.W. Song, S.H. Kim, Service life prediction of a concrete bridge structure subjected to carbonation, Constr. Build. Mater. 24 (2010) 1494–1501, http://dx.doi.org/10.1016/j.conbuildmat.2010.01.023.
[39] O.P. Kari, J. Puttonen, E. Skantz, Reactive transport modelling of long-term carbonation, Cem. Concr. Compos. 52 (2014) 42–53, http://dx.doi.org/10.1016/j.cemconcomp.2014.05.003.
[40] C.L. Page, Corrosion and protection of reinforcing steel in concrete, in: C.L. Page, M.M. Page (Eds.), Durab. Concr. Cem. Compos, Woodhead Publishing Ltd., Cambridge, U.K. 2007, pp. 136–186.
[41] H.-W. Song, S.-J. Kwon, Evaluation of chloride penetration in high performance concrete using neural network algorithm and micro pore structure, Cem. Concr. Res. 39 (2009) 814–824, http://dx.doi.org/10.1016/j.cemconres.2009.05.013.
[42] O.P. Kari, J. Puttonen, Simulation of concrete deterioration in Finnish rock cavern conditions for final disposal of nuclear waste, Ann. Nucl. Energy 72 (2014) 20–30, http://dx.doi.org/10.1016/j.anucene.2014.04.035.
[43] P. Schiessl, S. Lay, Influence of concrete composition, in: H. Böhni (Ed.), Corros. Reinf. Concr. Struct, Woodhead Publishing Limited, Cambridge, U.K. 2005, pp. 91–134.
[44] R. Neves, F. Branco, J. De Brito, Field assessment of the relationship between natural and accelerated concrete carbonation resistance, Cem. Concr. Compos. 41 (2013) 9–15, http://dx.doi.org/10.1016/j.cemconcomp.2013.04.006.
[45] fib (International Federation for Structural Concrete), Code-type Models for Concrete Behaviour: State-of-the-art Report, fib, Lausanne, 2013.
[46] fib (International Federation for Structural Concrete), fib Model Code for Concrete Structures 2010, Ernst & Sohn, Berlin, 2013.
[47] DuraCrete, DuraCrete Final Technical Report: Probabilistic Performance Based Durability Design of Concrete Structures, 2000.
[48] L. Tang, L.-O. Nilsson, P.A.M. Basheer, Resistance of Concrete to Chloride Ingress: Testing and Modelling, Boca Raton, FL, 2011, http://dx.doi.org/10.1201/b12603.
[49] J. Marchand, E. Samson, Predicting the service-life of concrete structures – limitations of simplified models, Cem. Concr. Compos. 31 (2009) 515–521, http://dx.doi.org/10.1016/j.cemconcomp.2009.01.007.
[50] C. Andrade, R. D'Andrea, N. Rebolledo, Chloride ion penetration in concrete: the reaction factor in the electrical resistivity model, Cem. Concr. Compos. 47 (2014) 41–46, http://dx.doi.org/10.1016/j.cemconcomp.2013.09.022.

[51] G. Morcous, Z. Lounis, Prediction of onset of corrosion in concrete bridge decks using neural networks and case-based reasoning, Comput. Civ. Infrastruct. Eng. 20 (2005) 108–117, http://dx.doi.org/10.1111/j.1467-8667.2005.00380.x.
[52] Y.-M. Sun, T.-P. Chang, M.-T. Liang, Kirchhoff transformation analysis for determining time/depth dependent chloride diffusion coefficient in concrete, J. Mater. Sci. 43 (2008) 1429–1437, http://dx.doi.org/10.1007/s10853-007-2304-4.
[53] J.C. Walraven, Design for service life: how should it be implemented in future codes, in: M.G. Alexander, H.-D. Beushausen, F. Dehn, P. Moyo (Eds.), Concr. Repair, Rehabil. Retrofit. II 2nd Int. Conf. Concr. Repair, Rehabil. Retrofit. ICCRRR-2, CRC Press, Leiden 2008, pp. 3–10, http://dx.doi.org/10.1201/9781439828403.sec1.
[54] R. Bekkerman, M. Bilenko, J. Langford, Scaling up machine learning: introduction, in: R. Bekkerman, M. Bilenko, J. Langford (Eds.), Scaling up Mach. Learn. Parallel Distrib. Approaches, Cambridge University Press, New York 2012, pp. 1–22.
[55] V. Cherkassky, F. Mulier, Learning From Data: Concepts, Theory, and Methods, second ed. John Wiley & Sons, Inc., Hoboken, NJ, 2007.
[56] J. Han, M. Kamber, J. Pei, Data Mining: Concepts and Techniques, Morgan Kaufmann, Waltham, MA, 2012.
[57] I.H. Witten, E. Frank, M.A. Hall, Data Mining: Practical Machine Learning Tools and Techniques: Practical Machine Learning Tools and Techniques, Morgan Kaufmann, Burlington, MA, 2011.
[58] E. Alpaydin, Introduction to Machine Learning, second ed. MIT Press, Cambridge, MA, 2010http://dx.doi.org/10.1017/S0269888910000056.
[59] Y. Reich, Machine learning techniques for civil engineering problems, Microcomput. Civ. Eng. 12 (1997) 295–310, http://dx.doi.org/10.1111/0885-9507.00065.
[60] V.M. Karbhari, L.S.-W. Lee, Vibration-based damage detection techniques for structural health monitoring of civil infrastructure systems, in: V.M. Karbhari, F. Ansari (Eds.), Struct. Heal. Monit. Civ. Infrastruct. Syst, Woodhead Publishing Limited, Cambridge, U.K. 2009, pp. 177–212.
[61] T. Mitchell, Machine Learning, McGraw Hill, 1997.
[62] M. Kanevski, V. Timonin, A. Pozdnukhov, Machine Learning for Spatial Environmental Data: Theory, Applications, and Software, EPFL Press, Lausanne, 2009http://dx.doi.org/10.1201/9781439808085.
[63] S. Marsland, Machine Learning: An Algorithmic Perspective, Chapman and Hall/CRC, Boca Raton, FL, 2009.
[64] K.P. Murphy, Machine learning: a probabilistic perspective, Machine Learning: A Probabilistic Perspective, Cambridge, MA, 2012.
[65] M. Ivanović, M. Radovanović, Modern machine learning techniques and their applications, in: A. Hussain, M. Ivanović (Eds.), Electron. Commun. Networks IV Proc. 4th Int. Conf. Electron. Commun. Networks, CRC Press, Leiden 2015, pp. 833–846, http://dx.doi.org/10.1201/b18592-153.
[66] T. Harris, Credit scoring using the clustered support vector machine, Expert Syst. Appl. 42 (2015) 741–750, http://dx.doi.org/10.1016/j.eswa.2014.08.029.
[67] A. Takeda, T. Kanamori, Using financial risk measures for analyzing generalization performance of machine learning models, Neural Netw. 57 (2014) 29–38, http://dx.doi.org/10.1016/j.neunet.2014.05.006.
[68] M.J. Kim, D.K. Kang, Ensemble with neural networks for bankruptcy prediction, Expert Syst. Appl. 37 (2010) 3373–3379, http://dx.doi.org/10.1016/j.eswa.2009.10.012.
[69] K. Di, W. Li, Z. Yue, Y. Sun, Y. Liu, A machine learning approach to crater detection from topographic data, Adv. Space Res. 54 (2014) 2419–2429, http://dx.doi.org/10.1016/j.asr.2014.08.018.
[70] G. Dede, M.H. Sazlı, Speech recognition with artificial neural networks, Digit. Signal Process. 20 (2010) 763–768, http://dx.doi.org/10.1016/j.dsp.2009.10.004.
[71] W.W. Hsieh, Machine Learning Methods in the Environmental Sciences: Neural Networks and Kernels, Cambridge University Press, Cambridge, 2009http://dx.doi.org/10.1017/CBO9780511627217.
[72] W.Z. Taffese, Case-based reasoning and neural networks for real estate valuation, in: V. Devedžic (Ed.), Proc. 25th IASTED Int. Multi-conference Artif. Intell. Appl, ACTA Press, Anaheim, CA 2007, pp. 84–89.
[73] B. Park, J.K. Bae, Using machine learning algorithms for housing price prediction: the case of Fairfax County, Virginia housing data, Expert Syst. Appl. 42 (2015) 2928–2934, http://dx.doi.org/10.1016/j.eswa.2014.11.040.
[74] W.Z. Taffese, A survey on application of artificial intelligence in real estate industry, in: M.Y. Hamid, A. Chekima, G. Sainarayanan, N. Prabhakaran, P. Anthony, F. Wong, et al., (Eds.), Proc. Third Int. Conf. Artif. Intell. Eng. Technol, Universiti Malaysia Sabah, Kota Kinabalu 2006, pp. 710–715.
[75] K.W. Chau, C.L. Wu, A hybrid model coupled with singular spectrum analysis for daily rainfall prediction, J. Hydroinformatics 12 (2010) 458–473, http://dx.doi.org/10.2166/hydro.2010.032.
[76] R. Taormina, K.-W. Chau, Data-driven input variable selection for rainfall–runoff modeling using binary-coded particle swarm optimization and extreme learning machines, J. Hydrol. 529 (2015) 1617–1632, http://dx.doi.org/10.1016/j.jhydrol.2015.08.022.
[77] W. Wang, K. Chau, D. Xu, X.-Y. Chen, Improving forecasting accuracy of annual runoff time series using ARIMA based on EEMD decomposition, Water Resour. Manag. 29 (2015) 2655–2675, http://dx.doi.org/10.1007/s11269-015-0962-6.
[78] C.L. Wu, K.W. Chau, Y.S. Li, Methods to improve neural network performance in daily flows prediction, J. Hydrol. 372 (2009) 80–93, http://dx.doi.org/10.1016/j.jhydrol.2009.03.038.
[79] A. Lavecchia, Machine-learning approaches in drug discovery: methods and applications, Drug Discov. Today 20 (2015) 318–331, http://dx.doi.org/10.1016/j.drudis.2014.10.012.
[80] G. Wang, K.-M. Lam, Z. Deng, K.-S. Choi, Prediction of mortality after radical cystectomy for bladder cancer by machine learning techniques, Comput. Biol. Med. 63 (2015) 124–132, http://dx.doi.org/10.1016/j.compbiomed.2015.05.015.
[81] D. Che, Q. Liu, K. Rasheed, X. Tao, Decision tree and ensemble learning algorithms with their applications in bioinformatics, in: H.R. Arabnia, Q.-N. Tran (Eds.), Softw. Tools Algorithms Biol. Syst, Springer-Verlag, New York 2011, pp. 191–199, http://dx.doi.org/10.1007/978-1-4419-7046-6.
[82] S. Zhang, K.-W. Chau, Dimension reduction using semi-supervised locally linear embedding for plant leaf classification, in: D.-S. Huang, K.-H. Jo, H.-H. Lee, H.-J. Kang, V. Bevilacqua (Eds.), Emerg. Intell. Comput. Technol. Appl. 5th Int. Conf. Intell. Comput. ICIC 2009, Ulsan, South Korea, Sept. 16-19, 2009. Proc, Springer, Berlin Heidelberg, Heidelberg 2009, pp. 948–955, http://dx.doi.org/10.1007/978-3-642-04070-2_100.
[83] A. Vaughan, S.V. Bohac, Real-time, adaptive machine learning for non-stationary, near chaotic gasoline engine combustion time series, Neural Netw. 70 (2015) 18–26, http://dx.doi.org/10.1016/j.neunet.2015.04.007.
[84] S. Jurado, À. Nebot, F. Mugica, N. Avellan, Hybrid methodologies for electricity load forecasting: entropy-based feature selection with machine learning and soft computing techniques, Energy 86 (2015) 276–291, http://dx.doi.org/10.1016/j.energy.2015.04.039.
[85] A. Kialashaki, J.R. Reisel, Development and validation of artificial neural network models of the energy demand in the industrial sector of the United States, Energy 76 (2014) 749–760, http://dx.doi.org/10.1016/j.energy.2014.08.072.
[86] T. Arciszewski, M. Mustafa, W. Ziarko, A methodology of design knowledge acquisition for use in learning expert systems, Int. J. Man Mach. Stud. 27 (1987) 23–32, http://dx.doi.org/10.1016/S0020-7373(87)80042-1.
[87] J.R. Stone, D.I. Blockley, B.W. Pilsworth, Towards machine learning from case histories, Civ. Eng. Syst. 6 (1989) 129–135, http://dx.doi.org/10.1080/02630258908970553.
[88] S. Zheng, Z. Li, H. Wang, A genetic fuzzy radial basis function neural network for structural health monitoring of composite laminated beams, Expert Syst. Appl. 38 (2011) 11837–11842, http://dx.doi.org/10.1016/j.eswa.2011.03.072.
[89] N.L. Khoa, B. Zhang, Y. Wang, F. Chen, S. Mustapha, Robust dimensionality reduction and damage detection approaches in structural health monitoring, Struct. Health Monit. 13 (2014) 406–417, http://dx.doi.org/10.1177/1475921714532989.
[90] S.-S. Jin, S. Cho, H.-J. Jung, Adaptive reference updating for vibration-based structural health monitoring under varying environmental conditions, Comput. Struct. 158 (2015) 211–224, http://dx.doi.org/10.1016/j.compstruc.2015.06.001.
[91] S. Yuan, L. Wang, G. Peng, Neural network method based on a new damage signature for structural health monitoring, Thin-Walled Struct. 43 (2005) 553–563, http://dx.doi.org/10.1016/j.tws.2004.10.003.
[92] S. Saadat, M.N. Noori, G.D. Buckner, T. Furukawa, Y. Suzuki, Structural health monitoring and damage detection using an intelligent parameter varying (IPV) technique, Int. J. Non Linear Mech. 39 (2004) 1687–1697, http://dx.doi.org/10.1016/j.ijnonlinmec.2004.03.001.
[93] F. Salazar, M.A. Toledo, E. Oñate, R. Morán, An empirical comparison of machine learning techniques for dam behaviour modelling, Struct. Saf. 56 (2015) 9–17, http://dx.doi.org/10.1016/j.strusafe.2015.05.001.
[94] J.-H. Chou, J. Ghaboussi, Genetic algorithm in structural damage detection, Comput. Struct. 79 (2001) 1335–1353, http://dx.doi.org/10.1016/S0045-7949(01)00027-X.
[95] B.A. Story, A Comparative Array of Artificial Neural Networks for Use in Structural Impairment Detection, Texas A&M University, 2012.
[96] M.Q. Feng, D.K. Kim, J.-H. Yi, Y. Chen, Baseline models for bridge performance monitoring, J. Eng. Mech. 130 (2004) 562–569, http://dx.doi.org/10.1061/(ASCE)0733-9399(2004)130:5(562).
[97] Y.-J. Cha, O. Buyukozturk, Modal strain energy based damage detection using multi-objective optimization, in: A. Wicks (Ed.), Struct. Heal. Monit. Vol. 5 Proc. 32nd IMAC, A Conf. Expo. Struct. Dyn. 2014, Springer, Cham 2014, pp. 125–133, http://dx.doi.org/10.1007/978-3-319-04570-2_14.
[98] V. Ranković, N. Grujović, D. Divac, N. Milivojević, A. Novaković, Modelling of dam behaviour based on neuro-fuzzy identification, Eng. Struct. 35 (2012) 107–113, http://dx.doi.org/10.1016/j.engstruct.2011.11.011.
[99] H.Z. Su, Z.P. Wen, Combination model monitoring dam safety with wavelet neural network, in: Z. Wu, M. Abe (Eds.), Proc. First Int. Conf. Struct. Heal. Monit. Intell. Infrastruct, A. A. Balkema, Lisse 2003, pp. 593–600.
[100] H. Hao, Y. Xia, Vibration-based damage detection of structures by genetic algorithm, J. Comput. Civ. Eng. 16 (2002) 222–229, http://dx.doi.org/10.1061/(ASCE)0887-3801(2002)16:3(222).
[101] B. Yan, Y. Cui, L. Zhang, C. Zhang, Y. Yang, Z. Bao, et al., Beam structure damage identification based on BP neural network and support vector machine, Math. Probl. Eng. 2014 (2014) 1–8, http://dx.doi.org/10.1155/2014/850141.
[102] C.-B. Yun, J.-H. Yi, E.Y. Bahng, Joint damage assessment of framed structures using a neural networks technique, Eng. Struct. 23 (2001) 425–435, http://dx.doi.org/10.1016/S0141-0296(00)00067-5.
[103] J.J. Lee, J.W. Lee, J.H. Yi, C.B. Yun, H.Y. Jung, Neural networks-based damage detection for bridges considering errors in baseline finite element models, J. Sound Vib. 280 (2005) 555–578, http://dx.doi.org/10.1016/j.jsv.2004.01.003.
[104] S.B. Satpal, A. Guha, S. Banerjee, Damage identification in aluminum beams using support vector machine: numerical and experimental studies, Struct. Control. Health Monit. (2015)http://dx.doi.org/10.1002/stc.1773.
[105] S. Soyoz, M.Q. Feng, Long-term monitoring and identification of bridge structural parameters, Comput. Civ. Infrastruct. Eng. 24 (2009) 82–92, http://dx.doi.org/10.1111/j.1467-8667.2008.00572.x.
[106] I. Karimi, N. Khaji, M.T. Ahmadi, M. Mirzayee, System identification of concrete gravity dams using artificial neural networks based on a hybrid finite element–boundary element approach, Eng. Struct. 32 (2010) 3583–3591, http://dx.doi.org/10.1016/j.engstruct.2010.08.002.
[107] M.P. González, J.L. Zapico, Seismic damage identification in buildings using neural networks and modal data, Comput. Struct. 86 (2008) 416–426, http://dx.doi.org/10.1016/j.compstruc.2007.02.021.

[108] J. Mata, Interpretation of concrete dam behaviour with artificial neural network and multiple linear regression models, Eng. Struct. 33 (2011) 903–910, http://dx.doi.org/10.1016/j.engstruct.2010.12.011.
[109] C.-Y. Kao, C.-H. Loh, Monitoring of long-term static deformation data of Fei-Tsui arch dam using artificial neural network-based approaches, Struct. Control. Health Monit. 20 (2013) 282–303, http://dx.doi.org/10.1002/stc.492.
[110] V. Ranković, N. Grujović, D. Divac, N. Milivojević, Development of support vector regression identification model for prediction of dam structural behaviour, Struct. Saf. 48 (2014) 33–39, http://dx.doi.org/10.1016/j.strusafe.2014.02.004.
[111] M.-Y. Cheng, J.-S. Chou, A.F.V. Roy, Y.-W. Wu, High-performance concrete compressive strength prediction using time-weighted evolutionary fuzzy support vector machines inference model, Autom. Constr. 28 (2012) 106–115, http://dx.doi.org/10.1016/j.autcon.2012.07.004.
[112] U. Atici, Prediction of the strength of mineral admixture concrete using multivariable regression analysis and an artificial neural network, Expert Syst. Appl. 38 (2011) 9609–9618, http://dx.doi.org/10.1016/j.eswa.2011.01.156.
[113] J.-S. Chou, C.-F. Tsai, A.-D. Pham, Y.-H. Lu, Machine learning in concrete strength simulations: multi-nation data analytics, Constr. Build. Mater. 73 (2014) 771–780, http://dx.doi.org/10.1016/j.conbuildmat.2014.09.054.
[114] I.-C. Yeh, L.-C. Lien, Knowledge discovery of concrete material using Genetic Operation Trees, Expert Syst. Appl. 36 (2009) 5807–5812, http://dx.doi.org/10.1016/j.eswa.2008.07.004.
[115] I. Saini, P. Chandramouli, Prediction of elastic modulus of high strength concrete by Gaussian process regression, Sci. Eng. Res. 4 (2013) 197–198.
[116] A.H. Gandomi, A.H. Alavi, Applications of computational intelligence in behavior simulation of concrete materials, in: X.-S. Yang, S. Koziel (Eds.), Comput. Optim. Appl. Eng. Ind, Springer, Berlin 2011, pp. 221–243, http://dx.doi.org/10.1007/978-3-642-20986-4_9.
[117] K. Yan, C. Shi, Prediction of elastic modulus of normal and high strength concrete by support vector machine, Constr. Build. Mater. 24 (2010) 1479–1485, http://dx.doi.org/10.1016/j.conbuildmat.2010.01.006.
[118] ACI (American Concrete Institute), Building Code Requirements for Structural Concrete (ACI 318-95) and Commentary (ACI 318R-95), AC1318-95 AC1318R-95, 1995.
[119] CEB (Comité Euro-International du Béton), CEB-FIP Model Code 90, 1993.
[120] M.Y. Mansour, M. Dicleli, J.Y. Lee, J. Zhang, Predicting the shear strength of reinforced concrete beams using artificial neural networks, Eng. Struct. 26 (2004) 781–799, http://dx.doi.org/10.1016/j.engstruct.2004.01.011.
[121] A. Behnood, K.P. Verian, M.M. Gharehveran, Evaluation of the splitting tensile strength in plain and steel fiber-reinforced concrete based on the compressive strength, Constr. Build. Mater. 98 (2015) 519–529, http://dx.doi.org/10.1016/j.conbuildmat.2015.08.124.
[122] J.-K. Kim, S.H. Han, Y.C. Song, Effect of temperature and aging on the mechanical properties of concrete: part I. Experimental results, Cem. Concr. Res. 32 (2002) 1087–1094, http://dx.doi.org/10.1016/S0008-8846(02)00744-5.
[123] F. Demir, K.A. Korkmaz, Prediction of lower and upper bounds of elastic modulus of high strength concrete, Constr. Build. Mater. 22 (2008) 1385–1393, http://dx.doi.org/10.1016/j.conbuildmat.2007.04.012.
[124] ACI (American Concrete Institute), Guide for Modeling and Calculating Shrinkage and Creep in Hardened Concrete, ACI 209.2R-08, 2008.
[125] Z.P. Bažant, S. Baweja, Creep and shrinkage prediction model for analysis and design of concrete structures: model B3-short form, in: A. Al-Manaseer (Ed.), Adam Nev. Symp. Creep Shrinkage-Structural Des. Eff. ACISP-194, American Concrete Institute (ACI), Farmington Hills, MI 2000, pp. 85–100.
[126] L. Bal, F. Buyle-Bodin, Artificial neural network for predicting drying shrinkage of concrete, Constr. Build. Mater. 38 (2013) 248–254, http://dx.doi.org/10.1016/j.conbuildmat.2012.08.043.
[127] T. Ji, T. Lin, X. Lin, A concrete mix proportion design algorithm based on artificial neural networks, Cem. Concr. Res. 36 (2006) 1399–1408, http://dx.doi.org/10.1016/j.cemconres.2006.01.009.
[128] M. Uysal, H. Tanyildizi, Estimation of compressive strength of self compacting concrete containing polypropylene fiber and mineral additives exposed to high temperature using artificial neural network, Constr. Build. Mater. 27 (2012) 404–414, http://dx.doi.org/10.1016/j.conbuildmat.2011.07.028.
[129] B.K.R. Prasad, H. Eskandari, B.V.V. Reddy, Prediction of compressive strength of SCC and HPC with high volume fly ash using ANN, Constr. Build. Mater. 23 (2009) 117–128, http://dx.doi.org/10.1016/j.conbuildmat.2008.01.014.
[130] R. Siddique, P. Aggarwal, Y. Aggarwal, Prediction of compressive strength of self-compacting concrete containing bottom ash using artificial neural networks, Adv. Eng. Softw. 42 (2011) 780–786, http://dx.doi.org/10.1016/j.advengsoft.2011.05.016.
[131] A.T.A. Dantas, M.B. Leite, K. de J. Nagahama, Prediction of compressive strength of concrete containing construction and demolition waste using artificial neural networks, Constr. Build. Mater. 38 (2013) 717–722, http://dx.doi.org/10.1016/j.conbuildmat.2012.09.026.
[132] Z.H. Duan, S.C. Kou, C.S. Poon, Prediction of compressive strength of recycled aggregate concrete using artificial neural networks, Constr. Build. Mater. 40 (2013) 1200–1206, http://dx.doi.org/10.1016/j.conbuildmat.2012.04.063.
[133] H. Naderpour, A. Kheyroddin, G.G. Amiri, Prediction of FRP-confined compressive strength of concrete using artificial neural networks, Compos. Struct. 92 (2010) 2817–2829, http://dx.doi.org/10.1016/j.compstruct.2010.04.008.
[134] A. Nazari, J.G. Sanjayan, Modelling of compressive strength of geopolymer paste, mortar and concrete by optimized support vector machine, Ceram. Int. 41 (2015) 12164–12177, http://dx.doi.org/10.1016/j.ceramint.2015.06.037.
[135] A. Nazari, S. Riahi, Prediction split tensile strength and water permeability of high strength concrete containing TiO2 nanoparticles by artificial neural network and genetic programming, Compos. Part B Eng. 42 (2011) 473–488, http://dx.doi.org/10.1016/j.compositesb.2010.12.004.
[136] M. Sarıdemir, Empirical modeling of splitting tensile strength from cylinder compressive strength of concrete by genetic programming, Expert Syst. Appl. 38 (2011) 14257–14268, http://dx.doi.org/10.1016/j.eswa.2011.04.239.
[137] B. Ahmadi-Nedushan, Prediction of elastic modulus of normal and high strength concrete using ANFIS and optimal nonlinear regression models, Constr. Build. Mater. 36 (2012) 665–673, http://dx.doi.org/10.1016/j.conbuildmat.2012.06.002.
[138] F. Demir, Prediction of elastic modulus of normal and high strength concrete by artificial neural networks, Constr. Build. Mater. 22 (2008) 1428–1435, http://dx.doi.org/10.1016/j.conbuildmat.2007.04.004.
[139] S. Lee, C. Lee, Prediction of shear strength of FRP-reinforced concrete flexural members without stirrups using artificial neural networks, Eng. Struct. 61 (2014) 99–112, http://dx.doi.org/10.1016/j.engstruct.2014.01.001.
[140] R. Bashir, A. Ashour, Neural network modelling for shear strength of concrete members reinforced with FRP bars, Compos. Part B Eng. 43 (2012) 3198–3207, http://dx.doi.org/10.1016/j.compositesb.2012.04.011.
[141] K. Nasrollahzadeh, M.M. Basiri, Prediction of shear strength of FRP reinforced concrete beams using fuzzy inference system, Expert Syst. Appl. 41 (2014) 1006–1020, http://dx.doi.org/10.1016/j.eswa.2013.07.045.
[142] K. Mermerdaş, M.M. Arbili, Explicit formulation of drying and autogenous shrinkage of concretes with binary and ternary blends of silica fume and fly ash, Constr. Build. Mater. 94 (2015) 371–379, http://dx.doi.org/10.1016/j.conbuildmat.2015.07.074.
[143] M.I. Khan, Mix proportions for HPC incorporating multi-cementitious composites using artificial neural networks, Constr. Build. Mater. 28 (2012) 14–20, http://dx.doi.org/10.1016/j.conbuildmat.2011.08.021.
[144] M. Marks, D. Jozwiak-Niedzwiedzka, M.A. Glinicki, Application of machine learning for prediction of concrete resistance to migration of chlorides, in: A.M. Brandt, J. Olek, I.H. Marshall (Eds.), Proc. Int. Symp. "Brittle Matrix Compos. 9", Woodhead Publishing Ltd. and Institute of Fundamental Technological Research, Warsaw 2009, pp. 227–236.
[145] F. Papworth, A whole of life approach to concrete durability—the CIA concrete durability series, in: F. Dehn, H.-D. Beushausen, M.G. Alexander, P. Moyo (Eds.), Concr. Repair, Rehabil. Retrofit. IV 4th Int. Conf. Concr. Repair, Rehabil. Retrofit. ICCRRR-4, CRC Press, Leiden 2015, pp. 213–219, http://dx.doi.org/10.1201/b18972-30.
[146] S.W. Tang, Y. Yao, C. Andrade, Z.J. Li, Recent durability studies on concrete structure, Cem. Concr. Res. 78 (2015) 143–154, http://dx.doi.org/10.1016/j.cemconres.2015.05.021.
[147] N.R. Buenfeld, N.M. Hassanein, A.J. Jones, An artificial neural network for predicting carbonation depth in concrete structures, in: I. Flood, N. Kartam (Eds.), Artif. Neural Networks Civ. Eng. Adv. Featur. Appl, American Society of Civil Engineers, Reston, VA 1998, pp. 77–117.
[148] C. Lu, R. Liu, Predicting carbonation depth of prestressed concrete under different stress states using artificial neural network, Adv. Artif. Neural Syst. 2009 (2009) 1–8, http://dx.doi.org/10.1155/2009/193139.
[149] W.Z. Taffese, F. Al-Neshawy, E. Sistonen, M. Ferreira, Optimized neural network based carbonation prediction model, Int. Symp. Non-Destructive Test. Civ. Eng. (NDT-CE 2015), Bundesanstalt für Materialforschung und –prüfung (BAM), Berlin 2015, pp. 1074–1083.
[150] R. Xiang, Prediction of concrete carbonation depth based on support vector regression, in: Q. Liu, M. Zhu (Eds.), Third Int. Symp. Intell. Inf. Technol. Appl, IEEE Computer Society, Los Alamitos, CA 2009, pp. 172–175, http://dx.doi.org/10.1109/IITA.2009.469.
[151] L. Zhitao, H. Hongming, Z. Shengli, Research on support vector machine's prediction of concrete carbonization, in: Q. Luo (Ed.), Int. Semin. Bus. Inf. Manag, IEEE Computer Society, Los Alamitos, CA 2008, pp. 319–322, http://dx.doi.org/10.1109/ISBIM.2008.206.
[152] N. Bu, G. Yang, H. Zhao, Prediction of concrete carbonization depth based on DE-BP neural network, in: Q. Luo, M. Zhu (Eds.), Third Int. Symp. Intell. Inf. Technol. Appl. IITA 2009, IEEE Computer Society, Los Alamitos, CA 2009, pp. 240–243, http://dx.doi.org/10.1109/IITA.2009.252.
[153] D. Luo, D. Niu, Z. Dong, Application of neural network for concrete carbonation depth prediction, in: J. Olek, J. Weiss (Eds.), Proc. 4th Int. Conf. Durab. Concr. Struct, Purdue University Press, West Lafayette, IN 2014, pp. 66–71, http://dx.doi.org/10.5703/1288284315384.
[154] Y. Liu, S. Zhao, C. Yi, The forecast of carbonation depth of concrete based on RBF neural network, in: Q. Zhou, J. Luo (Eds.), Second Int. Symp. Intell. Inf. Technol. Appl. IITA 2008, IEEE Computer Society, Los Alamitos, CA 2008, pp. 544–548, http://dx.doi.org/10.1109/IITA.2008.402.
[155] W.Z. Taffese, E. Sistonen, J. Puttonen, Prediction of concrete carbonation depth using decision trees, in: M. Verleysen (Ed.), Proc. 23rd Eur. Symp. Artif. Neural Networks, Comput. Intell. Mach. Learn, ESANN 2015, pp. 415–420.
[156] W.Z. Taffese, E. Sistonen, J. Puttonen, CaPrM: carbonation prediction model for reinforced concrete using machine learning methods, Constr. Build. Mater. 100 (2015) 70–82, http://dx.doi.org/10.1016/j.conbuildmat.2015.09.058.
[157] J. Peng, Z. Li, B. Ma, Neural network analysis of chloride diffusion in concrete, J. Mater. Civ. Eng. 14 (2002) 327–333, http://dx.doi.org/10.1061/(ASCE)0899-1561(2002)14:4(327).
[158] S. Inthata, W. Kowtanapanich, R. Cheerarot, Prediction of chloride permeability of concretes containing ground pozzolans by artificial neural networks, Mater. Struct. 46 (2013) 1707–1721, http://dx.doi.org/10.1617/s11527-012-0009-x.
[159] S.S. Gilan, H.B. Jovein, A.A. Ramezanianpour, Hybrid support vector regression – particle swarm optimization for prediction of compressive strength and RCPT of concretes containing metakaolin, Constr. Build. Mater. 34 (2012) 321–329, http://dx.doi.org/10.1016/j.conbuildmat.2012.02.038.

[160] N. Ghafoori, M. Najimi, J. Sobhani, M.A. Aqel, Predicting rapid chloride permeability of self-consolidating concrete: a comparative study on statistical and neural network models, Constr. Build. Mater. 44 (2013) 381–390, http://dx.doi.org/10.1016/j.conbuildmat.2013.03.039.
[161] A.R. Boğa, M. Öztürk, İ.B. Topçu, Using ANN and ANFIS to predict the mechanical and chloride permeability properties of concrete containing GGBFS and CNI, Compos. Part B Eng. 45 (2013) 688–696, http://dx.doi.org/10.1016/j.compositesb.2012.05.054.
[162] H. Yasarer, Y.M. Najjar, Characterizing the permeability of Kansas concrete mixes used in PCC pavements, Int. J. Geomech. 14 (2014), 04014017. http://dx.doi.org/10.1061/(ASCE)GM.1943-5622.0000362.
[163] Y.-Y. Kim, B.-J. Lee, S.-J. Kwon, Evaluation technique of chloride penetration using apparent diffusion coefficient and neural network algorithm, Adv. Mater. Sci. Eng. (2014)http://dx.doi.org/10.1155/2014/647243 (Article ID, 13 pages).
[164] J. Lizarazo-Marriaga, P. Claisse, Determination of the concrete chloride diffusion coefficient based on an electrochemical test and an optimization model, Mater. Chem. Phys. 117 (2009) 536–543, http://dx.doi.org/10.1016/j.matchemphys.2009.06.047.
[165] O.A. Hodhod, H.I. Ahmed, Developing an artificial neural network model to evaluate chloride diffusivity in high performance concrete, HBRC J. 9 (2013) 15–21, http://dx.doi.org/10.1016/j.hbrcj.2013.04.001.
[166] A. Tarighat, A.H. Erfanimanesh, Artificial neural network modeling of chloride diffusion coefficient and electrical resistivity for ordinary and high performance semi-lightweight concretes, 34th Our World Concr. Struct, CI-Premier Pte Ltd., 2009
[167] A. Delnavaz, A.A. Ramezanianpour, H.R. Ashrafi, The analysis of chloride diffusion coefficient in concrete based on neural network models, in: A.A. Tasnimi (Ed.), Third Int. Conf. Concr. Dev, Building and Housing Research Center, Tehran 2009, pp. 775–782.
[168] W. Mazer, M. Geimba de Lima, Numerical model based on fuzzy logic for predicting penetration of chloride ions into the reinforced concrete structures - first estimates, in: V.P. de Freitas, H. Corvacho, M. Lacasse (Eds.), XII DBMC 12th Int. Conf. Durab. Build. Mater. Compon, FEUP Edições, Porto, 2011.
[169] H.-C. Cho, H. Ju, J.-Y. Oh, K.J. Lee, K.W. Hahm, K.S. Kim, Estimation of concrete carbonation depth considering multiple influencing factors on the deterioration of durability for reinforced concrete structures, Adv. Mater. Sci. Eng. 2016 (2016) 1–18, http://dx.doi.org/10.1155/2016/4814609.
[170] A. Delnavaz, A.A. Ramezanianpour, The assessment of carbonation effect on chloride diffusion in concrete based on artificial neural network model, Mag. Concr. Res. 64 (2012) 877–884, http://dx.doi.org/10.1680/macr.11.00059.
[171] M. Marks, M.A. Glinicki, K. Gibas, Prediction of the chloride resistance of concrete modified with high calcium fly ash using machine learning, Materials (Basel) 8 (2015) 8714–8727, http://dx.doi.org/10.3390/ma8125483.
[172] M. Marks, D. Jozwiak-Niedzwiedzka, M.A. Glinicki, Automatic categorization of chloride migration into concrete modified with CFBC ash, Comput. Concr. 9 (2012) 375–387, http://dx.doi.org/10.12989/cac.2012.9.5.375.
[173] R. Parichatprecha, P. Nimityongskul, Analysis of durability of high performance concrete using artificial neural networks, Constr. Build. Mater. 23 (2009) 910–917, http://dx.doi.org/10.1016/j.conbuildmat.2008.04.015.
[174] B. Aygün, V.C. Gungor, Wireless sensor networks for structure health monitoring: recent advances and future research directions, Sens. Rev. 31 (2011) 261–276, http://dx.doi.org/10.1108/02602281111140038.
[175] N. Barroca, L.M. Borges, F.J. Velez, F. Monteiro, M. Górski, J. Castro-Gomes, Wireless sensor networks for temperature and humidity monitoring within concrete structures, Constr. Build. Mater. 40 (2013) 1156–1166, http://dx.doi.org/10.1016/j.conbuildmat.2012.11.087.
[176] W.J. McCarter, Ø. Vennesland, Sensor systems for use in reinforced concrete structures, Constr. Build. Mater. 18 (2004) 351–358, http://dx.doi.org/10.1016/j.conbuildmat.2004.03.008.
[177] D. Cusson, Z. Lounis, L. Daigle, Durability monitoring for improved service life predictions of concrete bridge decks in corrosive environments, Comput. Civ. Infrastruct. Eng. 26 (2011) 524–541, http://dx.doi.org/10.1111/j.1467-8667.2010.00710.x.
[178] W. McCarter, T. Chrisp, A. Butler, P.A. Basheer, Near–surface sensors for condition monitoring of cover-zone concrete, Constr. Build. Mater. 15 (2001) 115–124, http://dx.doi.org/10.1016/S0950-0618(00)00060-X.
[179] K. Kumar, S. Muralidharan, T. Manjula, M.S. Karthikeyan, N. Palaniswamy, Sensor systems for corrosion monitoring in concrete structures, Sens. Trans. Mag. 67 (2006) 553–560.
[180] J.M. Gandía-Romero, R. Bataller, P. Monzón, I. Campos, E. García-Breijo, M. Valcuende, et al., Characterization of embeddable potentiometric thick-film sensors for monitoring chloride penetration in concrete, Sensors Actuators B Chem. 222 (2016) 407–418, http://dx.doi.org/10.1016/j.snb.2015.07.056.
[181] S.P. Karthick, S. Muralidharan, V. Saraswathy, K. Thangavel, Long-term relative performance of embedded sensor and surface mounted electrode for corrosion monitoring of steel in concrete structures, Sensors Actuators B Chem. 192 (2014) 303–309, http://dx.doi.org/10.1016/j.snb.2013.10.123.
[182] A. Brenna, L. Lazzari, M. Ormellese, Monitoring chloride-induced corrosion of carbon steel tendons in concrete using a multi-electrode system, Constr. Build. Mater. 96 (2015) 434–441, http://dx.doi.org/10.1016/j.conbuildmat.2015.08.037.
[183] G. Qiao, G. Sun, Y. Hong, Y. Qiu, J. Ou, Remote corrosion monitoring of the RC structures using the electrochemical wireless energy-harvesting sensors and networks, NDT E Int. 44 (2011) 583–588, http://dx.doi.org/10.1016/j.ndteint.2011.06.007.
[184] W.Z. Taffese, E. Sistonen, Neural network based hygrothermal prediction for deterioration risk analysis of surface-protected concrete façade element, Constr. Build. Mater. 113 (2016) 34–48, http://dx.doi.org/10.1016/j.conbuildmat.2016.03.029.
[185] F. Al-Neshawy, J. Piironen, S. Peltola, E. Sistonen, J. Puttonen, Network system for assessing the moisture and thermal behaviour of repaired concrete building facades, Inf. Technol. Constr. 16 (2011) 601–616.
[186] A. Norris, M. Saafi, P. Romine, Temperature and moisture monitoring in concrete structures using embedded nanotechnology/microelectromechanical systems (MEMS) sensors, Constr. Build. Mater. 22 (2008) 111–120, http://dx.doi.org/10.1016/j.conbuildmat.2006.05.047.
[187] W.Z. Taffese, F. Al-Neshawy, J. Piironen, E. Sistonen, J. Puttonen, Monitoring, evaluation and long-term forecasting of hygrothermal performance of thick-walled concrete structure, Proc. OECD/NEA WGIAGE Work. Non-Destructive Eval. Thick. Concr. Struct, OECD, Prague 2014, pp. 121–143.
[188] M. Raupach, J. Gulikers, K. Reichling, Condition survey with embedded sensors regarding reinforcement corrosion, Mater. Corros. 64 (2012) 141–146, http://dx.doi.org/10.1002/maco.201206629.

Publication II

Taffese, Woubishet Zewdu; Sistonen, Esko; Puttonen, Jari. 2015. CaPrM: Carbonation prediction model for reinforced concrete using machine learning methods. Journal of Construction and Building Materials, volume 100, pages 70–82. ISSN 0950-0618. https://doi.org/10.1016/j.conbuildmat.2015.09.058.

Construction and Building Materials 100 (2015) 70–82

Contents lists available at ScienceDirect

Construction and Building Materials

journal homepage: www.elsevier.com/locate/conbuildmat

CaPrM: Carbonation prediction model for reinforced concrete using machine learning methods

Woubishet Zewdu Taffese *, Esko Sistonen, Jari Puttonen

Department of Civil and Structural Engineering, Aalto University, P.O. Box 12100, FI-00076 Aalto, Finland

HIGHLIGHTS

- Integrating machine learning methods enhances carbonation prediction accuracy.
- Feature selection method improves the performance of the carbonation prediction.
- Plasticizers, air and aggregate contents are also essential for predicting carbonation.
- Accelerated carbonation testing fails to represent fully the natural conditions.
- The median ratio of carbonation coefficients (k_{acc}/k_{nat}) varies with time.

ARTICLE INFO

Article history:
Received 20 March 2015
Received in revised form 14 August 2015
Accepted 27 September 2015

Keywords:
Carbonation
Concrete
Machine learning
Neural network
Decision tree
Bagged decision tree
Boosted decision tree
Model

ABSTRACT

Reliable carbonation depth prediction of concrete structures is crucial for optimizing their design and maintenance. The challenge of conventional carbonation prediction models is capturing the complex relationship between governing parameters. To improve the accuracy and methodology of the prediction a machine learning based carbonation prediction model which integrates four learning methods is introduced. The model developed considers parameters influencing the carbonation process and enables the user to choose the best alternative of the machine based methods. The applicability of the method is demonstrated by an example where the carbonation depths are estimated using the developed model and verified with unseen data. The evaluation proofs that the model predicts the carbonation depth with a high accuracy.

1. Introduction

Carbonation of concrete has been identified as one of the foremost cause of premature degradation, loss of serviceability and safety of reinforced concrete structures [1–5]. It is a natural physicochemical process caused by the penetration of carbon dioxide from the surrounding environment into the concrete through pores in the matrix where the carbon dioxide reacts with hydrated cement [6,7]. Calcium hydroxide ($Ca(OH)_2$) in contact with carbon dioxide (CO_2) forms calcium carbonate ($CaCO_3$) as shown in Eq. (1). This chemical reaction may gradually reduce the alkalinity of the pore fluid from pH value around 13–9 [7–11]

$$Ca(OH)_2 + CO_2 \xrightarrow{H_2O} CaCO_3 + H_2O \quad (1)$$

Even if the reduction of alkalinity caused by carbonation changes the chemical composition of concrete, its main practical consequence is that it destroys the passive oxide layer of steel reinforcement and eventually corrosion of the steel bars will be initiated [6–14]. It is a serious problem in many parts of the world and currently two-thirds of all structural concrete is exposed to environmental conditions that favor carbonation-induced corrosion [14,15]. Hence, accurate carbonation prediction model is a key to make realistic decisions on maintenance plan of reinforced concrete structures. In this work, a carbonation prediction model is developed using optimized and integrated machine learning methods. Neural network, decision tree, bagged decision tree and boosted decision tree are incorporated in the model with the purpose of achieving the best prediction.

* Corresponding author.
E-mail address: woubishet.taffese@aalto.fi (W.Z. Taffese).

http://dx.doi.org/10.1016/j.conbuildmat.2015.09.058
0950-0618/

2. Background

Conventionally, carbonation depth is reasonably estimated using a simplified version of Fick's second law of diffusion, Eq. (2) [5,6,9,13,16]

$$x_c(t) = k\sqrt{t}, \tag{2}$$

where $x_c(t)$ is carbonation depth at the time t in [mm] , k is coefficient of carbonation [mm/year$^{0.5}$] which is equals to $\sqrt{\frac{2 \cdot D_{CO_2}(C_1 - C_2)}{a}}$, D_{CO_2} is diffusion coefficient for CO_2 through carbonated concrete [mm^2/year], C_1 is concentration of CO_2 for the surrounding environment [kg/m^3], C_2 is concentration of CO_2 at the carbonation front [kg/m^3], a is mass of CO_2 per unit volume of concrete required to carbonate all the calcium hydroxide available [kg/m^3] and t time of exposure to the atmosphere containing carbon dioxide [year].

The assumptions in Eq. (2) are: (i) diffusion coefficient for CO_2 through carbonated concrete is constant, (ii) amount of CO_2 required to neutralise alkalinity within a unit volume of concrete is constant and (iii) CO_2 concentration varies linearly between fixed boundary values of C_1 at the external surface and C_2 at the carbonation front.

The carbonation coefficient k is a relative indicator of carbonation resistance of a concrete, which characterize the influence of concrete intrinsic factors on carbonation, curing and the exposed condition. The carbonation depth of the concrete should be measured first either by an accelerated carbonation test or by measuring the carbonation depth of an existing structure in order to determine the carbonation coefficient [17]. Since carbonation is a slow process, it is often investigated by performing accelerated test with higher CO_2 concentration in a controlled environment. Then, the measured carbonation depth is applied to calculate the equivalent carbonation coefficient using Eq. (2). This approach is used even if the accelerated test may not always describe the natural carbonation accurately enough [5]. Eq. (2) is valid as long as the diffusion coefficient for carbon dioxide is constant in time and location. But, in real exposure, diffusion of CO_2 cannot be constant and depends on several factors, such as CO_2 concentration, concrete composition, curing and environmental conditions [9,17,18]. Eq. (2) often fails to represent the actual condition of the concrete structures which may lead to inaccurate estimation of the carbonation depth [6,18,19]. To address these limitations, a number of improved models which considers the concrete quality and the environmental and execution factors have been developed, e.g. the model proposed in fib-MC2010 [20], Eq. (3)

$$x_c(t) = \sqrt{2 \cdot k_e \cdot k_c \cdot R_{NAC,0}^{-1} \cdot C_s} \cdot W(t) \cdot \sqrt{t}, \tag{3}$$

where $x_c(t)$ is carbonation depth at the time t in [mm], t is time in [year], k_e is environmental function [–], k_c is execution transfer parameter [–], C_s is CO_2 concentration in the air in [kg/m^3], $W(t)$ is weather function [–], $R_{NAC,0}^{-1}$ is inverse effective carbonation resistance of concrete in [(mm^2/year)/(kg/m^3)] which is determined at a certain time t_0 using the natural carbonation test NAC in [(mm^2/year)/(kg/m^3)].

This and many other models adopt Eq. (2) by linking the coefficient of carbonation with factors of the concrete material and the environment. The linked parameters have normally been regarded as random variables which define the concrete properties that dominate the ingress rate of CO_2 such as exposure, water to binder ratio (w/b) and compressive strength. Most of the improved models do not encompass all the influential parameters which govern the carbonation process. Combining two or more of these models does not address the problem. The combination of many assumptions and simplifications in the existing carbonation prediction models causes a considerable uncertainty in their performance. These models may fail to achieve conditions for optimized selection of appropriate design, maintenance and rehabilitation strategies that will assure a long service life. Hence, an advanced model that considers most of the parameters is absolutely necessary. Accurate prediction can be developed if all influential parameters evaluated as a group rather than individually because imperative dependencies may be overlooked.

Developing an advanced carbonation prediction model which addresses all the influential parameters, without adding many assumptions, is a challenging task since the behavior of concrete is a function of many parameters that are complex to describe mathematically. Standard laboratory tests alone are not reliable enough to predict long-term carbonation as the concrete microstructure alters due to time-dependent chemical processes of cement paste and in addition to its interaction with the environment. The lack of general agreement on how to translate result of accelerated carbonation test performed in laboratory to concrete exposed to natural conditions for long-term is another problem [1,18]. Therefore, developing carbonation prediction model that can learn from readily available long-term field data using machine learning methods is a lucrative alternative. Even though this approach is becoming a common practice in various engineering fields, its application in the assessment of the durability of concrete structures is yet limited.

3. Research problem and related work

The restrictions of the conventional Fick's law based carbonation prediction calls for the use of learning based models, as discussed in Section 2. Appropriate learning methods which map the input variables to output variables that closely approximate the target can be seen as a tempting alternative. A wide variety of machine learning methods are available for developing models based on experimental data. Neural networks, decision trees, and ensemble methods are among them. Even though, there are a number of machine learning techniques, only neural network method has been used for carbonation prediction [21–25]. Relative strengths of the available models based on machine learning are of keen interest to researchers. No one knows in advance which machine learning techniques will excel for a given problem unless otherwise experimented. Comparative strength of machine learning models strongly depends on the details of the problems addressed. One model (e.g. neural network) may perform best on problems of specific dataset, but may not be true for a different dataset. Therefore, the carbonation prediction ability of the well-known machine learning models needs to be investigated.

In another perspective, most of the existing neural network based carbonation prediction models do not employ all the necessary parameters that influence the microstructural properties of concrete. The common parameters utilized in most of the available models are composition and amount of cement and water to cement ratio (w/c) to describe the concrete properties. These parameters are not sufficient to predict the concrete carbonation since it is a function of many parameters and ignoring other influential variables weakens the prediction performance of the model. Indeed, there are few neural network based models which consider many parameters but lacked to perform certain essential preprocessing steps during the model development. It is known fact that incorporating more information regarding the concrete properties enhances the learning performance of the model. However, some parameters may be irrelevant or redundant for the carbonation prediction and even degrade the learning performance. For these reasons, it is essential to apply a special process to recognize the most important variables during the model development.

The aim of this work is to address the limitations of existing learning based carbonation prediction models. This work explores the applicability of machine learning methods for carbonation prediction. Based on the exploration, a better performing carbonation prediction model is developed using optimized and integrated machine learning techniques. The model integrates neural network, decision tree, bagged decision tree and boosted decision tree.

4. Machine learning

Machine learning is a major sub-field in artificial intelligence. It employs learning methods to recognize complex patterns from empirical data, without assuming a predetermined equation as a model, and make intelligent decisions [26–30]. The model can be predictive to make predictions in the future or descriptive to gain knowledge from data, or both [26,31]. Algorithms of machine learning characteristically fall into one of two learning types: supervised or unsupervised learning [30,32–34]. Supervised learning consists of input and output variables whereas in unsupervised learning there is no output. The former is trying to learn in order to predict a class or a value, while the latter is trying to group similar examples together or to find interesting patterns in the data. Supervised learning problems are classified into two clusters: classification and regression [29,32]. In classifications, the output domain is a finite discrete set of categories (classes), while in regression the output domain is the set of real numbers.

The carbonation prediction problem is a regression one since our main aim is predicting the numeric value of the carbonation depth knowing the value of the input variables. Regression is the problem of building a functional model which is the best predictor of y given input x using a given training data $D = \{y_i,\ x_i\}_1^N$ as described in Eq. (4)

$$y = \hat{F}(x_1,\ x_2, \ldots,\ x_n) = \hat{F}(X), \tag{4}$$

where y_i is the outputs variable, x_i is the input "vector" made of all the variable values for the ith observation, n is the number of variables; N is the number of observations.

Neural network, decision tree and ensemble methods are the foremost well-known machine learning techniques for their good capability at modeling uncertain and nonlinear regression problems. These techniques have been adopted with a great success for solving broad range complex nonlinear regression problems, for example, energy production [35], computational finance [36] and computational biology [37]. Nevertheless, in concrete research only neural network is commonly used to model nonlinear regression problems, for instance, chloride penetration in concrete [16], chloride threshold of pitting corrosion [38], time to corrosion [39], hygrothermal forecasting in thick-walled concrete [40] and corrosion currents of reinforced concrete [41]. The proposed carbonation prediction model integrates neural network, decision tree and ensemble (bagged and boosted decision tree) methods.

4.1. Neural network

Neural network consist of partially or fully interconnected simple processing units called artificial neurons [42–44]. Neural networks can be classified in a number of different ways depending on their architecture which is intimately linked with the learning algorithm used to train the network. Multilayer feedforward architecture and backpropagation training procedure is widely used for nonlinear regression problems [45–48]. This architecture usually has three or more layers. The first and the last layers are input and output layers whereas the intermediate layers (hidden layers) which aids in performing useful computations before directing the input into the output layer. The architectural graph in Fig. 1 illustrates the layout of a multilayer feedforward neural network with a single hidden layer. The network can be viewed as a flexible nonlinear parametric function from a set of inputs, x_i, to a set of outputs, y_m. First linear combinations of the weighted inputs are formed, and then transformed using a nonlinear activation function $\varphi(\cdot)$ [47–49], Eq. (5). The aim is to limit the amplitude of the output neuron. The outputs of these first-layer neurons are multiplied by the layer of the interconnection weights that connect them to the next layer of neurons. This process continues until the output nodes compute their outputs. For neurons in the same layer, the same activation functions are used. Various forms of activation functions can be defined depending on the characteristics of applications [49]

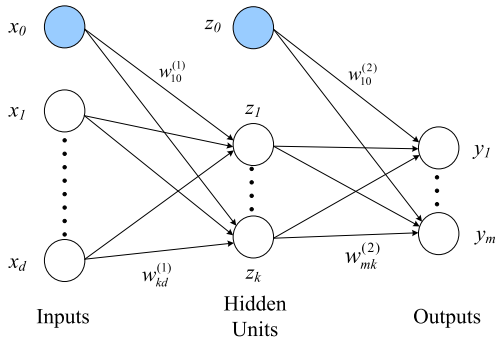

Fig. 1. A multilayer feedforward neural network with a single hidden layer.

$$z_j = \varphi\left(\sum_i w_{ji}^{(1)} x_i\right), \tag{5}$$

$$y_m = \sum_j w_{mj}^{(2)} z_j, \tag{6}$$

where $w_{ji}^{(1)}$ and $w_{mj}^{(2)}$ are the synaptic weights of the network which are initially set to random values, and then adjusted during training by back propagation using the response data.

4.2. Decision tree

Decision tree is a nonparametric hierarchical data structure implementing the divide-and-conquer strategy. It manages a complex regression problem by reducing them into simpler problems and recursively applies the same strategy to the sub-problems. Solutions of sub-problems can be combined to yield a solution of the complex problem. The power of this approach comes from the ability to split the instance-space into subspaces and each subspace is fitted with different models [26,50]. Decision trees can be applied to datasets having both a large number of cases and a large number of variables. They exhibit a high degree of interpretability [50,51] and composed of internal decision nodes and terminal leaves (see Fig. 2). The left subfigure plots the data points and partitions them while the right one shows the corresponding decision tree structure. Each *decision node* implements a test function with discrete outcomes labeling the branches. Given an input, at each node, a test is applied and one of the branches is taken depending on the outcome. This process starts at the root and is repeated recursively until a *leaf node* is hit, at which point the value written in the leaf constitutes the output [26].

4.3. Ensemble methods

Ensemble methods build a predictive model by integrating multiple models, each of which solves the same original task, in order

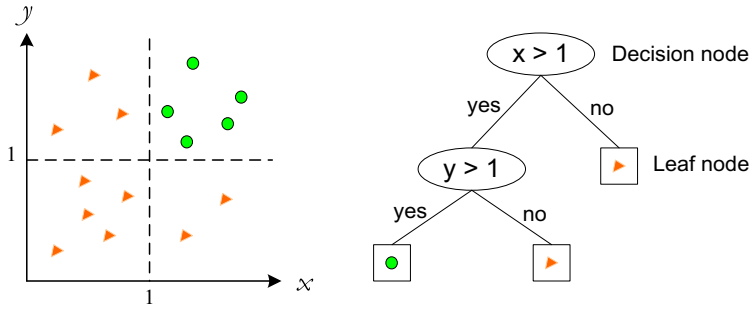

Fig. 2. Example of a dataset and the corresponding decision tree.

to improve the generalization ability, which in turn enhances prediction performance [26,32,51–53]. Among prominent types of ensemble methods, bagging and boosting are the ones used commonly [53,54]. Bagging technique draws multiple bootstrap random samples from the dataset to form a new training dataset. This is repeated until a large subset of training datasets is generated and the same observations can be drawn more than once. On average, each generated bootstrapped training set contains $n(1-\frac{1}{e}) \approx 0.63n$ observations, where n is actual dataset. Data points which are omitted in the training dataset are "out of bag" observation. Bagging trains each model in the ensemble using the randomly drawn subset of the training set. The final prediction value of the ensemble of trees for unseen (out of bag) data is the average of the predicted output of the individual trees [26,51,54,55]. Whereas boosting method trains the training dataset in sequence with improvement from one model to the next. It manipulates a data point weight for each training example in order to generate diverse models. The final output of the ensemble is the weighted average of the output from all its members [54,55].

5. CaPrM modeling process

In this section, the development steps of the proposed CaPrM model are presented. CaPrM is an optimized and integrated machine learning based carbonation prediction model. As any machine learning based models, the major development phases of CaPrM consists of data, training, validation and testing. The workflow of CaPrM model is illustrated in Fig. 3. The gray colored rectangular boxes represent the main processes/tasks of the modeling procedure. The major inputs into the process are shown in uncolored rectangular boxes.

As it is seen in Fig. 3, the first task is finding appropriate experimental dataset that includes features which influence the carbonation of concrete and then perform data exploration. The main aim of the data exploration task is to find a good set of features for developing a carbonation prediction model since some features are better for predicting the target than others. In machine learning modeling approach, data usually requires some pre-processing before they are analyzed further. For instance, there may be missing values in the data and these values need to be cleaned so the model can analyze the data properly. Pre-processing step could also involve other tasks such as data encoding and normalization. After making the data ready, the next step is dividing them into training, validation and test sets. Training dataset is used to build up carbonation prediction algorithms which includes neural network, decision tree, bagged and boosted decision trees. These learning algorithms are selected and integrated because they are widely used for nonlinear regression problems. Each integrated learning algorithms should run on the experimental training dataset. Some learning algorithms require the user to determine certain control parameters. These parameters may be adjusted by optimizing performance on a subset (a validation set) of the training set, e.g. neural network or via cross-validation in decision tree based models. If the obtained results in the validation process are unsatisfactory, variable selection based optimization technique will be adopted in order to select most relevant variables subset. After all the necessary parameter adjustment and learning are carried out, the performance of the resulting function should be measured on a test set that is separate from the training set. The integration gives the opportunity to select the best performing one among the four choices, by comparing the validation error matrix, since there is no single learning algorithm that works best all the time.

6. Application of the CaPrM model

In this section application of the CaPrM model is presented in detail using experimental data obtained from Finnish DuraInt-project. Details of the data, training and validation of the model are discussed in the following subsections.

6.1. Experimental data

In this work, the data used for the development of carbonation prediction model were prepared for Finnish DuraInt-project. This project was carried out in cooperation with Aalto University and VTT Technical Research Centre of Finland. In Finnish DuraInt-project concrete specimen from 23 different mix proportion, which represents mainly prevailing common industrial mixes in Finland, were prepared. Two specimens were prepared for each concrete mix types. All the specimens were casted in steel molds of size $100 \times 100 \times 500\ mm^3$ and demoulded after 24 h. Then, they were immersed into water for 7 days and cured in a controlled environment (21 °C temperature and 60% relative humidity). Field carbonation of the specimens started at about the age of 28 days in Espoo, southern Finland. The specimens were sheltered and kept on wooden racks as seen in Fig. 4. The yearly average CO_2 concentration, temperature and relative humidity at storage of specimens are 375 ppm, 6 °C and 79%, respectively.

The obtained dataset consists of information about the mixes used for the specimens as well as its fresh and hardened properties. The major ingredients that are used to produce the concrete mixes are presented in Table 1. A total of six types of cements, according to the classification of EN 197-1 [56], are utilized. These are Portland cement (CEM I 42,5 N-SR, CEM I 52,5 N and CEM I 52,5 R), Portland limestone cement (CEM II/A-LL 42,5 R), Portland composite cement (CEM II/A-M(S-LL) 42,5 N) and Portland slag cement (CEM II/B-S 42,5 N). Partially replaced Portland limestone cement, CEM II/A-LL 42,5 R, with pulverized blast-furnace slag and fly ash are also used in the experiment. The water to binder ratios (w/b) ranges from 0.40 to 0.60. Each concrete mix employs one plasticizer type from three producers, *VB-Parmix*, *Glenium G 51* or

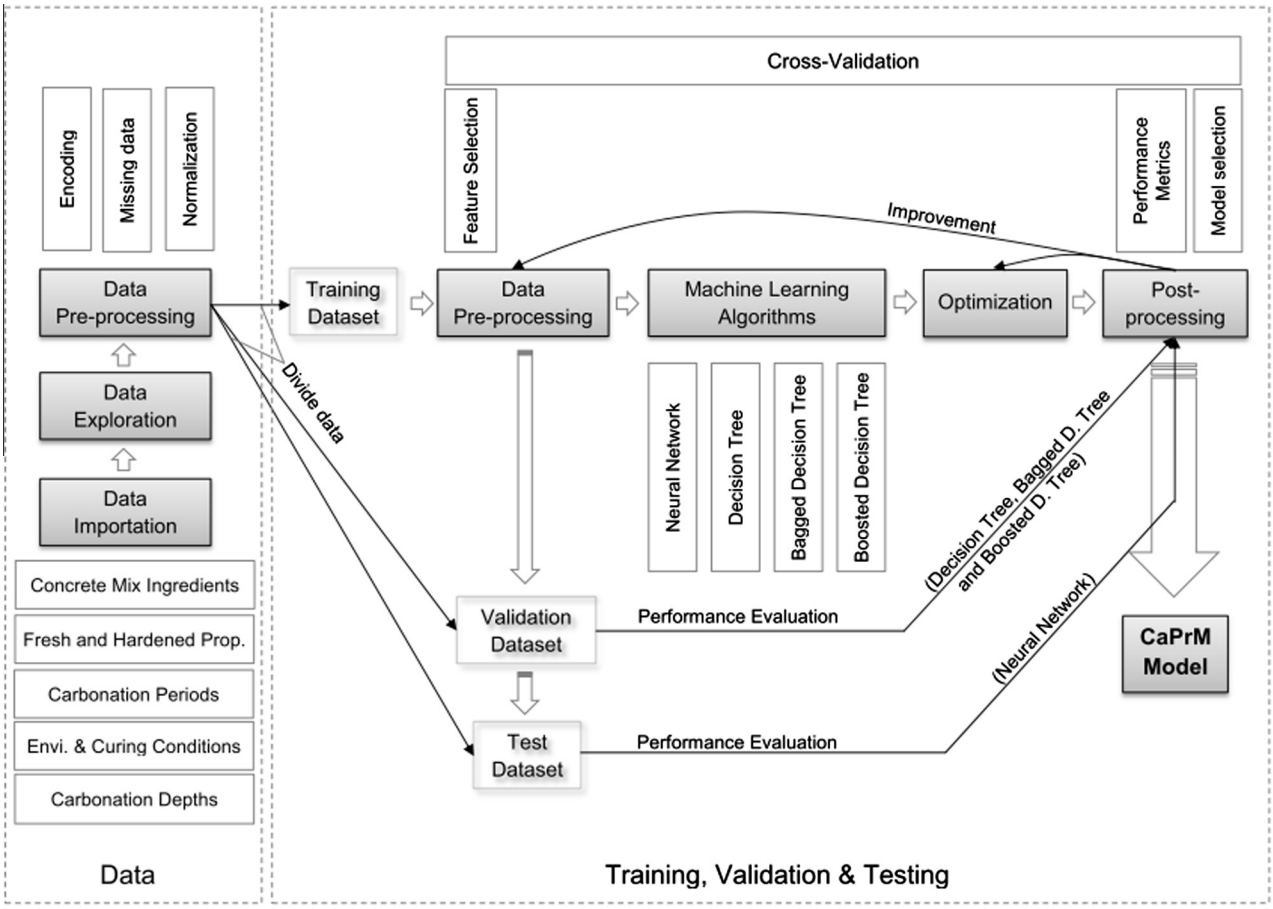

Fig. 3. Workflow of CaPrM model.

Fig. 4. Concrete specimen exposed to natural conditions at field.

Teho-Parmix. Every concrete mix types also employ an air-entraining agent (named either *Ilma-Parmix* or *Mischöl*). The fresh and the hardened concrete properties with curing and exposed conditions are also presented in Table 1. The fresh concrete properties comprised of slump, slump flow of self-compacting concrete (SCC) and air content. The properties defined for hardened concrete include compressive strength and accelerated carbonation. The compressive strength of the concrete specimens is tested at the age of 28 days. While accelerated carbonation test is performed by exposing the non-carbonated concrete specimens in a climatic control chamber for 28 and 56 days. The test chamber with the concrete specimens to be carbonated is filled with 1% of CO_2. The test chamber is placed in a room with RH 60% and temperature 21 °C. The carbonation depth is tested by 1% phenolphthalein in ethanol solution. The binder type and the w/b ratio of every concrete mixture are presented in Table 2.

In Finnish DuraInt-project carbonation front depth, from all sides, in a freshly broken surface of 100 × 100 mm^2 were measured at every time of measurement. The depth was determined by spraying a pH indicator solution of phenolphthalein. The arithmetic mean of carbonation depths measured from the four sides of every specimen was considered as the representative value. The carbonation reading was taken at the age of 268, 770, 1825 and 2585 days. The readings of the Finnish DuraInt project will continue far into the future. Carbonation front of two groups of concrete specimens after 56 days in the accelerated carbonation chamber is illustrated in Fig. 5. Surface areas with a pink color indicate the pH is above 9 and are non-carbonated part. The carbonated parts of the specimens are the area where the color of the concrete is unchanged.

6.1.1. Data types

In CaPrM model 25 input variables which control the carbonation process are considered. It includes concrete mixture ingredients, curing conditions, exposure environment, age of concrete at testing, and fresh and hardened properties of the specimens (listed in Table 1). The target variable is the carbonation depth of every concrete type measured at various ages. The input variables consist of continuous and nominal data types. Continuous variables are real numbers, such as results of quantitative measurements (e.g. amount of cement, density and compressive strength). Nominal variables are non-numeric and descriptive data types (e.g. types of cement, product name of plasticizers and air-entraining agents).

Table 1
Details of the concrete specimens and its exposure conditions.

Ingredients, fresh and hardened properties, curing and exposure conditions	Types and conditions	Units	Short name
Cement types	CEM I 42,5 N – SR	–	Cem. types
	CEM I 52,5 N	–	
	CEM I 52,5 R	–	
	CEM II/A-LL 42,5 R	–	
	CEM II/A-M(S-LL) 42,5 N	–	
	CEM II/B-S 42,5 N	–	
Additives	Pulverized blast-furnace slag	[kg/m^3]	BFS
	Fly ash (FA)	[kg/m^3]	FA
	Silica fume (SF)	[kg/m^3]	SF
Water/(Cement + BFS + FA + SF)	Ranged from 0.37 to 0.60	–	w/b
Cement content		[kg/m^3]	Cement
Total effective water		[kg/m^3]	Total eff. water
Aggregate content	Total aggregate	[kg/m^3]	Total Agg.
	Aggregate <0.125 mm	[%]*	Agg. <0.125 mm
	Aggregate <0.250 mm	[%]*	Agg.<0.250 mm
	Aggregate <4 mm	[%]*	Agg. <4 mm
Product name of plasticizers	Glenium G 51	–	Plas. pro. name
	Teho-Parmix	–	
	VB-Parmix	–	
Plasticizers		[%]**	Plasticizers
Product name of air-entraining agents	Ilma-Parmix	–	AEA pro. name
	Mischöl	–	
Air-entraining agents		[%]**	Air-ent. agents
Fresh concrete properties	Slump value	[mm]	Slump
	SCC slump-flow/T_{50}	[mm/s]	Slump-flow/T_{50}
	Air content	[%]	Air cont.
Curing conditions	Uncontrolled	–	Curing cond.
	Controlled	–	
	Wet	–	
Exposure conditions	Temperature	[°C]	Temp.
	Relative humidity	[%]	RH
	CO_2 concentration	[ppm]	CO_2 conc.
Hardened concrete properties	Compressive strength	[MPa]	Comp. str.
Carbonation properties	Accelerated carbonation depth	[mm]	Acc. carb. dep.
	Age of the concrete at carbonation testing	[days]	Carb. period
	Natural carbonation depth	[mm]	Nat. carb. dep.

* Compared with the total aggregate.
** Compared with the total binder materials.

6.1.2. Data pre-processing

In machine learning data pre-processing includes data encoding, missing data processing, data normalization and data partitioning. In CaPrM modeling the following data pre-processing tasks are performed.

6.1.2.1. Data encoding and normalization. Some of the machine learning techniques supports only continuous data types as input variables. For example, decision trees can process heterogeneous input data (continuous and nominal) without any problem but neural network lacks the ability to work with nominal variables. Since the proposed CaPrM model employs neural network, all non-numeric variables such as binder types, product name of plasticizers and air-entraining agents should be encoded as numerical variables. To do so, the most widely applied "1-of-N" encoding method is implemented. The encoded variables are listed in Table 3.

Normalization of the inputs and the target variables before processing them in the neural network is a standard practice. It puts different variables on a common scale and is very important especially where the inputs are generally on a wide different scale. Since MATLAB neural network toolbox is used for modeling, it automatically normalizes both the input and target variables. In

Table 2
Binder types and w/b ratios of the concrete specimens.

Mix number	Binder type	Water/binder
1	CEM II/B-S 42,5 N	0.41
2	CEM I 42,5 N – SR	0.42
3	CEM II/A-M(S-LL) 42,5 N	0.42
4	CEM II/A-LL 42,5 R	0.42
6	CEM I 52,5 R	0.42
6	CEM II/A-LL 42,5 R & BFS KJ400	0.37
7	CEM II/A-LL 42,5 R & FA – Fineness N, Class A	0.38
8	CEM II/A-M(S-LL) 42,5 N	0.42
9	CEM II/A-M(S-LL) 42,5 N	0.42
10	CEM II/A-M(S-LL) 42,5 N	0.42
11	CEM II/A-M(S-LL) 42,5 N	0.42
12	CEM II/A-M(S-LL) 42,5 N	0.42
13	CEM II/A-M(S-LL) 42,5 N	0.42
14	CEM II/B-S 42,5 N	0.47
15	CEM II/A-M(S-LL) 42,5 N	0.49
16	CEM I 52,5 N	0.46
17	CEM II/A-LL 42,5 R	0.51
18	CEM I 52,5 R	0.40
19	CEM II/A-M(S-LL) 42,5 N	0.50
20	CEM II/B-S 42,5 N	0.60
21	CEM II/A-M(S-LL) 42,5 N	0.58
22	CEM I 52,5 N	0.54
23	CEM II/A-LL 42,5 R	0.54

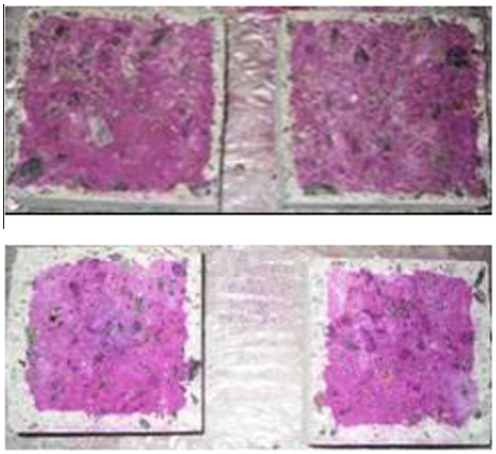

Fig. 5. Carbonation fronts of two groups of concrete specimens after 56 days in a climatic control chamber.

this way, the network output always falls into a normalized range [−1, 1]. It also transforms back into the units of the original target data. So, there is no need for a separate normalization process [57].

6.1.2.2. Missing data. Quality of input variables is one of the important factors in enhancing prediction accuracy of any machine learning based models. The presence of missing values is a recurrent problem in different research areas that affect quality of data. The Finnish DuraInt-project consist missing values for some variables. Fortunately, all the variables which are considered in CaPrM modeling have no missing values.

6.1.2.3. Data partitioning. For neural network the data is split into three subsets: training, validation and testing. The training dataset is used for computing the gradient and updating the network weights and biases. During the training process, neural network requires a validation procedure to halt the training when the generalization process stops improving. The test dataset is used to measure the predictive performance of the model. However, in decision tree based models, the data is divided into two subsets: training and validation. The training dataset is used for learning whereas the validation dataset is used to assess the performance of model built in the training phase. This is a common practice in machine learning methods since one has a limited amount of data.

6.2. Training

The prediction ability of machine learning based models highly depends on the quality and behavior of the data. One learning method may be superior over the other for specific training and validation dataset, but if the dataset is changed the performance may also change. As discussed in the above sections neural network, decision tree, bagged and boosted decision trees are integrated in CaPrM model. This integration provides the opportunity to select the best performing learning methods among the four choices.

The graphical representation of the neural network in the CaPrM model is basically identical with Fig. 1. The model has three layers: an input layer, a hidden layer and an output layer. Input variables are assigned as input neurons. The optimal number of neurons in the hidden layer is determined based on the generalization error after executing several trainings. The measured carbonation depth is assigned as output neuron. The applied learning algorithm is Levenberg–Marquardt [58]. It is the fastest backpropagation procedure that updates weight and bias values in the negative gradient direction. The activation functions selected for the hidden layer is tan-sigmoid transfer function so that the model can learn the nonlinear relationships between input and target variables. Linear transfer activation function is applied in the output layer.

The structure of the decision tree in the CaPrM model is the same as that of the tree presented in Fig. 2. The only difference is that the leaf contains real numbers (which are measured carbonation depth) instead of class labels. The learning process in decision tree follows the divide-and-conquer strategy. The bagged decision trees draw multiple bootstrap random samples from the training dataset to form a new training datasets. Using this new training datasets, the bagged decision trees make an ensemble of trees for predicting carbonation depth as a function of the input variables. The final prediction value of the ensemble of trees is the average of the predicted output of the individual trees. The boosted decision tree learns the training dataset in sequence with improvement from one model to the next. It uses least squares boosting algorithm to minimize mean-square error of the ensemble. The final output of the ensemble is weighted average of the output from all its members.

6.3. Validation and testing

Cross-validation technique is used to evaluate the performance of the developed CaPrM model. Several types of cross-validation methods can be applied for a given machine learning system. If the available dataset is limited, *k*-fold cross-validation method is the best alternative in order to achieve an unbiased estimate of the model performance [26]. In *k*-fold cross-validation, the original data is randomly divided into *k* subsets with roughly equal sizes. Each of the *k* sets is used as a validation dataset while the remaining dataset are used as a training set to fit the model. In total, *k* models are fit and *k* validation statistics are obtained. The predictive accuracy assessments from the *k*-folds are averaged to give a measure of the predictive performance of the model. The adopted value of *k* in this work is 10 which is a typical value in machine learning practice.

Table 3
1-of-N encoding process for non-numeric variables.

Binder materials		Curing conditions, product names of plasticizers and air-entraining agents		
Nominal input variables	Encoded output	Nominal input variables		Encoded output
CEM I 42,5 N – SR	[10000000]	Curing cond.	Uncontrolled	[100]
CEM I 52,5 N	[01000000]		Controlled	[010]
CEM I 52,5 R	[00100000]		Wet	[001]
CEM II/A-LL 42,5 R	[00010000]	Plasticizers	Glenium G 51	[100]
CEM II/A-M(S-LL) 42,5 N	[00001000]		Teho-Parmix	[010]
CEM II/B-S 42,5 N	[00000100]		VB-Parmix	[001]
CEM II/A-LL 42,5 R & BFS KJ400	[00000010]	Air-ent. agents	Ilma-Parmix	[10]
CEM II/A-LL 42,5 R & FA – fineness N, class A	[00000001]		Mischöl	[01]

Table 4
Important variables identified by bagged and boosted ensemble methods with their rank.

Variables	Rank	
	Bagged decision tree	Boosted decision tree
Acc. carb. dep.	1	1
Comp. str.	2	3
w/b	3	2
Plasticizers	4	4
Carb. period	5	6
Air cont.	6	5
Cement	8	7
Total Agg.	9	9
Agg. <0.250 mm	7	8
Agg. <0.125 mm	10	10

Performance of the trained CaPrM models is statistically measured using the validation dataset for decision tree based models. But, in neural network, test dataset is applied for evaluating the model performance since the validation dataset is used as part of training platform to optimize the hyperparameters of the learning algorithm. For regression model mean square error (MSE), root mean square errors (RMSE), and mean absolute error (MAE) are commonly used statistical measures. The MAE, also called the absolute loss, is an average of the absolute residuals/errors (the difference between the predicted and the actual value) and measured in the same units as the data. MSE is the mean of the squared difference between the target and its predicted value. It is the most widely employed loss function for regression model. RMSE is simply the square root of the MSE. Sometime RMSE is preferable than MSE because understanding of error values of MSE is difficult due to the squaring effect, particularly, if the target value represents quantities in units of measurements. RMSE retains the original units as MAE. MSE, RMSE, and MAE are calculated using Eqs. (7, 8 and 9), respectively

$$\mathrm{MSE} = \frac{1}{n}\sum_{i=1}^{n}\left(Y_i - \hat{Y}_i\right)^2, \tag{7}$$

$$\mathrm{RMSE} = \sqrt{\frac{1}{N}\sum_{i=1}^{N}\left(Y_i - \hat{Y}_i\right)^2}, \tag{8}$$

$$\mathrm{MAE} = \frac{1}{N}\sum_{i=1}^{N}\left|Y_i - \hat{Y}_i\right|, \tag{9}$$

where $\hat{Y}_i$ is the predicted output value, Y_i is the measured target value, and N is the number of observations.

If the obtained results in the validation process are unsatisfactory, variable selection based optimization technique will be adopted. The variable selection is a technique to select most relevant variables subset, and removes irrelevant and redundant variables according to some criterion from the original input variables to build robust learning models [26,30,32,59]. Indeed, having more information about the concrete properties, the performance of the learning method is expected to be better. It is also equally true that some variables may be irrelevant for predicting carbonation which ultimately degrades the learning performance. Therefore, pertinent variables have to be selected after the initial validation test.

There are three major categories of variable selection methods: filter, wrapper and embedded [60,61]. Ensemble methods can perform an embedded variable selection. These methods use all the variables to generate a carbonation prediction model and deduce the importance of the variables. A standalone decision tree also provides embedded measure of variable but it is not recommended. This is due the fact that standalone decision trees are produced by a greedy algorithm that generates an unstable model [60]. Therefore, in CaPrM model, ensemble methods are applied to select variables which have more predictive pieces of information compared to other variables. The important variables identified by bagged and boosted decision tree are presented in Table 4. These variables are identified after a number of iterations and ranked according to their occurrence. The ranks in bagged and boosted ensemble methods are quite similar.

Table 5
Average of ten round statistical performance measurements.

Dataset	Learning method	MSE	MAE	RMSE
Validation (before variable selection)	Neural network	0.3522	0.3860	0.5935
	Decision tree	0.5295	0.4491	0.7276
	Bagged decision tree	0.4907	0.4391	0.7005
	Boosted decision tree	0.3749	0.4116	0.6123
Validation (after variable selection)	Neural network	0.2417	0.2860	0.4916
	Decision tree	0.4189	0.3232	0.6473
	Bagged decision tree	0.3770	0.3415	0.6140
	Boosted decision tree	0.2649	0.3061	0.5147

7. Results and analysis

In this section, the training and testing performances of the CaPrM integrated models are presented. The performances of the models are described using the statistical measures discussed in Section 6.3 and the average of ten test results are listed in Table 5. In MSE, RMSE, and MAE, the lower the value of the error statistics is the better the prediction accuracy of the model. It can be easily observed from Table 5 that neural network has statistically outperformed all other models. Among the decision tree based models (decision tree, bagged and boosted decision trees), boosted decision tree performs best with better generalization capability. MAE of decision tree is smaller than bagged decision tree. However, their MSE value confirmed that decision tree generalized the test data poorly than bagged decision tree. It is worth to mention that these results are valid for the considered dataset. If a different dataset is employed, the performance may differ.

The initial validation test results of the CaPrM model before incorporating variable selection method is also presented in Table 5. The purpose is to demonstrate the contribution of variable selection in the improvement of the models performance. The same statistical performance evaluation methods were applied as the above cases. According to the result, variable selection enhances the performance of all the integrated models significantly. This confirms the advantage of considering variable selection in carbonation prediction modeling.

Experimentally measured and predicted carbonation depths obtained from training dataset for all integrated learning methods are shown in Fig. 6. As it is clearly seen, the correlation coefficients (R-values) for all methods are above 0.90. The higher the correlation coefficient indicates that all the models track the actual measured carbonation depth well during training phase. In Fig. 6, a slight tendency of an underestimation for higher carbonation depth is also observed. The reason for the underestimation is that the available dataset with higher carbonation depth are fewer compared to the lower carbonation depth. For instance, carbonation depths which are greater than 3 mm cover only about 9% of the total observation. The lack of sufficient training and validation dataset for higher carbonation depth leads to the underestimation in this range.

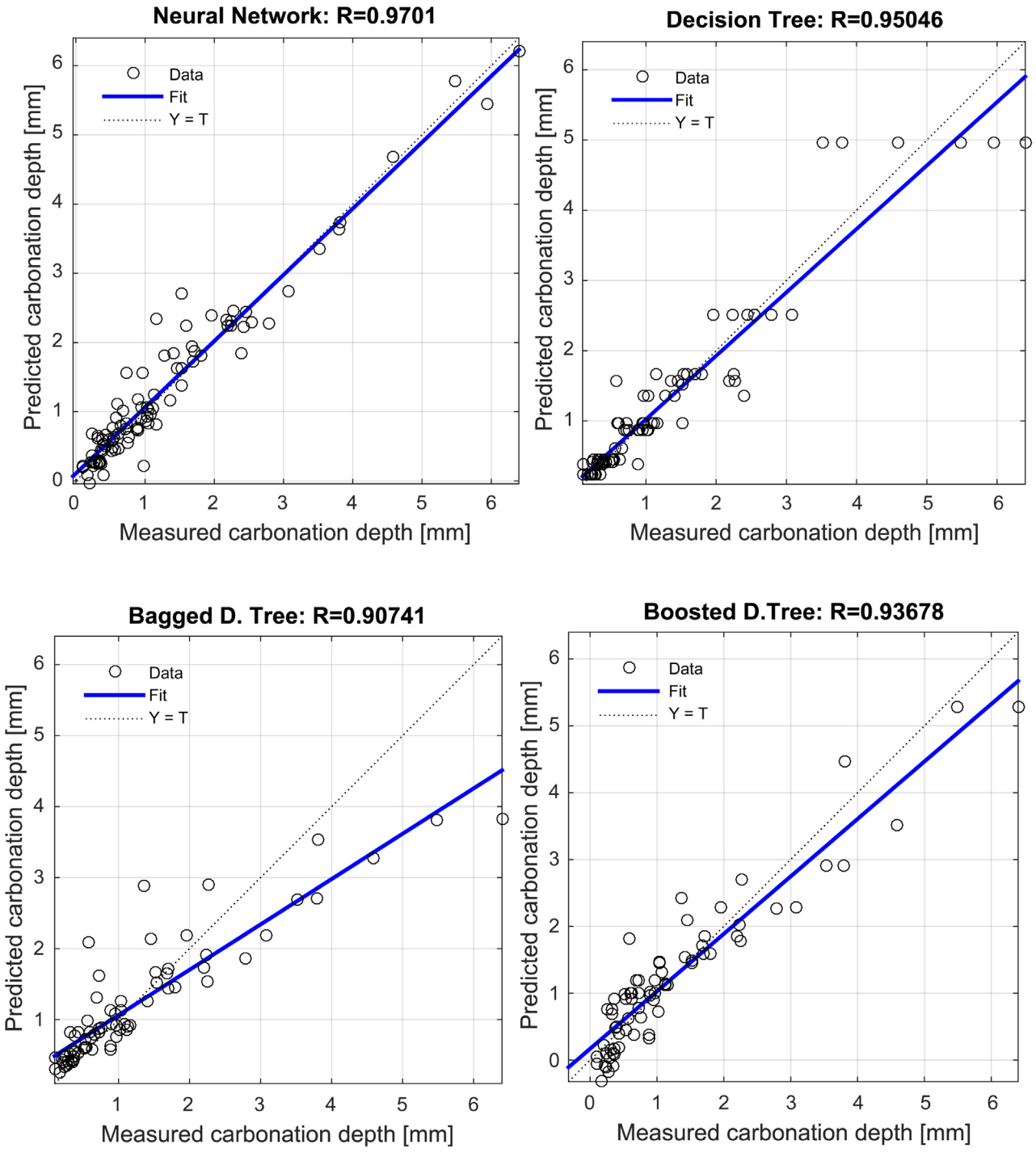

Fig. 6. Regression plot for predicted vs. measured carbonation depth for training dataset.

The distribution of the residuals of the CaPrM model is also analyzed. The residuals are calculated based on the differences between target and predicted carbonation depth values. The median, maximum, minimum and outlier values of residuals for the four integrated models are presented in Fig. 7 as a boxplot. The plot represents residuals of a random single run. The median is shown as a red line within the box. The blue box covers the middle 50% (25th–75th percentiles) of the residuals. The whiskers go down to the minimum and up to the maximum values. Residuals greater than 1.5 box lengths above the whiskers are outliers and shown as red plus sign.

The residuals median of the neural network model is almost in the middle of the box and distributed around zero. This shows that the residuals have a constant variance patterns and normally distributed. In the decision tree and bagged decision tree the median of residual is close to zero. The decision tree has fewer residuals far from the median. The median of bagged and boosted decision tree are nearer to the first quartile than to the third quartile, indicating

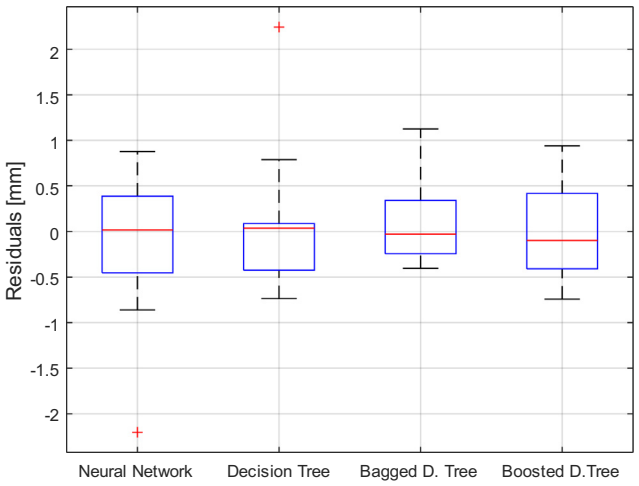

Fig. 7. Boxplot of residuals of CaPrM model.

that the residuals distributions are slightly skewed to the right. Generally, the boxplot of the residuals of a single run test demonstrate that all the models learn the nonlinear relation of the input variables and are able to capture the complex nature of the carbonation process with reasonably high accuracy.

8. Discussions

To avoid corrosion of steel reinforcement an accurate carbonation prediction model is crucial to make realistic decisions about service life of a structure or to evaluate possibilities for extending it. The complex nature of the carbonation process in combination with a wide variety of concrete mixtures and exposure conditions makes reaching at an equation which fully represent the carbonation process is challenging. As seen in the results received by the case study, machine learning based models are able to predict with a reasonably high accuracy without assuming a predetermined equation as a model.

Analysis of the results of the developed CaPrM model demonstrates its practical applicability in assisting service-life prediction of reinforced concrete structures. It captures the changes of the concrete due to aging and interaction with the exposure environment. The model is also easy to use and allows the users to switch

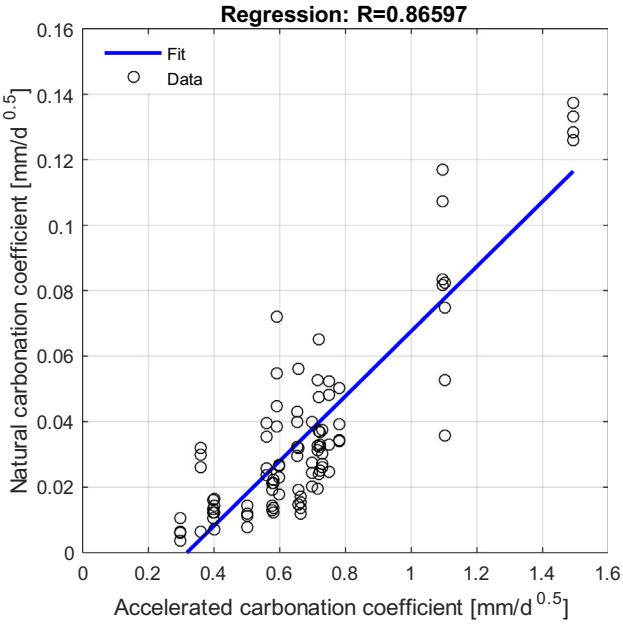

Fig. 9. Correlation between accelerated and natural carbonation coefficients.

from one learning method to another and make necessary adjustments for further optimization. The CaPrM model runs all the employed learning methods consequentially, measure their accuracy and provide their performance error in a matrix. In the CaPrM model the performance of each learning methods varies depending on the training dataset and the end user has the advantage of choosing the method that outperforms the others.

In the CaPrM modeling 25 input variables are processed. The predictive power of the variables is measured using ensemble methods. Typical importance weight of all the input variables inferred by bagged and boosted decision trees are shown in Fig. 8. It can be observed that accelerated carbonation depth, w/b and compressive strength are the most influential variables for prediction of the carbonation depth. These are well known parameters and have been considered in most of the analytical models. But next to these variables, plasticizers, air content, carbonation period and distribution of aggregate play considerable role in predicting the carbonation depth as clearly seen in Fig. 8. This is a useful finding because plasticizers, air content and aggregate

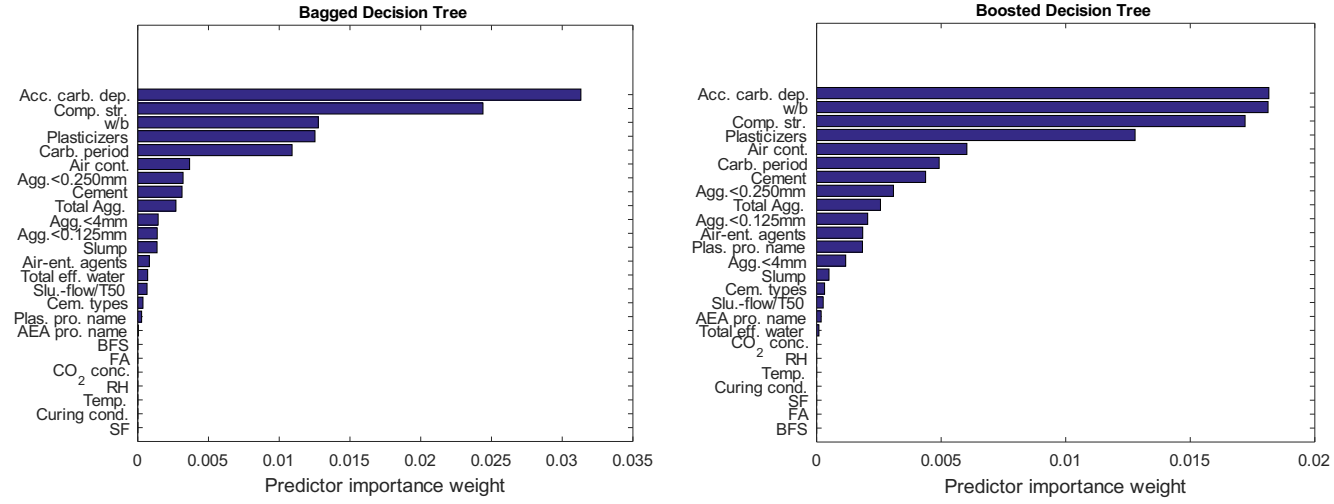

Fig. 8. Importance of relative variables of the ensemble learning methods.

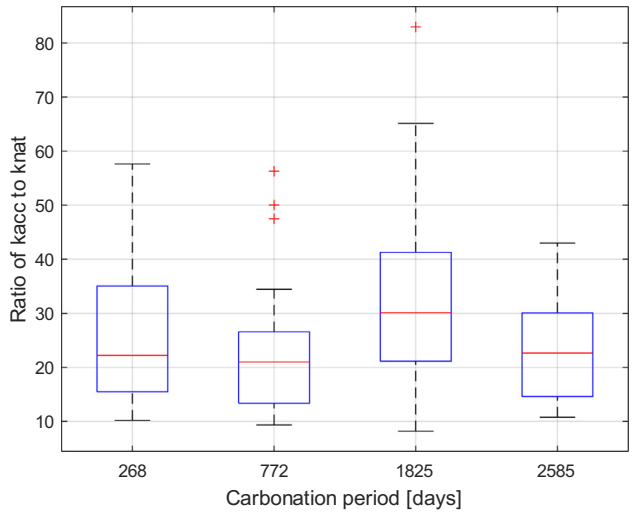

Fig. 10. Boxplot of k_{acc}/k_{nat} vs. carbonation periods.

distribution were overlooked in several existing analytical models. It is known that the role of CO_2, curing condition, relative humidity and temperature is significant in carbonation process but their importance is not shown in the figure. This is due to the use of one curing method and identical environmental exposure conditions for all concrete specimens in the Finnish DuraInt-project.

The accelerated and the field (natural) carbonation depth of the concrete specimens were obtained by following the procedure presented in Section 6.1. The accelerated carbonation was measured after exposing the concrete specimens in a climatic control chamber for 28 days, whereas the natural carbonations of the specimens were taken at the age of 268, 772, 1825 and 2585 days. The accelerated and the natural carbonation coefficients were calculated using Eq. (2) and their correlations is illustrated in Fig. 9. The accelerated coefficient generally shows a good correlation with the natural carbonation coefficient. The value of the correlation coefficient is 0.87. Other existing studies have also confirmed the good correlation between the accelerated and natural carbonation coefficients [18,62].

Analysis is performed to check the correctness of the conventional carbonation coefficient mathematical model which is expressed in Eq. (2). According to the mathematical model, the carbonation coefficient is assumed constant. If this assumption is valid the ratio of accelerated to natural carbonation coefficients (k_{acc}/k_{nat}) at different age should be about the same value. However, the median ratio (k_{acc}/k_{nat}) is not similar with time as demonstrated in Fig. 10. The variation is statistically significant, for example, about 26% difference in median ratio (k_{acc}/k_{nat}) between carbonation periods of 268 and 1825 days is observed. If the ratio of the accelerated to the natural carbonation at the age of 268 days is assumed to be correct, the conventional model expressed in Eq. (2) underestimate the carbonation depth at the age of 772 and 1825 days. This certainly confirms that the assumption of carbonation coefficient as constant with time leads to a considerable uncertainty in the prediction accuracy. Although the aim of the accelerated carbonation testing method is to provide a better understanding about what is likely to occur when the concrete is exposed to the natural environment, all the above findings of this study indicate that the accelerated testing fails to represent fully the natural conditions.

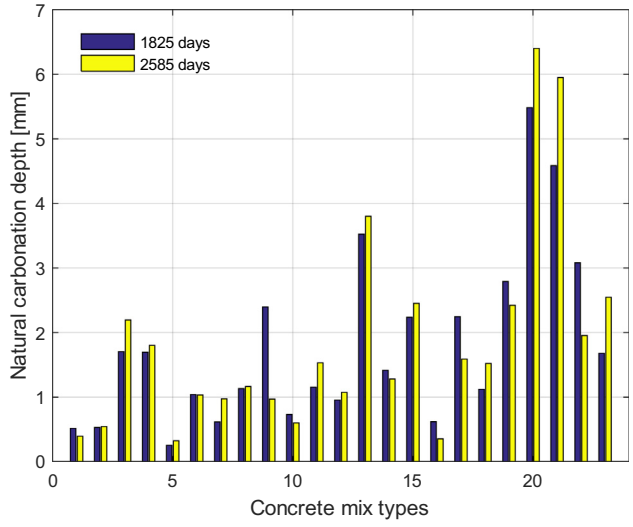

Fig. 11. Natural carbonation depths of all concrete mixes at the age of 1825 and 2585 days.

Another assumption in conventional models is that carbonation rate depends on square root of time. However the experimental data reveals that this assumption is invalid for some concrete mix types. As seen in Fig. 11, the carbonation depth at the age of 2585 days for concrete mix types 1, 9, 10, 14, 16, 17, 19 and 22 is less than that of 1825 days, which accounts for about 35%. Even if these results are different from other researches, it is not a new phenomenon, there are studies with the same findings [63,64]. Simply using time-independent carbonation rate as in the conventional models is not a valid approach generally. All these confirm the limitations of the conventional carbonation prediction model in providing reliable results.

In practice, carbonation depth prediction is often carried out up to the corresponding service life of concrete structures, which is typically 50 years or more. As similar learning based prediction models, CaPrM can generalize the problem at hand only within the range of the input variables. Thus, to make prediction for longer period, the model should be trained with new dataset consisting of long-term experimental data or long-term predictions can be achieved by using CaPrM and extrapolation. The CaPrM model determines the time dependence of carbonation depth within the time range of the training and the use of this dependency with an appropriate fitting function may allow extrapolation to longer periods.

The training data of CaPrM are acquired from Finnish DuraInt-project where the curing methods and environmental exposure conditions are the same for all concrete specimens. Indeed, it is possible to add more carbonation depths collected from various experimental data which encompass different concrete mix types, fresh and hardened concrete properties, exposure and curing conditions. This will make the CaPrM model more universal prediction model while enhancing the accuracy of the model as the generalization ability of the model increases because of the additional data. The CaPrM model can also be adopted with no or little effort by anyone who has experimental data.

9. Conclusions

An optimized and integrated machine learning based carbonation prediction model is developed and presented in this work. The novelty of the proposed model lies in its ability to integrate multiple powerful learning methods that can solve nonlinear regression problems efficiently. The integrated learning methods are neural network, decision tree and ensemble methods (bagged and boosted decision trees). The integration provides the opportunity to select the best performing learning methods among the four

choices because their relative performance alters when a dataset is changed. In addition, unlike the conventional models, the proposed model is able to consider almost all the influential parameters which govern the carbonation process. This allows evaluating all influential parameters as a group rather than individually which in turn ensures the reliability of the prediction since imperative dependencies are not overlooked.

The model is trained and tested using a dataset obtained from the Finnish DuraInt-project. The test performance of the presented model demonstrated that all the integrated learning methods predict the carbonation depth with rationally low error. The statistical performance indicators, MSE, RMSE, and MAE were applied to measure the prediction accuracy. In the utilized training dataset, neural network statistically outperformed all other models. The neural network had a MSE 0.2417, RMSE 0.4916, and MAE 0.2860. The employed variable selection method enhances the performance of all the integrated models. In addition, the ensemble trees identified important variables for prediction of the carbonation depth which was not considered in most of the existing analytical models. The performance results of the integrated model confirms the usability of the CaPrM model in assisting designers to optimize the concrete mix or structural design as well as to define proactive maintenance plan. Therefore, engineers as well as designers could incorporate the CaPrM model in practice to achieve more accurate results.

Acknowledgment

The authors would like to thank Research Scientist Hannele Kuosa from VTT Technical Research Centre of Finland for providing the experimental data.

References

[1] A. Muntean, S.A. Meier, M.A. Peter, M. Böhm, J. Kropp, A Note on Limitations of the Use of Accelerated Concrete-Carbonation Tests for Service-Life Predictions, Universität Bremen, Bremen, 2005.
[2] P.F. Marques, A. Costa, Service life of RC structures: carbonation induced corrosion. prescriptive vs. performance-based methodologies, Constr. Build. Mater. 24 (2010) 258–265, http://dx.doi.org/10.1016/j.conbuildmat.2009.08.039.
[3] J.C. Walraven,. Design for service life: how should it be implemented in future codes, in: Second Int. Conf. Concr. Repair, Rehabil. Retrofit, ICCRRR-2, 2008, pp. 3–11.
[4] W.Z. Taffese, E. Sistonen, Service life prediction of repaired structures using concrete recasting method: state-of-the-art, Proc. Eng. 57 (2013) 1138–1144, http://dx.doi.org/10.1016/j.proeng.2013.04.143.
[5] O.P. Kari, J. Puttonen, E. Skantz, Reactive transport modelling of long-term carbonation, Cem. Concr. Compos. 52 (2014) 42–53, http://dx.doi.org/10.1016/j.cemconcomp.2014.05.003.
[6] fib, Structural Concrete: Textbook on Behaviour, Design and Performance, Fédération internationale du béton (fib), Lausanne, 2009.
[7] B. Lagerblad, Carbon Dioxide Uptake During Concrete Life Cycle – State of the Art, vol. CBI 2005:2, 2005.
[8] Q. Huang, Z. Jiang, W. Zhang, X. Gu, X. Dou, Numerical analysis of the effect of coarse aggregate distribution on concrete carbonation, Constr. Build. Mater. 37 (2012) 27–35, http://dx.doi.org/10.1016/j.conbuildmat.2012.06.074.
[9] K.Y. Ann, S.W. Pack, J.P. Hwang, H.W. Song, S.H. Kim, Service life prediction of a concrete bridge structure subjected to carbonation, Constr. Build. Mater. 24 (2010) 1494–1501, http://dx.doi.org/10.1016/j.conbuildmat.2010.01.023.
[10] X.-Y. Wang, H.-S. Lee, A model for predicting the carbonation depth of concrete containing low-calcium fly ash, Constr. Build. Mater. 23 (2009) 725–733, http://dx.doi.org/10.1016/j.conbuildmat.2008.02.019.
[11] A.M. Neville, J.J. Brooks, Concrete Technology, second ed., Pearson Education Limited, Harlow, 2010.
[12] E. Sistonen, Service life of hot-dip galvanised reinforcement bars in carbonated and chloride-contaminated concrete, Helsinki University of Technology, 2009. <http://urn.fi/URN:ISBN:978-952-248-168-9>.
[13] C.L. Page, Corrosion and protection of reinforcing steel in concrete, in: C.L. Page, M.M. Page (Eds.), Durab. Concr. Cem. Compos., Woodhead Publishing Ltd., Cambridge, 2007, pp. 136–186.
[14] A. Köliö, T.A. Pakkala, J. Lahdensivu, M. Kiviste, Durability demands related to carbonation induced corrosion for Finnish concrete buildings in changing climate, Eng. Struct. 62–63 (2014) 42–52, http://dx.doi.org/10.1016/j.engstruct.2014.01.032.
[15] R. Neves, F.A. Branco, J. De Brito, A method for the use of accelerated carbonation tests in durability design, Constr. Build. Mater. 36 (2012) 585–591, http://dx.doi.org/10.1016/j.conbuildmat.2012.06.028.
[16] H.-W. Song, S.-J. Kwon, Evaluation of chloride penetration in high performance concrete using neural network algorithm and micro pore structure, Cem. Concr. Res. 39 (2009) 814–824, http://dx.doi.org/10.1016/j.cemconres.2009.05.013.
[17] P. Schiessl, S. Lay, Influence of concrete composition, in: H. Böhni (Ed.), Corros. Reinf. Concr. Struct., Woodhead Publishing Limited, Cambridge, 2005, pp. 91–134.
[18] R. Neves, F. Branco, J. De Brito, Field assessment of the relationship between natural and accelerated concrete carbonation resistance, Cem. Concr. Compos. 41 (2013) 9–15, http://dx.doi.org/10.1016/j.cemconcomp.2013.04.006.
[19] fib, Code-Type Models for Concrete Behaviour: State-of-the-Art Report, Fédération internationale du béton (fib), Lausanne, 2013.
[20] fib, Fib Model Code for Concrete Structures 2010, Ernst & Sohn, Berlin, 2013.
[21] Y. Liu, S. Zhao, C. Yi, The forecast of carbonation depth of concrete based on RBF neural network, in: Second Int. Symp. Intell. Inf. Technol. Appl. IITA 2008, vol. 3, IEEE Computer Society, Shanghai, 2008, pp. 544–548, http://dx.doi.org/10.1109/IITA.2008.402.
[22] D. Luo, D. Niu, Z. Dong, Application of neural network for concrete carbonation depth prediction, in: J. Weiss, J. Olek (Eds.), Fourth Int. Conf. Durab. Concr. Struct., ICDCS, West Lafayette, 2014, pp. 66–71, http://dx.doi.org/10.5703/1288284315384.
[23] C. Lu, R. Liu, Predicting carbonation depth of prestressed concrete under different stress states using artificial neural network, Adv. Artif. Neural Syst. 2009 (2009) 1–8, http://dx.doi.org/10.1155/2009/193139.
[24] N.R. Buenfeld, N.M. Hassanein, A.J. Jones, An artificial neural network for predicting carbonation depth in concrete structures, in: N. Kartam, I. Flood (Eds.), Artif. Neural Networks Civ. Eng. Adv. Featur. Appl., American Society of Civil Engineers, 1998, pp. 77–117.
[25] N. Bu, G. Yang, H. Zhao, Prediction of concrete carbonization depth based on DE-BP neural network, in: Third Int. Symp. Intell. Inf. Technol. Appl. IITA 2009, vol. 3, IEEE, Nanchang, 2009, pp. 240–243, http://dx.doi.org/10.1109/IITA.2009.252.
[26] E. Alpaydin, Introduction to Machine Learning, second ed., MIT press, Cambridge, 2010, http://dx.doi.org/10.1017/S0269888910000056.
[27] V. Cherkassky, F. Mulier, Learning From Data: Concepts, Theory, and Methods, second ed., John Wiley & Sons, Inc., Hoboken, 2007.
[28] J. Han, M. Kamber, J. Pei, Data Mining: Concepts and Techniques, Morgan Kaufmann, Waltham, 2012.
[29] R. Bekkerman, M. Bilenko, J. Langford, Scaling up machine learning: introduction, in: R. Bekkerman, M. Bilenko, J. Langford (Eds.), Scaling Up Mach. Learn. Parallel Distrib. Approaches, Cambridge University Press, New York, 2012, pp. 1–22.
[30] P. Wittek, Quantum Machine Learning: What Quantum Computing Means to Data Mining, First ed., Academic Press, San Diego, 2014.
[31] S. Marsland, Machine Learning: An Algorithmic Perspective, Chapman and Hall/CRC, Boca Raton, 2009.
[32] L. Rokach, O. Maimon, Data Mining With Decision Trees: Theory and Applications, World Scientific Publishing Co., Pte., Ltd., Singapore, 2008.
[33] J. Bell, Machine Learning: Hands-On For Developers and Technical Professionals, John Wiley & Sons, Inc., Indianapolis, 2015.
[34] O. Kramer, Dimensionality Reduction with Unsupervised Nearest Neighbors, Springer-Verlag, Berlin, 2013, http://dx.doi.org/10.1007/978-3-642-38652-7.
[35] A. Kialashaki, J.R. Reisel, Development and validation of artificial neural network models of the energy demand in the industrial sector of the United States, Energy 76 (2014) 749–760, http://dx.doi.org/10.1016/j.energy.2014.08.072.
[36] M.J. Kim, D.K. Kang, Ensemble with neural networks for bankruptcy prediction, Expert Syst. Appl. 37 (2010) 3373–3379, http://dx.doi.org/10.1016/j.eswa.2009.10.012.
[37] D. Che, Q. Liu, K. Rasheed, X. Tao, Decision tree and ensemble learning algorithms with their applications in bioinformatics, in: H.R. Arabnia, Q.-N. Tran (Eds.), Softw. Tools Algorithms Biol. Syst., vol. 696, Springer-Verlag, New York, 2011, pp. 191–199, http://dx.doi.org/10.1007/978-1-4419-7046-6.
[38] X. Shi, T.A. Nguyen, P. Kumar, Y. Liu, A phenomenological model for the chloride threshold of pitting corrosion of steel in simulated concrete pore solutions, Anti-Corrosion Methods Mater. 58 (2011) 179–189, http://dx.doi.org/10.1108/00035591111148894.
[39] E.M. Güneyisi, K. Mermerdaş, E. Güneyisi, M. Gesoğlu, Numerical modeling of time to corrosion induced cover cracking in reinforced concrete using soft-computing based methods, Mater. Struct. 48 (2014) 1739–1756, http://dx.doi.org/10.1617/s11527-014-0269-8.
[40] W.Z. Taffese, F. Al-Neshawy, J. Piironen, E. Sistonen, J. Puttonen, Monitoring, evaluation and long-term forecasting of hygrothermal performance of thick-walled concrete structure, in: Proc. OECD/NEA WGIAGE Work. Non-Destructive Eval. Thick. Concr. Struct., OECD, Prague, 2014, pp. 121–143.
[41] I.B. Topçu, A.R. Boğa, F.O. Hocaoğlu, Modeling corrosion currents of reinforced concrete using ANN, Autom. Constr. 18 (2009) 145–152, http://dx.doi.org/10.1016/j.autcon.2008.07.004.
[42] S. Samarasinghe, Neural Networks for Applied Sciences and Engineering: From Fundamentals to Complex Pattern Recognition, Auerbach Publications, Boca Raton, 2006, http://dx.doi.org/10.1201/9781420013061.fmatt.
[43] D. Graupe, Principles of Artificial Neural Networks, second ed., World Scientific Publishing Co., Pte., Ltd., Singapore, 2007, http://dx.doi.org/10.1142/9789812770578_fmatter.

[44] P. Gupta, R. Srinivasan, Missing data prediction and forecasting for water quantity data, in: Int. Conf. Model. Simul. Control. IPCSIT, vol. 10, IACSIT Press, Singapore, 2011, pp. 98–102, http://dx.doi.org/10.7763/IPCSIT.
[45] K. Vinaykumar, V. Ravi, C. Mahil, Software cost estimation using soft computing approaches, in: E.S. Olivas, J.D.M. Guerrero, M.M. Sober, J.R.M. Benedito, A.J.S. López (Eds.), Handb. Res. Mach. Learn. Appl. Trends Algorithms, Methods, Tech., IGI Global, Hershey, 2010, pp. 499–518, http://dx.doi.org/10.4018/978-1-60566-766-9.ch024.
[46] B.J. Taylor, Methods and Procedures For the Verification and Validation of Artificial Neural Networks, Springer Science & Business Media, New York, 2006, http://dx.doi.org/10.1007/0-387-29485-6.
[47] J. Wu, S. Coggeshall, Foundations of Predictive Analytics, CRC Press, Boca Raton, 2012.
[48] G. Dreyfus, Neural Networks: Methodology and Applications, Springer-Verlag, Berlin, 2005, http://dx.doi.org/10.1007/3-540-28847-3.
[49] S. Haykin, Neural Networks: A Comprehensive Foundation, Pearson Education Pte., Ltd., Singapore, 1999.
[50] J. Gama, Knowledge Discovery From Data Streams, Chapman and Hall/CRC, Boca Raton, 2010, http://dx.doi.org/10.1201/EBK1439826119-c1.
[51] C.D. Sutton, Classification and regression trees, bagging, and boosting, in: C.R. Rao, E.J. Wegman, J.L. Solka (Eds.), Handb. Stat. Data Min. data Vis., Elsevier B. V, Amsterdam, 2005, pp. 303–330, http://dx.doi.org/10.1016/S0169-7161(04)24001-9.
[52] G. Seni, J.F. Elder, Ensemble Methods in Data Mining: Improving Accuracy Through Combining Predictions, vol. 2, Morgan & Claypool, 2010, http://dx.doi.org/10.2200/S00240ED1V01Y200912DMK002.
[53] I.H. Witten, E. Frank, M.A. Hall, Data Mining: Practical Machine Learning Tools and Techniques: Practical Machine Learning Tools and Techniques, Morgan Kaufmann, Burlington, 2011.
[54] W.W. Hsieh, Machine Learning Methods in the Environmental Sciences: Neural Networks and Kernels, Cambridge University Press, Cambridge, 2009, http://dx.doi.org/10.1017/CBO9780511627217.
[55] M.R. Berthold, C. Borgelt, F. Höppner, F. Klawonn, Guide to Intelligent Data Analysis: How to Intelligently Make Sense of Real Data, Springer-Verlag, London, 2010, http://dx.doi.org/10.1007/978-1-84882-260-3.
[56] EN 197-1, Cement – Part 1: COMPOSITION, Specifications and Conformity Criteria for Common Cements, Eur Comm Stand, 2003.
[57] M.H. Beale, M.T. Hagan, H.B. Demuth, Neural Network Toolbox: User's Guide, Natick, 2013.
[58] G.H. Nguyen, A. Bouzerdoum, S.L. Phung, Efficient supervised learning with reduced training exemplars, in: IEEE Int. Jt. Conf. Neural Networks, IJCNN 2008, IEEE, Hong Kong, 2008, pp. 2981–2987, http://dx.doi.org/10.1109/IJCNN.2008.4634217.
[59] H. Wang, J. Ma, Simultaneous model selection and feature selection via BYY harmony, in: D. Liu, H. Zhang, M. Polycarpou, C. Alippi, H. He (Eds.), Adv. Neural Networks – ISNN 2011 8th Int. Symp. Neural Networks, ISNN 2011, Guilin, China, May 29–June 1, 2011, Proceedings, Part II, Springer-Verlag, Berlin, 2011, pp. 47–56, http://dx.doi.org/10.1007/978-3-642-21090-7.
[60] E. Tuv, A. Borisov, G. Runger, K. Torkkola, Feature selection with ensembles, artificial variables, and redundancy elimination, J. Mach. Learn. Res. 10 (2009) 1341–1366, http://dx.doi.org/10.1145/1577069.1755828.
[61] U. Stańczyk, Feature evaluation by filter, wrapper, and embedded approaches, in: U. Stańczyk, L.C. Jain (Eds.), Featur. Sel. Data Pattern Recognit., Springer-Verlag, Berlin, 2015, pp. 29–44, http://dx.doi.org/10.1007/978-3-662-45620-0.
[62] C. Gehlen, Probabilistische lebensdauerbemessung von stahlbetonbauwerken–zuverlässigkeitsbetrachtungen zur wirksamen vermeidung von bewehrungskorrosion (Ph.D. Thesis), DAfStb, 2000.
[63] J. Yaodong, B. Aruhan, P. Yan, Natural and accelerated carbonation of concrete containing fly ash and GGBS after different initial curing period, Mag. Concr. Res. 64 (2012) 143–150, http://dx.doi.org/10.1680/macr.10.00134.
[64] J. Sim, C. Park, Compressive strength and resistance to chloride ion penetration and carbonation of recycled aggregate concrete with varying amount of fly ash and fine recycled aggregate, Waste Manage. 31 (2011) 2352–2360, http://dx.doi.org/10.1016/j.wasman.2011.06.014.

Publication III

Taffese, Woubishet Zewdu; Sistonen, Esko. 2017. Significance of chloride penetration controlling parameters in concrete: Ensemble methods. Journal of Construction and Building Materials, volume 139, pages 9–23. ISSN 0950-0618. https://doi.org/10.1016/j.conbuildmat.2017.02.014.

Construction and Building Materials 139 (2017) 9–23

Contents lists available at ScienceDirect

Construction and Building Materials

journal homepage: www.elsevier.com/locate/conbuildmat

Significance of chloride penetration controlling parameters in concrete: Ensemble methods

Woubishet Zewdu Taffese *, Esko Sistonen

Department of Civil Engineering, Aalto University, P.O. Box 12100, FI-00076 Aalto, Finland

HIGHLIGHTS

- Ensemble methods are able to determine the optimal subset of influential variables.
- Chloride migration coefficient influences the chloride transport at earlier age.
- Several early age concrete tests are impotent in predicting the chloride ingress.
- Aggregate size distribution is among the predominant predictors of chloride ingress.
- Evaluation of long-term chloride transport using short-term tests is unrealistic.

ARTICLE INFO

Article history:
Received 7 December 2016
Received in revised form 5 February 2017
Accepted 6 February 2017

Keywords:
Reinforced concrete
Chloride ingress
Corrosion
Durability
Simplified models
Modelling
Ensemble methods
Variable importance analysis
Machine learning

ABSTRACT

Conventional chloride ingress prediction models rely on simplified assumptions, leading to inaccurate estimations. Reasonable simplifications can be achieved if and only if the effects of all interacting variables are clearly known. In this work, ensemble methods to discover significant parameters that control chloride ingress using long-term field data is developed and presented. The models are trained using dataset consisting of variables describing the concrete mix ingredients, fresh and hardened properties, field conditions as well as chloride profiles. The results analyses confirm that the models are able to determine the optimal subset of the influential variables that best predicts the chloride profile from the input dataset.

1. Introduction

Chloride attack is one of the predominant threats for the durability of reinforced concrete (RC) structures exposed to de-icing salts containing chloride [1–5]. The ingress of chloride ions is remarkable in countries at those latitudes where a large amount of de-icing salts are applied in winter to melt the ice on the roads. The melt ice slurry with extremely concentrated chloride ions from de-icing salt flows or splashes to RC structures by the moving vehicles. In some cases, chloride ions from de-icing salt is observed in RC structure situated 1.9 km from a busy highway and as high as 60th floor of a building [6]. In normal condition, the penetration of chloride does not result in damage to concrete directly. However, when the chloride concentration at the steel reinforcement bar (rebar) reaches a certain threshold value, they undergoes de-passivation and initiates corrosion [1–5]. Globally, corrosion of rebar induced by de-icing salt adversely affects the serviceability and safety of RC structures and has caused huge economic loss due to premature rehabilitation of civil infrastructures [1,5,7]. The total direct cost of chloride-induced corrosion in US highway bridges alone exceeds eight billion USD per annum. The indirect costs caused by traffic delays and lost productivity are predicted to be ten times more than the cost of corrosion related maintenance, repair and rehabilitation [7,8]. Hence, reliable quantitative evaluation of the amount of penetrated chloride concentration in the concrete is vital to mitigate premature failure of structures.

Through years of research, several models and input parameters have been established to foresee chloride concentration inside the concrete to make reliable and cost-effective maintenance and

* Corresponding author.
E-mail address: woubishet.taffese@aalto.fi (W.Z. Taffese).

http://dx.doi.org/10.1016/j.conbuildmat.2017.02.014
0950-0618/

repair decisions. The complexity level of the established models vary from simple analytical models assuming uniaxial diffusion into concrete, to more sophisticated numerical models which considers the physical, chemical, and electrochemical processes of gas and ion transport [9–11]. Some of the utilized analytical models and the associated value of input parameters have been incorrect, incomplete, and/or unsuitable for the prevailing conditions. Due to these facts, the prediction results differ substantially even for the same concrete matrix exposed in identical conditions [12]. Though the complex scientific models provide reasonably accurate predictions, they lack user friendliness and demand highly skilled professional, making them suitable only for research, but not for practical design applications. Despite the accessibility of numerous models, empirical ones are widely used to foresee the chloride concentration in concrete [13–17].

Empirical chloride ingress prediction models rely on simplified assumptions, leading to inaccurate estimations. Reliable simplification can be achieved if and only if the effect of the interacting variables is understood. In this work, models based on ensemble methods are developed to discover the significance of the parameters that influence the chloride ingress in concrete. The contributions of this work are: (i) chloride ingress prediction models using long-term field data (ii) evaluating the significance of early-age chloride transport property in determining long-term chloride penetration in concrete; (iii) determining the most influential variables which govern the penetration of chloride in concrete by employing three scenarios; and (iv) validating the identified subset of influential variables in improving chloride ingress prediction accuracy.

The structure of this paper is as follows. In Section 2, the importance of this research is elaborated. The fundamental knowledge on an ensemble method is presented in Section 3 since this technique is adopted to develop chloride ingress prediction models which ultimately used to investigate the significance of the parameters which govern chloride penetration in concrete. In Section 4, details of the chloride ingress prediction models development process is presented. The models are developed by utilizing ensemble methods. It is the core part of this work, since all the influential parameters are determined using these models. The models employ long-term experimental data exposed to de-icing environment. In Section 5 results and their analyses are explained in detail. Discussions of the findings and the conclusions of the work are presented in Sections 6 and 7, respectively.

2. Research significance

In practice, empirical chloride penetration prediction models in the form of simple analytical equations on the basis of Fick's second law of diffusion are commonly adopted to model penetration of chloride into concrete. Numerous models based on Eq. (1) have been published to predict the amount of chloride penetration and thus to evaluate the full or remaining service life of RC structure. Nevertheless, these models have several limitations that create uncertainty on the accuracy of the chloride ingress prediction. One of the foremost limitations of Eq. (1) is the assumption of the non-steady diffusion coefficient (D_{nss}) as invariant [13,18–20]. In real situation, D_{nss} cannot be recognized as constants. This is due to the transport properties of chloride relying on the intrinsic permeability of the concrete, which is changing during the process of cement hydration with time. In another perspective, the alteration of capillary pore structure of concrete is controlled by cement type, water to binder (w/b) ratio, exposure time, admixtures type, and exposure condition. Due to these, D_{nss} is varying with time and space [21,22]. In addition, in Eq. (1), the error function equation considers only diffusion mechanism. However, the penetration of chloride into concrete involves a complex physical and chemical process that combines various transport mechanisms other than diffusion such as capillary sorption, and permeation. All these facts explain why Eq. (1) based models fail to deliver accurate predictions in several instances [13].

$$C_x = C_i + (C_s - C_i)\left(1 - erf_{(x)}\left[\frac{x}{2\sqrt{D_{nss}t}}\right]\right) \quad (1)$$

where C_x is the content of chloride ion measured at average depth x [m] after exposure time t [s][% by mass of concrete]; C_s is the calculated content of ion at the exposed surface [% by mass of concrete]; C_i is the initial content of chloride ion [% by mass of concrete]; D_{nss} is the non-steady state diffusion coefficient of chloride ion [m^2/s.]; and $erf_{(x)}$ is the error function [−].

In order to address the time dependency of D_{nss} and effect of other influential factors different model codes have been proposed, e.g. in fib-MC2010 [23] and DuraCrete framework [24]. Most of the codes share the same expression as in Eq. (2).

$$D_{nss}(t) = k_e.k_t.k_c.D_0.\left(\frac{t_0}{t}\right)^n \quad (2)$$

where k_e is environmental function [–], k_t test method function [–], k_c curing function [–], D_0 is experimentally determined chloride diffusion coefficient at time t_0 [m^2/s], t_0 is age of concrete at D_0 is measured [year], t is the exposure duration [year], and n is the age factor [–].

The age factor describes the time dependency of the diffusion coefficient depending on the concrete composition. Its value is usually described by few parameters from concrete mixing ingredients, especially cementitious materials. The value of the age factor is usually determined based on various concrete specimens exposed to different environments for relatively short period of time and exhibits considerable scatter. Several studies demonstrated that the age factor is the most sensitive parameter in Eq. (2) [1,25–27]. A slight variation in its value causes a substantial uncertainty in chloride profile prediction, which in turn affects estimation of the time to corrosion initiation. This uncertainty may shorten the service life of the structure and increases the life-cycle cost due to improper prediction.

As discussed above, the widely applied chloride penetration prediction models (Eq. (1) and (2)) relies on limited factors. Indeed, examination of chloride transport in concrete is performed for several years to acquire a better understanding of various controlling parameters. To recognize the influence of various parameters, a large number of experiments should be performed since the microstructure of concrete is highly complex and its transport properties are controlled by numerous interacting variables. Nevertheless, it is usually challenging to isolate the influences of particular parameters because other controlling parameters are also vary naturally at the same time [28,29]. Hence, evaluating the importance of D_{nss} and other parameters that influence chloride ingression in concrete is essential in order to develop parsimonious and accurate chloride ingress prediction model.

Variable importance analysis technique can be applied to determine the main variables that influence the chloride ingress in concrete. Identifying important variables using traditional statistical methods, such as linear regression method is not achievable. The reason for this is that chloride ingress in concrete in field environment is a complex process controlled by numerous nonlinear factors, including concrete mix composition, external chloride concentration, climatic condition, exposure time, position and surface orientation of the concrete [30]. Variable importance analysis based on linear regression methods is only applicable for linear or nearly linear models. Therefore, alternative approaches which manage high-dimensional nonlinear features that reliably identify influential predictor variables are required.

Unlike conventional variable importance analysis approaches, machine learning algorithms are powerful in identifying and understanding the effect of complex interacting factors. Among machine learning algorithms, an ensemble method is a nonparametric algorithm that can handle highly nonlinear features with extensive interactions. Recently, the use of ensemble method to identify the influential parameters among numerous interacting factors has been proposed in certain civil engineering areas, e.g. hydrology [31], and building performance [32]. Though, the use of ensemble method has considerable advantage in determining complex relationship of nonlinear variables, it has not been commonly employed in concrete durability studies. Extended applications of machine learning in concrete durability including ensemble method are discussed in [33]. In this work, an ensemble method is developed to evaluate degree of importance of variables which govern the chloride ingress using long-term field experiments exposed in de-icing environment. The outcomes from this method not only benefit in understanding the characteristics of the chloride penetration in concrete, but also provide valuable information regarding the D_{nss} degree of significance in predicting chloride ingress in concrete.

3. Ensemble method

Since a machine learning ensemble method is developed to evaluate the effect of D_{nss}, it is worth to discuss the fundamentals of machine learning before elaborating on the applied ensemble method. Machine learning is one of a primary subfield in artificial intelligence. It utilizes learning algorithms to identify complex patterns from experimental data and perform intelligent decisions without assuming a predefined equation as a model [34–36]. Machine learning models can be either predictive to perform forecasts or descriptive to get new knowledge from a dataset, or both [34]. Characteristically, machine learning algorithms are classified into two learning types: supervised or unsupervised learning [37,38]. Supervised learning algorithms are increasingly adopted in modelling concrete properties [39–42]. Supervised learning comprises of input and output variables but unsupervised learning do not entails output variables. The former learning type is applied to predict a class or a value, while the latter learning type is used to cluster alike instances together or to discovery interesting patterns in the data. Supervised learning problems are categorized into two groups: classification and regression [37]. In classifications, the output domain is a finite discrete set of categories but in regression it is a set of real numbers. This research deals with regression learning problem as chloride profile is a numeric value that results from multiple nonlinear interacting factors. Regression problem generally defined as the problem of developing a practical model which is the best predictor of y given input x using a given training data $D = \{y_i, x_i\}_1^N$ as defined in Eq. (3).

$$y = \hat{F}(x_1, x_2, \ldots, x_n) = \hat{F}(X) \tag{3}$$

where y_i is the outputs variable, x_i is the input "vector" made of all the variable values for the *ith* observation, n is the number of variables; N is the number of observations.

In machine learning, ensemble methods are integration of several base models built within a given learning algorithm in order to enhance the generalization ability over a single model [34,37,43]. Unlike a statistical ensemble, a machine learning ensemble denotes finite set of alternative models and usually allows for a lot more flexible structure to exist among those alternatives. In this work, decision trees based ensemble of machine learning algorithms is adopted. Decision tree is a nonparametric hierarchical data structure, which apply the divide-and-conquer strategy. It handles complex problems by simplifying them into manageable extents and recursively implements the same approach to the sub-problems. Solutions of sub-problems can be integrated to deliver a solution of the complex problems. The ability of this approach arises from the capacity to divide the instance-space into subspaces and each sub-space is fitted with diverse models [34,44]. Decision tree applied for analysing regression problems known as regression tree. The fundamental structure of a regression tree is illustrated in Fig. 1. The left subfigure represents the data points and partitions them and the right subfigure displays the corresponding regression tree structure. As it is seen in the figure, regression tree is composed of decision and leaf nodes. Every decision node applies a test function with discrete outcomes labelling the branches. Given an input, at each node, a test is implemented and one of the branches is chosen based on the result. This procedure begins at the root and is recursively performed several times until a leaf node is hit, at which point the value listed in the leaf comprises the output [34]. Regression trees are fast learners that exhibit a high degree of interpretability and manage nonlinear numerical and categorical predictors with a large number of observations and input variables [43–45]. Indeed, a simple decision tree can be applied for variable importance (VI) analysis but a single tree may lead to overfitting since they are formed by a greedy algorithm where locally-optimal decisions are solved at each node. It

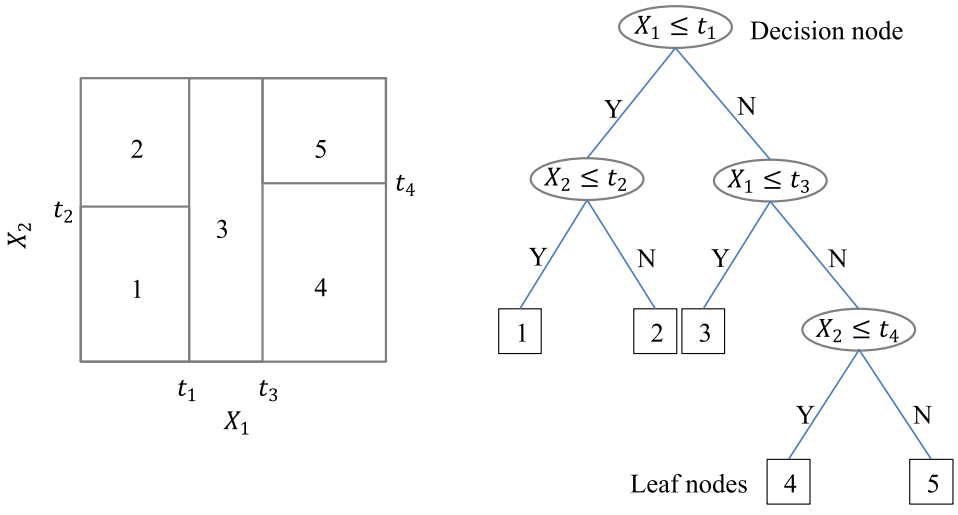

Fig. 1. Examples of a dataset and corresponding regression tree.

means that, a minor alteration to the data can provide a complete different output. Therefore, ensemble of multiple base models have to be adopted to avoid the effect of overfitting and increase generalization over a single decision tree [45].

Ensemble methods based on decision tree, bagging and boosting, are two of the most widely applied techniques [46]. Bagging method randomly draws multiple bootstrap observations from the dataset to build a new training dataset. This activity is carried out several times till a large subset of training datasets is produced and the identical samples can be drawn more than once. On average, every generated bootstrapped training dataset holds $N(1-\frac{1}{e}) \approx 0.63N$ observations, where N is the number of samples in the dataset. Samples which are excluded in the training dataset are known as out-of-bag observations. In the ensemble, bagging trains each model by utilizing the randomly drawn subset of the training set. The final output of the bagging ensemble of trees for out-of-bag dataset is the average of the estimated output of the single trees. Whereas boosting method trains the training dataset in sequence with enhancement from one model to the next. It employs a data point weight for each training observations in order to build various models. The final output of the boosting ensemble is the weighted mean of the output from all its members.

The developed ensemble method delivers measure of variable importance (the individual parameter effects of the inputs on the chloride profile output). In order to obtain the variable significance measure, for each decision tree, randomly permute the j-th predictor variable x_j with some permutation φ_j among the training set. Then compute the out-of-bag error on this perturbed dataset. The importance score for the j-th feature is evaluated by averaging the difference in out-of-bag error before and after the permutation over all trees. The score is normalized by the standard deviation of these differences. Variables which generate large values for this score are ranked as more significant than variables which induce small values. This procedure is described by Eq. (4)(6) [47].

Let $\overline{\beta}^{(t)}$ be the out-of-bag sample for a tree t, with $t \in \{1, 2, \ldots, T\}$. Then the variable importance of variable x_j in tree t is expressed by Eq. (4).

$$VI^{(t)}(x_j) = \frac{\sum_{i\overline{\beta}^{(t)}} I(y_i = \hat{y}_i^{(t)})}{|\overline{\beta}^{(t)}|} - \frac{\sum_{i\overline{\beta}^{(t)}} I(y_i = \hat{y}_{i,\varphi_j}^{(t)})}{|\overline{\beta}^{(t)}|} \tag{4}$$

where $\hat{y}_i^{(t)} = f^{(t)}(x_i)$ and $\hat{y}_{i,\varphi_j}^{(t)} = f^{(t)}(x_{i,\varphi_j})$ is predicted value for i-th observation before and after permuting its value of variable x_j, respectively. By definition, $VI^{(t)}(x_j) = 0$, if variable x_j is not in tree t).

The variable importance score for each variable is evaluated as the average importance over all trees, Eq. (5).

$$VI(x_j) = \frac{\sum_{t=1}^{T} VI^{(t)}(x_j)}{T} \tag{5}$$

The standardized variable importance is computed by utilizing Eq. (6). Its rationale is the following: As presented in Eq. (4), the individual importance scores $VI^{(t)}(x_j)$ are evaluated from T bootstrap samples which are randomly drawn from the original dataset and are identically distributed. Hence, if each individual variable importance $VI^{(t)}(x_j)$ has standard deviation σ, the average importance from T replications has standard error $\sigma/\sqrt{T}$.

$$\tilde{VI}(x_j) = \frac{VI(x_j)}{\frac{\sigma}{\sqrt{T}}} \tag{6}$$

In this work, the ensemble method using bagging approach is developed to analyse the variable importance of the inputs on the chloride profile. This method is a well appropriate method for measuring VI, at least, for three reasons: (i) they are random models; (ii) they use several base learners; (iii) they require a few hypotheses regarding the data and can manage large number variables. All these factors make the ensemble method robust against changes in data and avoid overfitting.

4. Model development for variable importance measure

In this section, the development steps of ensemble method based chloride profile prediction model and the process of variable importance measure are presented. The purpose of the model is to analyse importance of variables on chloride penetration. The workflow of the model development process is revealed in Fig. 2. From this figure, it can be noticed that the model development has four major steps: (i) data, (ii) bootstrap samples, (iii) building multiple models, and (iv) aggregation.

The first step, data, is the prerequisite for developing any machine learning based models. Data usually requires some preprocessing before they are utilized for model development. Data pre-processing often involves tasks of data encoding, missing data processing, data normalization and data partitioning. Performing such tasks before processing them in model training phase is almost a standard practice. Data encoding, missing data processing and data normalization tasks are not performed in this work because the developed model does not require data encoding and normalization as well as there are no missed values in the utilized experimental dataset. Data partitioning is presented as a second step after data pre-processing. The data is partitioned to training and testing set. The training sets are generated by randomly drawing multiple bootstrap samples from the original dataset using bagging method. On average, each training set comprises about 63% of the original dataset. Any left out instances from the original dataset (out-of-bag observations) are used as test sets. These data sets are necessary to evaluate the performance of the model. The third step is building multiple chloride profile prediction models by employing the bootstrap samples. The final step is aggregation of the models output, which is done by averaging the predicted output of each model built in step three in order to form an ensemble model. Once the model is formed, it is possible to analyse the VI measures. The whole process is iterated i times to achieve more reliable results and then the average value of i VI measures is considered for selection of the optimal subset of significant variables.

4.1. Data details

Long-term experimental data is utilized in this work. The experimental data were produced for Finnish DuraInt-project, which was performed in collaboration with Aalto University and VTT Technical Research Centre of Finland. In DuraInt-project concrete specimens with 18 dissimilar mix proportions, which mainly represent industrial mixes in Finland were prepared. The specimens were casted in upright position in wooden moulds of size $300 \times 300 \times 500$ mm^3 to carry out chloride field test. Surface treatments (impregnation, form lining, Cu-mortar) were applied on certain specimens to investigate their effect on chloride penetration. The concrete specimens were placed on the road side at Kotka, Finland and Borås, Sweden. The data utilized in this work is collected from the non-surface treated specimens situated on the side of highway 7 (HW 7) at Kotka. The geographical location of Kotka is shown in the map in Fig. 3.

The concrete specimens were exposed to NaCl de-icing agent for 6 years (2007–2013). The yearly average amount of de-icing salt that spread on HW7 during this period was about 0.99 kg/m^2 with an average of 102 salting occasions. The daily average number of vehicles passing on HW 7 was estimated about 27,000 in which

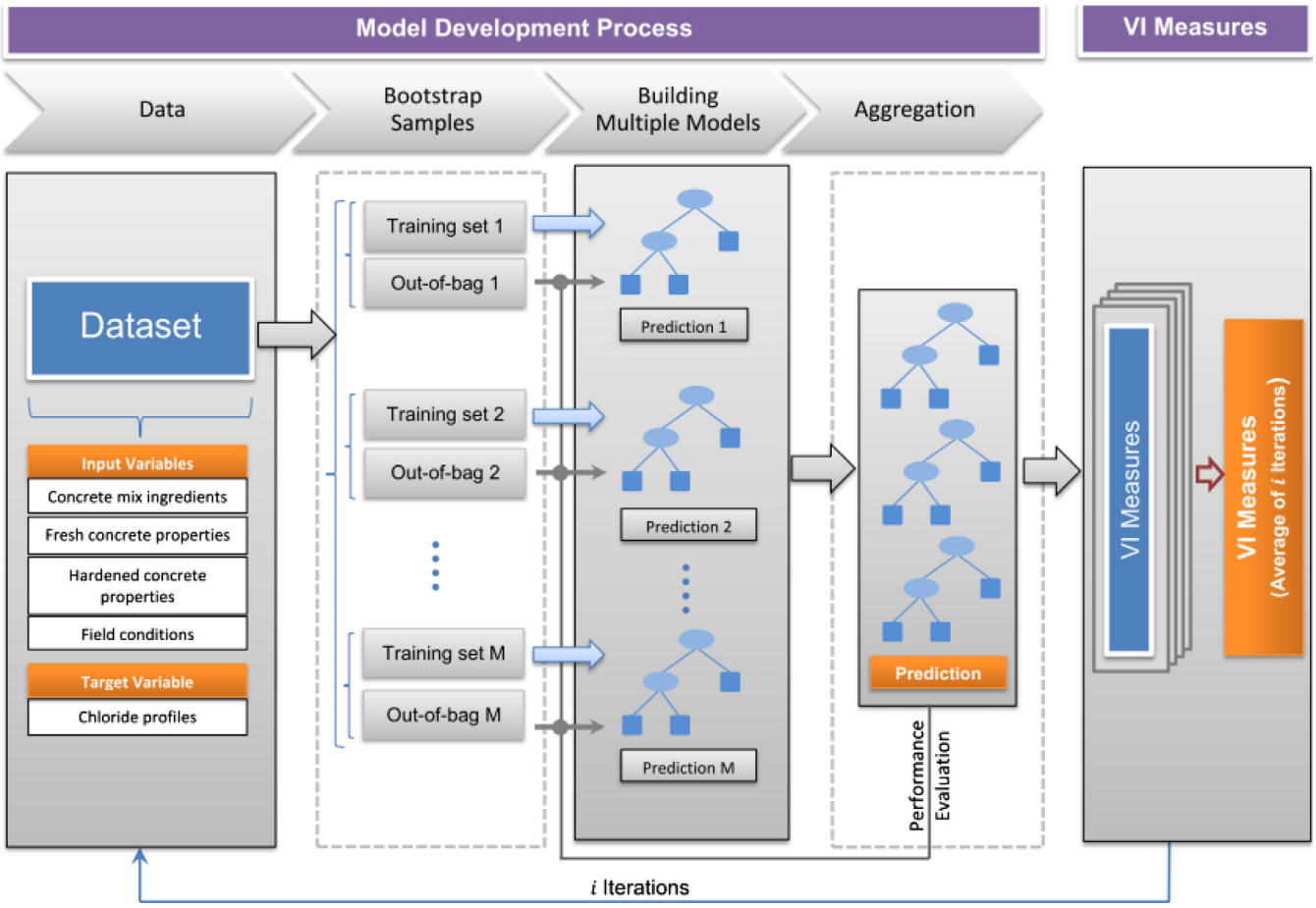

Fig. 2. workflow of the chloride ingress prediction model.

Fig. 3. Map of Finland and kotka where the concrete specimens are located.

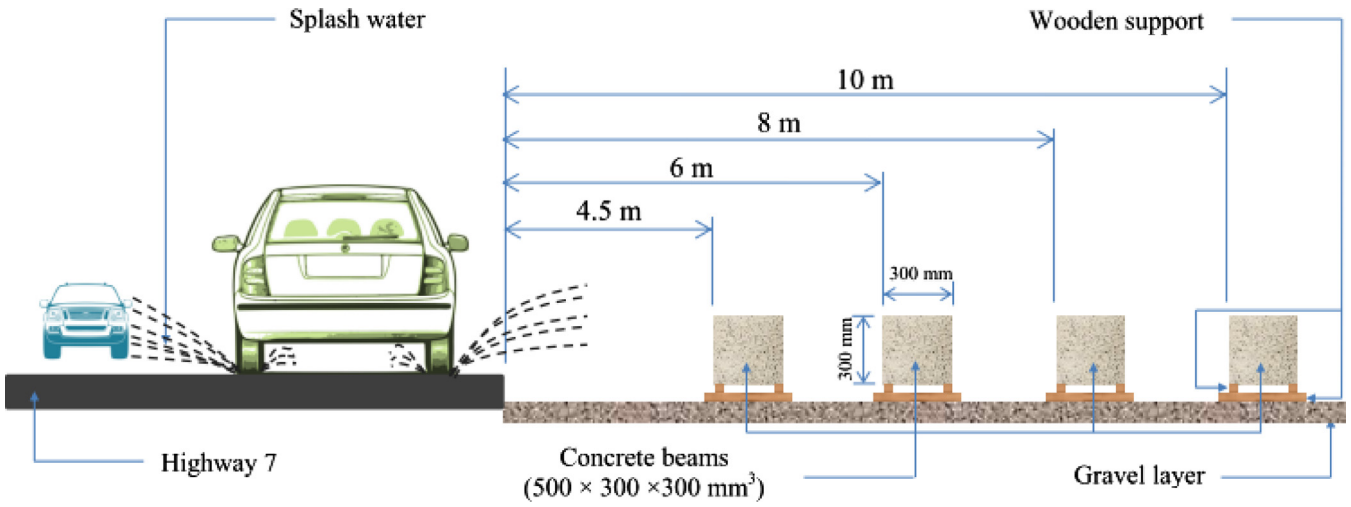

Fig. 4. Schematic representation of the concrete specimens for chloride penetration studies.

about 13% are heavy vehicles. A local weather station besides the HW 7 was installed. It continuously registered the weather variations including relative humidity, dew point temperature, road surface temperature and rain at every six minute intervals. The detailed description regarding the salting and the weather condition can be referred in [48]. The concrete specimens were positioned in array at a distance of 4.5 m, 6 m, 8 m, and 10 m from the HW 7 lane. The schematic illustration of the placement is shown in Fig. 4. All the specimens were kept on wooden stands which were installed on a gravel bed in order to avoid the probable water suction through the lower surfaces of the specimens. Regular field maintenance was executed to assure that the specimen's surfaces were exposed to splash water and water vapour. The amount of the splashed chloride on the specimens located at the same distance is assumed to be equal. The chloride profiles in concrete specimens were examined after 1, 3 and 6 years of exposure in the field environment. The chloride content analyses were carried out by taking cylinder cores with size of (ø 100 mm, h > 100 mm) from the field specimens. Dust samples were collected from the cored cylinders using a profile grinding method at different depths. The analysed chloride depth ranges from 0.5 mm to 26 mm with increments of diverse orders.

The data collected from the specimens and utilized in the model contains information about the concrete mix ingredients and the ingredients are listed in Table 1. A total of five kinds of cements, in accordance with the categorization of EN 197-1 [56], were employed. These are Portland cement (CEM I 42,5N-SR and CEM I 52,5 R), Portland limestone cement (CEM II/A-LL 42,5 R), Portland composite cement (CEM II/A-M(S-LL) 42,5N) and Portland slag cement (CEM II/B-S 42,5 N). Partially substituted Portland limestone cement, CEM II/A-LL 42,5 R, with pulverized blast-furnace slag (BFS) and fly ash (FA) are also utilized for preparing some of the specimens. The w/b ratio of the data ranges from 0.38 to 0.51. Each concrete specimen consists of one type of plasticizer (named VB-Parmix, or Glenium G 51 or Teho-Parmix) and an air-entraining agent (named either Ilma-Parmix or Mischöl). All the plasticizer and air-entraining agents were produced by different manufacturers. The typical mix compositions of concrete specimens which are placed at Kotka are presented in Table 2.

The dataset also comprised of fresh and hardened properties of the specimens. The fresh concrete properties include slump, density and air content. The air content was examined using pressure gauge method. Properties of the hardened specimen encompass laboratory test results of pore volume, density (wet and dry), air void, compressive strength, carbonation diffusion coefficient and chloride migration coefficient. The pore volume results provide information regarding the concrete porosity at early hardening phase. The wet and dry density of the specimens was determined at the same age with the pore volume analysis, at about the age of two days. The air void of the hardened concrete specimens was performed by thin section analysis. The size of the prepared thin sections, two from each specimen, was 35 mm × 55 mm × 25 μm. The compressive strength test was carried out using a set of three standard cube specimens with size of 150 × 150 × 150 mm^3 at the age of 28 days. The carbonation diffusion coefficients were also examined using accelerated carbonation test by exposing the specimens in a climatic control chamber filled with 1% of CO_2 for 28 days. Then the carbonation depths were tested using 1% phenolphthalein in ethanol solution to calculate the carbonation diffusion coefficients. The chloride diffusion coefficient is measured by the rapid chloride migration (RCM) and abbreviated as D_{nssm}. The concrete specimens were casted in cylinders (ø98 mm, h250 mm) to make this examination in laboratory. Three specimens were produced for each concrete mix categories. The specimens were sliced at a thickness of 50 mm to produce specimen size (ø98 mm, h50 mm) and perform the chloride penetration test at the age of three months in accordance with NT Build 492 [49]. All the discussed properties of the fresh and the hardened specimens are also presented in Table 1. In addition, the field conditions which contain information about the exposure time and distance from highway lane are included in Table 1.

It can be observed from Table 1 that there are a total of 33 variables representing the concrete mix ingredients, fresh and hardened properties, field conditions and chloride profiles. Variables numbered from 1 to 32 are designated as input variables and the last variable (chloride profile of every specimen) is assigned as a target variable. The input variables comprise of continuous and nominal data types whereas the target variable consist only continuous data type. In the table continuous variables are represented as C and nominal data types as N. Continuous variables are real numbers, such as results of quantitative measurements (e.g. w/b, cement and aggregate content) whereas nominal variables are non-numeric and descriptive data types (e.g. binder types, product name of plasticizers and air-entraining agents).

Table 1
Description of variables employed in the dataset (C: continuous and N: nominal).

Variables category	No.	Variable subcategories	Description	Units	Types and range	Short name
Concrete mix ingredients	1	Binder types	CEM I 42,5N – SR	–	N: (1 = CEM I 42,5N – SR, 2 = CEM I 52,5 R,	Bind. types
			CEM I 52,5 R	–	3 = CEM II/A-LL 42,5 R, 4 = CEM II/A-M(S-LL) 42,5N,	
			CEM II/A-LL 42,5 R	–	5 = CEM II/B-S 42,5N, 6 = CEM II/A-LL 42,	
			CEM II/A-M(S-LL) 42,5N	–	5 R & blast-furnace slag,	
			CEM II/B-S 42,5N	–	7 = CEM II/A-LL 42,5 R & fly ash)	
			CEM II/A-LL 42,5 R & blast-furnace slag	–		
			CEM II/A-LL 42,5 R & fly ash	–		
	2	Water to binder ratio		–	C: 0.37 to 0.51	w/b
	3	Cement content		[kg/m^3]	C: 217.22 to 451	Cement
	4	Blast-furnace slag content		[kg/m^3]	C: 0 to 217.22	BFS
	5	Fly ash content		[kg/m^3]	C: 0 to 106	FA
	6	Total effective water		[kg/m^3]	C: 159.50 to 180.40	Total eff. water
	7	Aggregate content	Total aggregate	[kg/m^3]	C: 1706 to 1895	Total Agg.
	8		Aggregate < 0.125 mm	[%]*	C: 2.40 to 4.50	Agg. <0.125 mm
	9		Aggregate < 0.250 mm	[%]*	C: 6.60 to 11.40	Agg. <0.250 mm
	10		Aggregate < 4 mm	[%]*	C: 36.30 to 52.50	Agg. <4 mm
	11	Product name of plasticizers	Glenium G 51	–	N: (1 = Glenium G 51, 2 = Teho-Parmix,	Plas. pro. name
			Teho-Parmix	–	3 = VB-Parmix)	
			VB-Parmix	–		
	12	Plasticizers content		[%]**	C: 0.60 to 2.54	Plasticizers
	13	Product name of air-entraining agents	Ilma-Parmix	–	N: (1 = Ilma-Parmix, 2 = Mischöl)	AEA pro. name
			Mischöl	–		
	14	Air-entraining agents content		[%]**	C: 0.01 to 0.06	Air-ent. agents
Fresh concrete properties	15	Basic properties	Slump	[mm]	C: 40 to 180	Slump
	16		Density	[kg/m^3]	C: 2287 to 2395	Density
	17		Air content	[%]	C: 3.40 to 6.90	Air cont.
Hardened concrete properties	18	Pore volumes and density	Air pores	[%]	C: 3.55 to 6.99	Air pores
	19		Total porosity	[%]	C: 17.52 to 20.39	T. porosity
	20		Capillary + gel porosity	[%]	C: 12.87 to 14.68	C + G porosity
	21		Density (wet)	[kg/m^3]	C: 2502 to 2581	Density (w)
	22		Density (dry)	[kg/m^3]	C: 2354 to 2427	Density (d)
	23	Thin section results	Total air pores	[%]	C: 1.90 to 5.90	T. air pores
	24		Air pores < 0.800 mm	[%]	C: 0.80 to 4.60	AP < 0.800 mm
	25		Air pores < 0.300 mm	[%]	C: 0.60 to 3.50	AP < 0.300 mm
	26		Specific surface	[mm^2/mm^3]	C: 12.80 to 36.50	S. surface
	27		Spacing factor (<0.800 mm pores)	[mm]	C: 0.18 to 0.51	SF < 0.800 mm
	28	Mechanical property	Compressive strength	[MPa]	C: 38 to 58.50	Comp. str.
	29	Durability properties	Accelerated carbonation coefficient	[mm/d$^{0.5}$]	C: 1.58 to 3.96	k_{acc}
	30		Chloride migration coefficient	[m^2/s]	C: 1.40 to 15.09 $\times$ 10^{-12}	D_{nssm}
Field conditions	31	Field conditions	Exposure time	[year]	C: 1 to 6	Expo. time
	32		Distance from highway lane	[m]	C: 4.50 to 10	Dis. from HW
Chloride profiles	33	Chloride profiles	Chloride concentration at various depth	[%]***	C: 0 to 0.10	Chloride profile

* Compared with the total aggregate.
** Compared with the total binder materials.
*** By weight of concrete.

Table 2
Concrete mix compositions of non-surface treated specimens situated on the side of HW 7 at Kotka.

Bind. types	w/b	Cement	BFS	FA	Total eff. water	Total Agg.	Plasticizer	Air-ent. agents
CEM II/B-S 42,5N	0.41	405	0	0	165	1746	0.69	0.01
CEM I 42,5N – SR	0.42	387	0	0	161	1796	0.78	0.02
CEM II/A-M(S-LL) 42,5N	0.42	428	0	0	179	1709	0.80	0.01
CEM II/A-LL 42,5 R	0.42	421	0	0	176	1748	0.82	0.02
CEM I 52,5 R	0.42	417	0	0	175	1737	0.87	0.06
CEM II/A-LL 42,5 R & BFS	0.38	217	217	0	163	1725	1.26	0.03
CEM II/A-LL 42,5 R & FA	0.38	344	0	106	173	1706	1.01	0.02
CEM II/B-S 42,5N	0.47	339	0	0	160	1808	0.67	0.01
CEM II/A-M(S-LL) 42,5N	0.49	333	0	0	163	1847	0.60	0.01
CEM II/A-LL 42,5 R	0.51	337	0	0	172	1833	0.78	0.01
CEM I 52,5 R	0.40	451	0	0	180	1722	2.54	0.05

4.2. Model building process

In this subsection, the process of ensemble method based model development and variable importance measure are discussed. The model is developed using Matlab programming language. The fundamental structure of the developed ensemble trees are identical as of the tree presented in Fig. 1 and uses bagging algorithm. The algorithm randomly generate a number of subsamples, or bootstrap replicas, from the original dataset which entails information regarding the concrete's mix ingredients, fresh and hardened properties, field conditions as well as chloride profiles. In the model, the bootstrap replicas are the training dataset, and out-of-bag observations are used as test dataset. Unlike other machine learning methods, there is no need to divide the data into training and test subsets since they are embedded in the sampling procedure.

In the model development process, the initial important step is identifying an appropriate leaf size for each regression trees. This can be achieved by constructing ensemble method utilizing the training dataset with different leaf size and reasonable number of trees. Then evaluate which of the tree configuration choice provides least mean square error (MSE). The MSE is computed by averaging the squared difference between the predicted responses of the out-of-bag and the target responses. To do so, an ensemble method with tree size of 100 and leaf sizes of 5, 10, 20, 50 and 100 was constructed. The mean square error attained by the ensemble method for the tested leaf and tree sizes is illustrated in Fig 5. Though the errors are comparable for two cases (leaf size 5 and 10), leaf size 5 yields the lowest mean square error. Hence, to perform efficient computations the size of leaf and trees were selected as 5 and 100, respectively for model development. Using this tree configuration, trees are grown for each bootstrap replica and train each regression trees in the ensemble. Two regression trees grown from two different bootstrap replicas often yield dissimilar predictions and due to this the ensemble combines by averaging the predictions of all the trees that are grown for all the bootstrap replicas.

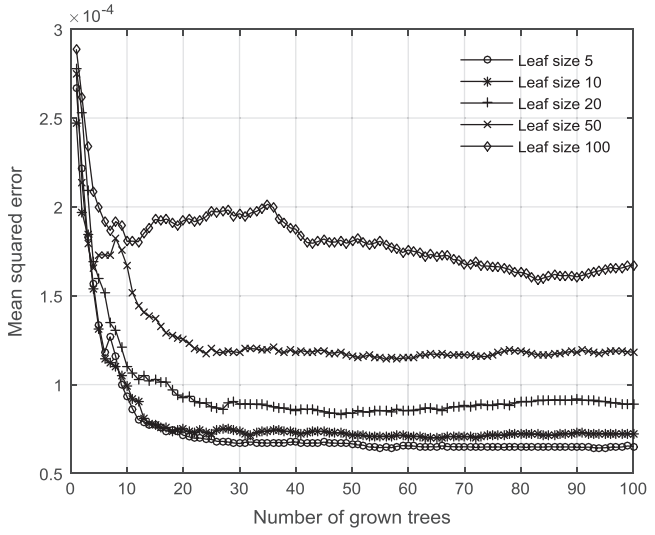

Fig. 5. Mean square error versus the number of grown trees for five different leaf sizes.

After performing chloride profile prediction using the developed ensemble method, the next main task is performing variable importance analysis. The purpose of the analysis is to figure out the degree of importance of each variable which are employed in the dataset in predicting the chloride profile. The variable importance was evaluated using a function which provides a numeric array of size (1-by-number of variables) comprising importance measure for each input variable. This is performed by randomly permuting out-of-bag data across a single variable at a time and predicting the increase in the out-of-bag error due to the permutation. This measure is evaluated for every regression tree in the ensemble, then averaged and the averaged value is divided by the standard deviation over the whole ensemble. This procedure is repeated ten times as this number of iteration tend to provide stable result with reasonable computational time. The final variable importance measure is considered by averaging the results of the ten iterations. The higher the variable importance score, the greater the influence of the variable on chloride profile predictions.

5. Results and analyses

The results of the degree of variable importance analyses based on the developed models are discussed in this section. Based on the analyses the influential factors, which control the penetration of chloride in concrete exposed to de-icing environment, were evaluated. To determine the influential factors, the results of ten models were analysed. The ten models were categorized into two groups: models A and models B according to the variables in their training dataset. The models in A category employs all variables presented in Table 1, except chloride profiles as input parameters. The models in category B utilize all variables concerning concrete mix ingredients, field exposure conditions, and chloride migration coefficients as inputs. In both model categories the target dataset is the chloride profile. The reason for this categorization is to examine the significance of fresh and hardened concrete test results in controlling chloride profile. Each group of the model further classified into three scenarios. In the first scenario the training dataset encompasses all respective input variables of the model A and B at which the chloride profiles measured on all specimens at different ages. The second scenario is the same as scenario one, the only difference is the included chloride profiles comes from the specimens

Table 3
Description of ten models.

Scenario	Model A			Model B			Description
	Model name	Input variables category	No. of variables	Model name	Input variables category	No. of variables	
1	**A.1**	All variables*	33	**B.1**	All concrete mix ingredients*, field conditions* and D_{nssm}	18	Entails data at which the chloride profiles measured on all specimens at different ages.
2	**A.2**	All variables* except dis. from HW	32	**B.2**	All concrete mix ingredients*, expo. time and D_{nssm}	17	Consists of data at which the chloride profiles measured on specimens only located at 4.5 m away from HW 7.
3	**A.3(i)**	All variables* except expo. time	32	**B.3(i)**	All concrete mix ingredients*, dis. from HW and D_{nssm}	17	Entails data of specimens at which the chloride profiles measured at 1 year of exposure.
	A.3(ii)			**B.3(ii)**			Ditto but at 3 years of exposure.
	A.3(iii)			**B.3 (iii)**			Ditto but at 6 years of exposure.

* Refer Table 1 for details of the variables.

located at 4.5 m. The purpose of this scenario is to eliminate the importance of distance on chloride profile prediction and focus on the remaining parameters. In the third scenario the focus is in removing the effect of exposure time by targeting the chloride profile measurement taken at specific year. Since the measurement of the specimen carried out at three different exposure times, there are three models under this scenario (1, 3, and 6 years). The detail of the classifications and the ten models are presented in Table 3. All the models considered the chloride profiles taken at the depths of 0.5 mm, 1.5 mm, 3 mm and 5 mm since the amount of chloride was analysed in all concrete specimens at these depths. Then the variable importance of each variable is averaged.

5.1. Scenario 1: variable importance measure for all conditions

Models A.1 and B.1 were developed according to the specifications given in Table 3 and the measure of the variable importance for both cases were carried out. The variable importance score of models is plotted in Fig. 6. It can be observed that distance from highway is the foremost factor which influences most the chloride profile in both models. This is the expected result because the amount of chlorides splashed on the concrete surfaces is heavily relay on the distance between the specimens and highway lane. The farther the distance, the lesser is the quantity of the splashed chlorides. The next five influential variables in model A.1 were compressive strength, cement content, total effective water, binder types, and exposure time. Though this model entails several variables from fresh and hardened concrete properties, the identified influential variables are mostly from concrete mix ingredients. This indicates that the effect of advanced laboratory tests carried out at early age is insignificant in predicting the chloride concentration in concrete. In case of model B.1, the influential variables next to distance from highway are cement content, exposure time, total effective water, binder types, exposure time, and w/b ratio. In both models, supplementary cementitious materials, product name of plasticizers, and air-entraining agents have the lowest effect in predicting the chloride profile. It is well known that supplementary cementitious materials are generally applied to increase the concrete resistance against chloride permeability since they can diminish the volume of large pores and capillaries. But they are not identified as influential variable since their amount and types are already explained by the combination of binder types and w/b ratio (which are already determined as significant variables). Laboratory based chloride transport test, D_{nssm}, is also identified as insignificant in predicting chloride profile in this scenario. This is due to the fact that transport properties of chloride depend on the intrinsic permeability of the concrete, which is changing with time during the process of cement hydration as well as the quantity of chloride concentration in the pore solution. In addition, the inclusion of chloride profiles measured from specimens placed at different distance with various exposure time plays a role in diminishing the importance of D_{nssm}. Hence, to make sure of the correctness of this result, other scenarios which eliminate the effect of specimens distance and exposure time have to be considered.

5.2. Scenario 2: variable importance measure at fixed distance

To make the analyses of variables importance independent of specimen's distance from highway, only chloride profile measured at 4.5 m were considered in the dataset of the model. The reason for choosing this distance is that the availability of highest number of specimens, allowing to acquire more chloride profile in the dataset. After performing successful training of the models, the embedded variable importance scores were computed. The top six most influential parameters are illustrated in Fig. 7. It can be clearly seen that exposure time is the leading parameters governing the penetration of chloride into concrete for A.2 and B.2 models with score of 0.43 and 0.44, respectively. The identified six uppermost significant variables have about 77% and 85% of collective contributions to the ensemble model A.2 and B.2, respectively. These are considerable amount of contributions considering the fact that the number of employed predictors for model A.2 is 31 whereas model B.2 is 16. It can also be noted that the variable importance measures of every respective parameters (according to their rank) of the two models are comparable. The importance variable measures and their percentile contribution of the influential predictors for both models are listed in Table 4. As it is seen from Table 4, exposure time of the concrete in field environment is the most influential variable with a relative contribution of 40.78% in model B.2. The w/b parameter with a 12.27% contribution is the second most predominant feature. Aggregate < 0.125 mm is another variable that had 10.43% contributions to prediction. Cumulatively, 63.47% of the total influence is attributed by these three influential factors. The variables D_{nssm}, plasticizers type, and aggregate < 4 mm are the next most influential parameters which represent 9.12%, 7.22% and 5.64% of contributions in predicting the chloride profile, respectively.

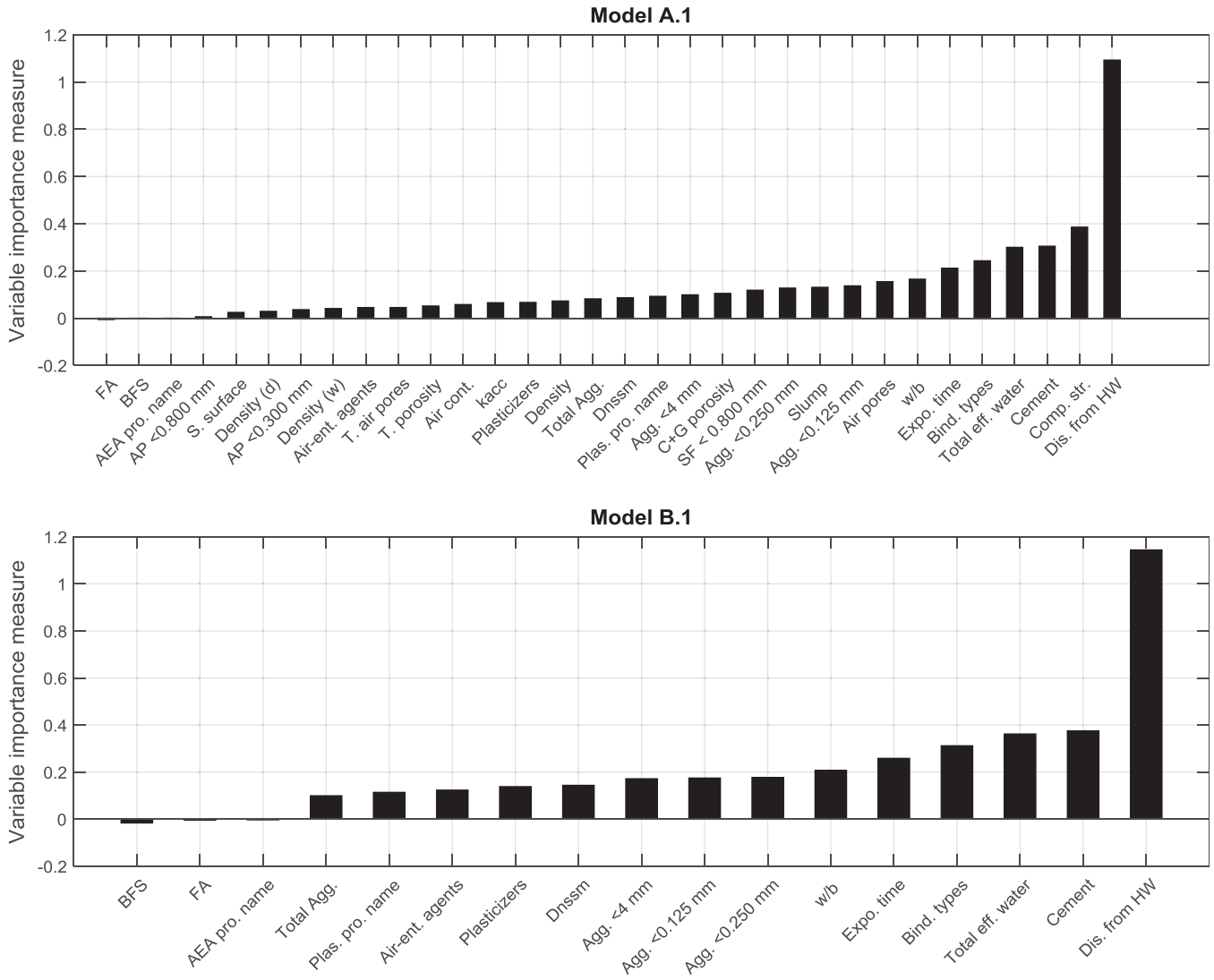

Fig. 6. Variable importance measures for chloride profile dataset based on scenario 1.

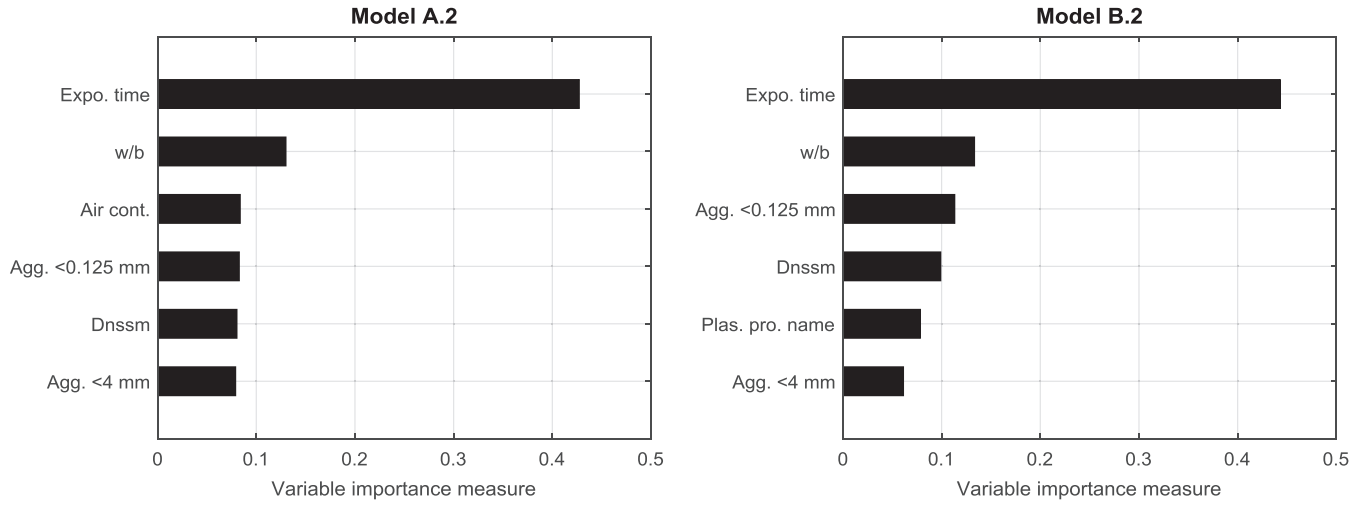

Fig. 7. Variable importance measures for chloride profile dataset based on scenario 2.

Table 4
Importance measure of influential variables and their percentile contribution for models A.2 and B.2.

Model A.2			Model B.2		
Variable name	VI measures [–]	Contribution [%]*	Variable name	VI measures [–]	Contribution [%]*
Expo. Time	0.4273	37.62	Expo. time	0.4431	40.78
w/b	0.1300	11.45	w/b	0.1333	12.27
Air cont.	0.0837	7.37	Agg. <0.125 mm	0.1133	10.43
Agg. <0.125 mm	0.0828	7.29	D_{nssm}	0.0991	9.12
D_{nssm}	0.0804	7.08	Plas. pro. Name	0.0784	7.22
Agg. <4 mm	0.0790	6.96	Agg. <4 mm	0.0613	5.64

* Compared with the total contributions of all input variables utilized in respective models.

The variable importance analysis revealed that most of the identified powerful predictors from both models are variables that describe the concrete mix ingredients as illustrated in Fig. 7. This demonstrated that almost all the advanced lab tests performed at early age, except D_{nssm}, are impotent in predicting the chloride profile in concrete. Among concrete mix ingredients, variables such as w/b and aggregate volume fraction are appeared to be the most significant parameters controlling chloride penetration. This is due to the fact that w/b and aggregates controls the pore structure of the cement paste which in turn impacts the transport properties. Indeed, aggregates utilized to produce concrete are often dense and thus chloride transportation through them is negligible. Nevertheless, at the presence of interfacial transition zone (ITZ) where the cement paste in the vicinity of aggregate surface reveals lower cement content and greater porosity compared with cement paste in regions far away from the aggregate. The ITZ covers a substantial portion of the total cement paste volume and controlled by the aggregate size distribution [28,50]. This may explain the observed significance of aggregate size distribution on the chloride transport property of concrete.

Unlike scenario 1, chloride migration coefficient is recognized as influential parameter where the effect of distance from highway lane is excluded. The chloride penetrations into the concrete specimens are controlled by their pore structures which are governed by the employed mix ingredients. The chloride profile primarily differs because of the continuous chemical reaction of chlorides with the dilute cement solution but not the amount of the splashed surface chloride as it is assumed as the same for all considered specimens in the model. Hence, finding the chloride migration coefficient, D_{nssm}, as influential predictor confirmed that it is a function of chloride content at the surface of the concrete.

5.3. Scenario 3: variable importance measure at three different ages

In this scenario, the focus is on the influence of input variables at specific exposure times. The variable importance measure for the chloride profile dataset at different ages is plotted in Fig. 8. It can be observed that distance from highway is the foremost influential parameters in all models. This is the expected result because the amount of chloride at the concrete surface differs according to the distance. The other most significant variables in model A.3 are compressive strength, total effective water and cement content. These properties and transport characteristics are linked to the concrete pore structure. Concrete with high compressive strength often have low porosity and thus high resistance to chloride penetration. The amount of cement and total effective water also influences the porosity of the concrete. These two parameters are identified as the most influential chloride profile predictor in all B.3 models too. The effect of these two parameters in controlling the chloride permeability is well noted by several studies and they are often expressed as water to cement ratio (w/c). In the developed models, w/b ratio was used as one of the training input variables but not w/c since there is other cementitious materials in the concrete mix ingredients. The considered binder types were cement, blast-furnace slag, and fly ash. In this scenario, the number of instances in the training dataset which entails blast-furnace slag and fly ash are very limited as shown in Table 2. Due to this the model identified the amount of cement, total effective water, and w/b as prominent predictors individually.

It can be noted that incorporation of supplementary cementitious materials have little influence on the chloride transport at the early age but its significance increases with years of exposure time. Similar to supplementary cementitious materials, aggregates size distribution appeared to be less influential in predicting chloride concentration in concrete at the early age. For instance, three predictors representing aggregates size distribution (Agg. <0.125 mm, Agg. <0.250 mm, and Agg. <4 mm) obtained importance ranks of 11th, 12th and 13th by model B.3(i), though only the first six important variables are shown in the Fig. 8 due to readability reason; 5th, 6th and 9th by model B.3(ii), and 4th, 6th and 8th by model B.3(iii). These three predictors have about 7%, 13%, and 15% contributions at the age of 1, 3 and 6 years, respectively. This can be explained by the characteristics change of the ITZ over time. In cases of plasticizers, opposite phenomenon is observed. In addition, the variable importance analyses of B.3 model revealed that the chloride transport properties of the concrete specimens can be described better by the chloride migration coefficient (D_{nssm}) values at earlier age than older age.

6. Discussions

The variable importance measure of the above three scenarios demonstrated that the influences on the chloride penetration into concrete exposed to de-icing environment mainly come from distance from highway, exposure time, and concrete mix ingredients. The most governing parameters from the concrete mix ingredients which are discovered by this work are cement content, amount of total effective water, aggregate size distribution and supplementary cementitious materials. The effect of cement content and amount of total effective water (often represented in the form of w/c ratio) is usually considered in several conventional chloride profiles prediction models. However, the effect of aggregate size distribution is often missed and controversial. Some studies reported that the influence of aggregate size distribution on chloride ingress is mainly due to the presence of ITZ which forms an interconnected network and facilitates chloride transport through them [50]. Other studies concluded that the aggregate content controls the chloride transport into concrete is significant but not aggregate size distribution [28,29]. These studies argued that increasing aggregate content produces more ITZ, but this is counteracted by the decrease in total porosity since more paste is substituted by the non-porous aggregate particles. The finding of this work agreed with the former studies. As presented in scenario 3 and shown in Fig. 9, the contribution of aggregate size distribution in controlling chloride penetration in model A.3 has

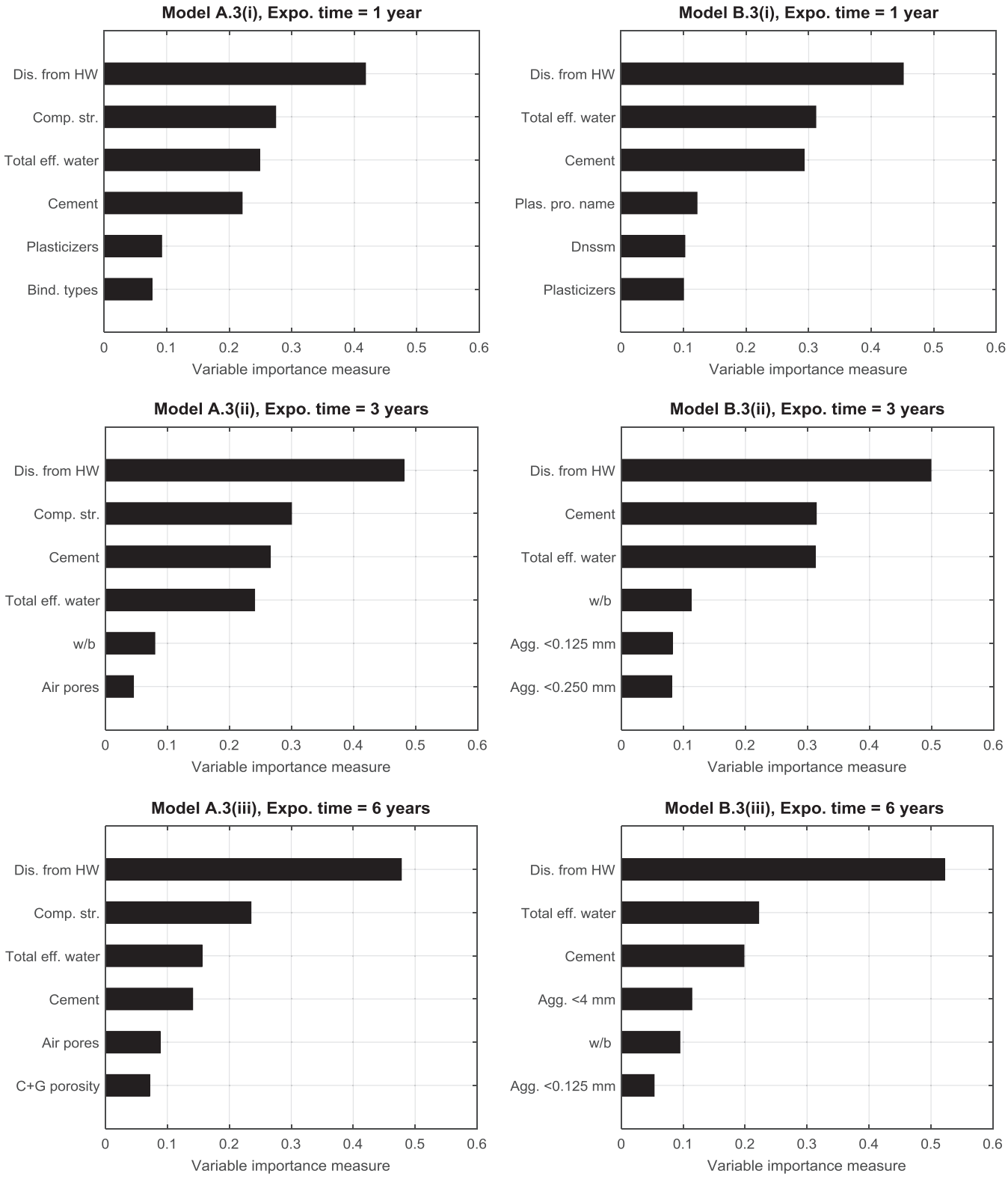

Fig. 8. Variable importance measures for chloride profile dataset based on scenario 3.

increased with exposure time but, in case of aggregate content, it is vice versa. The importance of aggregate size distribution in model B.3 is significant at exposure time of 3 and 6 years than earlier age. However, opposite phenomenon is observed in case of aggregate content. Even aggregate content with negative importance measure is noticed in both models. This implies that this variable do not have power in predicting chloride profile in concrete at some years of exposure. This study also revealed that, employment of supplementary cementitious materials in concrete mixes plays a role in controlling the ingression of chloride at later age. These effects are due to the continuous property change of the ITZ and binding capacity of the concrete [51–53]. All these results confirm the incapability of short-term laboratory or field examination in assessing the chloride profile. Hence, models should rely on data

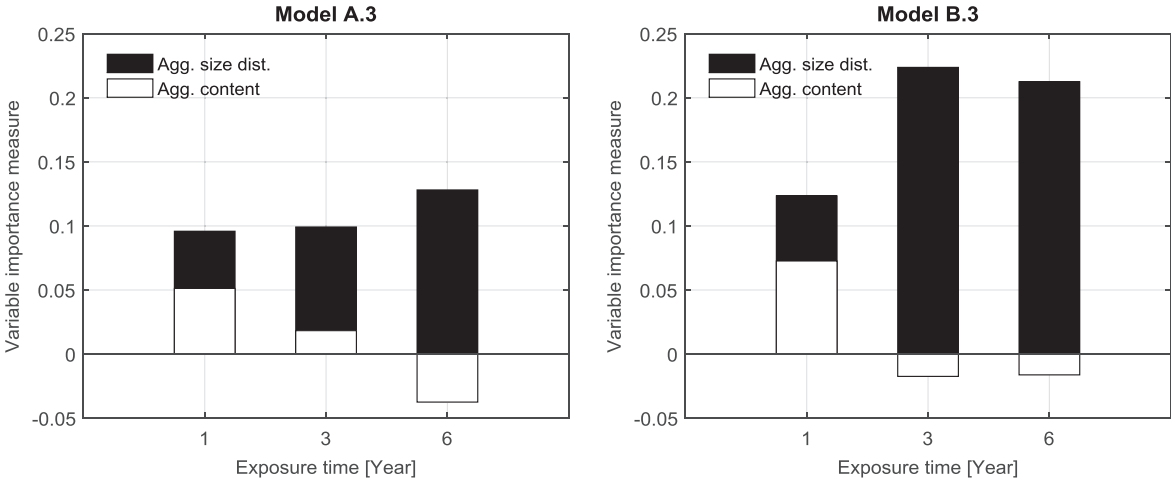

Fig. 9. Significance of aggregate size distribution and aggregate content vs exposure time in models A.3 and B.3.

from long-term field experiments for reliable chloride ingress prediction.

Though chloride transport in concrete is affected by several factors, most of the existing conventional models take into an account only the effect of w/c ratio and the chloride migration coefficients to represent the time dependency of the chloride penetration into concrete. To validate the importance of the newly determined subset of influential variables, the chloride profile prediction error is analysed using three input categories. In the first category, the input variables are the same as in Table 3 for all models. In the second category, only the determined top six influential variables are employed in their respective models. In the last category, the most commonly considered variables in the conventional models are utilized. These variables are the amount of cement and total effective water from concrete mix ingredient category, chloride migration coefficient and field conditions. The same ten models presented in Section 5 are adopted to predict the chloride profile by employing the input variables described in each category. The predictive power of the ensemble method is evaluated using out-of-bag observations. Mean square error (MSE) is adopted to evaluate the performance of the models in each category since it is the most common accuracy measure of a learning model. The MSE is computed by averaging the squared difference between the predicted responses of the out-of-bag and the target responses. The MSE results for all input categories are presented in Table 5. These MSE values are average of ten iterations. It can be noticed from Table 5 that the MSEs of all models which employ variables described in second category is small compared with the first category. The MSEs reduction is considerably large except models A.2 and B.2. It can also be recognized that the MSEs of all models in second category, except Model A.2 and A.3(i), is smaller than the MSEs of the third category. For instance, 19% decrease in MSE is observed in model B.3(iii) of second category compared to that of the third category. In the same model, the second category has 34% less MSE than the first category. This proofs that the developed models are more reliable in determining the subset of the significant variables, which can improve the generalization ability, for the chloride prediction models.

Table 5
Performance comparison of three categories.

Model names	Mean square error		
	Category 1	Category 2	Category 3
A.1	1.43E−04	1.21E−04	1.37E−04
B.1	1.37E−04	1.18E−04	1.35E−04
A.2	1.70E−04	1.64E−04	1.58E−04
B.2	1.60E−04	1.52E−04	1.59E−04
A.3(i)	8.66E−05	7.29E−05	6.93E−05
A.3(ii)	2.31E−04	1.62E−04	1.67E−04
A.3(iii)	4.10E−04	3.01E−04	3.36E−04
B.3(i)	8.66E−05	7.26E−05	7.80E−05
B.3(ii)	2.30E−04	1.62E−04	1.69E−04
B.3(iii)	3.75E−04	2.80E−04	3.33E−04

Evaluation of chloride penetration into concrete by employing many or very limited parameters lead to predictions with reduced accuracy as can be seen from Table 5. More improvements should be made to conventional models in order to represent the effect of the concrete mix design in more appropriate manner. This can be achieved by understanding the effect of the identified influential variables and their interactions quantitatively. As this study demonstrates the effect of influential parameter in different scenario is varying considerably with time. This makes translating chloride profile results from short-term tests to long-term as well as from one scenario result to another one is inappropriate. Thus, the effect of all influential concrete mix ingredients on chloride transport needs to be calibrated with long-term field data to yield reliable prediction.

According to the results of this work, variables from fresh and hardened concrete tests except compressive strength and D_{nssm} have insignificant influence on the chloride profile prediction. All concrete specimens are placed in the same elevation near to highway 7 at Kotka, Finland and experiencing similar multi-deteriorating actions over their life. Due to this, the effect of factors governing the boundary conditions of the concrete specimens including, the amount and frequency of sprinkled de-icing salt, elevation of the specimens, the actual climatic condition, amount of carbon dioxide in the environment and the traffic density are the same. It is obvious that these parameters play a significant role on the chloride penetration and thus incorporating data from different field experiments could help to measure the importance of factors affecting the boundary conditions of the concrete. The measure of the variable importance is based on the experimental dataset and thus the selected influential variables are only valid for the ranges of dataset provided in Table 1. Enrichment of the experimental dataset covering different exposure conditions enable to understand the combined effect of various deterioration mechanisms on chloride transport into concrete. Once the governing parameters and their interaction are understood, it is possible to enhance the reliability of the traditional models since reasonable simplifications can be established.

7. Conclusions

Ensemble methods based models to measure the importance of variables that control the chloride ingress in concrete exposed to de-icing environment were developed and presented in this work. The ensemble methods are based on bagged regression tree and utilized long-term field data. The input variables employed in the models were concrete mix ingredients, fresh and hardened properties, and field conditions and the chloride measurement at different depth in concrete was assigned as a target variable. Ten models were developed by employing different input dataset. The models were categorized into two groups in order to evaluate the effect of fresh and hardened tests. Each group was further divided into three scenarios in order to analyse the variables importance without the effect of exposure time and distance from highway. Using the ten models, variables of importance were analysed and the most influential ones were determined. The chloride profile prediction capacity of the most influential variables were analysed through MSE. Compared to results that employ conventionally agreed variables, up to 19% decrease in MSE result has been achieved by relying only on the determined subset of influential variables. The improvement in MSE results confirmed the models capacity in determining the optimal subset of influential variables that best predict the chloride profile from the input dataset. The main conclusions drawn from this work are:

- Chloride migration coefficient (D_{nssm}): It was identified that D_{nssm} carried out at early age in laboratory was recognized as influential parameter in the scenario where the dataset covers only concrete placed at the same distance. This demonstrated that the D_{nssm} is a function of chloride content at the surface of concrete in contrary to the assumption of conventional models. The influence of D_{nssm} on the chloride transport property was significant at earlier than older age. It was also discovered that fresh and hardened tests performed at early age are recognized, excluding compressive strength and D_{nssm}, to be impotent in predicting the chloride ingress in concrete.
- Concrete mix ingredients: It was noticed that binder types, cement content, total effective water and aggregate size distributions are the influential variables which controls the chloride penetration in concrete. These factors except aggregate size distribution are well known in controlling transport properties of concrete. The effect of aggregate size distribution in the chloride transport properties of concrete is controversial. The result of this work demonstrated that aggregate size distribution is among the predominant predictors and its influence increases with exposure time. The same phenomenon was also observed in case of supplementary cementitious materials. Plasticizers had considerable effect on the chloride transport at the early age but its contribution reduced significantly after some years of exposure.
- Short- and long-term tests: The results demonstrated that the contribution of each influential variable in the considered scenarios was noticeably changing with time. This indicates that evaluation of long-term chloride transport property of concrete using indicators obtained from short-term tests is unrealistic. Hence, long-term field data is essential to understand well the effect of all influential interacting variables on chloride permeability.

Therefore, using the ensemble method along with appropriate analyses is a promising approach to isolate the effect of complex interacting factors and determine the significance of variables, which in turn leads to better understanding of the chloride transport mechanisms in concrete.

Acknowledgment

The authors would like to thank Research Scientist Hannele Kuosa from VTT Technical Research Centre of Finland for providing the DuraInt-project experimental data.

References

[1] L. Tang, L.-O. Nilsson, P.A.M. Basheer, Resistance of Concrete to Chloride Ingress: Testing and Modelling, CRC Press, Boca Raton, FL, 2012, http://dx.doi.org/10.1201/b12603.
[2] T.S. Nguyen, S. Lorente, M. Carcasses, Effect of the environment temperature on the chloride diffusion through CEM-I and CEM-V mortars: an experimental study, Constr. Build. Mater. 23 (2009) 795–803, http://dx.doi.org/10.1016/j.conbuildmat.2008.03.004.
[3] H. Ye, X. Jin, C. Fu, N. Jin, Y. Xu, T. Huang, Chloride penetration in concrete exposed to cyclic drying-wetting and carbonation, Constr. Build. Mater. 112 (2016) 457–463, http://dx.doi.org/10.1016/j.conbuildmat.2016.02.194.
[4] X. Zhu, G. Zi, Z. Cao, X. Cheng, Combined effect of carbonation and chloride ingress in concrete, Constr. Build. Mater. 110 (2016) 369–380, http://dx.doi.org/10.1016/j.conbuildmat.2016.02.034.
[5] M. Torres-Luque, E. Bastidas-Arteaga, F. Schoefs, M. Sánchez-Silva, J.F. Osma, Non-destructive methods for measuring chloride ingress into concrete: state-of-the-art and future challenges, Constr. Build. Mater. 68 (2014) 68–81, http://dx.doi.org/10.1016/j.conbuildmat.2014.06.009.
[6] C. Houska, Stainless steel helps prevent deicing salt corrosion n.d. http://www.imoa.info/molybdenum-uses/molybdenum-grade-stainless-steels/architecture/global-deicing-salt-article.php.
[7] N. Ghafoori, M. Najimi, J. Sobhani, M.A. Aqel, Predicting rapid chloride permeability of self-consolidating concrete: a comparative study on statistical and neural network models, Constr. Build. Mater. 44 (2013) 381–390, http://dx.doi.org/10.1016/j.conbuildmat.2013.03.039.
[8] X. Shi, L. Fay, Z. Yang, T.A. Nguyen, Y. Liu, Corrosion of deicers to metals in transportation infrastructure: introduction and recent developments, Corros. Rev. 27 (2011) 23–52, http://dx.doi.org/10.1515/CORRREV.2009.27.1-2.23.
[9] Y. Hosokawa, K. Yamada, B. Johannesson, L.-O. Nilsson, Development of a multi-species mass transport model for concrete with account to thermodynamic phase equilibriums, Mater. Struct. 44 (2011) 1577–1592, http://dx.doi.org/10.1617/s11527-011-9720-2.
[10] K. Henchi, E. Samson, F. Chapdelaine, J. Marchand, Advanced finite-element predictive model for the service life prediction of concrete infrastructures in support of asset management and decision-making, in: L. Soibelman, B. Akinci (Eds.), Proc. 2007 Int. Work. Comput. Civ. Eng., American Society of Civil Engineers, Reston, 2007, pp. 870–880, http://dx.doi.org/10.1061/40937(261)103.
[11] E. Bastidas-Arteaga, A. Chateauneuf, M. Sánchez-Silva, P. Bressolette, F. Schoefs, A comprehensive probabilistic model of chloride ingress in unsaturated concrete, Eng. Struct. 33 (2011) 720–730, http://dx.doi.org/10.1016/j.engstruct.2010.11.008.
[12] F. Papworth, A whole of life approach to concrete durability—the CIA concrete durability series, in: F. Dehn, H.-D. Beushausen, M.G. Alexander, P. Moyo, (Eds.), Concr. Repair, Rehabil. Retrofit. IV Proc. 4th Int. Conf. Concr. Repair, Rehabil. Retrofit., Leiden, CRC Press 2015, pp. 213–219. doi:10.1201/b18972-30.
[13] C. Andrade, R. D'Andrea, N. Rebolledo, Chloride ion penetration in concrete: the reaction factor in the electrical resistivity model, Cem. Concr. Compos. 47 (2014) 41–46, http://dx.doi.org/10.1016/j.cemconcomp.2013.09.022.
[14] H. Ye, Y. Tian, N. Jin, X. Jin, C. Fu, Influence of cracking on chloride diffusivity and moisture influential depth in concrete subjected to simulated environmental conditions, Constr. Build. Mater. 47 (2013) 66–79, http://dx.doi.org/10.1016/j.conbuildmat.2013.04.024.
[15] G. de Vera, M. Climent, E. Viqueira, C. Antón, M. López, Chloride penetration prediction in concrete through an empirical model based on constant flux diffusion, J. Mater. Civ. Eng. 27 (2015), http://dx.doi.org/10.1061/(ASCE)MT.1943-5533.0001173.
[16] Z. Yu, Y. Chen, P. Liu, W. Wang, Accelerated simulation of chloride ingress into concrete under drying–wetting alternation condition chloride environment, Constr. Build. Mater. (2015) 205–213, http://dx.doi.org/10.1016/j.conbuildmat.2015.05.090.
[17] L. Pang, Q. Li, Service life prediction of RC structures in marine environment using long term chloride ingress data: comparison between exposure trials and real structure surveys, Constr. Build. Mater. 113 (2016) 979–987, http://dx.doi.org/10.1016/j.conbuildmat.2016.03.156.
[18] L. Tang, L.-O. Nilsson, P.A.M. Basheer, Resistance of Concrete to Chloride Ingress: Testing and Modelling. Boca Raton, FL, 2011. doi:10.1201/b12603.
[19] J. Marchand, E. Samson, Predicting the service-life of concrete structures – Limitations of simplified models, Cem. Concr. Compos. 31 (2009) 515–521, http://dx.doi.org/10.1016/j.cemconcomp.2009.01.007.
[20] B. Saassouh, Z. Lounis, Probabilistic modeling of chloride-induced corrosion in concrete structures using first- and second-order reliability methods, Cem. Concr. Compos. 34 (2012) 1082–1093, http://dx.doi.org/10.1016/j.cemconcomp.2012.05.001.
[21] G. Morcous, Z. Lounis, Prediction of onset of corrosion in concrete bridge decks using neural networks and case-based reasoning, Comput. Civ. Infrastruct. Eng. 20 (2005) 108–117, http://dx.doi.org/10.1111/j.1467-8667.2005.00380.x.

[22] Y.-M. Sun, T.-P. Chang, M.-T. Liang, Kirchhoff transformation analysis for determining time/depth dependent chloride diffusion coefficient in concrete, J. Mater. Sci. 43 (2008) 1429–1437, http://dx.doi.org/10.1007/s10853-007-2304-4.
[23] fib (International Federation for Structural Concrete). fib model Code for Concrete Structures 2010. Berlin: Ernst & Sohn, 2013.
[24] DuraCrete. DuraCrete Final Technical Report: Probabilistic Performance Based Durability Design of Concrete Structures, 2000.
[25] L. Tang, A. Lindvall, Validation of models for prediction of chloride ingress in concrete exposed in de-icing salt road environment, Int. J. Struct. Eng. 4 (2013) 86–99, http://dx.doi.org/10.1504/IJSTRUCTE.2013.050766.
[26] G. Markeset, O. Skjølsvold, Time dependent chloride diffusion coefficient – field studies of concrete exposed to marine environment in Norway, in: K. van Breugel, G. Ye, Y. Yuan (Eds.), 2nd Int Symp. Serv. Life Des. Infrastructures, RILEM Publications SARL, 2010, pp. 83–90.
[27] T. Luping, J. Gulikers, On the mathematics of time-dependent apparent chloride diffusion coefficient in concrete, Cem. Concr. Res. 37 (2007) 589–595, http://dx.doi.org/10.1016/j.cemconres.2007.01.006.
[28] J. Zheng, H.S. Wong, N.R. Buenfeld, Assessing the influence of ITZ on the steady-state chloride diffusivity of concrete using a numerical model, Cem. Concr. Res. 39 (2009) 805–813, http://dx.doi.org/10.1016/j.cemconres.2009.06.002.
[29] S.D. Abyaneh, H.S. Wong, N.R. Buenfeld, Modelling the diffusivity of mortar and concrete using a three-dimensional mesostructure with several aggregate shapes, Comput. Mater. Sci. 78 (2013) 63–73, http://dx.doi.org/10.1016/j.commatsci.2013.05.024.
[30] Xianming Shi, N. Xie, K. Fortune, J. Gong, Durability of steel reinforced concrete in chloride environments: an overview, Constr. Build. Mater. 30 (2012) 125–138, http://dx.doi.org/10.1016/j.conbuildmat.2011.12.038.
[31] B. Merz, H. Kreibich, U. Lall, Multi-variate flood damage assessment: a tree-based data-mining approach, Nat. Hazards Earth Syst. Sci. 13 (2013) 53–64.
[32] W. Tian, R. Choudhary, G. Augenbroe, S.H. Lee, Importance analysis and meta-model construction with correlated variables in evaluation of thermal performance of campus buildings, Build. Environ. 92 (2015) 61–74, http://dx.doi.org/10.1016/j.buildenv.2015.04.021.
[33] W.Z. Taffese, E. Sistonen, Machine learning for durability and service-life assessment of reinforced concrete structures: recent advances and future directions, Autom. Constr. 77 (2017) 1–14, http://dx.doi.org/10.1016/j.autcon.2017.01.016.
[34] E. Alpaydin, Introduction to Machine Learning, second ed., MIT Press, Cambridge, MA, 2010, http://dx.doi.org/10.1017/S0269888910000056.
[35] V. Cherkassky, F. Mulier, Learning From Data: Concepts, Theory, and Methods, second ed., John Wiley & Sons, Inc., Hoboken, NJ, 2007.
[36] J. Han, M. Kamber, J. Pei, Data Mining: Concepts and Techniques, Morgan Kaufmann, Waltham, MA, 2012.
[37] L. Rokach, O. Maimon, Data Mining with Decision Trees: Theory and Applications, World Scientific Publishing Co., Pte. Ltd., Singapore, 2008.
[38] J. Bell, Machine Learning: Hands-on for Developers and Technical Professionals, John Wiley & Sons, Inc., Indianapolis, 2015.
[39] W.Z. Taffese, F. Al-Neshawy, E. Sistonen, M. Ferreira, Optimized neural network based carbonation prediction model, in: Int. Symp. Non-Destructive Test. Civ. Eng. (NDT-CE 2015), Bundesanstalt für Materialforschung und –prüfung (BAM), Berlin (2015) 1074–1083.
[40] W.Z. Taffese, E. Sistonen, Neural network based hygrothermal prediction for deterioration risk analysis of surface-protected concrete façade element, Constr. Build. Mater. 113 (2016) 34–48, http://dx.doi.org/10.1016/j.conbuildmat.2016.03.029.
[41] İ.B. Topçu, A.R. Boğa, F.O. Hocaoğlu, Modeling corrosion currents of reinforced concrete using ANN, Autom. Constr. 18 (2009) 145–152, http://dx.doi.org/10.1016/j.autcon.2008.07.004.
[42] W.Z. Taffese, E. Sistonen, J. Puttonen, CaPrM: carbonation prediction model for reinforced concrete using machine learning methods, Constr. Build. Mater. 100 (2015) 70–82, http://dx.doi.org/10.1016/j.conbuildmat.2015.09.058.
[43] C.D. Sutton, Classification and regression trees, bagging, and boosting, in: C.R. Rao, E.J. Wegman, J.L. Solka (Eds.), Handb. Stat. Data Min. data Vis., Elsevier B. V., Amsterdam, 2005, pp. 303–330, http://dx.doi.org/10.1016/S0169-7161(04)24001-9.
[44] J. Gama, Knowledge discovery from data streams, Chapman and Hall/CRC, Boca Raton, 2010, http://dx.doi.org/10.1201/EBK1439826119-c1.
[45] E. Tuv, A. Borisov, G. Runger, K. Torkkola, Feature selection with ensembles, artificial variables, and redundancy elimination, J. Mach. Learn Res. 10 (2009) 1341–1366, http://dx.doi.org/10.1145/1577069.1755828.
[46] I.H. Witten, E. Frank, M.A. Hall, Data Mining: Practical Machine Learning Tools and Techniques: Practical Machine Learning Tools and Techniques, Morgan Kaufmann, Burlington, MA, 2011.
[47] C. Strobl, Statistical Issues in Machine Learning: Towards Reliable Split Selection and Variable Importance Measures. Ludwig-Maximilians-Universität München, 2008.
[48] H. Kuosa, Concrete durability field testing Field and laboratory results 2007–2010 in DuraInt-project. Espoo, 2011.
[49] NT Build 492. Concrete, Mortar and Cement-based Repair Materials: Chloride Migration Coefficient from Non-steady-state migration Experiments, 1999.
[50] S. Caré, Influence of aggregates on chloride diffusion coefficient into mortar, Cem. Concr. Res. 33 (2003) 1021–1028, http://dx.doi.org/10.1016/S0008-8846(03)00009-7.
[51] X. Lu, C. Li, H. Zhang, Relationship between the free and total chloride diffusivity in concrete. Cem. Concr. Res. n.d. (32) 323–326. doi:10.1016/S0008-8846(01)00664-0
[52] Y.-S. Choi, J.-G. Kim, K.-M. Lee, Corrosion behavior of steel bar embedded in fly ash concrete, Corros. Sci. 48 (2006) 1733–1745, http://dx.doi.org/10.1016/j.corsci.2005.05.019.
[53] M. Uysal, K. Yilmaz, M. Ipek, The effect of mineral admixtures on mechanical properties, chloride ion permeability and impermeability of self-compacting concrete, Constr. Build. Mater. 27 (2012) 263–270, http://dx.doi.org/10.1016/j.conbuildmat.2011.07.049.

Publication IV

Taffese, Woubishet Zewdu; Sistonen, Esko. 2016. Neural network based hygrothermal prediction for deterioration risk analysis of surface-protected concrete façade element. Journal of Construction and Building Materials, volume 113, pages 34–48. ISSN 0950-0618. https://doi.org/10.1016/j.conbuildmat.2016.03.029.

Construction and Building Materials 113 (2016) 34–48

Contents lists available at ScienceDirect

Construction and Building Materials

journal homepage: www.elsevier.com/locate/conbuildmat

Neural network based hygrothermal prediction for deterioration risk analysis of surface-protected concrete façade element

Woubishet Zewdu Taffese *, Esko Sistonen

Department of Civil and Structural Engineering, Aalto University, P.O. Box 12100, FI-00076 Aalto, Finland

HIGHLIGHTS

- Neural network can realistically predict hygrothermal condition in concrete.
- Hygrothermal prediction model can be adopted to evaluate the corrosion rate.
- Hygrothermal prediction model is vital to foresee risk of various deteriorations.
- Exploratory data analysis assists in selecting appropriate protection systems.
- Performance of surface treatments is influenced by their application method.

ARTICLE INFO

Article history:
Received 2 October 2015
Received in revised form 25 February 2016
Accepted 5 March 2016

Keywords:
Hygrothermal
Concrete façade
Surface protection
Neural network
Modelling
In-service monitoring
Deterioration
Corrosion rate
Frost attack
Chemical attack

ABSTRACT

Accurate prediction of hygrothermal behavior in the concrete is vital requirements to make more realistic service-life extension decisions. In this work, a neural network based hygrothermal prediction model to estimate a temporal hygrothermal condition in surface-protected concrete façade members is developed and presented. The model learns the case-specific features of hygrothermal behavior using the two years temperature and relative humidity data obtained from the installed probes. The performance evaluation confirms that the model describes the hygrothermal behavior inside the concrete façade with a high accuracy. This in turn enables to assess the corrosion rate as well as deterioration risk levels caused by frost and chemical attacks while identifying the appropriate surface protection system.

1. Introduction

Environmental agents cause different types of physical and chemical damage, such as corrosion of reinforcing bar (rebar), frost and chemical attacks in reinforced concrete (RC) structures. Corrosion-induced deterioration of RC structures is one of the most serious problem throughout the world [1–6]. It has been reported that corrosion related maintenance and repair of RC structures costs multibillion USD annually worldwide. Even, some industrial countries, spend as much as 3.5% of their gross national product (GNP) for corrosion associated damage and control [7]. The total building repair cost in Finland is estimated about 5.5 billion Euro per annum, of which about 30% involves external structures such as façades, balconies and roofs. The repair volume of corrosion-induced damage on prefabricated RC façade is predicted to be about 15 million m^2 per year and will grow 2% annually since it is the dominant technology in Finnish building industry [8]. Depending on the surface finishing type of the façades, it accounts for about 11–40% of the repair costs [9]. Frost attack is another most common cause of deterioration to concrete façades in Nordic climate [10–12].

The moisture content is the main factor in controlling the corrosion rate through their influence on the electrochemical reactions at the rebar/concrete interface and through their influence on ion transport between anodes and cathodes [13]. Not only the moisture content but also the surrounding temperature influence the rate of the electrochemical reactions and the amount of the

* Corresponding author.
E-mail address: woubishet.taffese@aalto.fi (W.Z. Taffese).

http://dx.doi.org/10.1016/j.conbuildmat.2016.03.029
0950-0618/

moisture that the concrete retains [14]. The corrosion rate varies by more than a factor of ten in a common seasonal temperature range from 5 to 30 °C [4,14,15]. In cold climate, concrete may be damaged by freezing and thawing if the pore system of the concrete is filled with moisture and has reached a critical degree of saturation. Moreover, in the presence of high moisture and aggressive substances, some chemical reactions which cause damage on the concrete can take place [16–19]. For instance, alkali reaction may occur in concrete when alkalis from the cement, or from an external sources, react with certain aggregates to form products that are deleterious to concrete.

A large number of RC structures are subjected to deteriorations due to uncontrolled hygrothermal factors and the significant repair costs related to them calls for cost-effective repair measures. In the past few decades, considerable efforts have been put into devising economical repair techniques to extend the service life of RC structures. Limiting the moisture penetration into RC structure is one of the potential ways to prolong their service life since all the major degradation mechanisms, such as corrosion of rebar, frost and chemical attacks, require high moisture content in the concrete. European Standard – EN 1504 suggests that surface protection systems to reduce moisture content and control corrosion of rebar by increasing concrete resistivity under rehabilitation principles P2 – *Moisture control of concrete* and P8 – *Increase of the electric resistivity of concrete*, respectively [20]. According to EN 1504, the surface protection treatments for concrete are classified into three groups. i) hydrophobic impregnation: produces a water-repellent surface with no pores filling effect; ii) impregnation: reduces the surface porosity with partial or total pores filling effect; and iii) coatings: produces a continuous protective film on the concrete surface.

Since compositions of the surface protection materials to limit the penetration of moisture into concrete vary widely, the surface protection systems may behave differently and even cause unintentional damage to the structure. In addition, it may provide different levels of protection against moisture even with similar generic chemical composition. Due to these, selection of appropriate surface protection system for a given structure is challenging. Thus, continuous hygrothermal monitoring of surface-protected concrete is necessary. This provides more reliable information about the actual hygrothermal behavior of the concrete. Nevertheless, in-service monitoring the hygrothermal performance of the concrete throughout its service life is not practical due to cost and time limitations. Hence, developing an efficient model which can predict the hygrothermal situation inside the surface-protected concrete based on ambient climatic condition is essential. In another perspective, to select appropriate surface protection system, analysis of data obtained from monitoring system and/or model is crucial. Data are useless on their own until one extracts knowledge or inferences from them. The lack of advanced data analysis makes the selection process suboptimal and even dangerous in some cases. The objectives of this work are threefold: i) to develop a hygrothermal prediction model for surface-protected Finnish concrete façade elements using long-term in-service monitored data; ii) to foresee the corrosion rate and deterioration risk levels due to frost and chemical attacks; and iii) to analyze the performance of various surface protection system in regulating the hygrothermal behavior of the concrete panel.

The structure of this paper is as follows. In Section 2, the significance of this research is presented. Architecture of artificial neural network is discussed in Section 3 since it is used to model the hygrothermal behavior of the case structure. In Section 4, detail of the case structure and the hygrothermal monitoring procedure is presented. Section 5 elaborates the hygrothermal prediction model development procedure. The model is trained, validated and tested using two years hygrothermal data of the case structure. The performance of the developed hygrothermal prediction model is analyzed in Section 6. In Section 7, the time-variant corrosion rate of rebar in surface-protected concrete elements is quantitatively evaluated using the monitored and predicted hygrothermal data. The deterioration risk levels associated with corrosion, frost and chemical attack is performed by adopting advanced exploratory data analysis techniques. Performance of surface protection systems against moisture is also analyzed and presented in this section. Finally, Section 8 presents the summary, conclusions and applicability of the study.

2. Research significance

Long-term in-service hygrothermal monitoring of surface-protected concrete using sensors is necessary for assessing the performance of the applied protection material. There are earlier works which demonstrate the use of sensors for monitoring hygrothermal status inside concrete element [21–24]. Although implementation of long-term monitoring system (which consists of probes, cables, and data acquisition equipment) is necessary, such a system cannot be implemented to monitor continuously for the whole service life time of the structure due to resource limitations. Thus, modelling the hygrothermal performance of the concrete using the monitored data as well as the ambient air temperature and relative humidity is vital. Indeed, hygrothermal transport phenomena through concrete and many other exterior building envelopes are well understood and numerical models have already been developed. A comprehensive review of relevant building envelope simulation models is found in [25]. Even though hygrothermal prediction models have been proposed in the past, none has explicitly incorporated various concrete surface protection materials and application methods in their material libraries. Numerical models can provide reliable simulations of an actual process only if appropriate material models are available and utilized.

Modelling of hygrothermal performance inside a surface-protected concrete member requires information of the temporal change of properties of coating materials under environmental and service conditions, which can be obtained by on-site monitoring. In addition, fundamental understanding of the interaction of various surface protection systems with an existing concrete is highly required. Some of the surface protection materials can penetrate inside the concrete pores and react with the hydration products of concrete but some of the other materials form a continuous layer at the concrete surface.

Due to the complex characteristics of interactions, developing a model to predict hygrothermal performance inside surface-protected concrete is challenging. Such a problem requires approach where the most essential features of a complex problem with multiple interactions are modelled so that the system behavior can be predicted reliably. Learning system behavior from observed data using machine learning methods is an effective alternative. Among several machine learning techniques, artificial neural network is commonly used due to its capability of capturing nonlinear and complex underlying characteristics of any physical process with a high degree of accuracy [26,27]. Artificial neural networks have been successfully used for various tasks in civil engineering applications, for example, structural behavior [28–31], earthquake prediction [32–34], and prediction of concrete properties [35–40]. However, their application in the research field of concrete repair is yet limited. In this work, hygrothermal prediction model for surface-protected Finnish concrete façades using artificial neural network is developed. The model is trained, validated and tested using two years of in-service monitored hygrothermal data.

3. Artificial neural network

Artificial neural networks, commonly referred to as neural networks, are computational networks inspired by biological neural networks which consists of partially or fully interconnected simple processing units called artificial neurons [41–43]. The model of an artificial neuron, which forms the basis for designing neural networks, is shown in Fig. 1. It basically consists of a set of synapses, an adder, an activation function and a bias. A set of synapses is characterized by a weight of its own. Specifically, a single x_j at the input of synapse j connected to network k is multiplied by synaptic weight w_{kj}. An adder is used for summing the input signals, weighted by the respective synapses of the neuron. An activation function, $\varphi(.)$, is applied for limiting the amplitude of the output of a neuron. Various forms of activation functions can be defined depending on the characteristics of applications. The bias b_k has the effect of increasing or lowering the net input of the activation function, depending on whether it is positive or negative, respectively.

A neuron k, can be mathematically described by Eqs. (1) and (2).

$$\beta_k = \sum_{j=1}^{m} w_{kj} x_j, \tag{1}$$

$$y_k = \varphi(v_k) = \varphi(\beta_k + b_k), \tag{2}$$

where β_k is the linear combiner output due to the input signal; $x_1, x_2, \ldots, x_m$ are the input signals; $w_{k1}, w_{k2}, \ldots, w_{km}$ are the synaptic weights of neuron k; b_k is the bias; $\varphi(.)$ is the activation function; and y_k is the output signal of the neuron.

Neural networks can be classified in a number of different ways depending on their architecture (pattern of connections between the neurons) which is intimately linked with the learning algorithm used to train the network. Fundamentally neural network architectures are classified into three classes: single-layer feedforward network, multilayer feedforward networks, and recurrent network [41]. Recurrent network has one or more feedback loops and is widely used for nonlinear time-series problems. It attempts to incrementally build the autocorrelation structure of a series into the model internally, using feedback connections relying solely on the current values of the input(s) provided externally. The idea behind such networks is that a network should learn the dynamics of the series over time from the present state of the series, which is continuously fed into it, and that the network should then use this memory when forecasting [41,42]. Based on the kinds of time-series problems, the architectural layout of recurrent network takes many different forms. Non-linear autoregressive with exogenous inputs (NARX) model is one of the popular subclass of recurrent neural network. It has a capacity in capturing long-term dependencies as it includes inputs at explicit time lags [42,44].

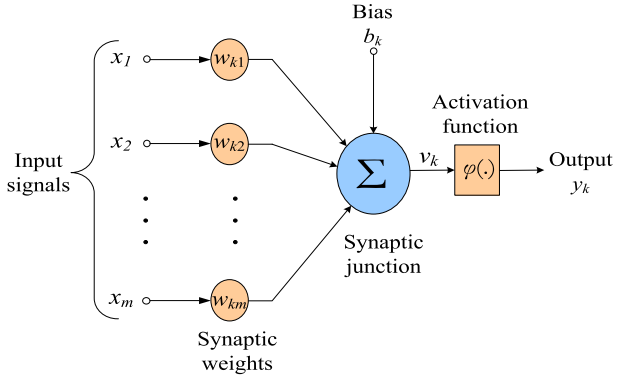

Fig. 1. Nonlinear model of a neuron, labelled k [41].

In NARX model, external inputs are presented to the network with those fed back from the output [41,42]. The architecture of a generic NARX model is shown in Fig. 2. The model has a single input that is applied to a tapped-delay-line memory of q units. It has a single output that is fed back to the input via another tapped-delay-line memory also of q units. The contents of these two tapped-delay-line memories are used to feed the input layer of the multilayer perceptron. The present value of the model input is denoted by $u(n)$, and the corresponding value of model output is denoted by $\hat{y}(n+1)$; that is, the output is ahead of the input by one time unit. Thus, the signal vector applied to the input layer of the multilayer perceptron consists of a data window made up as follows:

- Present and past values of the input, namely, $u(n)$, $u(n-1)$, …, $u(n-q+1)$, which represent exogenous inputs originating from outside the network,
- Delayed values of the output, namely, $\hat{y}(n)$, $\hat{y}(n-1)$, …, $\hat{y}(n-q+1)$, on which the model output $\hat{y}(n+1)$ is regressed and represents the value of the endogenous variables.

The dynamic behavior of the NARX model is described by Eq. (3).

$$\hat{y}(n+1) = F(\hat{y}(n), \ldots, \hat{y}(n-q+1); u(n), \ldots, u(n-q+1)) \tag{3}$$

In this work NARX network is adopted to develop a hygrothermal prediction model inside surface-protected concrete façade elements using in-service monitored data since it provides a concise representation for a wide class of nonlinear problems.

4. Hygrothermal monitoring of case structure

In this section detail of the case structure and the hygrothermal monitoring strategy is presented.

4.1. Case structure

In this work a six-story building with prefabricated RC sandwich panels was selected for investigating its hygrothermal performance. The building is situated in the city of Vantaa, Finland. It was constructed in 1972 and the finishing of the exterior concrete façade elements were brushed and painted. The panels used in exterior wall are sandwich-type panels where thermal insulation lies between two RC panels. The two concrete panels are connected to each other by steel trusses. The average thickness of the outermost layers of the concrete panels is 53 mm and their surface area is 7.84 m^2 with 2.82 m width and 2.78 m height. This type of concrete façade panels were, and still are, mainly used in Finnish multistory residential buildings [8,12,45,46]. Concrete façade elements of the case structure are illustrated in Fig. 3.

Six concrete façade elements from the southeast side of the case building were designated for examination. All the necessary surface preparations were done before repairing the concrete façade elements with surface protection systems. The old paint of concrete façade elements was removed by sand water blasting. Surface protective systems were applied on five elements (S1, S2, S4, S5, and S6) as shown in Fig. 3. The applied surface protection systems, based on the outermost layer, can be grouped into two: cementitious and organic coatings. The outermost layer of the façade elements labelled S1 and S2 are coated with *cementitious materials, whereas S4, S5, and S6 are treated with organic coating materials* from various manufacturers. Cementitious coatings and layers form a wide category that ranges from true cement-based coatings

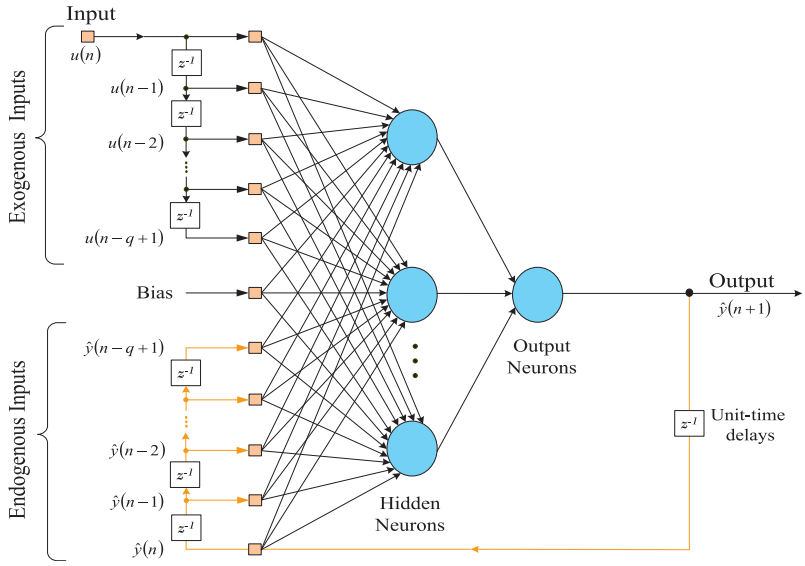

Fig. 2. NARX network with q delayed input and outputs.

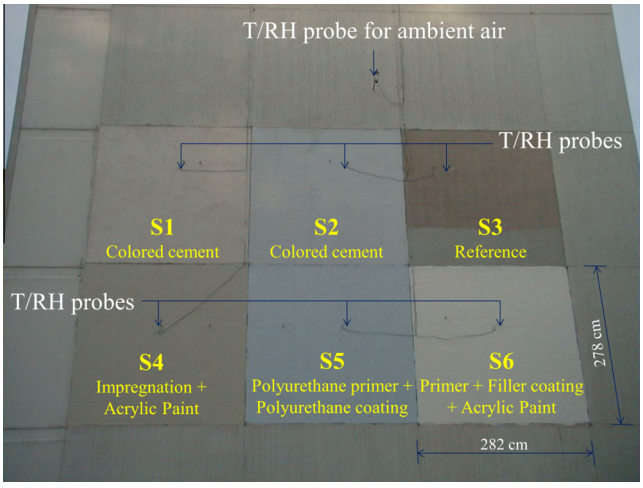

Fig. 3. Concrete façade elements of the case structure.

of a few to less than 10 mm thick. Whereas, organic coatings form a continuous polymeric film on the surface of the concrete, of a thickness ranging from 100 to 300 μm [13]. According to EN 1504, all the applied surface protection systems can be used to limit moisture content and thereby to increase the concrete resistivity under rehabilitation principles P2 and P8, respectively. Cleaned façade element labelled S3 was left uncoated for reference purpose. The type of the applied concrete surface protection materials with the application methods are presented in Table 1.

Table 1
Surface protection materials applied on concrete façade elements of the case structure.

Façade labels	Treatment types	Application methods
S1	Colored cement coating	1 × trowel
S2	Colored cement coating	2 × brush
S4	Impregnation	1 × roller
	Acrylic Paint	2 × roller
S5	Polyurethane primer	1 × brush
	Polyurethane coating	2 × brush
S6	Primer	1 × roller
	Filler coating	1 × roller
	Acrylic Paint	2 × roller

4.2. Hygrothermal monitoring procedure

A total of six relative humidity/temperature probes were utilized to measure relative humidity and temperature at the surface and inside the concrete façade elements. Five of the probes were installed into the façade members to measure the inner relative humidity and temperature, whereas one probe was mounted on the surface of a façade to measure the ambient hygrothermal condition. The probes were calibrated using two-point calibration method before installation in accordance with the manufacturer guide. The same calibration method was also applied every six months after installation. This calibration method adjusts both offset and gain. In order to install the probes, five holes were bored to a depth of about 40 mm at an approximate angle of 45° at the center area of the concrete façade elements. Then the holes were cleaned out and plastic sleeves were inserted into it. At this point, the probes were pushed into the plastic sleeve and sealed. The cable probes were connected to a data logger to record the hygrothermal measurements. Schematic representation of the installed probe is shown in Fig. 4. The length of the probe is 69 mm and it can measure the hygrothermal condition inside concrete at a desire depth from 30 to 90 mm. In the case structure, the concrete panel at the bottom of the holes releases humidity into the space around the probe until equilibrium is reached. Then the hygrothermal measurements were taken with a regular time interval of half an hour for 719 days. The same type of probe was used to measure surface shade air temperature and relative humidity of the concrete panel.

The reliability and the accuracy of the measured data depend on the reliability and the accuracy of the utilized monitoring system. The measurement ranges of the probe for relative humidity is 0–100% and temperature is −20 to +60 °C. The accuracy of the relative humidity probe is ±2% and ±3% when the relative humidity is ranged from 0 to 90% and 90 to 100%, respectively. In case of temperature, the accuracy is ±0.4 °C at +20 °C [47]. All these confirm that the monitoring system is reliable and accurate enough for the intended purpose.

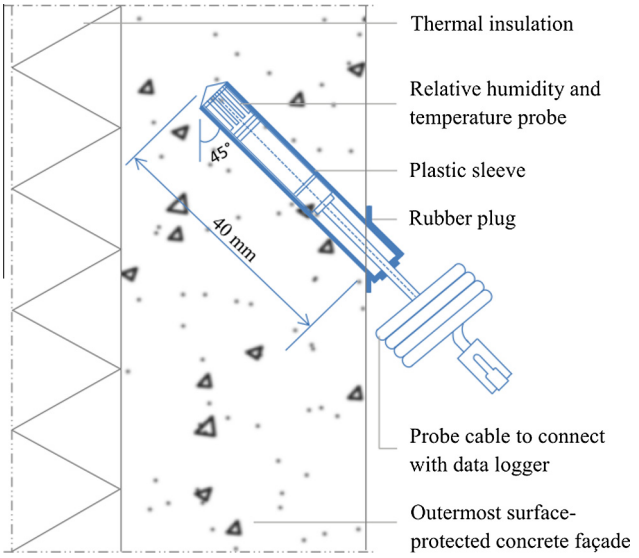

Fig. 4. Schematic representation of the installed probe.

5. Hygrothermal modelling process

In this section, the development steps of the proposed hygrothermal prediction model are presented. As any model based on the machine learning, the major development phases consist of data, training, validation, and testing. The workflow of this hygrothermal prediction model is illustrated in Fig. 5. The grey colored rectangular boxes represent the main processes or tasks of the modelling procedure. The major inputs into the process are shown in uncolored rectangular boxes.

It can be noted from the workflow that the modelling task is started by importing a dataset which includes the monitored hygrothermal measurements of the ambient air and from inside the concrete façade members. Then data exploration is performed

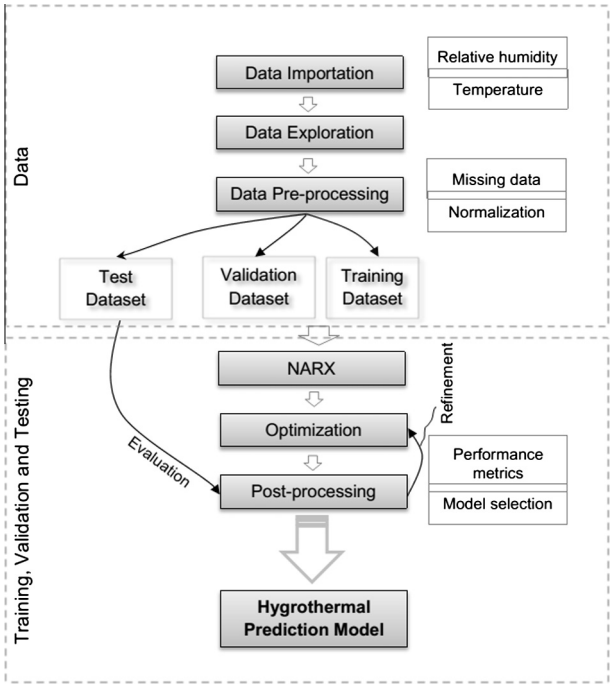

Fig. 5. Workflow of the developed hygrothermal prediction model.

in order to understand and visualize the main characteristics of the dataset. This part is often performed using visual analytic tools. In any machine learning based models, data pre-processing is often performed before they are analyzed further. For instance, there may be missing values in the data and these values need to be cleaned so the model can analyze the data properly. Pre-processing step, especially in neural network based model, could also involve other tasks such as data normalization in order to put different variables on a common scale. After making the data ready, the next step is splitting them into training, validation and test sets. Training dataset is a set of examples used for training the neural network. Validation dataset is used to prevent overfitting. After making the necessary optimization, the predictive power of the network is evaluated using the test dataset. In the next subsections, all the major tasks are discussed in detail.

5.1. Data

As discussed in the previous section, about two years monitored hygrothermal data inside surface-protected concrete façade were collected in the earlier research. These data are analyzed and employed to develop a hygrothermal model based on a neural network.

5.1.1. Data types

In the hygrothermal model proposed, four variables in which two are input and two target variables are considered. Outdoor relative humidity and temperature of ambient air are the input variables. The target variables are the values of relative humidity and temperature of concrete façade members measured inside the concrete façade member. The value of the temperature and relative humidity is numeric and units used for them are °C and %, respectively.

5.1.2. Data exploration

The recorded hygrothermal data covers about a period of two years, from 21 October 1998 to 08 October 2000. The daily-averaged values of relative humidity and temperature are illustrated in Figs. 6 and 7, respectively. Both figures shows hygrothermal data of the ambient and the inner which was measured inside surface-protected façades and the reference concrete façade. It can be seen that some data are missing from the hygrothermal observations for consecutive days at different patch of time. Data missing from certain measured parameters is a recurrent problem in different fields because of various reasons. In this case, technical errors were the main cause for the loss of data. The hygrothermal data of all the panels, except the reference façade element, were lost during the same period of time. There are more missed data in the reference façade member, but this does not affect the comparison of hygrothermal trends between the reference and surface-protected concrete façade elements.

As it can be seen in Fig. 6, the ambient relative humidity fluctuates widely. The inner relative humidity in all surface-protected concrete façades, except for about the first 200 days, do not follow the same trend as the reference. After about a year, the inner relative humidity of surface-protected concrete façade elements (except S1) is lower compared to the inner relative humidity of the reference panel. However, a strong association is observed among the relative humidity values measured from the concrete façade S5 and S6. In the case of temperature, all the surface-protected concrete façades inner temperature seems to have a similar trend with temperature of the reference concrete panel and the ambient as shown in Fig. 7.

In order to visualize the stability of the relative humidity across the thickness of the panel, a contour plot is generated using MATLAB. A contour plot is a graphic representation of the relation-

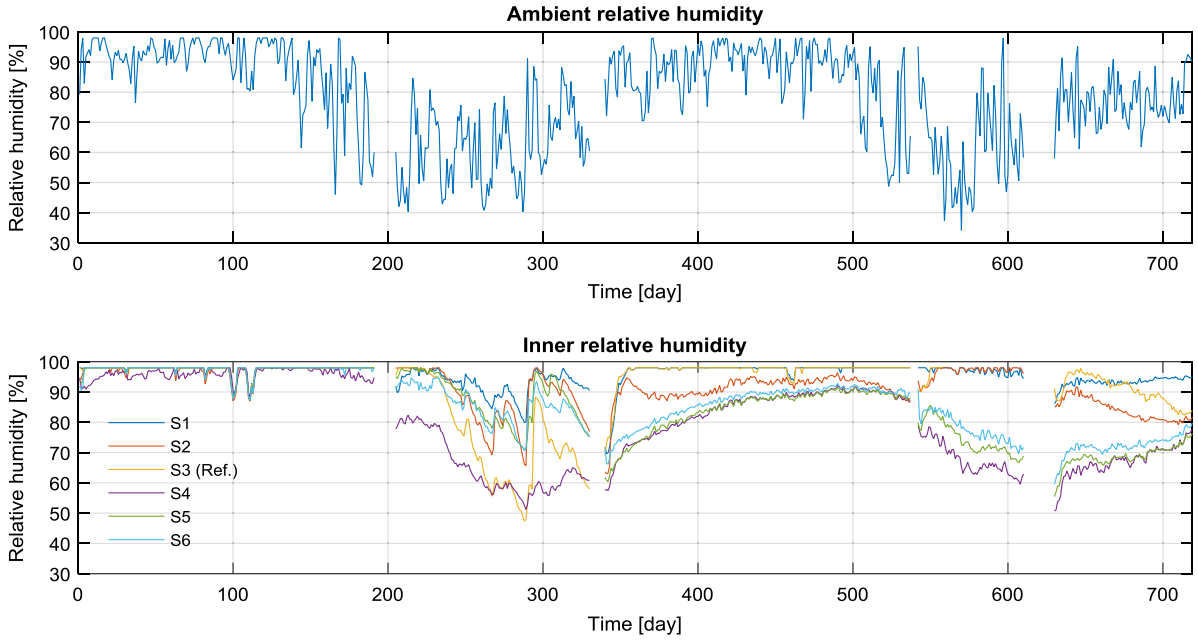

Fig. 6. Daily-averaged relative humidity values of the ambient shade air and inside concrete façade elements.

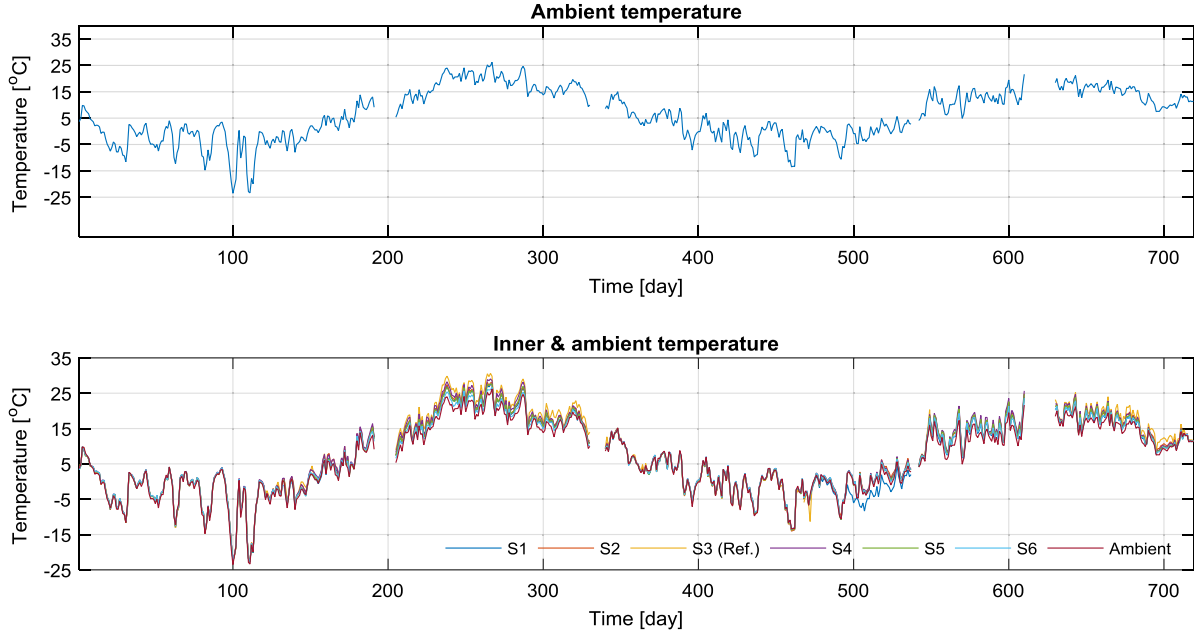

Fig. 7. Daily-averaged temperature values of the ambient shade air and inside concrete façade elements.

ships among three variables in two dimensions. Two variables are for *x* and *y* axes, and a third variable z is for contour levels. Axis *x* represents the time and axis *y* represents the cross sectional depth of the façade elements. Element z is a 2-by-2 matrix that contains values of relative humidity at the surface and inside the concrete façade elements (at a diagonal depth of 40 mm or a perpendicular depth of about 30 mm from the surface). The *x* values correspond to the column indices of z and the *y* values correspond to the row indices of z. The contour levels are chosen automatically and plotted as isolines. The area between the isolines is color-coded to indicate the values interpolated. Fig. 8 is a contour plot which illustrates the depth-time dependency of relative humidity of the panels for the last 90 days. The choice of 90 days is for better visualization. The outer surface of the panel is represented by the depth value 0 mm. From the contour plot, it is also possible to estimate the relative humidity at various depths across the thickness of the façade elements. It can be observed that the relative humidity in the concrete façade elements S1, S2, and S3 is mostly above 80%, whereas in the façade elements S4, S5, and S6 it remains below 80%.

5.1.3. Data pre-processing

Data pre-processing includes data encoding, missing data processing, data normalization, and data partitioning. They are commonly considered in all the models based on the machine

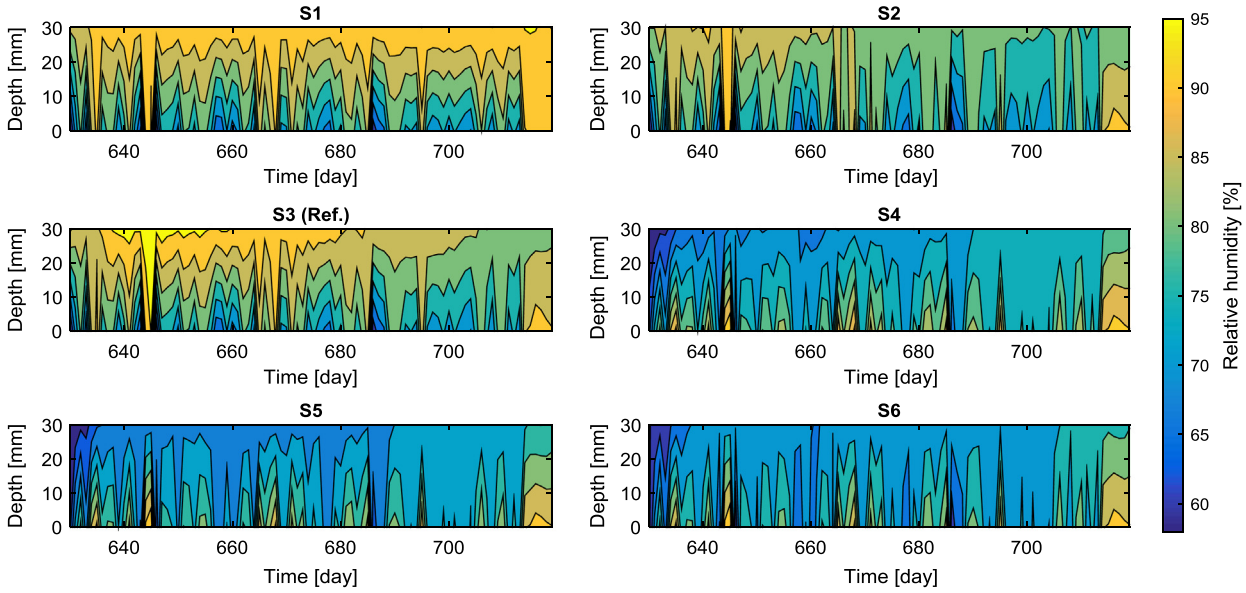

Fig. 8. Relative humidity inside concrete façade elements for the last 90 days.

learning. In the proposed hygrothermal modelling the following data pre-processing tasks are performed.

5.1.3.1. Data normalization. Normalization of the inputs and the target variables before processing them in the neural network is a standard practice. It puts different variables on a common scale and is very important especially where the inputs generally have widely different scales. All the input and target variables are normalized using the algorithm expressed in Eq. (4) [48]. In this way, the normalized inputs and targets that are returned will all fall in the interval $[-1, 1]$.

$$y = (y_{max} - y_{min}) * \frac{(x - x_{min})}{(x_{max} - x_{min})} + y_{min}, \tag{4}$$

where y is the normalized value of the variable; y_{max} is the maximum value of the normalization range, (+1); y_{min} is the minimum value of the normalization range, (-1); x is the original inputs or target variables; x_{max} is the maximum value for variable x ; and x_{min} is the minimum value for variable x. If $x_{max} = x_{min}$ or if either x_{max} or x_{min} are non-finite, then $y = x$ and no change occurs.

5.1.3.2. Missing data. Quality of input variables is one of the important factors in enhancing prediction accuracy of any machine learning models. Missing values are a recurrent problem in different research areas that affect quality of data. The amount of missing data <1% is generally considered trivial, 1–5% manageable. Nevertheless, 5–15% require advanced methods to handle, and >15% may severely impact any kind of interpretation [49]. In our case structure, in total about 6% of hygrothermal data are missed for consecutive days at different patch of time from each surface-protected façade members. For supplementing the missed values of the time series within the range of known data it is important to develop accurate prediction model [50,51]. In order to replace the missing data as well as to eliminate the noise of the monitored hygrothermal data in surface-protected façade elements, a moving average filter method is applied. This technique smooths and substitutes the missing data with the average of the neighboring data points defined within the span [52]. It is represented by the difference equation, Eq. (5).

$$x_s(i) = \frac{1}{2M+1}(x(i+M) + x(i+M-1) + \cdots + x(i-M)), \tag{5}$$

where $x_s(i)$ is the smoothed value for the *ith* data point, M is the number of neighboring data points on either side of $x_s(i)$, and $2M + 1$ is the span.

5.1.3.3. Data partitioning. As seen in the work flow figure, the monitored hygrothermal data is divided into three subsets: training, validation, and testing. The training dataset is used for computing the gradient and updating the network weights and biases. During the training process, neural network requires a validation procedure to halt the training when the generalization process stops improving. The test dataset is used to measure the predictive performance of the model.

5.2. Model training

In this section, the structure of the model for predicting the relative humidity and temperature of the façade element S4 is presented. One façade member is sufficient since the fundamental technique of hygrothermal performance prediction is the same for all members. So there is no special reason for choosing façade element S4 for illustrating the model training.

NARX network is adopted to train the hygrothermal behavior of the case structure using the monitored temperature and relative humidity data of the ambient air and inside concrete façade elements. The model has one target (e.g. inner temperature/relative humidity) and two inputs, one is an external input (e.g. ambient shade air temperature/relative humidity), and the other is a feedback connection from the output of the model (e.g. predicted inner temperature/relative humidity). Since all the conditions of the concrete panels are identical, other influential factors which govern the inner hygrothermal performance, such as concrete composition, concrete depth, curing time and condition are not assigned as input parameters to the model.

The NARX network codes were written in MATLAB to model and simulate hygrothermal prediction model using two years of in-service monitored data. The fundamental graphical representation of the developed NARX network is identical with Fig. 2. A tapped-delay-line memory of two units was assigned for both the input and feedback. The network consists of ten hidden neurons and one output neuron. The optimal number of neurons in the hidden layer and a tapped-delay-line memory were determined based on the generalization error after several trainings. The input and tar-

get values are randomly divided into three clusters: training, validation, and testing. The training dataset holds 75% of the dataset. Training begins with the third data point since a tapped-delay-line memory of two units is assigned. The applied training algorithm is the Levenberg-Marquardt [48]. This algorithm is an iterative technique that locates the minimum of a multivariate function that is expressed as the sum of squares of non-linear real-valued functions and is the fastest method for training [53–55]. The type of the activation functions selected for the hidden layers is a hyperbolic tangent transfer function as this is a common approach [48]. The hyperbolic tangent transfer function generates outputs between −1 and 1 since the input of the neuron net goes from negative to positive infinity. Linear transfer function is applied as activation function in the output layer because a non-linear activation function may distort the predicted output. It calculates the output of the neurons by simply returning the value passed to it. The input layer has not an activation function as its role is to transfer the inputs to the hidden layer.

5.3. Model validation and testing

The validation and testing dataset represent 15% and 10%, respectively. Validation dataset is used to measure the network generalization, and to halt training when the generalization stops improving. Test dataset are used to measure network performance during and after training. The mean square error (MSE), the root mean square error (RMSE), and the mean absolute error (MAE) are used to measure the performance of the model statistically. All these indicators measure the spread between the monitored and the predicted output from the network.

MSE is the mean of the squared difference between the target and its predicted value. It is the most widely employed loss function and described in Eq. (6).

$$\mathrm{MSE} = \frac{1}{n}\sum_{i=1}^{n}(Y_i - \hat{Y}_i)^2, \tag{6}$$

RMSE is simply the square root of the MSE, Eq. (7) and measured in the same units as the data. Sometime the RMSE is preferable to the MSE because understanding error values of the MSE is difficult due to a squaring effect, particularly, if the target value represents quantities in units of measurements.

$$\mathrm{RMSE} = \sqrt{\frac{1}{N}\sum_{i=1}^{N}(Y_i - \hat{Y}_i)^2} \tag{7}$$

MAE, also called the absolute loss, is an average of the absolute residuals/errors (the difference between the predicted and the actual value). It is mathematically expressed by Eq. (8). MAE retains original units as also RMSE.

$$\mathrm{MAE} = \frac{1}{N}\sum_{i=1}^{N}|Y_i - \hat{Y}_i| \tag{8}$$

where $\hat{Y}_i$ is the predicted output value, Y_i is the measured target value, and N is the number of observations.

6. Performance evaluation of the hygrothermal model

Hygrothermal prediction for concrete façade members were conducted using the neural network model developed in Section 5. The training, validation and testing performance of the proposed model is presented in this section. A successfully trained network is characterized by its ability to predict the hygrothermal behavior inside concrete façade members for the data on which it was trained. The training performance of the developed hygrothermal model for predicting temperature and relative humidity is shown in Fig. 9. As it is clearly seen, the correlation coefficients (R-values) for relative humidity and temperature predictions are close to 1. The high correlation coefficient indicates that the developed model track the actual measured relative humidity and temperature well during the training phases.

The validity of any effectively trained machine learning based model is determined by its ability to generalize its predictions beyond the training data and to perform well when it is presented with unseen data from within the range of the input parameters used in the training. The validity of the developed model was tested using the dataset which covers the measurements of the last 90 days (11 July 2000 to 8 October 2000). The model was trained in this environmental conditions (from within the range of the input parameters used in the training) only once, i.e., from July to October 1999. The prediction performance of the developed hygrothermal model for the last 90 days was analyzed statistically. The MSE of relative humidity and temperature were 7.8890 and 2.4421, respectively. The MAE of relative humidity and temperature were 4.0426 and 0.8876, respectively. The test result confirms that the model predicts the hygrothermal performance inside the concrete with a reasonably low error despite the limitation of the representative data from the specific testing period in the training dataset. The errors, MSE and MAE, of temperature are smaller than relative humidity. This is because there is a strong correlation between the

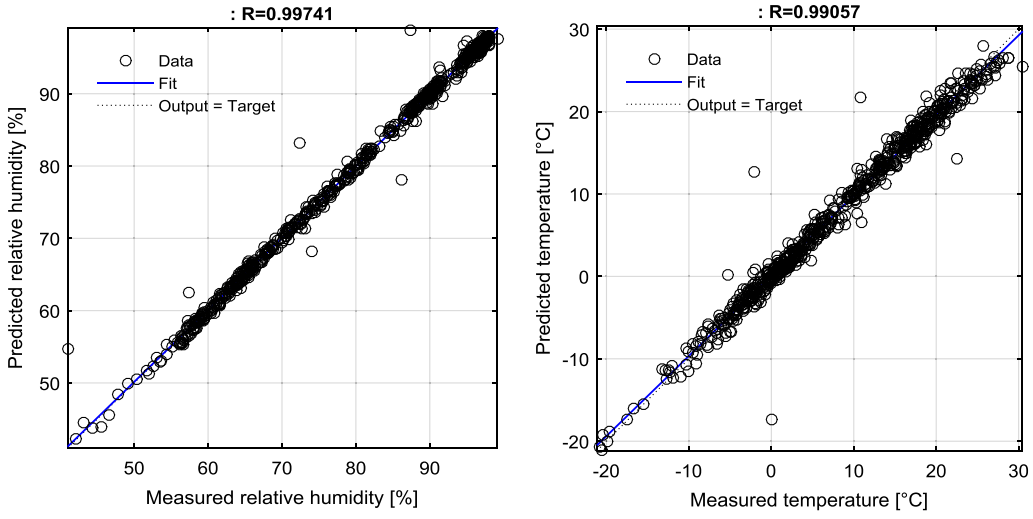

Fig. 9. Regression plot for predicted vs. measured relative humidity and temperature for training dataset in concrete façade element S4.

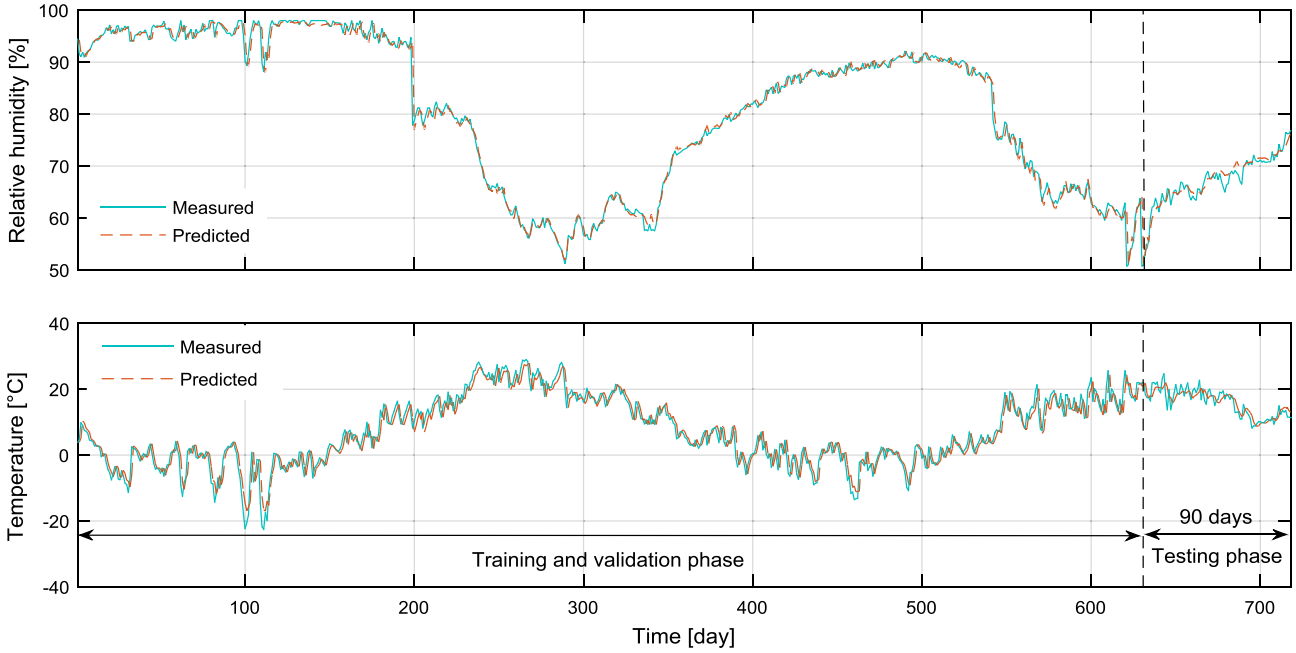

Fig. 10. Measured and predicted hygrothermal performance in concrete façade element S4.

inner and the ambient temperature. In addition, the ambient temperature does not fluctuate widely unlike the ambient relative humidity. When the model is trained with large dataset the error will definitely be reduced. The measured and predicted relative humidity and temperature in concrete façade element S4 is shown in Fig. 10.

The residuals, the differences between the measured and predicted relative humidity and temperature values, are computed using the test dataset. The median values of the residuals with their median, maximum, minimum, and outlier values for concrete façade member S4 are presented in Fig. 11 as a boxplot. The plot represents residuals of a random single run. The median is shown as a red line within the box. The blue box covers the middle 50% (25th to 75th percentiles) of the residuals. The whiskers go down to the minimum and up to the maximum values. Residuals greater than 1.5 box lengths above the whiskers are outliers and shown as red plus sign. The residual median for temperature is about in the middle of the box and distributed around zero. This shows that the residuals have a constant variance patterns and they are normally distributed. The residual median for relative humidity is closer to zero and nearer to the third quartile than to the first quartile, indicating that the residuals distributions are slightly skewed to the left. A single outlier is observed in residuals box blot of temperature. Generally, the boxplot of the residuals of a single run test demonstrates that the developed hygrothermal model learns from the nonlinear relation of the input variables and is able to capture the complex nature of the hygrothermal interaction with a good accuracy.

The accuracy of the developed hygrothermal model is measured using the statistical measures which are discussed in Section 5 and the average of ten test results are listed in Table 2. Though the principles of the model development are the same, the model is optimized for each façade member to achieve a better performance since surface-protection materials and methods are different for every member. The lower the value of the error statistics (MSE, RMSE, and MAE) is, the better the prediction accuracy of the model. The small MSE values of the predicted relative humidity and temperature confirm that the model has high ability to generalize. MSE of the temperature is smaller than MSE value of the relative humidity. They are also nearly equal for all façade members. The MAE errors of the temperature are small compared to their corresponding values of the relative humidity. Generally, from the error metrics presented in Table 2, it can be observed that the error values are reasonably low. This proves the suitability of the proposed model for evaluating the hygrothermal status in the surface-protected façade members of the case structure.

7. Deterioration risk and coating performance analysis

In this section, the necessity of hygrothermal monitoring and modelling of surface-protected concrete façade members from controlling of corrosion rate, frost and chemical attacks perspectives is discussed. Performance of surface protection systems against moisture and thermal is also presented by analysing the monitored hygrothermal data.

7.1. Corrosion rate

In practice, corrosion rate is often estimated by taking instantaneous electrochemical measurements. The value of corrosion current is determined from the Tafel plots of polarization curves which are used to calculate the corrosion rate and the state of corrosion. Table 3 presents the four groups of the state of corrosion which are classified based on values of corrosion current or corrosion rate.

Carbonation-induced corrosion of rebar is the most common degradation mechanism of concrete façades in Finland [10,12]. The carbonation process breaks the passive protection layer of rebar and thus causing the initiation of corrosion. Once initiated, the deterioration of rebar depends on the corrosion rate. Though, corrosion rate is influenced by several factors, in carbonated concrete, it is greatly governed by moisture-relative terms [4,13,18]. Corrosion rate is much lower when the relative humidity inside the concrete is less than 75%. It increases significantly when the inner relative humidity increases at 95%. The inner temperature has a significant impact on the corrosion rate [4,13–15]. The rate of corrosion of rebar in concrete is computed using Eq. (9) [58–60].

$$r = C_T r_o, \tag{9}$$

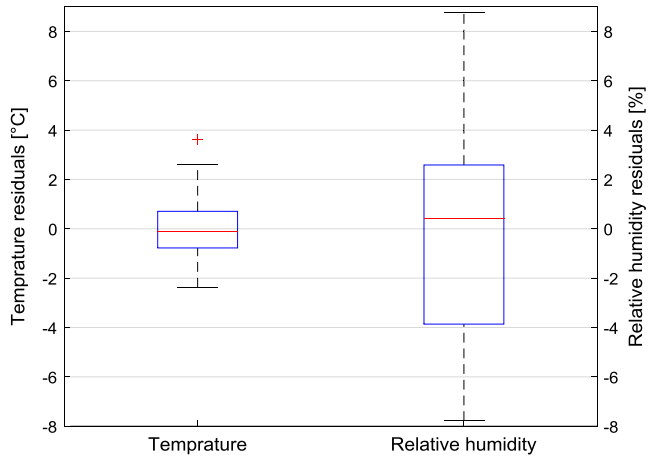

Fig. 11. Residuals boxplot of temperature and relative for concrete façade element S4.

where r is the rate of corrosion [μm/year], C_T is the temperature coefficient, and r_o is the rate of corrosion at +20 °C [μm/year]. C_T and r_o are time-variant variables which are dependent on the temperature and relative humidity inside the concrete, respectively. And, for carbonated concrete, they can be described by Eqs. (10)–(12) [58,60].

$$C_T = 1.6 \cdot 10^{-7}(30+T)^4, \tag{10}$$

$$r_o = 190 \cdot (RH)^{26}, \text{ when } RH \leqslant 0.95, \tag{11}$$

$$r_o = 2000 \cdot (1-RH)^2, \text{ when } RH > 0.95, \tag{12}$$

where T is inner temperature in °C and RH is relative humidity.

The corrosion rate of rebar in the concrete façades is computed using the above equations. The computation is done using the monitored and the predicted hygrothermal data only for the last one year of the monitoring period. The computed corrosion rate values are translated to corrosion progress based on the classification (passive, low, moderate, and high) presented in Table 3 and shown in Fig. 12. The unknown value of the corrosion rate due to the malfunction of the hygrothermal probes in the reference façade element is left blank in the figure (white color). It can be observed from Fig. 12 that the difference of corrosion progress evaluated using the monitored data and data predicted by the hygrothermal model is insignificant. In both cases, the state of corrosion for the concrete façade elements S4, S5, and S6 is low and passive; whereas for S1, S2, and S3 it ranges from passive to high. Among all façade members, S1 and S2 offer poor protection against the progress of rebar corrosion. Even though, both of the elements were protected by the same coating materials from different manufacturers, S1 provides the poorest protection. This indicates that, not only the type of the coating materials but also the working method as well as the source affect the performance of the protection against corrosion. In addition, it can be seen that the state of corrosion is varying within a short period of time in S1 and S2. This reveals that prediction of corrosion rate based on the conventional instantaneous electrochemical measurement will under or overestimates the value. Therefore, implementation of a long-term hygrothermal monitoring and modelling strategy is necessary. If long-term monitoring strategy is applied, it is possible to track the corrosion status reasonably well which in turn enable determination of the optimum intervention time improving the cost-effectiveness of the maintenance and repairing measures.

7.2. Frost and chemical attacks

Earlier in this paper, it is presented that concrete surface protection systems act as a physical barrier to control the penetration of moisture and thus slows down the corrosion rate. However, some surface protection methods may cause unintended consequences of damage. Hence, the effectiveness of the surface protections must be evaluated by considering its effect on other deterioration mechanisms which are governed by the hygrothermal interactions such as frost and chemical attacks.

Concrete may be severely damaged by frost action if the pore system of the concrete is filled with moisture and has reached a critical degree of saturation. In most cases, critical saturation corresponds to very high moisture contents and normally it requires long time exposure to moisture flow [61]. Indeed, the mechanisms leading to frost damage are not entirely clarified. However, it is generally accepted that because of the surface tension in the small capillaries pores, the water freezes at temperatures below 0 °C and the amount of frozen water increases continuously as the temperature decreases. It may increase in volume of approximately 9% [13,17–19]. Hydrostatic pressure on the unfrozen water caused by the volume increase of the ice which has already formed, osmotic pressures as well as a redistribution of water in the pore system may lead to high internal stresses which may seriously damage the concrete, particularly as the number of freeze-thaw cycles increases [16–18,62].

Chemical attacks on concrete manifest themselves into detrimental physical effects, such as increase in the porosity and permeability, decrease in the strength, cracking, and spalling. Concrete deteriorations caused by chemical attacks are associated primarily with chemical changes occurring within the hydrated cement matrix. Two forms of chemical attacks, namely, sulfate attack and alkali-aggregate reaction in their various forms are the most widespread threat to concrete durability. Sulfate attack results from the deleterious chemical reaction between soluble sulfates and constituents of cement in the occurrence of moisture [13,17–19,63]. Sulfates ions may present in concrete from gypsum (calcium sulfate), often present as an additive in blended cements, or from external environment. The chemical reaction products produced occupy a greater volume than the compounds they replace and the cement paste may be destroyed; thus expansion and disruption of the concrete may result. Examples of sulfate attack include formation of ettringite, delayed ettringite, and thaumasite [63]. Alkali-aggregate reaction occurs in concrete when alkalis from the cement, or from an external sources, react with certain

Table 2
Statistical performance measurement of the developed hygrothermal model.

Façade element	MSE		MAE		RMSE	
	Relative humidity	Temperature	Relative humidity	Temperature	Relative humidity	Temperature
S1	3.5074	2.8867	5.0236	0.7265	1.8728	1.6990
S2	4.3062	2.7960	4.4686	0.7756	2.0751	1.6721
S4	5.8039	2.8320	3.9995	0.8875	2.4091	1.6829
S5	4.0053	2.5812	4.1923	0.8125	2.0013	1.6066
S6	3.9371	2.5936	4.4386	0.6289	1.9842	1.6105

Table 3
Ranges of the corrosion rate [56,57].

Corrosion current [μA/cm^2]	Corrosion rate [μm/year]	State of corrosion
<0.1	<1	Passive
0.1–0.5	1–5	Low
0.5–1.0	5–10	Moderate
>1.0	>10	High

aggregates in the presence of moisture to form products that are deleterious to concrete [13,17–19]. The expansion, deterioration and perhaps even failure of concrete structural elements resulting from alkali-aggregate reaction in the concrete are due to swelling pressures developing as a result of the reactivity within the fabric of the concrete which are sufficient to produce and propagate microfractures [64]. Different forms of alkali-aggregate reaction have been occurred, such as: alkali-silica reaction, alkali-silicate reaction and alkali-carbonate reaction.

Frost and chemical attacks will occur only when there is sufficient moisture in the concrete pores. According to [16,65], concrete members with a medium internal relative humidity of 65–85% have an insignificant risk for deterioration by frost attack. This is because the presence of air in capillary pores reduces the pressure upon freezing as they act as expansion chambers. However, for concrete with high internal relative humidity (85–95%) and a saturated concrete (>98%), the damage risk related with frost attack is medium and high, respectively. Similarly, the risk of the concrete damage caused by chemical reactions with the presence of low or medium amount of moisture in the concrete is insignificant. Whereas, concrete with high moisture content (internal relative humidity >98%) the risk of concrete damage is high [16,18,65]. Frost and chemical attacks sensitivity of the concrete façade elements for the last one year is analyzed and illustrated in Fig. 13. The analysis is carried out using the data from the probes and the predicted data by the hygrothermal model. The unknown deterioration risk levels due to the failure of the hygrothermal probes in the reference façade member is left blank and represented in the figure by white color. It can be observed from Fig. 13 that the frost and chemical attacks sensitivity difference using the data from the model and probes is insignificant. The performance of organic coatings is superior to the cementitious ones in protecting the concrete against frost and chemical attacks while hindering the corrosion rate as presented in the above subsection. The cementitious coatings applied on façade elements S1 and S2 are not effective enough in protecting the concrete against frost and chemical attacks. Cementitious coating material applied in S1 is less protecting than the cementitious material applied in S2 concrete façade. This confirms that the coating application methods and the source of the product influence the performance of the surface treatment.

7.3. Performance of coatings

The performance of the applied surface protection systems in controlling moisture and thermal transport to the concrete façade members is analyzed. The monthly difference in values of relative humidity ($RH_{diff} = RH_{amb} - RH_{inside}$) and temperature ($T_{diff} = T_{amb} - T_{inside}$) between ambient air and inner part of the concrete façade member for the last one year is illustrated as boxplots in Figs. 14 and 15, respectively. The green line represents the mean values of RH_{diff} and T_{diff}. It can be observed that there is a strong match in the trends of RH_{diff} between organic coatings S4, S5, and S6 as well as between cementitious coatings S1 and S2. As the box size of the plots indicates, RH_{diff} from March to May 2000 is large for almost for all concrete façade members. The mean of RH_{diff} of S1 and S2 is below zero with relatively high values throughout the year. This confirms that the surface treatments applied on façade elements S1 and S2 encapsulate the internal moisture; indicating cementitious coatings are not effective enough in protecting the concrete against moisture. Accordingly, the risk of concrete damage will be high since it offers favorable conditions for several major degradation mechanisms. However, this kind of coating might have positive effect to lower risk of other deterioration types. In several instances, the mean of RH_{diff} in S4, S5 and S6 is above zero. This demonstrated that organic coatings offer an effective and reliable solution in controlling the moisture and thus minimizes deterioration risks associated with moisture. From Fig. 15, it can be observed that the box size of S1 is small throughout the year except March and April 2000. This revealed that the temperature difference between ambient air and inside S1 falls within a small range. The mean temperature curves of concrete façade members S4, S5, and S6 which are treated by organic coatings have similar trend. In all concrete façade elements the mean T_{diff} is below zero

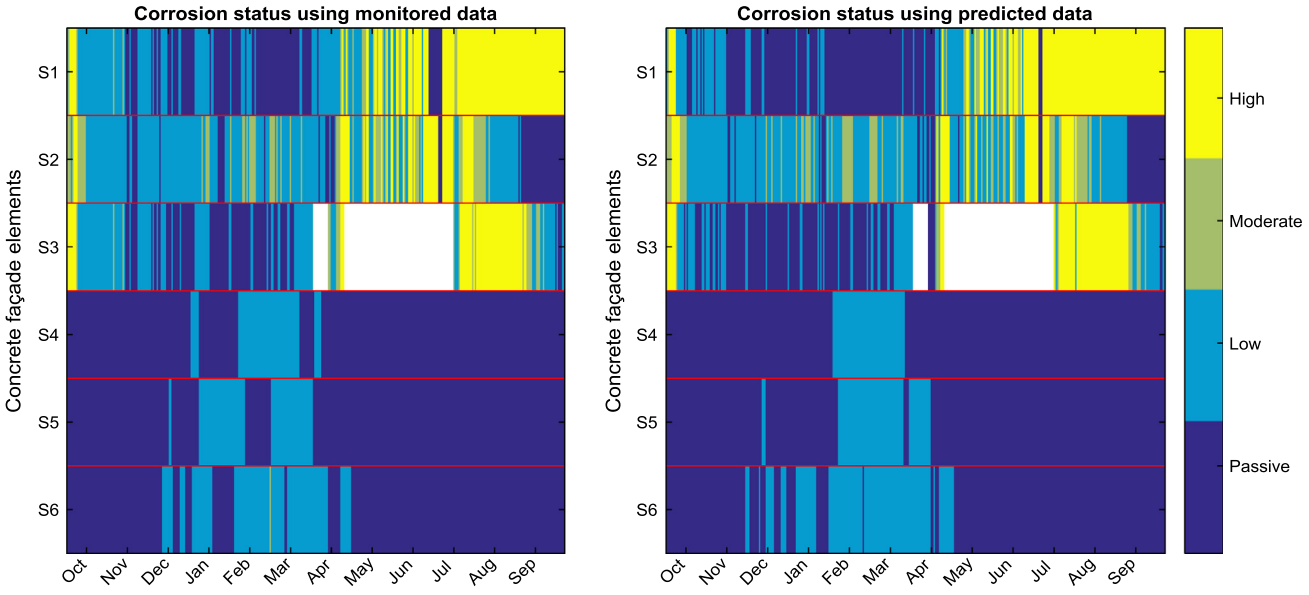

Fig. 12. One year corrosion status in the concrete façade elements of the case structure (1999–2000).

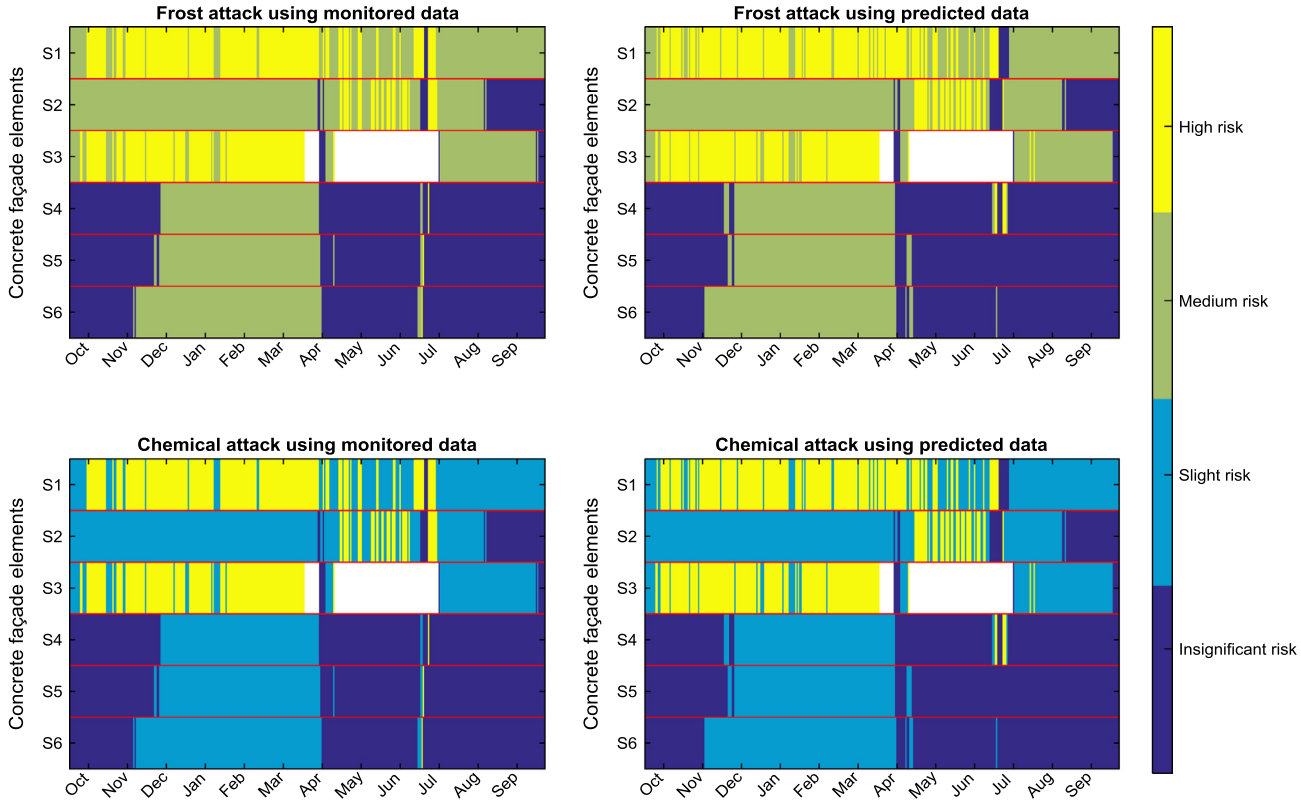

Fig. 13. One year frost and chemical attacks sensitivity of concrete façade elements (1999–2000).

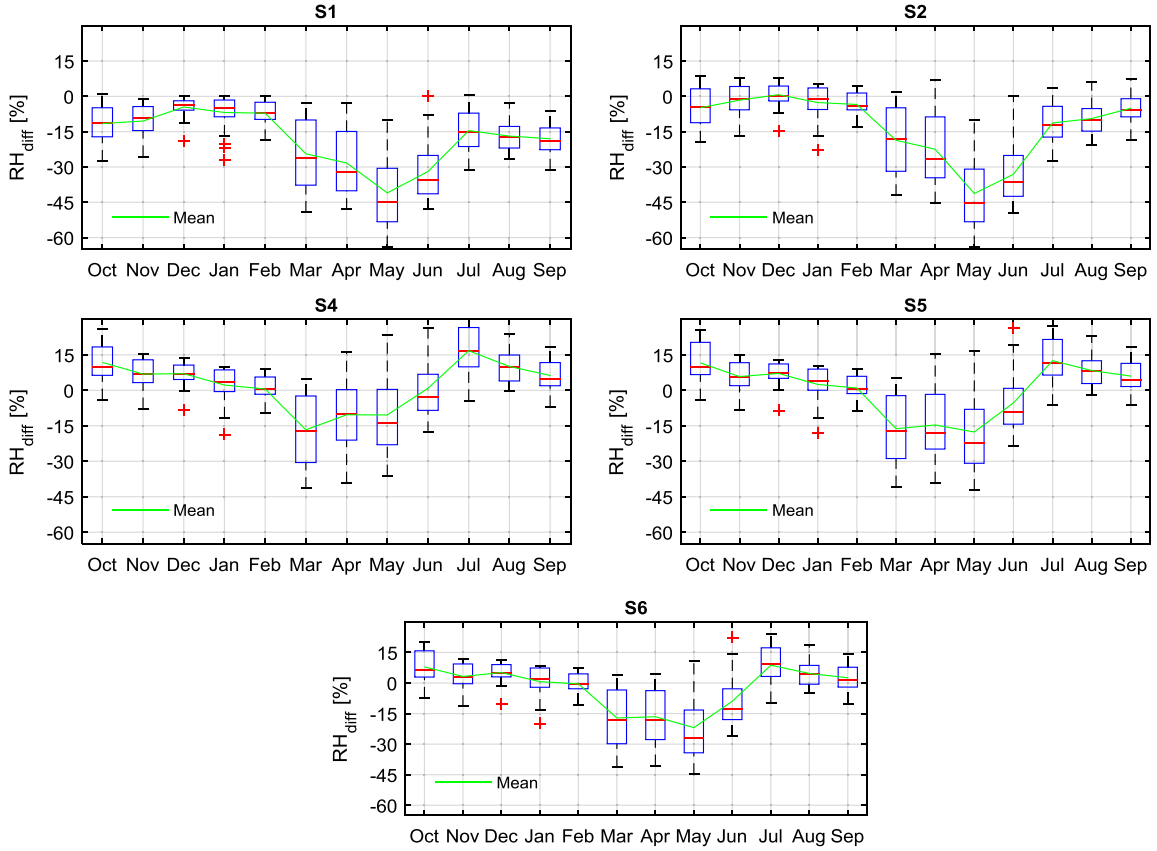

Fig. 14. Boxplot of relative humidity difference between ambient air and inside façade members (1999–2000).

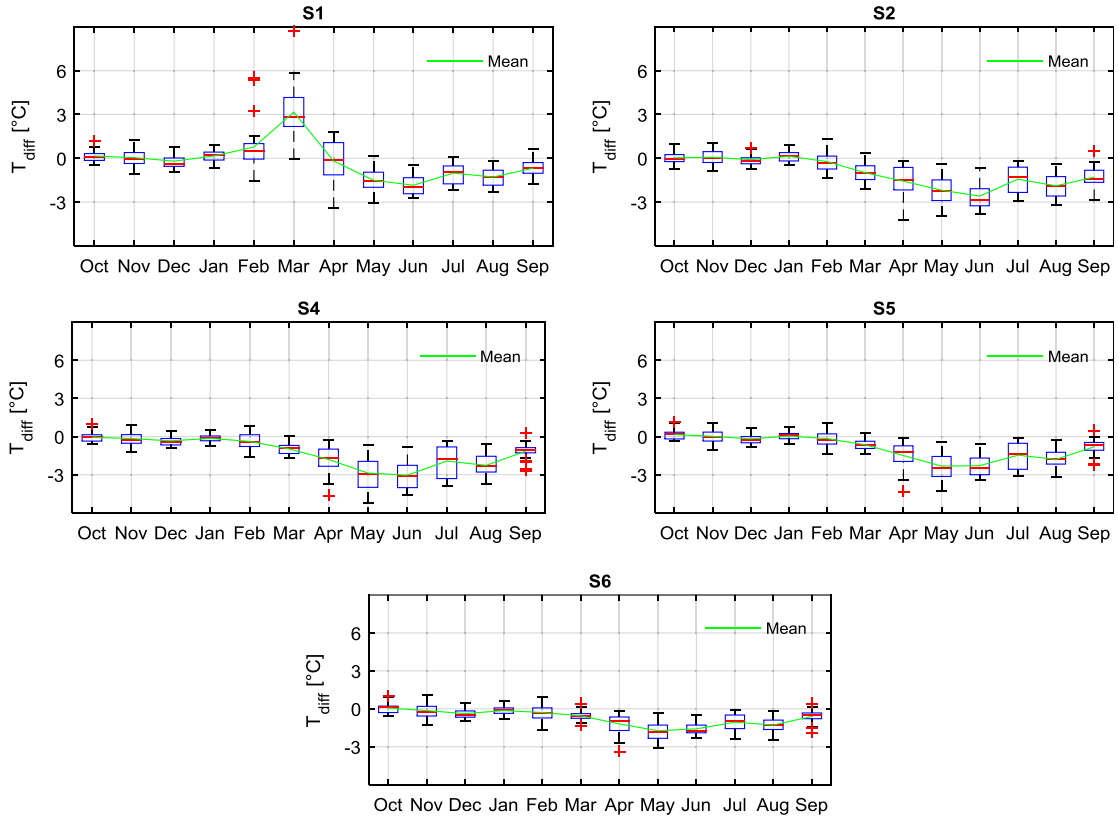

Fig. 15. Boxplot of temperature difference between ambient air and inside façade members (1999–2000).

throughout the year, except S1, and around zero from October to January. This reveals that temperature inside concrete façade member is higher than the ambient air. However, in many instances, the mean temperature inside reference façade member is greater than all surface protected members, indicating that the coating systems limit the temperature gradient.

8. Discussions

Hygrothermal monitoring and modelling can be seen as intertwined actions. The monitoring system provides information about the hygrothermal performance of surface-protected concrete panel for a specific period of time. The hygrothermal prediction model estimates the hygrothermal state of the panel using meteorological ambient air temperature and relative humidity after learning the interrelation using the monitored data. Hygrothermal data obtained from monitoring system/model can be used to evaluate the corrosion rate and other potential deterioration caused unintentionally by the applied surface protection systems, such as frost and chemical attacks. This allows for a more rational approach to a realistic assessment of the structure and reasonably timed repair measures, which in turn reduce the maintenance costs significantly. As the amount of available data for learning increase, the performance of neural network based model adaptively improve to produce meaningful and reliable predictions. In addition, the adopted advanced exploratory data analysis techniques would allow identifying essential relations and patterns. Without systematic monitoring and modelling, it is not plausible to maintain significant level of reliability regarding the performance of coatings, corrosion rate and deterioration caused by frost and chemical attacks in surface-protected concrete elements.

The developed hygrothermal prediction model will significantly promote the management of various deteriorations controlled by hygrothermal interactions in the case structure. Indeed, the model can be used globally if necessary features are included. These features may include concrete composition, geolocation, concrete geometry, façade orientation, various surface protection materials, and distance from aggressive environments. The features shall be monitored in several case studies and the monitored data used for training the model. The adopted advanced exploratory data analysis techniques can also be used to analyze other types of monitored data in research field of concrete. In the present work, the developed model was tested using 90 days and the hygrothermal behavior was predicted with a reasonably low error. The authors plan to test the model using a long-term data in order to investigate whether the two years data is sufficient for capturing the ageing effect of the surface protection materials until their life-time.

9. Conclusions

In this work, hygrothermal prediction model was developed. The model was carried out using NARX recurrent neural network architecture. It used ambient relative humidity and ambient temperature data as input. Relative humidity and temperature data measured inside surface-protected concrete façade member at a diagonal depth of 40 mm were assigned as target. The proposed model was trained, validated, and tested using data of two years. The test performance of the presented model demonstrated that the model predicts the hygrothermal performance inside the concrete with a reasonably low error. The hygrothermal data obtained from the model were used to compute the corrosion rate and to foresee the deterioration risk levels caused by frost and chemical attacks. In addition, with exploratory data analysis techniques, the performance of the applied surface protection systems against moisture and thermal was analyzed. The proposed model as well

as the adopted advanced exploratory data analysis techniques allows for a more rational approach to a realistic assessment of various deterioration mechanisms controlled by hygrothermal interactions as well as the performance of the surface treatments. It allows identifying appropriate surface protection system against moisture, which in turn enables a considerable minimization in maintenance and lifecycle costs.

References

[1] Z. Wang, Q. Zeng, L. Wang, Y. Yao, K. Li, Corrosion of rebar in concrete under cyclic freeze–thaw and chloride salt action, Constr. Build. Mater. 53 (2014) 40–47, http://dx.doi.org/10.1016/j.conbuildmat.2013.11.063.

[2] B. Pradhan, Corrosion behavior of steel reinforcement in concrete exposed to composite chloride–sulfate environment, Constr. Build. Mater. 72 (2014) 398–410, http://dx.doi.org/10.1016/j.conbuildmat.2014.09.026.

[3] E. Sistonen, Service Life of Hot-Dip Galvanised Reinforcement Bars in Carbonated and Chloride-Contaminated Concrete, Helsinki University of Technology, 2009. <http://urn.fi/URN:ISBN:978-952-248-168-9>.

[4] M. El-Reedy, Steel-Reinforced Concrete Structures: Assessment and Repair of Corrosion, CRC Press, Boca Raton, 2008, http://dx.doi.org/10.1201/9781420054316.

[5] W.Z. Taffese, E. Sistonen, Service life prediction of repaired structures using concrete recasting method: state-of-the-art, Proc. Eng. 57 (2013) 1138–1144, http://dx.doi.org/10.1016/j.proeng.2013.04.143.

[6] B. Yu, L. Yang, M. Wu, B. Li, Practical model for predicting corrosion rate of steel reinforcement in concrete structures, Constr. Build. Mater. 54 (2014) 385–401, http://dx.doi.org/10.1016/j.conbuildmat.2013.12.046.

[7] J.R. Mackechnie, M.G. Alexander, Repair Principles for Corrosion-Damaged Reinforced Concrete Structures, Department of Civil Engineering, University of Cape Town, 2001.

[8] J. Lahdensivu, Durability Properties and Actual Deterioration of Finnish Concrete Facades and Balconies, Tampere University of Technology, 2012. <http://urn.fi/URN:ISBN:978-952-15-2823-1>.

[9] A. Köliö, M. Honkanen, J. Lahdensivu, M. Vippola, M. Pentti, Corrosion products of carbonation induced corrosion in existing reinforced concrete facades, Cem. Concr. Res. 78 (2015) 200–207, http://dx.doi.org/10.1016/j.cemconres.2015.07.009.

[10] J. Lahdensivu, H. Mäkelä, P. Pirinen, Corrosion of reinforcement in existing concrete façades, in: V.P. de Freitas, A. Costa, J.M.P.Q. Delgado (Eds.), Durab. Build. Mater. Components, Springer Berlin Heidelberg, Heidelberg, 2013, pp. 253–274, http://dx.doi.org/10.1007/978-3-642-37475-3_10.

[11] T.A. Pakkala, A. Köliö, J. Lahdensivu, M. Pentti, The effect of climate change on freeze-thaw cycles in nordic climate, in: C. Andrade, J. Gulikers, R. Polder (Eds.), Durab. Reinf. Concr. From Compos to Prot., Cham, Springer International Publishing, 2014, pp. 145–154, http://dx.doi.org/10.1007/978-3-319-09921-7_13.

[12] F. Al-Neshawy, Computerised Prediction of the Deterioration of Concrete Building Facades Caused by Moisture and Changes in Temperature, Aalto University, 2013. <http://urn.fi/URN:ISBN:978-952-60-5203-8>.

[13] L. Bertolini, B. Elsener, P. Pedeferri, R.B. Polde, Corrosion of Steel in Concrete: Prevention, Diagnosis, Repair, Wiley-VCH Verlag GmbH & Co. KGaA, Weinheim, 2004, http://dx.doi.org/10.1002/3527603379.

[14] F. Hunkeler, Corrosion in reinforced concrete: processes and mechanisms, in: H. Böhni (Ed.), Corros. Reinf. Concr. Struct., CRC Press, Boca Raton, 2005, pp. 1–45.

[15] R. Akid, Corrosion of engineering materials, in: J.K. Wessel (Ed.), Handb. Adv. Mater. Enabling New Des., John Wiley & Sons, Inc., Hoboken, 2004, pp. 487–542, http://dx.doi.org/10.1002/0471465186.ch11.

[16] fib, Structural Concrete: Textbook on Behaviour, Design and Performance, Fédération internationale du béton (fib), Lausanne, 2009.

[17] A.M. Neville, J.J. Brooks, Concrete Technology, Prentice Hall, Harlow, 2010.

[18] Z. Li, Advanced Concrete Technology, John Wiley & Sons, Inc., Hoboken, 2011, http://dx.doi.org/10.1002/9780470950067.

[19] P.K. Mehta, P.J.M. Monteiro, Concrete: Microstructure, Properties, and Materials, third ed., McGraw-Hill Professional, 2006, http://dx.doi.org/10.1036/0071462899.

[20] Dansk Standard, Repair of Concrete Structures to EN 1504, Elsevier Butterworth-Heinemann, Oxford, 2004.

[21] F. Al-Neshawy, J. Piironen, S. Peltola, E. Sistonen, J. Puttonen, Network system for assessing the moisture and thermal behaviour of repaired concrete building facades, Inf. Technol. Constr. 16 (2011) 601–616.

[22] D.A. Lange, Z.C. Grasley, R. Rodden, Embedded sensors for measuring environmental parameters in concrete, ACI Special Publ. 252 (2008) 41–52.

[23] M.N.A. Said, D. Duchesne, A.H.P. Maurenbrecher, K. Ibrahim, C. Lumsdon, D. Stephenson, Monitoring the long-term performance of the Peace Tower in Ottawa, J. Preserv. Technol. 36 (2005) 53–59.

[24] W.Z. Taffese, F. Al-Neshawy, J. Piironen, E. Sistonen, J. Puttonen, Monitoring, evaluation and long-term forecasting of hygrothermal performance of thick-walled concrete structure OECD/NEA WGIAGE Work, in: Non-Destructive Eval. Thick. Concr. Struct., OECD, Prague, 2014, pp. 121–143.

[25] A. Janssens, M. Woloszyn, C. Rode, A. Sasic-Kalagasidis, M. De Paepe, From EMPD to CFD – overview of different approaches for heat air and moisture modeling in IEA Annex 41, in: C. Rode, H. Hens, H. Janssen (Eds.), Proc. IEA ECBCS Annex 41 Closing Semin., Technical University of Denmark, Department of Civil Engineering, Copenhagen, 2008, pp. 9–20.

[26] M. Khashei, M. Bijari, An artificial neural network (p, d, q) model for timeseries forecasting, Expert Syst. Appl. 37 (2010) 479–489, http://dx.doi.org/10.1016/j.eswa.2009.05.044.

[27] H.-U. Löffler, D. Raabe, F. Roters, F. Barlat, L-Q Chen, Microstructure modeling using artificial neural networks, in: Contin. Scale Simul. Eng. Mater. Fundam. – Microstruct. – Process Appl., Wiley-VCH Verlag GmbH & Co. KGaA, Weinheim, 2004, pp. 829–844, http://dx.doi.org/10.1002/3527603786.ch46.

[28] W. Graf, S. Freitag, M. Kaliske, J.-U. Sickert, Recurrent neural networks for uncertain time-dependent structural behavior, Comput. Civ. Infrastruct. Eng. 25 (2010) 322–323, http://dx.doi.org/10.1111/j.1467-8667.2009.00645.x.

[29] U. Reuter, B. Möller, Artificial neural networks for forecasting of fuzzy time series, Comput. Civ. Infrastruct. Eng. 25 (2010) 363–374, http://dx.doi.org/10.1111/j.1467-8667.2009.00646.x.

[30] S. Freitag, W. Graf, M. Kaliske, J.-U. Sickert, Prediction of time-dependent structural behaviour with recurrent neural networks for fuzzy data, Comput. Struct. 89 (2011) 1971–1981, http://dx.doi.org/10.1016/j.compstruc.2011.05.013.

[31] S. Lee, C. Lee, Prediction of shear strength of FRP-reinforced concrete flexural members without stirrups using artificial neural networks, Eng. Struct. 61 (2014) 99–112, http://dx.doi.org/10.1016/j.engstruct.2014.01.001.

[32] H. Adeli, A. Panakkat, A probabilistic neural network for earthquake magnitude prediction, Neural Networks 22 (2009) 1018–1024, http://dx.doi.org/10.1016/j.neunet.2009.05.003.

[33] M. Moustra, M. Avraamides, C. Christodoulou, Artificial neural networks for earthquake prediction using time series magnitude data or seismic electric signals, Expert Syst. Appl. 38 (2011) 15032–15039, http://dx.doi.org/10.1016/j.eswa.2011.05.043.

[34] T.K. Šipoš, V. Sigmund, M. Hadzima-Nyarko, Earthquake performance of infilled frames using neural networks and experimental database, Eng. Struct. 51 (2013) 113–127, http://dx.doi.org/10.1016/j.engstruct.2012.12.038.

[35] W.Z. Taffese, E. Sistonen, J. Puttonen, CaPrM: carbonation prediction model for reinforced concrete using machine learning methods, Constr. Build. Mater. 100 (2015) 70–82, http://dx.doi.org/10.1016/j.conbuildmat.2015.09.058.

[36] İ.B. Topçu, M. Sarıdemir, Prediction of rubberized concrete properties using artificial neural network and fuzzy logic, Constr. Build. Mater. 22 (2008) 532–540, http://dx.doi.org/10.1016/j.conbuildmat.2006.11.007.

[37] M.M. Alshihri, A.M. Azmy, M.S. El-Bisy, Neural networks for predicting compressive strength of structural light weight concrete, Constr. Build. Mater. 23 (2009) 2214–2219, http://dx.doi.org/10.1016/j.conbuildmat.2008.12.003.

[38] Z.H. Duan, S.C. Kou, C.S. Poon, Using artificial neural networks for predicting the elastic modulus of recycled aggregate concrete, Constr. Build. Mater. 44 (2013) 524–532, http://dx.doi.org/10.1016/j.conbuildmat.2013.02.064.

[39] L. Bal, F. Buyle-Bodin, Artificial neural network for predicting drying shrinkage of concrete, Constr. Build. Mater. 38 (2013) 248–254, http://dx.doi.org/10.1016/j.conbuildmat.2012.08.043.

[40] W.Z. Taffese, F. Al-Neshawy, E. Sistonen, M. Ferreira, Optimized neural network based carbonation prediction model, in: Int. Symp. Non-Destructive Test. Civ. Eng., Bundesanstalt für Materialforschung und -prüfung (BAM), Berlin, 2015, pp. 1074–1083.

[41] S. Haykin, Neural Networks and Learning Machines, third ed., Pearson Education, Inc., Upper Saddle River, 2009.

[42] S. Samarasinghe, Neural Networks for Applied Sciences and Engineering: From Fundamentals to Complex Pattern Recognition, Auerbach Publications, Boca Raton, 2006, http://dx.doi.org/10.1201/9781420013061.fmatt.

[43] S.T. Skias, Background of the verification and validation of neural networks, in: B.J. Taylor (Ed.), Methods Proced. Verif. Valid. Artif. neural networks, Springer Science + Business Media, Inc., New York, 2006, pp. 1–12, http://dx.doi.org/10.1007/0-387-29485-6_1.

[44] H.R. Maier, G.C. Dandy, Neural networks for the prediction and forecasting of water resources variables: a review of modelling issues and applications, Environ. Modell. Software 15 (2000) 101–124, http://dx.doi.org/10.1016/S1364-8152(99)00007-9.

[45] J. Mattila, On the Durability of Cement-Based Patch Repairs on Finnish Concrete Facades and Balconies, Tampere University of Technology, 2003.

[46] T.A. Pakkala, A. Köliö, J. Lahdensivu, M. Kiviste, Durability demands related to frost attack for Finnish concrete buildings in changing climate, Build. Environ. 82 (2014) 27–41, http://dx.doi.org/10.1016/j.buildenv.2014.07.028.

[47] Vaisala, HM44 Concrete Humidity Measurement System, 2009. pp. 1–2, <http://www.vaisala.com/Vaisala> Documents/Catalogues/HM44.pdf.

[48] M.H. Beale, M.T. Hagan, H.B. Demuth, Neural Network toolboxTM: User's Guide, The MathWorks, Inc., 2015.

[49] E. Acuña, C. Rodriguez, The treatment of missing values and its effect in the classifier accuracy, in: D. Banks, R.F. McMorris, P. Arabie, W. Gaul (Eds.), Classif. Clust. Data Min. Appl., Springer Berlin Heidelberg, Berlin, 2004, pp. 639–647, http://dx.doi.org/10.1007/978-3-642-17103-1_60.

[50] P. Gupta, R. Srinivasan, Missing data prediction and forecasting for water quantity data, Int. Conf. Model. Simul. Control, IACSIT Press, Singapore, 2011. 98–102.

[51] A. Sorjamaa, Methodologies for time series prediction and missing value imputation, Aalto University, 2010. <http://lib.tkk.fi/Diss/2010/isbn9789526034539/>.

[52] MathWorks, Curve Fitting toolbox™: User's Guide, The MathWorks, Inc., 2015.

[53] H. Mirzaee, Long-term prediction of chaotic time series with multi-step prediction horizons by a neural network with Levenberg–Marquardt learning algorithm, Chaos, Solitons Fractals 41 (2009) 1975–1979, http://dx.doi.org/10.1016/j.chaos.2008.08.016.
[54] T. Wang, K. Yang, Y. Guo, River ice conditions forecast by artificial neural networks, in: C. Zhang, H. Tang (Eds.), Adv. Water Resour. Hydraul. Eng. Proc. 16th IAHR-APD Congr. 3rd Symp. IAHR-ISHS, Springer-Verlag, Berlin, 2009, pp. 1918–1923, http://dx.doi.org/10.1007/978-3-540-89465-0.
[55] M. Štencl, J. Šťastny, Artificial neural networks numerical forecasting of economic time series, in: C.-L.P. Hui (Ed.), Artif. Neural Networks – Appl., InTech, Rijeka, 2011, pp. 13–28, http://dx.doi.org/10.5772/15341.
[56] C. Andrade, I. Martínez, Techniques for measuring the corrosion rate (polarization resistance) and the corrosion potential of reinforced concrete structures, in: C. Maierhofer, H.-W. Reinhardt, G. Dobmann (Eds.), Non-Destructive Eval. Reinf. Concr. Struct. Non-Destructive Test. Methods, Woodhead Publishing Limited, Cambridge, 2010, pp. 284–316. 10.1533/9781845699604.2.284..
[57] N.J. Carino, Methods to evaluate corrosion of reinforcement, in: V.M. Malhotra, N.J. Carino (Eds.), Handb. Nondestruct. Test. Concr., second ed., CRC Press, Boca Raton, 2004, p. 384.
[58] K. Jolkkonen, S. Huovinen, Influence of Coatings on the Service Life of Concrete Sandwich-Facades, 2000. Espoo (in Finnish).
[59] A. Sarja, E. Vesikari, Durability Design of Concrete Structures: Report of RILEM Technical Committee 130-CSL, E & FN Spon, London, 1996.
[60] Finnish Association of Civil Engineers. RIL 183-4.9, Service life of construction materials and structures, in: Methods of Appraisal. 4.9: Service Life Design of Concrete Structures, Finnish Association of Civil Engineers (RIL), Vantaa, 1995 (in Finnish).
[61] G. Fagerlund, Moisture mechanics as a tool for service life prediction, in: C. Sjöström (Ed.), Durab. Build. Mater. Components 7 Proc. 7th Int. Conf. Durab. Build. Mater. Components, Taylor & Francis, London, 1996, pp. 21–32.
[62] R.O. Heckroodt, Guide to Deterioration and Failure of Building Materials, Thomas Telford Publishing, London, 2002.
[63] G.K. Glass, Deterioration of steel reinforced concrete, in: I. Milne, R.O. Ritchie, B. Karihaloo (Eds.), Compr. Struct. Integr., vol. 6, Elsevier Ltd., 2003, pp. 321–350, http://dx.doi.org/10.1016/B0-08-043749-4/06140-1.
[64] A.B. Poole, Introduction to alkali-aggregate reaction in concrete, in: R.N. Swamy (Ed.), Alkali-Silica React. Concr., Spon Press, 1998, http://dx.doi.org/10.4324/9780203036631.ch1.
[65] CEB, Durable Concrete Structures: Design Guide, Thomas Telford Services Ltd., London, 1992.

Turku Centre for Computer Science
TUCS Dissertations

1. **Marjo Lipponen**, On Primitive Solutions of the Post Correspondence Problem
2. **Timo Käkölä**, Dual Information Systems in Hyperknowledge Organizations
3. **Ville Leppänen**, Studies on the Realization of PRAM
4. **Cunsheng Ding**, Cryptographic Counter Generators
5. **Sami Viitanen**, Some New Global Optimization Algorithms
6. **Tapio Salakoski**, Representative Classification of Protein Structures
7. **Thomas Långbacka**, An Interactive Environment Supporting the Development of Formally Correct Programs
8. **Thomas Finne**, A Decision Support System for Improving Information Security
9. **Valeria Mihalache**, Cooperation, Communication, Control. Investigations on Grammar Systems.
10. **Marina Waldén**, Formal Reasoning About Distributed Algorithms
11. **Tero Laihonen**, Estimates on the Covering Radius When the Dual Distance is Known
12. **Lucian Ilie**, Decision Problems on Orders of Words
13. **Jukkapekka Hekanaho**, An Evolutionary Approach to Concept Learning
14. **Jouni Järvinen**, Knowledge Representation and Rough Sets
15. **Tomi Pasanen**, In-Place Algorithms for Sorting Problems
16. **Mika Johnsson**, Operational and Tactical Level Optimization in Printed Circuit Board Assembly
17. **Mats Aspnäs**, Multiprocessor Architecture and Programming: The Hathi-2 System
18. **Anna Mikhajlova**, Ensuring Correctness of Object and Component Systems
19. **Vesa Torvinen**, Construction and Evaluation of the Labour Game Method
20. **Jorma Boberg**, Cluster Analysis. A Mathematical Approach with Applications to Protein Structures
21. **Leonid Mikhajlov**, Software Reuse Mechanisms and Techniques: Safety Versus Flexibility
22. **Timo Kaukoranta**, Iterative and Hierarchical Methods for Codebook Generation in Vector Quantization
23. **Gábor Magyar**, On Solution Approaches for Some Industrially Motivated Combinatorial Optimization Problems
24. **Linas Laibinis**, Mechanised Formal Reasoning About Modular Programs
25. **Shuhua Liu**, Improving Executive Support in Strategic Scanning with Software Agent Systems
26. **Jaakko Järvi**, New Techniques in Generic Programming – C++ is more Intentional than Intended
27. **Jan-Christian Lehtinen**, Reproducing Kernel Splines in the Analysis of Medical Data
28. **Martin Büchi**, Safe Language Mechanisms for Modularization and Concurrency
29. **Elena Troubitsyna**, Stepwise Development of Dependable Systems
30. **Janne Näppi**, Computer-Assisted Diagnosis of Breast Calcifications
31. **Jianming Liang**, Dynamic Chest Images Analysis
32. **Tiberiu Seceleanu**, Systematic Design of Synchronous Digital Circuits
33. **Tero Aittokallio**, Characterization and Modelling of the Cardiorespiratory System in Sleep-Disordered Breathing
34. **Ivan Porres**, Modeling and Analyzing Software Behavior in UML
35. **Mauno Rönkkö**, Stepwise Development of Hybrid Systems
36. **Jouni Smed**, Production Planning in Printed Circuit Board Assembly
37. **Vesa Halava**, The Post Correspondence Problem for Market Morphisms
38. **Ion Petre**, Commutation Problems on Sets of Words and Formal Power Series
39. **Vladimir Kvassov**, Information Technology and the Productivity of Managerial Work
40. **Frank Tétard**, Managers, Fragmentation of Working Time, and Information Systems

41. **Jan Manuch**, Defect Theorems and Infinite Words
42. **Kalle Ranto**, Z_4-Goethals Codes, Decoding and Designs
43. **Arto Lepistö**, On Relations Between Local and Global Periodicity
44. **Mika Hirvensalo**, Studies on Boolean Functions Related to Quantum Computing
45. **Pentti Virtanen**, Measuring and Improving Component-Based Software Development
46. **Adekunle Okunoye**, Knowledge Management and Global Diversity – A Framework to Support Organisations in Developing Countries
47. **Antonina Kloptchenko**, Text Mining Based on the Prototype Matching Method
48. **Juha Kivijärvi**, Optimization Methods for Clustering
49. **Rimvydas Rukšėnas**, Formal Development of Concurrent Components
50. **Dirk Nowotka**, Periodicity and Unbordered Factors of Words
51. **Attila Gyenesei**, Discovering Frequent Fuzzy Patterns in Relations of Quantitative Attributes
52. **Petteri Kaitovaara**, Packaging of IT Services – Conceptual and Empirical Studies
53. **Petri Rosendahl**, Niho Type Cross-Correlation Functions and Related Equations
54. **Péter Majlender**, A Normative Approach to Possibility Theory and Soft Decision Support
55. **Seppo Virtanen**, A Framework for Rapid Design and Evaluation of Protocol Processors
56. **Tomas Eklund**, The Self-Organizing Map in Financial Benchmarking
57. **Mikael Collan**, Giga-Investments: Modelling the Valuation of Very Large Industrial Real Investments
58. **Dag Björklund**, A Kernel Language for Unified Code Synthesis
59. **Shengnan Han**, Understanding User Adoption of Mobile Technology: Focusing on Physicians in Finland
60. **Irina Georgescu**, Rational Choice and Revealed Preference: A Fuzzy Approach
61. **Ping Yan**, Limit Cycles for Generalized Liénard-Type and Lotka-Volterra Systems
62. **Joonas Lehtinen**, Coding of Wavelet-Transformed Images
63. **Tommi Meskanen,** On the NTRU Cryptosystem
64. **Saeed Salehi**, Varieties of Tree Languages
65. **Jukka Arvo**, Efficient Algorithms for Hardware-Accelerated Shadow Computation
66. **Mika Hirvikorpi**, On the Tactical Level Production Planning in Flexible Manufacturing Systems
67. **Adrian Costea**, Computational Intelligence Methods for Quantitative Data Mining
68. **Cristina Seceleanu**, A Methodology for Constructing Correct Reactive Systems
69. **Luigia Petre**, Modeling with Action Systems
70. **Lu Yan**, Systematic Design of Ubiquitous Systems
71. **Mehran Gomari**, On the Generalization Ability of Bayesian Neural Networks
72. **Ville Harkke**, Knowledge Freedom for Medical Professionals – An Evaluation Study of a Mobile Information System for Physicians in Finland
73. **Marius Cosmin Codrea**, Pattern Analysis of Chlorophyll Fluorescence Signals
74. **Aiying Rong**, Cogeneration Planning Under the Deregulated Power Market and Emissions Trading Scheme
75. **Chihab BenMoussa**, Supporting the Sales Force through Mobile Information and Communication Technologies: Focusing on the Pharmaceutical Sales Force
76. **Jussi Salmi**, Improving Data Analysis in Proteomics
77. **Orieta Celiku**, Mechanized Reasoning for Dually-Nondeterministic and Probabilistic Programs
78. **Kaj-Mikael Björk**, Supply Chain Efficiency with Some Forest Industry Improvements
79. **Viorel Preoteasa**, Program Variables – The Core of Mechanical Reasoning about Imperative Programs
80. **Jonne Poikonen**, Absolute Value Extraction and Order Statistic Filtering for a Mixed-Mode Array Image Processor
81. **Luka Milovanov**, Agile Software Development in an Academic Environment
82. **Francisco Augusto Alcaraz Garcia**, Real Options, Default Risk and Soft Applications
83. **Kai K. Kimppa**, Problems with the Justification of Intellectual Property Rights in Relation to Software and Other Digitally Distributable Media
84. **Dragoş Truşcan**, Model Driven Development of Programmable Architectures
85. **Eugen Czeizler**, The Inverse Neighborhood Problem and Applications of Welch Sets in Automata Theory

86. **Sanna Ranto**, Identifying and Locating-Dominating Codes in Binary Hamming Spaces
87. **Tuomas Hakkarainen**, On the Computation of the Class Numbers of Real Abelian Fields
88. **Elena Czeizler**, Intricacies of Word Equations
89. **Marcus Alanen**, A Metamodeling Framework for Software Engineering
90. **Filip Ginter**, Towards Information Extraction in the Biomedical Domain: Methods and Resources
91. **Jarkko Paavola**, Signature Ensembles and Receiver Structures for Oversaturated Synchronous DS-CDMA Systems
92. **Arho Virkki**, The Human Respiratory System: Modelling, Analysis and Control
93. **Olli Luoma**, Efficient Methods for Storing and Querying XML Data with Relational Databases
94. **Dubravka Ilić**, Formal Reasoning about Dependability in Model-Driven Development
95. **Kim Solin**, Abstract Algebra of Program Refinement
96. **Tomi Westerlund**, Time Aware Modelling and Analysis of Systems-on-Chip
97. **Kalle Saari**, On the Frequency and Periodicity of Infinite Words
98. **Tomi Kärki**, Similarity Relations on Words: Relational Codes and Periods
99. **Markus M. Mäkelä**, Essays on Software Product Development: A Strategic Management Viewpoint
100. **Roope Vehkalahti**, Class Field Theoretic Methods in the Design of Lattice Signal Constellations
101. **Anne-Maria Ernvall-Hytönen**, On Short Exponential Sums Involving Fourier Coefficients of Holomorphic Cusp Forms
102. **Chang Li**, Parallelism and Complexity in Gene Assembly
103. **Tapio Pahikkala**, New Kernel Functions and Learning Methods for Text and Data Mining
104. **Denis Shestakov**, Search Interfaces on the Web: Querying and Characterizing
105. **Sampo Pyysalo**, A Dependency Parsing Approach to Biomedical Text Mining
106. **Anna Sell**, Mobile Digital Calendars in Knowledge Work
107. **Dorina Marghescu**, Evaluating Multidimensional Visualization Techniques in Data Mining Tasks
108. **Tero Säntti**, A Co-Processor Approach for Efficient Java Execution in Embedded Systems
109. **Kari Salonen**, Setup Optimization in High-Mix Surface Mount PCB Assembly
110. **Pontus Boström**, Formal Design and Verification of Systems Using Domain-Specific Languages
111. **Camilla J. Hollanti**, Order-Theoretic Mehtods for Space-Time Coding: Symmetric and Asymmetric Designs
112. **Heidi Himmanen**, On Transmission System Design for Wireless Broadcasting
113. **Sébastien Lafond**, Simulation of Embedded Systems for Energy Consumption Estimation
114. **Evgeni Tsivtsivadze**, Learning Preferences with Kernel-Based Methods
115. **Petri Salmela**, On Commutation and Conjugacy of Rational Languages and the Fixed Point Method
116. **Siamak Taati**, Conservation Laws in Cellular Automata
117. **Vladimir Rogojin**, Gene Assembly in Stichotrichous Ciliates: Elementary Operations, Parallelism and Computation
118. **Alexey Dudkov**, Chip and Signature Interleaving in DS CDMA Systems
119. **Janne Savela**, Role of Selected Spectral Attributes in the Perception of Synthetic Vowels
120. **Kristian Nybom**, Low-Density Parity-Check Codes for Wireless Datacast Networks
121. **Johanna Tuominen**, Formal Power Analysis of Systems-on-Chip
122. **Teijo Lehtonen**, On Fault Tolerance Methods for Networks-on-Chip
123. **Eeva Suvitie**, On Inner Products Involving Holomorphic Cusp Forms and Maass Forms
124. **Linda Mannila**, Teaching Mathematics and Programming – New Approaches with Empirical Evaluation
125. **Hanna Suominen**, Machine Learning and Clinical Text: Supporting Health Information Flow
126. **Tuomo Saarni**, Segmental Durations of Speech
127. **Johannes Eriksson**, Tool-Supported Invariant-Based Programming

128. **Tero Jokela**, Design and Analysis of Forward Error Control Coding and Signaling for Guaranteeing QoS in Wireless Broadcast Systems
129. **Ville Lukkarila**, On Undecidable Dynamical Properties of Reversible One-Dimensional Cellular Automata
130. **Qaisar Ahmad Malik**, Combining Model-Based Testing and Stepwise Formal Development
131. **Mikko-Jussi Laakso**, Promoting Programming Learning: Engagement, Automatic Assessment with Immediate Feedback in Visualizations
132. **Riikka Vuokko**, A Practice Perspective on Organizational Implementation of Information Technology
133. **Jeanette Heidenberg**, Towards Increased Productivity and Quality in Software Development Using Agile, Lean and Collaborative Approaches
134. **Yong Liu**, Solving the Puzzle of Mobile Learning Adoption
135. **Stina Ojala**, Towards an Integrative Information Society: Studies on Individuality in Speech and Sign
136. **Matteo Brunelli**, Some Advances in Mathematical Models for Preference Relations
137. **Ville Junnila**, On Identifying and Locating-Dominating Codes
138. **Andrzej Mizera**, Methods for Construction and Analysis of Computational Models in Systems Biology. Applications to the Modelling of the Heat Shock Response and the Self-Assembly of Intermediate Filaments.
139. **Csaba Ráduly-Baka**, Algorithmic Solutions for Combinatorial Problems in Resource Management of Manufacturing Environments
140. **Jari Kyngäs**, Solving Challenging Real-World Scheduling Problems
141. **Arho Suominen**, Notes on Emerging Technologies
142. **József Mezei**, A Quantitative View on Fuzzy Numbers
143. **Marta Olszewska**, On the Impact of Rigorous Approaches on the Quality of Development
144. **Antti Airola**, Kernel-Based Ranking: Methods for Learning and Performace Estimation
145. **Aleksi Saarela**, Word Equations and Related Topics: Independence, Decidability and Characterizations
146. **Lasse Bergroth**, Kahden merkkijonon pisimmän yhteisen alijonon ongelma ja sen ratkaiseminen
147. **Thomas Canhao Xu**, Hardware/Software Co-Design for Multicore Architectures
148. **Tuomas Mäkilä**, Software Development Process Modeling – Developers Perspective to Contemporary Modeling Techniques
149. **Shahrokh Nikou**, Opening the Black-Box of IT Artifacts: Looking into Mobile Service Characteristics and Individual Perception
150. **Alessandro Buoni**, Fraud Detection in the Banking Sector: A Multi-Agent Approach
151. **Mats Neovius**, Trustworthy Context Dependency in Ubiquitous Systems
152. **Fredrik Degerlund**, Scheduling of Guarded Command Based Models
153. **Amir-Mohammad Rahmani-Sane**, Exploration and Design of Power-Efficient Networked Many-Core Systems
154. **Ville Rantala**, On Dynamic Monitoring Methods for Networks-on-Chip
155. **Mikko Pelto**, On Identifying and Locating-Dominating Codes in the Infinite King Grid
156. **Anton Tarasyuk**, Formal Development and Quantitative Verification of Dependable Systems
157. **Muhammad Mohsin Saleemi**, Towards Combining Interactive Mobile TV and Smart Spaces: Architectures, Tools and Application Development
158. **Tommi J. M. Lehtinen**, Numbers and Languages
159. **Peter Sarlin**, Mapping Financial Stability
160. **Alexander Wei Yin**, On Energy Efficient Computing Platforms
161. **Mikołaj Olszewski**, Scaling Up Stepwise Feature Introduction to Construction of Large Software Systems
162. **Maryam Kamali**, Reusable Formal Architectures for Networked Systems
163. **Zhiyuan Yao**, Visual Customer Segmentation and Behavior Analysis – A SOM-Based Approach
164. **Timo Jolivet**, Combinatorics of Pisot Substitutions
165. **Rajeev Kumar Kanth**, Analysis and Life Cycle Assessment of Printed Antennas for Sustainable Wireless Systems
166. **Khalid Latif**, Design Space Exploration for MPSoC Architectures

167. **Bo Yang**, Towards Optimal Application Mapping for Energy-Efficient Many-Core Platforms
168. **Ali Hanzala Khan**, Consistency of UML Based Designs Using Ontology Reasoners
169. **Sonja Leskinen**, m-Equine: IS Support for the Horse Industry
170. **Fareed Ahmed Jokhio**, Video Transcoding in a Distributed Cloud Computing Environment
171. **Moazzam Fareed Niazi**, A Model-Based Development and Verification Framework for Distributed System-on-Chip Architecture
172. **Mari Huova**, Combinatorics on Words: New Aspects on Avoidability, Defect Effect, Equations and Palindromes
173. **Ville Timonen**, Scalable Algorithms for Height Field Illumination
174. **Henri Korvela**, Virtual Communities – A Virtual Treasure Trove for End-User Developers
175. **Kameswar Rao Vaddina**, Thermal-Aware Networked Many-Core Systems
176. **Janne Lahtiranta**, New and Emerging Challenges of the ICT-Mediated Health and Well-Being Services
177. **Irum Rauf**, Design and Validation of Stateful Composite RESTful Web Services
178. **Jari Björne**, Biomedical Event Extraction with Machine Learning
179. **Katri Haverinen**, Natural Language Processing Resources for Finnish: Corpus Development in the General and Clinical Domains
180. **Ville Salo**, Subshifts with Simple Cellular Automata
181. **Johan Ersfolk**, Scheduling Dynamic Dataflow Graphs
182. **Hongyan Liu**, On Advancing Business Intelligence in the Electricity Retail Market
183. **Adnan Ashraf**, Cost-Efficient Virtual Machine Management: Provisioning, Admission Control, and Consolidation
184. **Muhammad Nazrul Islam**, Design and Evaluation of Web Interface Signs to Improve Web Usability: A Semiotic Framework
185. **Johannes Tuikkala**, Algorithmic Techniques in Gene Expression Processing: From Imputation to Visualization
186. **Natalia Díaz Rodríguez**, Semantic and Fuzzy Modelling for Human Behaviour Recognition in Smart Spaces. A Case Study on Ambient Assisted Living
187. **Mikko Pänkäälä**, Potential and Challenges of Analog Reconfigurable Computation in Modern and Future CMOS
188. **Sami Hyrynsalmi**, Letters from the War of Ecosystems – An Analysis of Independent Software Vendors in Mobile Application Marketplaces
189. **Seppo Pulkkinen**, Efficient Optimization Algorithms for Nonlinear Data Analysis
190. **Sami Pyöttiälä**, Optimization and Measuring Techniques for Collect-and-Place Machines in Printed Circuit Board Industry
191. **Syed Mohammad Asad Hassan Jafri**, Virtual Runtime Application Partitions for Resource Management in Massively Parallel Architectures
192. **Toni Ernvall**, On Distributed Storage Codes
193. **Yuliya Prokhorova**, Rigorous Development of Safety-Critical Systems
194. **Olli Lahdenoja**, Local Binary Patterns in Focal-Plane Processing – Analysis and Applications
195. **Annika H. Holmbom**, Visual Analytics for Behavioral and Niche Market Segmentation
196. **Sergey Ostroumov**, Agent-Based Management System for Many-Core Platforms: Rigorous Design and Efficient Implementation
197. **Espen Suenson**, How Computer Programmers Work – Understanding Software Development in Practise
198. **Tuomas Poikela**, Readout Architectures for Hybrid Pixel Detector Readout Chips
199. **Bogdan Iancu**, Quantitative Refinement of Reaction-Based Biomodels
200. **Ilkka Törmä**, Structural and Computational Existence Results for Multidimensional Subshifts
201. **Sebastian Okser**, Scalable Feature Selection Applications for Genome-Wide Association Studies of Complex Diseases
202. **Fredrik Abbors**, Model-Based Testing of Software Systems: Functionality and Performance
203. **Inna Pereverzeva**, Formal Development of Resilient Distributed Systems
204. **Mikhail Barash**, Defining Contexts in Context-Free Grammars
205. **Sepinoud Azimi**, Computational Models for and from Biology: Simple Gene Assembly and Reaction Systems
206. **Petter Sandvik**, Formal Modelling for Digital Media Distribution

207. **Jongyun Moon**, Hydrogen Sensor Application of Anodic Titanium Oxide Nanostructures
208. **Simon Holmbacka**, Energy Aware Software for Many-Core Systems
209. **Charalampos Zinoviadis**, Hierarchy and Expansiveness in Two-Dimensional Subshifts of Finite Type
210. **Mika Murtojärvi**, Efficient Algorithms for Coastal Geographic Problems
211. **Sami Mäkelä**, Cohesion Metrics for Improving Software Quality
212. **Eyal Eshet**, Examining Human-Centered Design Practice in the Mobile Apps Era
213. **Jetro Vesti**, Rich Words and Balanced Words
214. **Jarkko Peltomäki**, Privileged Words and Sturmian Words
215. **Fahimeh Farahnakian**, Energy and Performance Management of Virtual Machines: Provisioning, Placement and Consolidation
216. **Diana-Elena Gratie**, Refinement of Biomodels Using Petri Nets
217. **Harri Merisaari**, Algorithmic Analysis Techniques for Molecular Imaging
218. **Stefan Grönroos**, Efficient and Low-Cost Software Defined Radio on Commodity Hardware
219. **Noora Nieminen**, Garbling Schemes and Applications
220. **Ville Taajamaa**, O-CDIO: Engineering Education Framework with Embedded Design Thinking Methods
221. **Johannes Holvitie**, Technical Debt in Software Development – Examining Premises and Overcoming Implementation for Efficient Management
222. **Tewodros Deneke**, Proactive Management of Video Transcoding Services
223. **Kashif Javed**, Model-Driven Development and Verification of Fault Tolerant Systems
224. **Pekka Naula**, Sparse Predictive Modeling – A Cost-Effective Perspective
225. **Antti Hakkala**, On Security and Privacy for Networked Information Society – Observations and Solutions for Security Engineering and Trust Building in Advanced Societal Processes
226. **Anne-Maarit Majanoja**, Selective Outsourcing in Global IT Services – Operational Level Challenges and Opportunities
227. **Samuel Rönnqvist**, Knowledge-Lean Text Mining
228. **Mohammad-Hashem Hahgbayan**, Energy-Efficient and Reliable Computing in Dark Silicon Era
229. **Charmi Panchal**, Qualitative Methods for Modeling Biochemical Systems and Datasets: The Logicome and the Reaction Systems Approaches
230. **Erkki Kaila**, Utilizing Educational Technology in Computer Science and Programming Courses: Theory and Practice
231. **Fredrik Robertsén**, The Lattice Boltzmann Method, a Petaflop and Beyond
232. **Jonne Pohjankukka**, Machine Learning Approaches for Natural Resource Data
233. **Paavo Nevalainen**, Geometric Data Understanding: Deriving Case-Specific Features
234. **Michal Szabados**, An Algebraic Approach to Nivat's Conjecture
235. **Tuan Nguyen Gia**, Design for Energy-Efficient and Reliable Fog-Assisted Healthcare IoT Systems
236. **Anil Kanduri**, Adaptive Knobs for Resource Efficient Computing
237. **Veronika Suni**, Computational Methods and Tools for Protein Phosphorylation Analysis
238. **Behailu Negash**, Interoperating Networked Embedded Systems to Compose the Web of Things
239. **Kalle Rindell**, Development of Secure Software: Rationale, Standards and Practices
240. **Jurka Rahikkala**, On Top Management Support for Software Cost Estimation
241. **Markus A. Whiteland**, On the k-Abelian Equivalence Relation of Finite Words
242. **Mojgan Kamali**, Formal Analysis of Network Routing Protocols
243. **Jesús Carabaño Bravo**, A Compiler Approach to Map Algebra for Raster Spatial Modeling
244. **Amin Majd**, Distributed and Lightweight Meta-heuristic Optimization Method for Complex Problems
245. **Ali Farooq**, In Quest of Information Security in Higher Education Institutions: Security Awareness, Concerns, and Behaviour of Students
246. **Juho Heimonen**, Knowledge Representation and Text Mining in Biomedical, Healthcare, and Political Domains

247. **Sanaz Rahimi Moosavi**, Towards End-to-End Security in Internet of Things based Healthcare
248. **Mingzhe Jiang**, Automatic Pain Assessment by Learning from Multiple Biopotentials
249. **Johan Kopra**, Cellular Automata with Complicated Dynamics
250. **Iman Azimi**, Personalized Data Analytics for Internet-of-Things-based Health Monitoring
251. **Jaakko Helminen**, Systems Action Design Research: Delineation of an Application to Develop Hybrid Local Climate Services
252. **Aung Pyae**, The Use of Digital Games to Enhance the Physical Exercise Activity of the Elderly: A Case of Finland
253. **Woubishet Zewdu Taffese**, Data-Driven Method for Enhanced Corrosion Assessment of Reinforced Concrete Structures

Turku Centre *for* Computer Science

http://www. tucs.fi

tucs@abo.fi

University of Turku
Faculty of Science and Engineering
- Department of Future Technologies
- Department of Mathematics and Statistics

Turku School of Economics
- Institute of Information Systems Science

Åbo Akademi University
Faculty of Science and Engineering
- Computer Engineering
- Computer Science

Faculty of Social Sciences, Business and Economics
- Information Systems

ISBN 978-952-12-3952-6
ISSN 1239-1883

Woubishet Z. Taffese

Data-Driven Method for Enhanced Corrosion Assessment of Reinforced Concrete Structures

Woubishet Z. Taffese

Data-Driven Method for Enhanced Corrosion Assessment of Reinforced Concrete Structures

Woubishet Z. Taffese

Data-Driven Method for Enhanced Corrosion Assessment of Reinforced Concrete Structure